MUNI
FACULTY
OF MEDICINE

MASARYK UNIVERSITY
FACULTY OF MEDICINE

The Cardiomyocyte Is Not the Whole Story

Developmental and Cellular Perspectives on Dystrophin-Associated Cardiomyopathy

HABILITATION THESIS

VLADIMÍR ROTREKL

DEPARTMENT OF BIOLOGY

Bibliographic record

Author: Vladimír Rotrekl
Faculty of Medicine
Masaryk University
Department of Biology
Title of Thesis: The Cardiomyocyte Is Not the Whole Story Developmental and Cellular Perspectives on Dystrophin-Associated Cardiomyopathy
Field: Medical biology
Year: 2026
Number of Pages: 155
Keywords: Duchenne muscular dystrophy, cardiomyopathy, stem cells, disease modeling

ORIGINALITY AND CONFLICT OF INTEREST DECLARATION

The presented experimental data comes from original research that was carried out by the author himself and in collaboration with other colleagues. Submitted thesis consists of my own text except for the parts properly cited from other authors. AI was used solely to polish grammar and style of the thesis.

Conflict of interest statement: None declared

Brno, 14. 9. 2026 ……..

Mgr. Vladimír Rotrekl, Ph.D.

ABSTRACT

Dystrophin-associated cardiomyopathy is a major manifestation of dystrophinopathies and has traditionally been understood primarily as a consequence of progressive dysfunction and loss of dystrophin-deficient cardiomyocytes. Increasing evidence, however, indicates that disease-associated abnormalities may extend to earlier cellular and developmental stages and to non-cardiomyocyte populations of the postnatal heart. Investigating these different dimensions requires complementary experimental models, as no single system provides access to the full temporal, developmental and cellular complexity of the disease. The work presented in this habilitation therefore combines DMD hPSC models to investigate early disease-associated cellular and developmental processes, three-dimensional dystrophin-deficient hPSC-derived cardiac models for quantitative functional characterization, human BMD myocardium for direct assessment of the affected human heart, and the mdx mouse model for examining cellular changes over time within the intact dystrophin-deficient myocardium.

Dystrophin-deficient hPSC-derived cardiac models reproduced multiple disease-relevant functional phenotypes, including abnormalities of electrophysiology, calcium handling and contractile function. Importantly, differences were also observed at the level of cardiac differentiation outcome, with a reduced proportion of spontaneously contracting cardiac aggregates. Looking further upstream, dystrophin-deficient pluripotent cells exhibited altered redox homeostasis and compromised genome integrity before cardiac differentiation. In parallel, studies of hPSC biology demonstrated redox-sensitive regulation of PI3K/AKT signalling, identifying this pathway as one component of the broader relationship between cellular redox state and stem-cell signalling.

A second, biologically distinct dimension emerged from studies of the postnatal heart. Human BMD myocardium showed a reduced resident cardiac population with stem/progenitor-like properties, accompanied by reduced ex vivo survival and reduced capacity to support cardiac fibroblast migration. In the mdx model, a similarly defined population showed an early increase followed by progressive age-dependent decline in the context of developing cardiac pathology. Cells isolated from this population also exhibited increased DNA damage.

Together, these findings extend the cellular framework of dystrophin-associated cardiac disease in two directions: upstream of the differentiated cardiac phenotype, towards earlier cellular states and developmental processes, and outside the cardiomyocyte compartment, towards resident populations with stem/progenitor-like properties in the postnatal myocardium. These observations raise several questions that warrant further investigation, including which cellular processes underlie the altered cardiac differentiation outcome, whether redox-sensitive signalling contributes to this phenotype in dystrophin-deficient cells, and what mechanisms underlie the alterations of resident populations in the postnatal heart and whether these changes influence disease progression. The relationship between the developmental and postnatal abnormalities also remains to be defined, as they arise in distinct biological contexts and cannot presently be assumed to represent a continuous or mechanistically unified process. Determining whether abnormalities arising in either context contribute causally to the development or progression of dystrophin-associated cardiomyopathy, rather than representing secondary manifestations of dystrophin deficiency, therefore remains an important challenge.

ACKNOWLEDGEMENTS

I must say that I feel blessed by so many wonderful people who have guided me through my life and professional endeavors. The list would be far too long if I were to name everyone who has helped me reach this milestone.

First and foremost, I must thank my family and those closest to me, especially my children, Adam and Adéla, and their mother, Dáša, for their patience, forgiveness, and understanding when I was more a piece of laboratory inventory than a husband and father at home. I also thank my partner, Kamila, for her deep understanding and support, and simply for showing me the colors I cannot see myself.

In my professional life, I feel particularly indebted to my students and the lab members who have wandered through my lab. The least I can do is to list their names here, alphabetically rather than in any particular order: Aneta Kohutova, Anton Salykin, Debbie Beckerová, Dita Munzová, Ivana Acimovic, Jan Raška, Lukáš Bálek, Martin Pešl, Mirek Vařecha, Miriama Krutá, Monika Šeneklová, Petr Fojtík, Renata Hejnová, Šárka Jelínková, Tereza Juráková, and Tereza Váňová.

I must also express my gratitude to my colleagues and collaborators Albano Meli, Christi A. Walter, Guido Caluori, Michaela Kunová, Jan Vrbský, and Jana Gregorová for their support in many aspects of my work. For setting me on the path towards becoming an independent scientist, I owe my thanks to Prof. Ing. Petr Dvořák, CSc., Doc. MVDr. Aleš Hampl, CSc., Christi A. Walter, PhD, Patrick Sung, PhD, and Prof. RNDr. Břetislav Brzobohatý, CSc.

TABLE OF CONTENTS

The Cardiomyocyte Is Not the Whole Story Developmental and Cellular Perspectives on Dystrophin-Associated Cardiomyopathy 1
ORIGINALITY AND CONFLICT OF INTEREST DECLARATION 3
ABSTRACT 4
ACKNOWLEDGEMENTS 5
TABLE OF CONTENTS 6
LIST OF FIGURES 8
GLOSSARY 9
1. INTRODUCTION 11
1.1. Central hypothesis 13
2. THEORETICAL BACKGROUND 13
2.1. Dystrophinopathies and cardiac disease 13
2.2. Experimental access to the early stages of dystrophin-associated cardiac pathology 17
2.3. Dystrophin deficiency and stem/progenitor-cell fate 20
2.4. From stem-cell damage to altered cardiovascular lineage formation 22
2.5. The adult heart as a multicellular homeostatic niche 25
2.6. Integrated model and unresolved questions 29
3. COMMENTARY TO PUBLISHED WORK 32
3.1. Commentary to published work – Annex 1 32
3.2. Commentary to published work – Annex 2 33
3.3. Commentary to published work – Annex 3 34
3.4. Commentary to published work – Annex 4 36
3.5. Commentary to published work – Annex 5 37
3.6. Commentary to published work – Annex 6 38
3.7. Commentary to published work – Annex 7 39
4. CONCLUSIONS 41
5. BIBLIOGRAPHY 42
6. SUPPLEMENT MATERIAL 50
6.1. Annex 1 50
6.2. Annex 2 56
6.3. Annex 3 64
6.4. Annex 4 84
6.5. Annex 5 107

6.6. Annex 6 126
6.7. Annex 7 135

LIST OF FIGURES

Figure 1. Developmental axis of human cardiomyocyte differentiation from hPSCs and potential effects of dystrophin deficiency.

Figure 2: Lineage contributions and paracrine functions of proposed resident cardiac stem/progenitor populations in the postnatal/adult heart.

Figure 3. Potential role of resident cardiac progenitor-like cells in dystrophin-deficient myocardium and contribution to disease progression.

GLOSSARY

AFM	Atomic force microscopy
AKT	Protein kinase B (AKT)
BMD	Becker muscular dystrophy
BMP	Bone morphogenetic protein
CM	Cardiomyocyte
CMR	Cardiac magnetic resonance
CRISPR/Cas9	Clustered regularly interspaced short palindromic repeats/CRISPR-associated protein 9
CVPCs	Cardiovascular progenitor cells
DDR	DNA damage response
DGC	Dystrophin-associated glycoprotein complex
DMD	Duchenne muscular dystrophy
Dp412e	Embryonic dystrophin isoform Dp412e
Dp427	Full-length dystrophin isoform
Dp427m	Full-length muscle dystrophin isoform
DSB	DNA double-strand break
EGFR	Epidermal growth factor receptor
EPDCs	Epicardium-derived cells
hESC	Human embryonic stem cell
hiPSC	Human induced pluripotent stem cell
hPSC	Human pluripotent stem cell
KDR	Kinase insert domain receptor (VEGFR2)
LGE	Late gadolinium enhancement
MAPK	Mitogen-activated protein kinase
MEA	Microelectrode array
MESP1	Mesoderm posterior bHLH transcription factor 1
nNOS	Neuronal nitric oxide synthase
NO	Nitric oxide
NOS	Nitric oxide synthase
NOX2	NADPH oxidase 2
NOX4	NADPH oxidase 4
PDGFRα	Platelet-derived growth factor receptor alpha
PI3K	Phosphoinositide 3-kinase
PTEN	Phosphatase and tensin homolog
RNS	Reactive nitrogen species
ROS	Reactive oxygen species
RyR2	Ryanodine receptor 2
SP	Side population
SR	Sarcoplasmic reticulum
WT	Wild type
WNT	Wingless/Integrated (WNT) signaling pathway

"The colors are always there, you just can't see them."
— David K., *Prism: Shedding Light on Life with Duchenne*

In *Prism*, David K. recalls the prisms hanging in the kitchen window of his childhood home and his fascination with discovering that apparently ordinary light contained colours invisible until the prism separated them. Living with Duchenne muscular dystrophy, he later returned to this image as a metaphor for the difference between what disability looks like from the outside and the considerably richer reality of the life within it.

Years ago, rarity was raised as one consideration against prioritizing a grant proposal in which we sought to study Duchenne muscular dystrophy. The argument stayed with me—not because rarity is irrelevant when limited research resources must be distributed, but because prevalence describes the frequency of a disease remarkably well and the experience of having it remarkably poorly. A number necessarily reduces complexity. Behind every number is an individual whose life extends far beyond the diagnosis by which that individual entered the statistic.

Perhaps Duchenne muscular dystrophy itself needs to be viewed through a prism. What first meets the eye is skeletal muscle: its progressive weakening gives the disease its name, its characteristic phenotype and much of its clinical identity. Yet this is only one part of the spectrum cast by dystrophin deficiency. Less immediately visible, but no less consequential, is the progressive involvement of the heart. Yet even the failing heart reveals only the visible endpoint of a process whose beginnings may lie much deeper—in cellular changes that precede overt myocardial disease by years.

This thesis is concerned with looking beneath that visible endpoint.

1. INTRODUCTION

Duchenne muscular dystrophy (DMD) is a severe, progressive X-linked neuromuscular disorder caused by pathogenic variants in the *DMD* gene, resulting in the absence or profound deficiency of functional dystrophin (Duan et al., 2021). Although DMD has historically been regarded predominantly as a disease of skeletal muscle, improved respiratory and multidisciplinary care and the resulting prolongation of survival have increasingly exposed cardiac involvement as a major determinant of morbidity and mortality (Jung et al., 2013; Landfeldt et al., 2024). DMD predominantly affects males. Estimates of its frequency vary according to population and methodology; a systematic review and meta-analysis estimated a global birth prevalence of 19.8 per 100,000 live male births—approximately 1 in 5,000—while demonstrating substantial heterogeneity between studies (Crisafulli et al., 2020).

The *DMD* gene is located at Xp21.2, spans approximately 2.4 Mb, and comprises 79 exons (Koenig et al., 1988). Multiple tissue-specific promoters and alternative splicing give rise to several full-length and shorter dystrophin isoforms with distinct patterns of tissue and developmental expression (Gao and McNally, 2015). The full-length muscle isoform Dp427m is predominantly expressed in skeletal and cardiac muscle, where dystrophin forms a central component of the dystrophin-associated glycoprotein complex (DGC) (Hoffman et al., 1987; Gao and McNally, 2015). Through its interactions with cytoskeletal F-actin and components of the DGC, dystrophin participates in a molecular complex linking the intracellular cytoskeleton to laminin in the extracellular matrix, thereby contributing to sarcolemmal stability during muscle contraction (Ervasti and Campbell, 1993).

The function of the dystrophin-associated complex is not exclusively structural; it also provides a molecular platform for proteins involved in intracellular signaling. Of particular relevance, neuronal nitric oxide synthase (nNOS) associates with the dystrophin complex at the sarcolemma, and dystrophin deficiency results in marked loss of sarcolemmal nNOS protein and activity in DMD muscle (Brenman et al., 1995). Thus, the consequences of dystrophin deficiency extend beyond mechanical destabilization of the sarcolemma and include disruption of NO-dependent signaling. This signaling function of the dystrophin complex is particularly relevant to the work presented in this thesis and will be considered further in the context of NOS-dependent oxidative stress and cellular pathology.

The mutational spectrum of the *DMD* gene is highly heterogeneous. Large exon deletions account for approximately two thirds of pathogenic variants, followed by exon duplications and smaller sequence variants, including nonsense variants, small insertions or deletions, and splice-altering variants, whereas pathogenic missense variants are comparatively rare (Bladen et al., 2015). The molecular consequence of an individual variant depends not only on its genomic classification but also on its effect on pre-mRNA processing, preservation of the open reading frame, transcript stability, and ultimately the structure, stability and function of the resulting dystrophin protein. Variants disrupting the reading frame generally result in premature translation termination and little or no functional dystrophin, whereas in-frame exon rearrangements may permit production of an internally altered dystrophin retaining partial function. This relationship forms the basis of the classical reading-frame rule, according to which out-of-frame variants are predominantly associated with DMD, whereas variants preserving the reading frame more frequently result in the generally milder Becker muscular dystrophy (BMD) phenotype; clinically important exceptions nevertheless occur (Monaco et al., 1988; Aartsma-Rus et al., 2006).

The first clinical manifestations of DMD usually become evident during early childhood. Progressive weakness predominantly affects proximal musculature and is accompanied by delayed motor development, difficulty running or climbing stairs, Gowers' sign, and progressive loss of motor function (Birnkrant et al., 2018). Repeated cycles of muscle damage, inflammation, and incomplete regeneration lead to progressive replacement of functional skeletal muscle by fibrotic and adipose tissue (Duan et al., 2021). As the disease progresses, affected individuals typically lose independent ambulation and develop respiratory muscle weakness, skeletal deformities, and additional systemic complications (Birnkrant et al., 2018). Improvements in corticosteroid treatment, respiratory support, orthopedic management, and multidisciplinary care have substantially changed the natural history of DMD and extended survival into adulthood (Birnkrant et al., 2018).

Cardiac involvement is a major manifestation of dystrophinopathies, although the molecular mechanisms linking *DMD* mutations to the development and progression of the cardiac phenotype remain incompletely understood. At the cardiomyocyte level, dystrophin deficiency or dysfunction is associated with sarcolemmal instability, disturbed Ca^{2+} homeostasis, and increased oxidative stress, which together contribute to progressive cellular dysfunction and injury (Williams and Allen, 2007a, 2007b; Jung et al., 2008; Meyers and Townsend, 2019). Progressive cardiomyocyte damage and loss are accompanied by myocardial remodeling and fibrotic replacement, ultimately contributing to ventricular dysfunction, arrhythmias, and heart failure (Meyers and Townsend, 2019).

Cardiac involvement becomes increasingly prevalent with age in DMD (Spurney et al., 2014). Progressive cardiac disease represents a major contributor to morbidity and mortality, particularly in older patients (Nigro et al., 1990). Importantly, structural myocardial changes may be detectable before deterioration of global cardiac function becomes evident. Cardiac magnetic resonance imaging (CMR), particularly late gadolinium enhancement (LGE), can identify myocardial fibrosis in patients with preserved left ventricular systolic function, demonstrating that myocardial remodeling may already be present during a clinically less apparent stage of cardiac disease (Puchalski et al., 2009; Panovský et al., 2019). The onset and subsequent progression of cardiac involvement nevertheless show substantial interindividual variability among patients with DMD (Landfeldt et al., 2024).

The progression of DMD-associated cardiomyopathy is highly heterogeneous, with considerable interindividual variability in the onset and severity of myocardial fibrosis, ventricular dysfunction, and arrhythmias. Although associations between specific *DMD* variants and cardiac outcomes have been reported, mutation type or position alone does not reliably predict the individual cardiac phenotype. Available evidence indicates that cardiac disease progression is influenced by multiple additional factors, including genetic modifiers and exposure to glucocorticoid and cardioprotective therapies, although the strength of evidence for individual predictors varies considerably (Landfeldt et al., 2024).

Current concepts of DMD-associated cardiomyopathy have predominantly centered on pathological processes occurring within dystrophin-deficient cardiomyocytes, and studies using patient-specific human pluripotent stem cell models have similarly focused largely on cardiomyocytes differentiated from these cells (Pioner et al., 2020b; Eisen and Binah, 2023). This cardiomyocyte-centered view has provided important insight into the mechanisms of DMD-associated cardiac dysfunction, but it does not necessarily establish the developmental stage at which the pathological process begins. The heart is a multicellular organ whose development, homeostasis, and response to injury depend on coordinated interactions among cardiomyocytes and multiple non-myocyte cell populations. These observations raise the broader question of whether dystrophin-associated cardiac pathology may involve cellular abnormalities beyond the differentiated cardiomyocyte, including both processes affecting stem/progenitor-cell fate and function and alterations of resident non-cardiomyocyte populations within the heart.

1.1. Central hypothesis

We hypothesize that dystrophin deficiency can alter the fate and function of stem/progenitor cells and lead to functional impairment or depletion of resident cardiac cell populations with stem/progenitor-like properties. We further propose that impairment or depletion of these resident cell populations may contribute to the development and/or progression of dystrophin-associated cardiomyopathy through disruption of their non-cardiomyogenic contributions to myocardial homeostasis.

Because the relevant cellular states and processes cannot all be examined within a single experimental system, different components of this hypothesis are investigated using complementary models. The causal and mechanistic relationships between these components remain to be established.

2. THEORETICAL BACKGROUND

2.1. Dystrophinopathies and cardiac disease

2.1.1. DMD gene and dystrophin

The DMD gene is located at Xp21.2 and, spanning approximately 2.4 Mb of genomic DNA, is among the largest genes in the human genome. Its 79 exons encode a full-length transcript of approximately 14 kb and the 427-kDa dystrophin protein (Dp427) (Koenig et al., 1988; Roberts et al., 1993). Expression of full-length dystrophin is controlled by tissue-specific promoters, giving rise to brain (Dp427B), muscle (Dp427M), and Purkinje-cell (Dp427P) isoforms. Multiple promoters, together with alternative splicing, generate a complex repertoire of tissue- and developmentally regulated dystrophin transcripts, including several shorter dystrophin products (Feener et al., 1989; Boyce et al., 1991; Lederfein et al., 1992; Byers et al., 1993; Lederfein et al., 1993; D'Souza et al., 1995; Lidov et al., 1995). Of particular relevance to the developmental perspective of this thesis, dystrophin expression is not restricted to differentiated muscle. The embryonic isoform Dp412e is transiently expressed during early differentiation of hPSCs and has also been detected in early human embryonic tissues (Massouridès et al., 2015). Although its function remains unresolved, this observation demonstrates that expression from the *DMD* locus occurs at developmental stages preceding terminal muscle differentiation.

Full-length dystrophin itself is a large cytoskeletal protein composed of an N-terminal actin-binding domain, an extended central rod domain containing spectrin-like repeats, a cysteine-rich domain, and a C-terminal region that interacts with components of the dystrophin-associated glycoprotein complex (DGC) (Koenig et al., 1988). Through these interactions, dystrophin contributes to the organization of a transmembrane molecular complex connecting the intracellular actin cytoskeleton to laminin in the extracellular matrix, thereby providing mechanical stabilization of the sarcolemma (Ervasti and Campbell, 1991; Ervasti and Campbell, 1993). The functional consequences of dystrophin deficiency, however, cannot be understood solely as loss of this mechanical linkage, because the DGC also serves as a platform organizing proteins involved in cellular signaling.

The best-characterized example of this signaling function comes from skeletal muscle, where neuronal nitric oxide synthase (nNOS) is associated in normal skeletal muscle with the sarcolemma through interactions involving dystrophin and syntrophin. Dystrophin deficiency in DMD results in pronounced loss of sarcolemmal nNOS, thereby disrupting the spatial organization of nitric oxide signaling (Brenman et al., 1995). α1-Syntrophin participates directly in recruitment of nNOS through PDZ-domain-mediated interactions (Brenman et al., 1996), but syntrophin alone is insufficient to account for its sarcolemmal localization: genetic disruption of α1-syntrophin causes loss of sarcolemmal nNOS without producing the muscle degeneration characteristic of dystrophin deficiency (Kameya et al., 1999). Moreover, spectrin-like repeats 16 and 17 within the dystrophin rod domain are specifically required for efficient sarcolemmal targeting of nNOS, demonstrating that dystrophin itself has a direct organizational role in this signaling complex (Lai et al., 2009). These observations establish dystrophin not only as a structural component of the muscle membrane but also as an organizer of spatially restricted signaling pathways, a distinction that becomes particularly relevant when considering the consequences of dystrophin deficiency for nitric oxide/redox homeostasis discussed later in this thesis.

2.1.2. Duchenne and Becker muscular dystrophy

Duchenne muscular dystrophy (DMD) and Becker muscular dystrophy (BMD) represent allelic dystrophinopathies caused by pathogenic variants in the *DMD* gene, but they differ substantially in the amount and functionality of dystrophin that can be produced. The classical molecular explanation for this difference is provided by the reading-frame rule. Mutations disrupting the translational reading frame generally result in premature termination and severe reduction or absence of functional dystrophin, leading to the DMD phenotype. In contrast, mutations that preserve the reading frame can permit synthesis of an internally altered dystrophin that retains sufficient function to produce the generally milder BMD phenotype (Monaco et al., 1988). This relationship is highly predictive but not absolute. Analysis of large dystrophinopathy cohorts has identified clinically relevant exceptions in both directions, reflecting effects of mutation type and location, altered splicing or translation, and disruption or preservation of functionally important dystrophin domains (Aartsma-Rus et al., 2006; Kesari et al., 2008; Juan-Mateu et al., 2015). In a cohort of 576 dystrophinopathy families, for example, the reading-frame rule was fulfilled in 90.4% of DMD and 82.4% of BMD cases, illustrating both its general validity and the limitations of predicting phenotype solely from the genomic reading frame (Juan-Mateu et al., 2015).

At the clinical level, DMD is generally associated with an earlier onset and more rapidly progressive skeletal-muscle phenotype, whereas BMD encompasses a considerably broader spectrum, ranging from substantial muscle weakness to mild or even subclinical skeletal-muscle

involvement. The distinction between DMD and BMD should therefore not be regarded as a simple binary consequence of the presence or absence of dystrophin, but rather as part of a phenotypic spectrum determined by the quantity, molecular structure and functional properties of the dystrophin products retained in individual patients. This distinction is particularly important when considering cardiac disease, because the severity of myocardial involvement does not necessarily parallel that of skeletal muscle. Longitudinal analysis of patients with BMD demonstrated progressive cardiac involvement and showed that severe cardiomyopathy can occur independently of the severity of skeletal-muscle disease (Nigro et al., 1995). Similarly, frequent myocardial abnormalities have been documented in patients with only mild or subclinical BMD skeletal-muscle manifestations, demonstrating that substantial cardiac disease may coexist with relatively preserved skeletal-muscle function (Melacini et al., 1996).

Cardiac involvement is therefore an important component of both DMD and BMD and may remain clinically inconspicuous during its earlier stages. In BMD, progressive myocardial disease can ultimately result in ventricular dysfunction and dilated cardiomyopathy, while cardiac magnetic resonance imaging has demonstrated myocardial abnormalities and fibrosis before advanced global ventricular dysfunction is apparent (Yilmaz et al., 2008). The relationship between *DMD* genotype and cardiac phenotype is itself complex: specific mutations and the dystrophin domains they affect can influence cardiac manifestations, but skeletal-muscle severity does not provide a reliable measure of the extent or progression of myocardial disease (Nigro et al., 1995; Melacini et al., 1996; Kaspar et al., 2009). Consequently, the biological effects of pathogenic *DMD* variants cannot be inferred simply from their overall effect on the skeletal-muscle phenotype. Differences in the amount, molecular composition and tissue-specific expression of residual dystrophin provide potential determinants of phenotypic variability, although their individual contributions to cardiac disease remain incompletely resolved.

From the perspective of this thesis, DMD and BMD therefore provide complementary manifestations of dystrophin-associated cardiac disease rather than entirely separate biological entities. DMD provides the principal disease context investigated here, whereas BMD offers an informative setting in which partial dystrophin expression may coexist with substantial cardiac pathology. The dissociation between skeletal-muscle and cardiac disease severity further emphasizes the need to investigate the myocardium directly rather than infer cardiac pathology from the systemic neuromuscular phenotype. This provides the basis for considering dystrophin-associated cardiomyopathy as a distinct component of the dystrophinopathy spectrum and for examining the cellular mechanisms through which dystrophin deficiency or dysfunction affects the heart.

2.1.3. Dystrophin-associated cardiomyopathy

Loss of dystrophin renders cardiomyocytes abnormally susceptible to mechanical stress and disrupts cellular processes involved in maintaining sarcolemmal and ionic homeostasis. Dystrophin-deficient cardiomyocytes show increased vulnerability to mechanical stress-induced contractile failure and membrane injury, providing a direct link between loss of the structural function of dystrophin and cardiomyocyte damage (Danialou et al., 2001). However, membrane instability alone does not adequately account for the cardiac phenotype. Experimental studies have identified abnormalities in intracellular Ca^{2+} handling and oxidative stress as closely interconnected mechanisms capable of amplifying the initial cellular disturbance. In *mdx* cardiomyocytes, increased activity of stretch-activated channels promotes abnormal Ca^{2+} entry and is enhanced by reactive oxygen species (ROS), establishing reciprocal interactions between

mechanical stress, Ca^{2+} dysregulation and ROS production (Jung et al., 2008). Increased NOX2 activity provides an additional source of pathological ROS production in the dystrophic heart, with downregulation of miR-448-3p associated with increased expression of the NOX2 regulatory subunit p47^phox^ and enhanced NOX2-derived ROS production (Kyrychenko et al., 2015a).

Abnormal Ca^{2+} handling also involves intracellular Ca^{2+} stores and several components of cardiomyocyte excitation–contraction coupling. In *mdx* hearts, S-nitrosylation of the cardiac ryanodine receptor (RyR2), accompanied by depletion of the channel-stabilizing protein calstabin2 (FKBP12.6), increases diastolic Ca^{2+} leak from the sarcoplasmic reticulum and contributes to ventricular arrhythmogenesis (Fauconnier et al., 2010). Alterations are not restricted to RyR2. Voltage-gated ion-channel dysfunction, including changes affecting NaV1.5 and L-type Ca^{2+} currents, has been demonstrated in dystrophin-deficient cardiomyocytes, with some electrophysiological abnormalities detectable before the development of overt cardiomyopathy in *mdx* mice (Koenig et al., 2011; Koenig et al., 2014). Importantly, Ca^{2+} dysregulation, oxidative stress and mitochondrial dysfunction should not be regarded as independent pathways. Progressive mitochondrial oxidation, structural damage, increased mitochondrial Ca^{2+} sequestration and membrane depolarization have been demonstrated in *mdx* cardiomyocytes, with mitochondrial dysfunction associated with oxidative stress and cellular Ca^{2+} overload (Kyrychenko et al., 2015b). Thus, mechanical instability, abnormal Ca^{2+} handling, redox imbalance and mitochondrial dysfunction form interacting rather than strictly sequential components of dystrophin-deficient cardiomyocyte pathology.

Persistent Ca^{2+} and redox disturbances, mitochondrial dysfunction and repeated mechanical stress ultimately contribute to cardiomyocyte injury and loss. Progressive loss of functional myocardium is accompanied by inflammatory and reparative responses and by increasing extracellular-matrix deposition, resulting in the characteristic myocardial fibrosis of dystrophin-associated cardiomyopathy. With disease progression, replacement of functional myocardium by fibrotic tissue and continued cardiomyocyte dysfunction contribute to adverse ventricular remodeling, impaired contractile function and ultimately dilated cardiomyopathy (Kamdar and Garry, 2016; Meyers and Townsend, 2019).

Importantly, detectable cellular and functional abnormalities can precede advanced myocardial remodeling. Ion-channel dysfunction has been demonstrated before overt cardiomyopathy in dystrophin-deficient mice (Koenig et al., 2011), while abnormalities of cardiac function can be detected in patients before the development of established dilated cardiomyopathy (Markham et al., 2006). Together with the early myocardial fibrosis detectable by cardiac magnetic resonance discussed above, these observations indicate that dystrophin-associated cardiomyopathy develops through a prolonged phase preceding overt ventricular dysfunction, during which molecular, cellular and tissue abnormalities progressively accumulate. Although the conventional model provides a compelling explanation for the progressive dysfunction, injury and loss of dystrophin-deficient cardiomyocytes, it remains predominantly cardiomyocyte-centered. It therefore does not fully resolve when the pathological trajectory begins, or whether abnormalities arising in other cardiac cell populations—or at earlier developmental or progenitor-cell stages—may contribute to the subsequent development of cardiomyopathy.

Our contribution to the field

Our work approached dystrophin-associated cardiac pathology using complementary human *in vitro*, animal and human myocardial models, with particular emphasis on whether disease-

associated abnormalities extend beyond differentiated cardiomyocytes. We established patient-specific DMD hiPSC lines and demonstrated that hPSC-derived DMD cardiac cells reproduce functional abnormalities associated with dystrophic cardiomyopathy, thereby providing a human experimental system in which early disease mechanisms could be investigated (Jelinkova et al., 2019a; Jelinkova et al., 2020). Importantly, our studies identified abnormalities already at the pluripotent stem-cell level, where dystrophin deficiency was associated with NOS-dependent oxidative stress and compromised genomic stability (Jelinkova et al., 2019b). Extending the investigation to native myocardium, we subsequently identified reduced abundance and impaired properties of c-kit^+/CD45^− cardiovascular progenitor cells in human myocardium affected by Becker muscular dystrophy (Pesl et al., 2020) and demonstrated age-dependent changes in cardiovascular progenitor populations during progression of cardiac pathology in *mdx* mice (Jelinkova et al., 2021). Collectively, these studies support consideration of dystrophin-associated cardiomyopathy not exclusively as a consequence of progressive dysfunction of differentiated cardiomyocytes, but as a disease process in which abnormalities of stem/progenitor-cell populations may also contribute to disturbed cardiac tissue homeostasis.

2.2. Experimental access to the early stages of dystrophin-associated cardiac pathology

2.2.1. Complementary experimental models

Clinical investigation of dystrophin-associated cardiomyopathy provides increasingly sensitive means of detecting and following cardiac involvement. Echocardiography allows longitudinal assessment of ventricular structure and function, whereas cardiac magnetic resonance imaging provides additional tissue characterization and can detect myocardial fibrosis before overt systolic dysfunction becomes apparent in patients with DMD (Puchalski et al., 2009). Electrocardiographic and ambulatory rhythm monitoring further reveal conduction and rhythm abnormalities associated with dystrophin-deficient hearts (Perloff, 1984; McNally et al., 2015). These approaches are indispensable for defining the clinical phenotype and its progression, but they interrogate predominantly organ- and tissue-level manifestations of disease and provide limited direct access to the cellular and molecular events from which these manifestations arise. Consequently, identification of early disease mechanisms requires experimental access to cardiac cells and tissues at stages preceding advanced myocardial remodeling.

Human myocardial tissue provides more direct access to cellular and molecular pathology, but with substantial practical and interpretative limitations. Endomyocardial biopsy permits histological and molecular analysis of living myocardium, yet samples only a small fraction of the heart and is restricted to defined clinical indications (Cooper et al., 2007). Explanted and post-mortem hearts provide more extensive material but predominantly represent advanced or end-stage disease, after extensive myocardial remodeling has already occurred. Such material can therefore establish that an abnormality is present in the diseased human heart, but generally cannot determine when it arose or whether it contributed to disease development or emerged secondarily during disease progression.

Animal models provide access to this temporal dimension because genetically defined disease can be examined within the intact myocardium at successive stages of disease progression. The most widely used murine model of DMD, the *mdx* mouse, carries a nonsense mutation in exon 23 of *Dmd* resulting in loss of full-length dystrophin (Sicinski et al., 1989). Its phenotype nevertheless differs substantially from human DMD, with comparatively mild skeletal-muscle disease and a

cardiac phenotype that develops relatively late (Quinlan et al., 2004). These differences limit direct extrapolation of disease kinetics and severity, but the progressive cardiac phenotype makes the *mdx* model particularly useful for examining age-dependent changes within the native dystrophin-deficient myocardium. Indeed, cellular abnormalities can be detected before overt cardiomyopathy develops in *mdx* mice (Koenig et al., 2011). Importantly, however, cardiac stem/progenitor-cell biology cannot be assumed to translate directly between experimental models or species. Even within the mouse heart, lineage-tracing experiments have shown that endogenous c-kit$^+$ cells contribute only extremely rarely to cardiomyocyte formation and predominantly generate endothelial cells (van Berlo et al., 2014). Thus, the *mdx* model provides temporal access to cellular changes within native dystrophin-deficient myocardium, but cannot by itself establish how corresponding cellular states behave in the human system.

Human pluripotent stem-cell models provide access to a different biological dimension. Human somatic cells can be reprogrammed to pluripotency while retaining their donor-specific genetic background (Takahashi et al., 2007), and patient-specific iPSCs can subsequently be differentiated into cardiomyocytes that reproduce genetically determined cardiac phenotypes *in vitro* (Moretti et al., 2010). Importantly for the question developed in this thesis, pluripotent cells also provide experimental access to successive stages of differentiation, allowing disease-associated abnormalities to be investigated before as well as after acquisition of the differentiated cardiomyocyte phenotype. Their interpretation nevertheless requires caution, because hPSC-derived cardiomyocytes retain important structural, electrophysiological and metabolic features of immature rather than adult cardiomyocytes (Veerman et al., 2015). Human myocardial tissue, longitudinal animal models and hPSC-based systems therefore provide different and non-interchangeable experimental windows: human myocardium establishes relevance to the diseased human heart, the *mdx* model provides temporal access to pathology within the native dystrophin-deficient myocardium, and hPSCs permit investigation of human cellular phenotypes across developmental and differentiation states.

2.2.2. From pluripotent stem cells to functional cardiac models

Differentiation of hPSCs toward the cardiac lineage is not simply a means of producing cardiomyocytes, but an *in vitro* process that reproduces key principles of early human cardiac development. Pluripotent cells progressively acquire mesodermal and cardiovascular identities before generating differentiated cardiac cell types, with cell-fate transitions influenced by the timing and combination of developmental signaling cues (Yang et al., 2008; Lian et al., 2012). Similarly to early embryonic cardiogenesis, cardiac differentiation of hPSCs is governed by temporally coordinated developmental signals; for example, canonical WNT/β-catenin signaling promotes early mesoderm induction, whereas its subsequent inhibition favors cardiac specification (Lian et al., 2012). Thus, cardiac differentiation provides not only a source of cardiac cells but also an experimentally accessible developmental trajectory during which disease-associated abnormalities may arise before the differentiated cardiac phenotype becomes apparent.

Three-dimensional differentiation systems permit the development of multicellular, spontaneously contracting cardiac preparations that can be functionally investigated *in vitro* (Schaaf et al., 2011; Mannhardt et al., 2016). For consistency, such preparations are referred to throughout this thesis as **3D hPSC-derived cardiac models**, with distinctions between individual model types considered separately in the corresponding Concept Box. Three-dimensional hPSC-

derived cardiac models allow integrated cardiac properties, including contractile behavior and responses to physiological and pharmacological stimulation, to be examined experimentally (Schaaf et al., 2011; Mannhardt et al., 2016). Functional analysis of these models therefore provides a means of determining whether abnormalities arising during differentiation are accompanied by a disease-relevant cardiac phenotype.

The principal cellular abnormalities associated with dystrophin-deficient myocardium have been discussed in Section 2.1.3 and include disturbed Ca^{2+} homeostasis, electrophysiological abnormalities, oxidative and mitochondrial dysfunction, and impaired contractile function. A biologically informative hPSC-derived cardiac model should therefore reproduce at least a subset of these interconnected phenotypes. The relevant question is not whether such a model reproduces the complete clinical cardiomyopathy, but whether dystrophin deficiency generates cardiac cellular phenotypes corresponding to abnormalities observed in the dystrophic heart.

Several independent groups have successfully recapitulated key cellular features of dystrophin-deficient myocardium using hiPSC-derived cardiomyocytes. Early studies demonstrated elevated resting cytosolic Ca^{2+}, mitochondrial damage and increased apoptosis, with membrane stabilization reducing Ca^{2+} overload and apoptotic signaling (Lin et al., 2015). Subsequent studies identified electrophysiological abnormalities, including irregular automaticity, prolonged action-potential duration and altered ion currents (Eisen et al., 2019), as well as impaired structural maturation and contractile function in patient-derived and genetically engineered dystrophin-deficient cardiomyocytes (Pioner et al., 2020a). Abnormal Ca^{2+} handling and arrhythmic activity have also been demonstrated across patient-derived and isogenic dystrophin-deficient hiPSC lines, including increased susceptibility to arrhythmic Ca^{2+} transients during β-adrenergic stimulation (Kamdar et al., 2020). Oxidative and mitochondrial abnormalities were subsequently confirmed in DMD hiPSC-derived cardiomyocytes, where increased ROS production was associated with mitochondrial depolarization and increased NOX4 expression; correction of the *DMD* mutation restored ROS levels, while suppression of NOX4-dependent oxidative stress improved the cellular phenotype (Duelen et al., 2022). More recent three-dimensional models have extended these observations beyond isolated cardiomyocyte phenotypes. Isogenic dystrophin-deficient engineered cardiac tissues reproduced reduced contractile force, abnormal contraction and relaxation kinetics, elevated resting Ca^{2+} and impaired Ca^{2+} cycling (Bremner et al., 2022), while long-term culture of patient-derived DMD cardiac organoids revealed progressive cardiomyocyte deterioration together with fibrosis and aberrant adipogenesis compared with mutation-corrected isogenic controls (Marini et al., 2022). Together, these studies demonstrate that hiPSC-derived cardiac models reproduce multiple interconnected components of dystrophin-deficient cardiac pathology across different genetic backgrounds and experimental platforms, with more complex 3D systems additionally providing access to aspects of progressive tissue remodeling.

Our contribution to the field

Our work established patient-specific pluripotent stem-cell models for investigating dystrophin-associated cardiac pathology. We generated and characterized hiPSC lines from two independent patients with DMD, providing renewable human pluripotent cell models that retained the respective patient-specific *DMD mutations and lacked full-length dystrophin expression (Jelinkova et al., 2019a). These patient-specific* hPSC lines, together with a CRISPR/Cas9-generated dystrophin-deficient hESC line, were subsequently differentiated

toward the cardiac lineage. The resulting dystrophin-deficient hPSC-derived cardiac cells recapitulated several functional abnormalities associated with dystrophin-deficient cardiac pathology, including altered electrophysiological properties, abnormal Ca^{2+} handling, hypocontractility and a blunted β-adrenergic response (Jelinkova et al., 2020). Importantly, however, dystrophin deficiency affected not only the functional phenotype of the resulting cardiac cells but also the efficiency of cardiac differentiation, which was reduced across the dystrophin-deficient hPSC models (Jelinkova et al., 2020). This observation raised the possibility that the consequences of dystrophin deficiency may arise before acquisition of the differentiated cardiomyocyte phenotype and may influence processes occurring during cardiac lineage formation.

2.3. Dystrophin deficiency and stem/progenitor-cell fate

Although the pathological consequences of dystrophin deficiency have traditionally been attributed predominantly to dysfunction and progressive loss of differentiated muscle cells, increasing evidence indicates that dystrophin deficiency also affects stem and progenitor cell populations. This concept was established most clearly in skeletal muscle, where dystrophin was shown to be expressed in activated satellite cells and to participate directly in the establishment of cell polarity and asymmetric division (Dumont et al., 2015). Subsequent studies extended these observations beyond a defect in asymmetric division, demonstrating abnormalities in progenitor commitment, self-renewal and differentiation, as well as in signaling and cellular homeostatic processes that regulate these transitions (Chang et al., 2018; Wang et al., 2019; Granet et al., 2025). Importantly, involvement of the stem/progenitor compartment cannot be equated simply with its numerical depletion. Depending on disease stage and experimental context, dystrophic progenitor populations may undergo initial expansion followed by decline, or remain numerically preserved despite impaired regenerative function (Jiang et al., 2014; Ribeiro et al., 2019). Altered cell fate and function, rather than depletion per se, therefore provide a broader framework for considering the involvement of stem/progenitor populations in DMD pathology.

Evidence that such abnormalities may extend beyond the skeletal-muscle satellite-cell compartment remains more limited. Cardiac progenitor cells isolated from GRMD dogs were reported to exhibit impaired self-renewal and cardiac differentiation, together with earlier senescence and impaired proliferation, providing early evidence that dystrophin-associated progenitor-cell dysfunction may also occur in the heart (Cassano et al., 2012). In parallel, studies using human pluripotent stem-cell models of skeletal myogenesis have shifted the temporal boundary of DMD-associated abnormalities toward earlier developmental stages. Multi-omic analysis identified extensive molecular dysregulation beginning at the somite stage, before activation of the skeletal-muscle program and before upregulation of Dp427m (Mournetas et al., 2021). These observations raise the broader possibility that dystrophin deficiency can influence cell-state transitions at both developmental and tissue-resident progenitor stages, rather than exerting its pathological consequences only after formation of differentiated muscle cells.

The mechanisms through which dystrophin deficiency may alter stem/progenitor-cell fate are likely to be multiple and interconnected rather than attributable to a single pathway. Within this complex network, two complementary conceptual axes appear particularly relevant to the present discussion. The first links loss of dystrophin to altered cell polarity and organization of stem-cell division, thereby affecting the balance between self-renewal and generation of

committed progenitors. The second encompasses alterations in intracellular signaling and redox-metabolic and cellular homeostasis that modify proliferation, survival, commitment and differentiation. These axes are not mechanistically independent: signaling and metabolic state influence polarity and division, while cell organization itself determines the spatial context in which signaling pathways operate. They provide, however, a useful framework for considering how the consequences of dystrophin deficiency may converge on a common biological outcome—altered stem/progenitor-cell fate.

2.3.1. Dystrophin, cell polarity and stem/progenitor-cell fate

Dystrophin participates directly in the regulation of satellite stem-cell polarity and asymmetric division. In activated satellite cells, dystrophin becomes asymmetrically localized and interacts with the polarity regulator MARK2; its absence disrupts MARK2 expression, PARD3 localization and mitotic-spindle orientation, resulting in reduced asymmetric division and reduced generation of committed myogenic progenitors, thereby disturbing the balance between stem-cell maintenance and lineage commitment (Dumont et al., 2015). The consequences extend to molecular specification of daughter-cell fate. The dystrophin-associated glycoprotein complex organizes β1-syntrophin/p38γ signaling required for CARM1-dependent modification of PAX7 and activation of the myogenic determinant *Myf5*, thereby linking dystrophin-dependent cellular organization to epigenetic regulation of lineage commitment (Chang et al., 2018).

The functional importance of this polarity–fate axis is supported by restoration of asymmetric division in dystrophin-deficient satellite cells through EGFR–AURKA signaling. Increased asymmetric division enhanced generation of myogenic progenitors and improved muscle regeneration and strength in *mdx* mice (Wang et al., 2019). Thus, dystrophin deficiency can alter stem/progenitor-cell fate through disruption of cell polarity, division organization and lineage commitment, thereby extending the consequences of dystrophin deficiency beyond its canonical structural effects in differentiated muscle cells.

2.3.2. Redox homeostasis and stem/progenitor-cell fate

Cellular redox homeostasis is closely coupled to stem/progenitor-cell state and fate. In hPSCs, oxygen availability can influence the balance between pluripotency and differentiation, with hypoxia capable of reverting early committed cells toward a pluripotent state (Mathieu et al., 2013), illustrating the close interrelationship between environmental oxygen, metabolic state and cell fate. Reactive oxygen species (ROS) represent an important component of this regulatory environment.

One mechanism linking redox state to cell fate involves maintenance of genome integrity. In neural stem cells, oxidative mitochondrial DNA damage altered differentiation outcome, with impaired repair of oxidized DNA shifting differentiation toward an astrocytic lineage, whereas protection of mitochondrial DNA favored neurogenesis (Wang et al., 2011). Importantly, DNA damage is not exclusively a pathological consequence of oxidative stress. Redox-dependent oxidation of IGFBP2 in neural stem cells was shown to repress BRCA1-dependent DNA-repair programs and promote DNA double-strand breaks required for neuronal commitment (Shahin et al., 2023), suggesting that DNA damage can function as an instructive signal in the regulation of stem-cell fate.

ROS can also influence cell fate through modulation of intracellular signaling. Experimentally increased ROS promoted mesendodermal differentiation of hESCs and reduced expression of

pluripotency markers, while ROS scavenging attenuated this response; several fate-regulatory signaling pathways, including MAPK and AKT, were affected by ROS manipulation (Ji et al., 2010). In neural stem/progenitor cells, physiological ROS promoted proliferation and self-renewal through oxidation of PTEN and activation of PI3K/AKT signaling (Le Belle et al., 2011). In hPSCs, we further demonstrated that ROS regulate PI3K/AKT activity through redox-sensitive mechanisms involving PTEN and upstream PI3K signaling, while mild hypoxia attenuates AKT phosphorylation through suppression of ROS (Fojtík et al., 2021). Thus, PTEN–PI3K–AKT provides one experimentally defined example of a broader principle whereby ROS can modify signaling networks controlling stem/progenitor-cell behavior.

This framework is directly relevant to dystrophin deficiency. In dystrophin-deficient hPSCs, we identified dysregulated NOS activity, increased ROS production, DNA damage and compromised genomic stability (Jelinkova et al., 2019b). Pharmacological inhibition of NOS or ROS scavenging reduced DNA damage, while NOS inhibition also restored ROS levels toward those observed in control hPSCs, establishing a causal contribution of NOS-dependent ROS production to the DNA-damage phenotype. Together with the capacity of ROS to influence stem/progenitor-cell fate through genome integrity and redox-sensitive signaling, these findings provide a mechanistic framework through which dystrophin deficiency could alter cell fate already at the pluripotent or progenitor-cell stage.

Our contribution to the field

Our work identified redox homeostasis as a regulator of signaling in human pluripotent stem cells and subsequently linked its disturbance to dystrophin deficiency. In hPSCs, we demonstrated that ROS modulate PI3K/AKT signaling through redox-sensitive mechanisms involving PTEN and upstream PI3K regulation, providing a mechanistic link between the cellular redox environment and signaling pathways involved in maintenance of pluripotency and cell-fate regulation (Fojtík et al., 2021). In dystrophin-deficient hPSCs, we identified increased NOS-dependent ROS production accompanied by DNA damage and compromised genomic stability, with pharmacological inhibition of NOS and ROS scavenging reducing the DNA-damage phenotype (Jelinkova et al., 2019b). Together, these studies indicate that dystrophin deficiency can perturb redox-dependent cellular processes already at the pluripotent stem-cell stage and provide a mechanistic basis for considering altered redox homeostasis as one potential contributor to subsequent abnormalities of stem/progenitor-cell fate.

2.4. From stem-cell damage to altered cardiovascular lineage formation

2.4.1. Cardiovascular lineage specification and fate decisions during hPSC differentiation

Cardiac differentiation of hPSCs proceeds through transient mesodermal and progressively cardiac-specified states before the emergence of differentiated cardiovascular lineages. During hESC differentiation, a KDR^low^/C-KIT^−^ population with cardiomyocyte, endothelial and vascular smooth-muscle potential identified an early multipotent cardiovascular progenitor state (Yang et al., 2008). Subsequent studies showed that cardiac mesoderm arising from both hESCs and hiPSCs can be distinguished by co-expression of KDR and PDGFRα and that its specification is highly sensitive to the level and timing of developmental signals, including Activin/Nodal and BMP signaling (Kattman et al., 2011). Reporter-based studies further resolved the temporal progression of cardiac specification, with transient MESP1 expression preceding the emergence

of NKX2-5-expressing cardiac cells (Elliott et al., 2011; Den Hartogh et al., 2015). Importantly, these marker-defined populations should not be interpreted as a rigid sequence of discrete progenitor compartments: MESP1-expressing cells showed preferential cardiac differentiation but also generated endothelial and smooth-muscle derivatives, while their surface-marker profile did not completely overlap with previously defined KDR^+/PDGFRα^+ cardiac mesoderm (Den Hartogh et al., 2015).

Progression through these developmental states is highly dependent on the timing and magnitude of extracellular signaling cues. Canonical WNT/β-catenin signaling provides a particularly clear example of this stage dependence. Activation of WNT/β-catenin signaling during early differentiation promotes mesoderm formation, whereas subsequent inhibition of the pathway after mesoderm induction promotes cardiomyocyte differentiation (Paige et al., 2010; Lian et al., 2012). Similarly, the efficiency of cardiac mesoderm specification depends on the levels of Activin/Nodal and BMP signaling, with optimal conditions varying between individual hPSC lines (Kattman et al., 2011). Thus, cardiac differentiation is a temporally regulated developmental process in which the consequences of a signaling input depend on the developmental state in which it occurs.

Lineage specification is not the sole determinant of cell fate during cardiac differentiation, because the proliferative and differentiation behavior of intermediate progenitor populations can also influence the number and relative abundance of their differentiated descendants. During hPSC cardiac differentiation, inhibition of EGFR signaling increased cardiac differentiation efficiency by promoting proliferation of NKX2-5-expressing cardiac progenitors while reducing proliferation of SOX2-expressing neural progenitors, demonstrating that differential expansion of progenitor populations can modify lineage output after cardiac mesoderm formation (Shim et al., 2016). Similarly, GREM2-dependent inhibition of canonical BMP signaling promoted proliferation of cardiac progenitors, whereas their subsequent differentiation required additional GREM2-dependent signaling through JNK, demonstrating that progenitor expansion and differentiation are distinct but coordinated processes (Bylund et al., 2017). Thus, the abundance of differentiated cardiac cells can be influenced not only by initial lineage specification but also by the proliferation and subsequent differentiation of intermediate progenitor populations.

Cellular stress and genome-surveillance pathways provide an additional mechanism through which disturbances arising before or during differentiation can influence these fate decisions. In hiPSCs, experimentally induced DNA damage during a defined window of definitive-endoderm differentiation activated a p53-dependent differentiation checkpoint that altered lineage progression without inducing apoptosis, demonstrating that the DNA-damage response can modify cell fate rather than acting solely through elimination of damaged cells (Eldridge et al., 2020). Although demonstrated outside the cardiac lineage, this principle is complemented by the marked stage-dependent sensitivity of cardiac differentiation to p53 activity. Pharmacological stabilization of p53 during early hiPSC cardiac differentiation induced cell-cycle arrest and apoptosis and markedly reduced subsequent cardiomyocyte formation, whereas later cardiac progenitor and cardiomyocyte stages were substantially less susceptible to the same perturbation (Brandt et al., 2021). In a separate hPSC cardiac-differentiation model, mTOR inhibition reduced mitochondrial ROS production, DNA-damage signaling and p53-dependent apoptosis during early differentiation and was associated with increased cardiomyocyte yield (Qiu et al., 2017). Together, these findings indicate that cellular stress and genome-surveillance responses acting during early developmental states can influence subsequent cardiac-cell output through effects on cell-cycle progression and survival, while evidence from other hPSC

differentiation systems demonstrates that DNA damage can also directly influence lineage choice.

2.4.2. Consequences of altered progenitor fate for cardiac model composition

The consequences of altered progenitor fate during cardiac differentiation extend beyond changes in the efficiency of cardiomyocyte generation, because the differentiation process gives rise to heterogeneous populations of cardiac and non-cardiac cells. Single-cell transcriptomic analysis of hPSC cardiac differentiation has identified coexisting cardiac progenitors, endothelial cells and endodermal populations at intermediate stages, followed by the emergence of cardiomyocytes together with non-contractile, fibroblast-like populations (Friedman et al., 2018). Subsequent single-cell studies have further demonstrated that directed cardiac differentiation generates multiple progenitor and differentiated cell states and that their relative abundance can vary substantially between hPSC lines (Churko et al., 2018; Elorbany et al., 2022). Thus, perturbations that alter the specification, expansion, survival or differentiation of intermediate progenitor populations have the potential to modify not only cardiomyocyte yield but also the cellular composition of the resulting cardiac model.

Evidence from skeletal myogenesis provides a disease-specific precedent that dystrophin deficiency can perturb developmental and stem/progenitor-cell trajectories before entry into the skeletal-muscle compartment. During skeletal differentiation of DMD hPSCs, mesoderm commitment was preserved, but extensive transcriptional dysregulation emerged at the somite stage, before expression of the skeletal-muscle program, indicating that disease-associated abnormalities can arise within intermediate developmental populations (Mournetas et al., 2021). Single-cell analysis subsequently resolved this phenomenon further, showing that dystrophin-deficient cells diverged from the normal myogenic trajectory at the somite stage and entered an alternative developmental branch associated with dysregulated cell-junction programs and altered epithelialization (Mozin et al., 2024). Complementary evidence from postnatal skeletal-muscle stem cells demonstrated a direct role of dystrophin in regulating satellite-cell polarity and asymmetric division: dystrophin deficiency disrupted MARK2/PARD3-dependent polarity, reduced asymmetric divisions and consequently impaired generation of myogenic progenitors (Dumont et al., 2015). Although developmental myogenic progenitors and postnatal satellite cells represent distinct cell populations, these findings collectively demonstrate that the consequences of dystrophin deficiency are not restricted to differentiated muscle cells and can include altered behavior and developmental progression of stem/progenitor populations.

Dystrophin isoform expression is itself developmentally regulated during cardiac differentiation, with induction of additional isoforms, including the muscle-specific Dp427m isoform, during progression of hPSCs toward the cardiac lineage (Dick et al., 2013). Nevertheless, whether dystrophin deficiency alters the specification or fate of cardiovascular progenitor populations during human cardiac differentiation remains insufficiently resolved. Most hPSC-based studies of DMD cardiomyopathy have focused on phenotypes of the differentiated cardiomyocytes, while comparatively little attention has been directed toward the developmental populations from which these cells arise. Consequently, it remains unclear whether abnormalities observed in DMD cardiac models reflect dysfunction manifesting in differentiated cardiomyocytes alone or may also incorporate alterations established during preceding stages of cardiovascular differentiation.

Our contribution to the field

Our work provided evidence that dystrophin deficiency can influence the outcome of human cardiac differentiation before analysis of the functional cardiomyocyte phenotype. Using multiple patient-derived DMD hiPSC lines together with a CRISPR/Cas9-engineered dystrophin-deficient hESC model, we observed a reduced proportion of spontaneously contracting cardiac aggregates compared with WT hPSCs (Jelinkova et al., 2020). The experimental design did not resolve the developmental stage at which this difference arose and therefore does not distinguish between altered cardiovascular specification, progenitor expansion or survival, subsequent differentiation, or the acquisition of functional properties required for spontaneous contraction. Nevertheless, in the context of the developmental mechanisms discussed above, the reduced generation of beating cardiac aggregates identifies the differentiation process itself as a potentially informative component of the DMD phenotype and raises the possibility that abnormalities preceding the differentiated cardiomyocyte state contribute to the subsequent phenotype of DMD cardiac models.

Figure 1. Developmental axis of human cardiomyocyte differentiation from hPSCs and potential effects of dystrophin deficiency

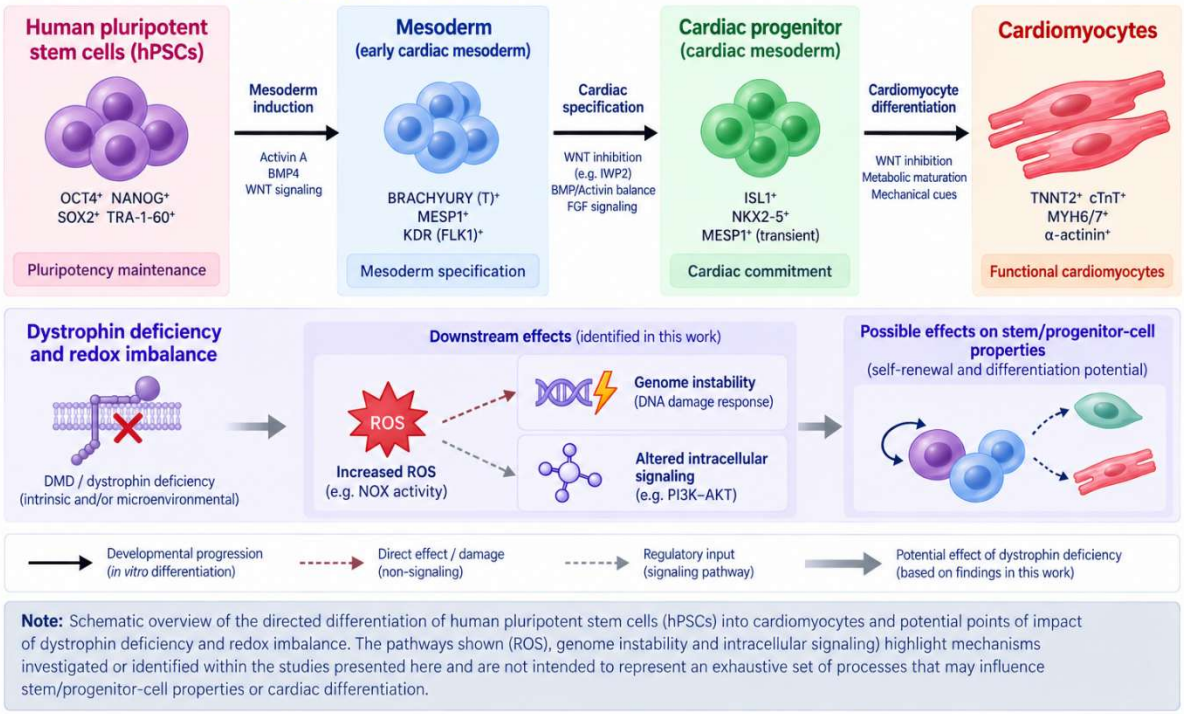

Note: Schematic overview of the directed differentiation of human pluripotent stem cells (hPSCs) into cardiomyocytes and potential points of impact of dystrophin deficiency and redox imbalance. The pathways shown (ROS), genome instability and intracellular signaling) highlight mechanisms investigated or identified within the studies presented here and are not intended to represent an exhaustive set of processes that may influence stem/progenitor-cell properties or cardiac differentiation.

2.5. The adult heart as a multicellular homeostatic niche

The developmental progenitor populations identified during *in vitro* cardiac differentiation should not be assumed to be equivalent to, or developmentally continuous with, resident cardiac cell populations with stem/progenitor-like properties detected in the postnatal myocardium. Nevertheless, observations in these distinct systems raise a related question: whether dystrophin deficiency can compromise stem/progenitor-cell states not only during

cardiovascular differentiation, but also within the cellular environment of the native heart. In the postnatal myocardium, where cardiomyocyte renewal is limited, the significance of resident stem/progenitor-like populations need not depend on their capacity to generate new cardiomyocytes. Rather, their potential contribution must be considered within the broader multicellular mechanisms that maintain myocardial homeostasis and regulate responses to injury. The following sections therefore examine resident cardiac stem/progenitor-like populations in the context of the myocardial cellular niche, their potential non-cardiomyogenic functions, and evidence that their abundance or functional state may be altered in dystrophin-deficient myocardium.

2.5.1. Adult cardiac cell populations and tissue homeostasis

The adult myocardium contains heterogeneous populations of non-cardiomyocytes that have been described as resident cardiac stem or progenitor cells on the basis of marker expression, isolation properties, clonogenicity or differentiation potential under experimental conditions (Santini et al., 2016). Several populations have consequently been proposed, including c-kit+ and Sca-1+ cells, cardiac side-population cells, Isl1+ progenitors, PDGFRα+ populations and epicardium-derived progenitor cells, which were identified using distinct molecular markers or experimental properties (Beltrami et al., 2003; Oh et al., 2003; Martin et al., 2004; Laugwitz et al., 2005; Smart et al., 2007; Chong et al., 2013). These populations were defined using different experimental criteria and show substantial phenotypic and functional heterogeneity, while the relationships between many of them and their physiological functions *in vivo* remain incompletely resolved (Santini et al., 2016). For this reason, the term resident cardiac cell populations with stem/progenitor-like properties is used here operationally to encompass cardiac-resident cell populations exhibiting one or more progenitor-associated properties, without implying bona fide stem-cell identity or a capacity for physiologically meaningful cardiomyocyte regeneration.

Despite the progenitor-associated properties attributed to these populations under experimental conditions, their contribution to cardiomyocyte formation in the adult heart appears to be very limited. Genetic lineage-tracing studies of Sca-1-expressing cells demonstrated predominantly vascular contributions, whereas their contribution to the cardiomyocyte population was extremely low during postnatal development, aging and following cardiac injury (Zhang et al., 2018; Vagnozzi et al., 2018). More broadly, lineage tracing of the non-cardiomyocyte compartment provided no evidence that resident non-myocytes constitute a quantitatively meaningful source of new cardiomyocytes during adult cardiac homeostasis or following myocardial infarction (Li et al., 2018). These observations distinguish progenitor-associated properties identified by marker expression or experimental manipulation from physiologically significant cardiomyogenic activity *in vivo*.

c-kit expression was initially used to identify a putative multipotent cardiac stem-cell population with cardiomyogenic, endothelial and smooth-muscle differentiation potential (Beltrami et al., 2003). Subsequent genetic lineage-tracing studies, however, demonstrated that endogenous c-kit+ cells contribute only minimally to cardiomyocyte formation, while substantially greater contributions were observed within endothelial lineages (van Berlo et al., 2014; Sultana et al., 2015). Moreover, lineage tracing using a *Kit*-CreER knock-in model indicated that at least part of the apparent cardiomyocyte contribution could arise from pre-existing Kit-expressing cardiomyocytes rather than differentiation of a resident progenitor population (Liu et al., 2016). Thus, c-kit expression should not itself be interpreted as evidence of bona fide cardiomyogenic stem-cell identity, while the biological significance of c-kit-expressing resident cardiac cells may extend beyond their capacity for direct cardiomyocyte generation.

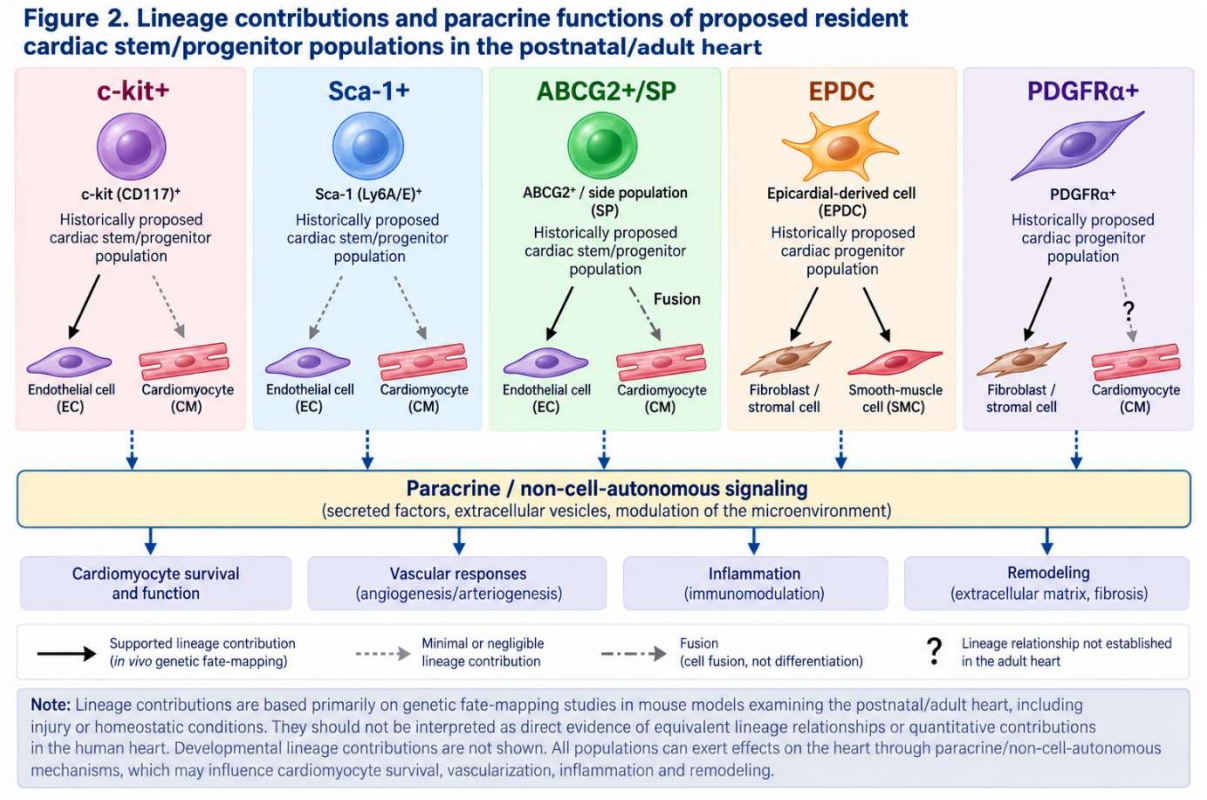

2.5.2. Non-cardiomyogenic functions in myocardial homeostasis and injury

The limited cardiomyogenic contribution of resident stem/progenitor-like populations does not exclude their participation in myocardial maintenance or responses to injury through non-cell-autonomous mechanisms. Studies of isolated human cardiac progenitor cells have demonstrated secretion of biologically active factors capable of influencing surrounding cardiac cells and the response of injured myocardium. Proteomic analysis of human cardiac progenitor cells identified a complex secretome containing factors associated with cell survival, angiogenesis and tissue repair, while administration of conditioned medium from neonatal cardiac progenitor cells improved cardiac function, neovascularization and myocardial remodeling after experimental myocardial infarction (Sharma et al., 2017). Extracellular vesicles provide an additional mechanism of intercellular signaling, as human cardiovascular-progenitor-derived vesicles reproduced cardioprotective effects of their parent cells, whereas inhibition of vesicle secretion reduced the beneficial effect of transplanted progenitor cells after myocardial infarction (El Harane et al., 2018). Together, these findings support non-cell-autonomous signaling as an important property of experimentally characterized cardiac stem/progenitor-like populations, independently of their capacity for direct cardiomyocyte generation.

The effects of these secreted signals extend across several cellular processes relevant to myocardial injury and remodeling. Conditioned medium from cardiac mesenchymal stromal cells protected hPSC-derived cardiomyocytes against oxidative and pharmacological injury, preserving mitochondrial membrane potential, reducing ROS accumulation and suppressing transcriptional programs associated with cell death (Constantinou et al., 2020). In parallel, cardiovascular-progenitor-derived extracellular vesicles have been shown to influence the inflammatory response to myocardial injury by modifying monocyte recruitment and promoting a reparative immune environment, thereby linking progenitor-cell signaling to regulation of post-

injury inflammation (Lima Correa et al., 2021). Together with the effects on neovascularization and myocardial remodeling observed following administration of cardiac-progenitor conditioned medium (Sharma et al., 2017), these findings indicate that cardiac stem/progenitor-like populations can influence cardiomyocyte survival, vascular responses, inflammation and tissue remodeling through signals acting on neighboring cell populations.

These experimental findings demonstrate the capacity of cardiac stem/progenitor-like populations to influence myocardial cells through non-cell-autonomous mechanisms, but they do not establish that isolated or culture-expanded populations reproduce the physiological functions of their endogenous counterparts *in vivo*. Their contribution to normal myocardial homeostasis therefore remains less clearly defined than their experimentally demonstrated effects in models of cardiac injury. Nevertheless, the ability of these populations and their secreted products to regulate cardiomyocyte survival, vascularization, inflammation and remodeling provides a mechanistic basis for considering changes in their abundance or functional state as potentially relevant to myocardial disease even in the absence of meaningful cardiomyocyte replacement. This possibility becomes particularly relevant when resident stem/progenitor-like populations themselves are altered in the diseased myocardium.

2.5.3. Alteration of resident stem/progenitor-like populations in dystrophin-deficient myocardium

Evidence from dystrophin-deficient animal models indicates that abnormalities of resident cardiac stem/progenitor-like populations can accompany myocardial disease. Cardiac progenitor cells isolated from golden retriever muscular dystrophy (GRMD) dogs showed impaired self-renewal and proliferation, earlier senescence and reduced cardiomyogenic differentiation compared with cells isolated from healthy animals, indicating that dystrophin deficiency is associated with functional impairment of cardiac progenitor-like cells (Cassano et al., 2012). In mdx mice, dystrophin-deficient myocardium exhibited expansion of a Sca-1+/PDGFRα+/CD31−/CD45− coronary adventitial population associated with increased collagen expression and TGF-β1-dependent perivascular fibrosis, linking altered behavior of resident non-cardiomyocyte populations to pathological myocardial remodeling (Ieronimakis et al., 2013). Together, these observations indicate that dystrophin-associated cardiac pathology is accompanied not only by cardiomyocyte abnormalities but also by changes in resident cell populations with progenitor or stromal properties.

Alterations have also been identified within the c-kit+/CD45− population of dystrophin-deficient myocardium. In an explanted heart from a patient with BMD-associated end-stage heart failure, the proportion of c-kit+/CD45− cells was markedly reduced compared with donor myocardium, accompanied by reduced ex vivo survival of c-kit+ cells and impaired tissue plasticity (Pesl et al., 2020). Because these observations were obtained from end-stage human myocardium, they could not determine whether the reduced abundance of c-kit+/CD45− cells preceded cardiac dysfunction or developed during disease progression. Analysis of mdx hearts across different ages subsequently revealed an initially increased c-kit+/CD45− population in young dystrophin-deficient animals followed by its rapid age-dependent decline, coinciding with the progressive development of cardiac dysfunction (Jelinkova et al., 2021). Cardiovascular progenitor cells isolated from mdx hearts also exhibited increased DNA damage compared with age-matched WT cells, indicating that altered population dynamics were accompanied by cellular abnormalities within the progenitor-like compartment (Jelinkova et al., 2021).

Collectively, these studies suggest that dystrophin deficiency is associated with changes in both the functional properties and population dynamics of resident cardiac stem/progenitor-like and stromal populations. Importantly, the available evidence does not establish whether these abnormalities represent a primary consequence of dystrophin deficiency, a secondary response to chronic myocardial injury, or a process that subsequently amplifies pathological remodeling. Nevertheless, in view of the non-cell-autonomous activities of cardiac stem/progenitor-like populations described above, their altered abundance or functional state provides a potential mechanism through which the non-cardiomyocyte compartment may contribute to the progression of dystrophin-associated cardiomyopathy.

Our contribution

Our work extended the evidence for involvement of resident cardiac stem/progenitor-like populations in dystrophin-associated cardiomyopathy from functional abnormalities of experimentally isolated cells to changes in their abundance and temporal dynamics within the diseased myocardium. Analysis of explanted myocardium from a patient with end-stage BMD-associated heart failure revealed a marked reduction of the c-kit+/CD45− population together with impaired ex vivo survival of c-kit+ cells and reduced tissue plasticity (Pesl et al., 2020). Because this observation represented an endpoint of advanced human disease, it could not resolve whether depletion of the resident population preceded cardiac dysfunction or developed as a consequence of progressive myocardial pathology. We therefore examined the c-kit+/CD45− population across disease progression in mdx mice and identified a dynamic trajectory characterized by an increased population at young age followed by rapid age-dependent decline coinciding with the development of cardiac dysfunction (Jelinkova et al., 2021). The increased DNA damage detected in mdx cardiovascular progenitor cells further indicated that population loss was accompanied by compromised cellular integrity, although a causal relationship between DNA damage and subsequent depletion was not established (Jelinkova et al., 2021). Together, these findings replaced a simple endpoint model of progenitor depletion with a dynamic model in which early expansion or recruitment of resident progenitor-like cells is followed by their progressive loss during dystrophin-associated cardiac disease. We propose that such altered population dynamics may reduce the capacity of the non-cardiomyocyte compartment to support myocardial homeostasis and thereby contribute to a self-reinforcing cycle of injury and pathological remodeling; however, whether progenitor-cell dysfunction is a driver, consequence or amplifier of dystrophin-associated cardiomyopathy remains to be determined.

2.6. Integrated model and unresolved questions

Dystrophin-associated cardiomyopathy has traditionally been interpreted primarily as a consequence of progressive dysfunction and loss of dystrophin-deficient cardiomyocytes. While cardiomyocyte-autonomous abnormalities clearly constitute a major component of the disease, evidence from independent studies together with our own findings, as discussed in the preceding sections, indicates that the cardiac consequences of dystrophin deficiency may extend beyond the differentiated cardiomyocyte. Abnormalities associated with dystrophin deficiency have been identified at the pluripotent stem-cell stage, during lineage differentiation and within resident non-cardiomyocyte populations of the dystrophin-deficient myocardium. These observations arise from biologically distinct experimental systems and do not establish

developmental continuity or a common causal mechanism between the affected cell populations. Rather, they support a broader view of dystrophin-associated cardiomyopathy as a temporally and cellularly distributed process in which abnormalities occurring at different stages and within different cellular compartments may collectively influence the development and progression of cardiac disease.

Within this broader framework, two conceptually distinct axes emerge from the evidence discussed above. Along the developmental axis, dystrophin deficiency is associated with altered redox homeostasis and genomic instability already at the pluripotent stem-cell stage, while the sensitivity of subsequent lineage decisions to cellular stress provides a mechanistic basis for considering whether these early abnormalities may influence cardiovascular specification, progenitor behavior or the outcome of cardiac differentiation. This developmental connection remains hypothetical, because the causal sequence linking pluripotent-cell abnormalities to altered cardiovascular progenitor fate has not yet been demonstrated. In the postnatal heart, a separate body of evidence indicates that dystrophin-associated disease is accompanied by altered abundance and functional properties of resident stem/progenitor-like and stromal populations. Given the capacity of such populations to influence cardiomyocyte survival, vascular responses, inflammation and tissue remodeling through non-cell-autonomous mechanisms, their dysfunction or progressive loss may modify the myocardial response to chronic injury without requiring direct cardiomyocyte replacement. Here too, however, it remains unresolved whether alterations of resident cell populations contribute causally to disease progression or arise primarily as a consequence of the dystrophic myocardial environment.

Several critical questions therefore remain unresolved. It is not yet known when during cardiovascular differentiation the consequences of dystrophin deficiency first become functionally relevant, whether altered specification, expansion, survival or differentiation of intermediate progenitor populations contributes to the cardiac phenotype, or to what extent abnormalities established before cardiomyocyte differentiation persist in or influence the resulting cardiac cells. In the postnatal myocardium, the mechanisms underlying the changing abundance and functional state of resident stem/progenitor-like populations remain similarly uncertain, as does the extent to which their alteration modifies rather than merely accompanies disease progression. Whether disturbed redox homeostasis and genome integrity represent mechanistic links between dystrophin deficiency and altered stem/progenitor-cell behavior across these distinct experimental and biological contexts also remains to be determined. Resolving these questions will require experimental approaches capable of distinguishing primary consequences of dystrophin deficiency from secondary responses to cellular and tissue injury and of determining when, and in which cellular compartments, potentially disease-modifying abnormalities arise. Taken together, the available evidence supports investigating dystrophin-associated cardiomyopathy not solely as the progressive failure of dystrophin-deficient cardiomyocytes, but as a multicellular and temporally distributed disease process in which cardiomyocyte-autonomous dysfunction may interact with abnormalities arising during cardiac differentiation and with altered homeostatic responses of the postnatal myocardium.

Figure 3. Potential role of resident cardiac progenitor-like cells in dystrophin-deficient myocardium and contribution to disease progression

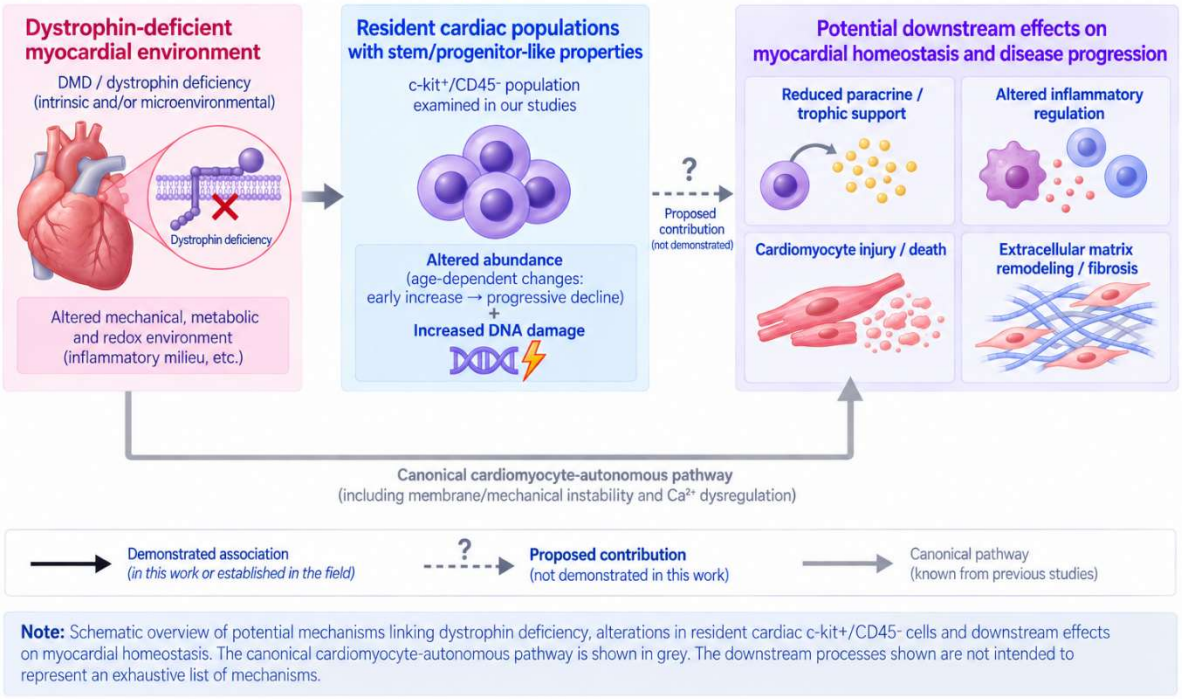

Note: Schematic overview of potential mechanisms linking dystrophin deficiency, alterations in resident cardiac c-kit+/CD45- cells and downstream effects on myocardial homeostasis. The canonical cardiomyocyte-autonomous pathway is shown in grey. The downstream processes shown are not intended to represent an exhaustive list of mechanisms.

3. COMMENTARY TO PUBLISHED WORK

3.1. Commentary to published work – Annex 1

Generation of two Duchenne muscular dystrophy patient-specific induced pluripotent stem cell lines DMD02 and DMD03 (MUNIi001-A and MUNIi003-A)

Original article published in Stem Cell Research, 2019, Q2, IF(2019): 4,489

Jelinkova S, Markova L, Pesl M, Valaskova I, Makaturova E, Jurikova L, Vondracek P, Lacampagne A, Dvorak P, Meli AC, ***Rotrekl V****

*- Corresponding author

Duchenne muscular dystrophy is a progressive X-linked disorder in which cardiac involvement represents a major component of disease morbidity and mortality. Investigation of dystrophin-associated cardiac pathology requires experimental models that retain the human disease-associated genetic background while providing access to cardiac cells that cannot readily be obtained from affected patients. Patient-specific human induced pluripotent stem cells provide such a system, because they retain the donor genotype and can subsequently be differentiated toward the cardiac lineage. The first step in establishing our experimental platform was therefore the generation and characterization of hiPSC lines derived from patients with DMD.

In this work, we generated two patient-specific hiPSC lines, DMD02 (MUNIi001-A) and DMD03 (MUNIi003-A), from two independent patients with DMD carrying deletions of exons 45–50 and 48–50 of the DMD gene, respectively. The resulting lines expressed pluripotency markers and retained the capacity to differentiate into derivatives of all three germ layers. Their identity and patient-specific DMD mutations were confirmed by STR analysis and MLPA, respectively, and both lines displayed a normal 46,XY karyotype. Together, these analyses established two independently derived, well-characterized patient-specific DMD hiPSC lines suitable for subsequent disease-modeling studies.

The generated hiPSC lines provided the experimental basis for subsequent investigation of dystrophin deficiency at both the pluripotent stem-cell stage and after differentiation into disease-relevant cell types. Their intended application included the study of abnormalities arising in DMD hiPSCs themselves as well as the characterization of phenotypes in subsequently derived cardiomyocytes and skeletal myotubes. This established a patient-specific human model in which the consequences associated with dystrophin deficiency could be investigated at the pluripotent stage and following differentiation while retaining the genetic background of the respective donor.

Within the research programme presented in this habilitation, the principal contribution of this work was the establishment and validation of a renewable patient-specific human DMD experimental platform. The availability of two independently derived DMD hiPSC lines subsequently enabled us to investigate disease-associated cellular abnormalities at the pluripotent stem-cell stage and to examine the phenotype of their differentiated cardiac derivatives. This experimental platform therefore provided the foundation for the subsequent studies of dystrophin deficiency discussed in the following annexes.

3.2. Commentary to published work – Annex 2

Non-invasive electromechanical cell-based biosensors for improved investigation of 3D cardiac models

Original article published in Biosensors and Bioelectronics, 2019, Q1, IF(2019): 10,257

Caluori G, Pribyl J, Pesl M, Jelinkova S, ***Rotrekl V****, Skladal P, Raiteri R*

Spontaneous contraction is a readily recognizable feature of hPSC-derived cardiac models, but its quantitative assessment is technically more demanding. Optical approaches can be used to derive contraction parameters from recorded movement, whereas direct measurement of the force generated by three-dimensional cardiac aggregates requires dedicated biomechanical methods. In our previous work, we addressed this limitation by coupling spontaneously beating hPSC-derived cardiac aggregates to an atomic-force-microscopy cantilever, establishing a micromechanical cell-based biosensor for direct and prolonged measurement of their contractile activity (Pesl et al., 2016). This approach provided quantitative information on the mechanical component of cardiac function, but did not simultaneously resolve the electrical events initiating contraction. The subsequent methodological objective was therefore to integrate mechanical and electrophysiological measurements within the same three-dimensional cardiac model, enabling direct analysis of cardiac excitation–contraction coupling.

To achieve this, we combined atomic force microscopy with microelectrode-array recording to obtain simultaneous and synchronized measurements of the mechanical and electrical activity of three-dimensional hPSC-derived cardiac models. The cardiac aggregates were positioned on the MEA sensing area, where extracellular field potentials were recorded, while an AFM cantilever simultaneously detected the displacement and force generated during contraction. Synchronization of the two signals enabled individual electrical events to be related directly to the corresponding mechanical contractions and allowed extraction of parameters describing beating frequency, contraction and relaxation kinetics, generated force and electromechanical delay. The resulting platform therefore provided an integrated quantitative assessment of cardiac excitation–contraction coupling within the same spontaneously contracting three-dimensional cardiac model.

The analytical capability of the platform was evaluated using physiological and pharmacological perturbations and subsequently applied to a patient-specific DMD cardiac model. Changes in extracellular Ca^{2+} concentration and pharmacological modulation with isoproterenol and verapamil demonstrated that the combined electromechanical measurements could resolve model- and treatment-dependent responses that were not uniformly captured by individual functional parameters. When applied to cardiac models derived from the DMD02 hiPSC line established in the preceding study, the platform revealed functional differences from WT cardiac models, including a distinct relationship between beating rate and generated force and differential responses to pharmacological stimulation. These experiments demonstrated that simultaneous electromechanical analysis could discriminate between hPSC-derived cardiac models and provided an initial demonstration of the platform in a patient-specific DMD cardiac model. The approach subsequently provided the methodological basis for a more comprehensive functional characterization of dystrophin-deficient cardiac models.

3.3. Commentary to published work – Annex 3

DMD Pluripotent Stem Cell Derived Cardiac Cells Recapitulate *in vitro* Human Cardiac Pathophysiology

Original article published in Frontiers in Bioengineering and Biotechnology, 2020, Q1, IF(2020): 5,126

Jelinkova S, Vilotic A, Pribyl J, Aimond F, Salykin A, Acimovic I, Pesl M, Caluori G, Klimovic S, Urban T, Dobrovolna H, Soska V, Skladal P, Lacampagne A, Dvorak P, Meli AC, ***Rotrekl V****
*- Corresponding author

The establishment of patient-specific DMD hiPSC lines provided access to human cells carrying disease-associated DMD mutations, while quantitative functional analysis of hPSC-derived cardiac models enabled their electromechanical properties to be interrogated in vitro. The next question was whether dystrophin-deficient hPSCs could reproduce functional abnormalities associated with DMD cardiac pathology after differentiation toward the cardiac lineage. To address this question across complementary experimental backgrounds, we used multiple patient-derived DMD hiPSC lines together with a dystrophin-deficient hESC line and its isogenic WT control and characterized the resulting cardiac models using electrophysiological, Ca^{2+}-handling and contractile measurements. This complementary design combined patient-specific models, which captured phenotypes across independent disease-associated genetic backgrounds, with an engineered isogenic model that strengthened attribution of observed abnormalities to dystrophin deficiency.

Cardiac models derived from dystrophin-deficient hPSCs reproduced multiple functional abnormalities associated with DMD cardiac pathology. Compared with their respective WT models, dystrophin-deficient cardiac cells exhibited altered spontaneous electrical activity, including reduced beating frequency and increased beat-rate variability, together with impaired contractile function and progressive loss of viable cardiomyocytes during prolonged culture. Electrophysiological analysis further revealed abnormalities in action-potential characteristics and ion-channel function, demonstrating that dystrophin deficiency affected several interconnected components of cardiomyocyte physiology rather than producing an isolated functional defect. Collectively, these findings demonstrated that hPSC-derived dystrophin-deficient cardiac models reproduce multiple functional abnormalities previously associated with cardiac pathology in DMD patients and experimental animal models, providing a human cellular system in which the mechanisms underlying individual components of the cardiac phenotype could subsequently be investigated.

Abnormal Ca^{2+} handling represented a particularly prominent component of the dystrophin-deficient cardiac phenotype. Ca^{2+} imaging revealed prolonged intracellular Ca^{2+} transients, including delayed time to peak and altered decay kinetics, together with small secondary Ca^{2+} release events occurring during diastole. These spontaneous diastolic events were consistent with the abnormal sarcoplasmic-reticulum Ca^{2+} release previously described in dystrophin-deficient cardiomyocytes and provided a cellular correlate of the arrhythmogenic Ca^{2+} instability associated with dystrophic cardiac disease.

A blunted response to β-adrenergic stimulation represented another disease-relevant functional abnormality reproduced in the patient-derived DMD cardiac models. Reduced β-adrenergic responsiveness had previously been demonstrated in dystrophin-deficient myocardium, where it was associated with altered Ca^{2+}-handling protein phosphorylation and reduced β1-adrenergic receptor density and sensitivity. In our DMD cardiac models, however, the attenuated chronotropic and inotropic responses to β-adrenergic stimulation were accompanied by increased expression of β1- and β2-adrenergic receptors. This apparent dissociation between receptor abundance and functional responsiveness suggested that the impaired response could not be explained simply by reduced receptor expression and pointed instead toward altered regulation or desensitization of the β-adrenergic signaling pathway.

In addition to the abnormalities identified in the resulting cardiac cells, we observed a reduced proportion of spontaneously contracting cardiac aggregates across the dystrophin-deficient hPSC models. The experimental design did not determine whether this difference resulted from altered cardiovascular lineage specification, progenitor expansion or survival, subsequent differentiation, or the acquisition of functional properties required for spontaneous contraction. Nevertheless, this unresolved observation shifted the focus of our subsequent research upstream from the phenotype of dystrophin-deficient cardiomyocytes toward the possibility that dystrophin deficiency may already influence the biology of stem and progenitor cells from which disease-relevant cardiac cells arise. It thereby provided the conceptual impetus for investigating DMD not exclusively as a disease of differentiated muscle cells, but also as a disorder in which abnormalities at the stem/progenitor-cell level may contribute to the subsequent disease phenotype.

3.4. Commentary to published work – Annex 4

Dystrophin Deficiency Leads to Genomic Instability in Human Pluripotent Stem Cells via NO Synthase-Induced Oxidative Stress

Original article published in Cells, 2019, Q1, IF(2019): 4,366

Jelinkova S, Fojtik P, Kohutova A, Vilotic A, Markova L, Pesl M, Jurakova T, Kruta M, Vrbsky J, Gaillyova R, Valaskova I, Frak I, Lacampagne A, Forte G, Dvorak P, Meli AC, ***Rotrekl V****
*- Corresponding author

The altered outcome of cardiac differentiation observed in our preceding study raised the question of whether the consequences of dystrophin deficiency might already be detectable before differentiation toward the cardiac lineage. Human pluripotent stem cells provided an experimentally accessible system in which this question could be addressed before the emergence of lineage-specific cardiac physiology, while retaining cellular processes central to stem-cell maintenance, including stringent regulation of genome integrity and cellular homeostasis. Importantly, high-molecular-weight dystrophin isoforms were expressed in WT hPSCs but absent from the dystrophin-deficient models, indicating that dystrophin is already present at this early cellular state.

Dystrophin-deficient hPSCs exhibited increased intracellular ROS, indicating disturbed redox homeostasis already at the pluripotent stage. This increase was accompanied by elevated DNA damage. Analysis of candidate enzymatic sources of ROS, together with pharmacological and genetic interventions, identified dysregulated NOS activity as a major contributor to the increased ROS production in dystrophin-deficient cells. Importantly, pharmacological inhibition of NOS and knockdown of individual NOS isoforms reduced DNA damage, while NOS inhibition also reduced ROS accumulation and ROS scavenging attenuated the DNA-damage phenotype. These interventions therefore provided functional evidence for a causal sequence in which dysregulated NOS activity promotes ROS accumulation that, in turn, contributes to DNA damage in dystrophin-deficient hPSCs.

The identification of NOS-dependent redox disturbance and DNA damage in undifferentiated DMD hPSCs demonstrated that cellular consequences associated with dystrophin deficiency can arise before acquisition of a differentiated muscle phenotype and at a stage preceding the contractile activity and tissue-level injury that characterize dystrophic muscle. Together with the altered outcome of cardiac differentiation observed in our preceding study, these findings raised the possibility that abnormalities already present in the pluripotent population might influence subsequent stem/progenitor-cell behavior or lineage differentiation. However, no causal relationship between the redox and DNA-damage phenotype of DMD hPSCs and the altered outcome of cardiac differentiation was established. This unresolved connection shifted our attention toward a more fundamental question: whether redox homeostasis itself participates in the signaling mechanisms that regulate the state and fate of human pluripotent stem cells.

3.5. Commentary to published work – Annex 5

Both Hypoxia-Inducible Factor 1 and MAPK Signaling Pathway Attenuate PI3K/AKT via Suppression of Reactive Oxygen Species in Human Pluripotent Stem Cells

Original article published in Frontiers in Cell and Developmental Biology, 2021, Q1, IF(2021): 6,081

Fojtik P, Beckerova D, Holomkova K, Senfluk M, ***Rotrekl V****
*- Corresponding author

The identification of increased NOS-dependent ROS production in dystrophin-deficient hPSCs raised the broader question of whether changes in the cellular redox environment might influence signaling mechanisms involved in stem-cell fate regulation. We therefore investigated whether intracellular ROS can modulate PI3K/AKT signaling in human pluripotent stem cells, a pathway with an established role in the regulation of cell-fate decisions.

Experimental modulation of intracellular ROS demonstrated a direct relationship between the cellular redox state and PI3K/AKT signaling in hPSCs. Reduction of ROS decreased AKT phosphorylation, whereas increasing ROS enhanced AKT phosphorylation, and inhibition of PI3K prevented the ROS-induced increase in AKT activity. Mechanistic analysis further identified PTEN as a redox-sensitive component of this regulation, with ROS-dependent oxidation of PTEN providing a mechanism through which changes in the cellular redox state can modulate PI3K/AKT pathway activity. Together, these findings established a regulatory role for intracellular ROS in PI3K/AKT signaling in human pluripotent stem cells.

Within our research programme, these findings provided a mechanistic basis for considering altered redox homeostasis not only as a consequence of dystrophin deficiency, but also as a potential regulator of stem/progenitor-cell fate. Together with the increased NOS-dependent ROS production identified in DMD hPSCs, the demonstrated redox sensitivity of PI3K/AKT signaling raised the possibility that dystrophin-associated changes in the cellular redox environment could influence signaling processes governing stem/progenitor-cell maintenance and differentiation. Although this relationship remained hypothetical and was not demonstrated in dystrophin-deficient cells, it broadened the questions arising from our hPSC studies and provided a conceptual basis for asking whether abnormalities of stem/progenitor-cell regulation might also be detectable within the dystrophin-deficient heart.

3.6. Commentary to published work – Annex 6

Cardiovascular progenitor cells and tissue plasticity are reduced in a myocardium affected by Becker muscular dystrophy

Original article published in *Orphanet Journal of Rare Diseases*, 2020, Q1, IF(2020): 4,123

Pesl M, Jelinkova S, Caluori G, Holicka M, Krejci J, Nemec P, Kohutova A, Zampachova V, Dvorak P, ***Rotrekl V****
*- Corresponding author

Our studies in hPSCs indicated that the consequences of dystrophin deficiency can extend to the stem-cell state and raised the broader question of whether cellular populations other than differentiated muscle cells might also be affected in dystrophin-associated disease. We therefore extended our investigation to the non-myocyte compartment of the dystrophin-deficient heart, focusing on a resident c-kit+/CD45− population with stem/progenitor-like properties. Access to explanted myocardium from a patient with BMD-associated end-stage heart failure provided the opportunity to examine whether the abundance and functional properties of this population were altered in human dystrophin-associated cardiac disease.

Analysis of the explanted BMD myocardium revealed a marked reduction in the c-kit+/CD45− population compared with non-dystrophic donor myocardium. Cells isolated from the BMD heart also exhibited reduced ex vivo survival, showing that the population abnormality was not restricted to a quantitative difference in the myocardium. In parallel, ex vivo culture of myocardial explants revealed reduced tissue plasticity, further indicating that end-stage dystrophin-associated heart disease involved alterations extending beyond the cardiomyocyte compartment.

The observation that the c-kit+/CD45− population was markedly reduced in end-stage human dystrophin-associated heart disease raised the question of when this alteration emerges during disease progression. Because the BMD myocardium represented an endpoint of advanced cardiac disease, the study could not determine whether the reduced abundance of the resident population preceded cardiac dysfunction or developed as a consequence of the progressively diseased myocardial environment. Resolving this temporal relationship therefore required analysis of the resident cardiac stem/progenitor-like compartment at different stages of dystrophin-associated cardiac disease. This question provided the basis for our subsequent investigation of the c-kit+/CD45− population during disease progression in the mdx mouse model.

3.7. Commentary to published work – Annex 7

Dystrophin Deficiency Causes Progressive Depletion of Cardiovascular Progenitor Cells in the Heart

Original article published in *International Journal of Molecular Sciences*, 2021, Q1, IF(2020): 6,208

Jelinkova S, Sleiman Y, Fojtik P, Aimond F, Finan A, Hugon G, Scheuermann V, Beckerova D, Cazorla O, Vincenti M, Amedro P, Richard S, Jaros J, Dvorak P, Lacampagne A, Carnac G, ***Rotrekl V****, Meli AC*

The reduced abundance of the c-kit+/CD45− population identified in end-stage human BMD myocardium could not determine when this alteration emerged during the course of cardiac disease. We therefore extended our analysis to the mdx mouse model, which enabled the resident cardiac stem/progenitor-like compartment to be examined across different ages. The study was designed to determine how the abundance and distribution of the c-kit+/CD45− population change over time and whether alterations of this population are accompanied by detectable cellular abnormalities.

Dystrophin-deficient hearts developed progressive myocardial fibrosis together with abnormalities of left-ventricular mechanics detected by speckle-tracking echocardiography, demonstrating an age-dependent cardiac phenotype in the mdx model. These findings established the pathological context in which subsequent changes in the resident cardiac cell population could be evaluated.

Analysis of the c-kit+/CD45− population revealed a dynamic age-dependent pattern rather than a simple progressive reduction. Young mdx hearts contained an increased proportion of c-kit+/CD45− cells compared with WT hearts, followed by a marked decline at later ages. This change in abundance was accompanied by altered spatial distribution, with c-kit+/CD45− cells detected predominantly in the right atrial and subepicardial regions of young mdx hearts and becoming progressively scarce in older animals. These findings complemented the endpoint observation from human BMD myocardium by demonstrating that alteration of the resident c-kit+/CD45− population in dystrophin-deficient hearts can involve an early increase followed by subsequent age-dependent loss.

To determine whether the changing abundance of the resident population was accompanied by a cellular abnormality, c-kit+/CD45− cells isolated from mdx and WT hearts were examined for DNA damage. Cells derived from mdx hearts exhibited increased γH2AX staining compared with WT cells, indicating increased DNA damage within the dystrophin-deficient c-kit+/CD45− population. In contrast, ROS levels measured by CellROX after cell isolation did not differ significantly between mdx and WT cells, and the mechanism responsible for the DNA-damage phenotype therefore remained unresolved. These findings demonstrated that, in addition to the age-dependent alteration of the c-kit+/CD45− population, cells isolated from the dystrophin-deficient heart exhibited increased DNA damage.

Within the research program presented in this habilitation, this study transformed the endpoint observation of a reduced c-kit+/CD45− population in human dystrophin-deficient myocardium into a dynamic model of population change during disease progression. The early increase in c-kit+/CD45− cells in mdx hearts, followed by their progressive age-dependent decline, suggested that the resident population may initially be recruited or expanded in response to the dystrophin-

deficient myocardial environment and subsequently become depleted as cardiac pathology progresses. The detection of increased DNA damage in isolated mdx c-kit+/CD45− cells additionally identified a cellular abnormality within this resident population, although its relationship to the subsequent population loss was not established. Together, these findings raised the possibility that progressive impairment or depletion of the resident progenitor-like compartment may reduce its capacity to participate in myocardial homeostasis and thereby contribute to disease progression. Whether these changes represent a driver, consequence or amplifier of dystrophin-associated cardiac pathology remains unresolved.

4. CONCLUSIONS

Understanding the cellular processes underlying dystrophin-associated cardiomyopathy requires experimental models providing access to aspects of the disease that cannot be resolved directly in patients. Human myocardial tissue provides the closest representation of the affected heart, but is available only to a limited extent and predominantly reflects advanced stages of disease, when extensive tissue remodeling has already occurred. Animal models complement this endpoint view by allowing cellular changes to be examined over time within the intact dystrophin-deficient myocardium, although differences between species limit their direct translation to human disease. Human pluripotent stem-cell models provide access to yet another dimension, allowing disease-associated processes to be investigated in a human cellular context across successive stages of differentiation. Their differentiation into three-dimensional cardiac models further enables disease-associated cardiac phenotypes to be examined through quantitative assessment of electrophysiological, mechanical and pharmacological properties. Yet each of these experimental systems provides access to only part of a disease process that unfolds across different cellular states, biological scales and stages of progression. It is their complementarity that allows the affected human heart to be connected with the temporal evolution of pathology *in vivo* and, looking further upstream, with cellular processes preceding and accompanying human cardiac differentiation.

Our work contributes to extending the current understanding of dystrophin-associated cardiac disease beyond dysfunction of the differentiated cardiomyocyte alone. The functional abnormalities reproduced in dystrophin-deficient hPSC-derived cardiac models remain consistent with this established disease paradigm, but differences were also apparent at the level of cardiac differentiation outcome, with a reduced proportion of spontaneously contracting cardiac aggregates. Looking further upstream, dystrophin-deficient pluripotent cells already exhibited altered redox homeostasis and compromised genome integrity before cardiac differentiation. In parallel, our studies of hPSC biology demonstrated redox-sensitive regulation of PI3K/AKT signaling, identifying one pathway through which changes in cellular redox state can influence stem-cell signaling. The present studies therefore do not establish whether this redox-sensitive signaling contributes to the altered cardiac differentiation outcome observed in dystrophin-deficient cells. A second, biologically distinct extension emerged in the postnatal heart, where our findings implicated resident cardiac populations with stem/progenitor-like properties as another cellular compartment altered in dystrophin-associated disease. Evidence from human BMD myocardium established the relevance of this compartment to the diseased human heart, while the mdx model provided a temporal perspective on its alteration during disease progression. Together, these findings extend the cellular framework of dystrophin-associated cardiac disease in two directions: upstream of the differentiated cardiac phenotype, towards earlier cellular states and developmental processes, and outside the cardiomyocyte compartment, towards resident populations with stem/progenitor-like properties in the postnatal myocardium. Their significance becomes particularly apparent when viewed alongside skeletal-muscle dystrophinopathy. In skeletal muscle, disease biology has already expanded beyond the differentiated myofibre, with abnormalities arising during myogenic development and direct evidence that dystrophin regulates satellite-cell polarity and asymmetric division. Our findings begin to address an analogous gap in cardiac dystrophinopathy by providing evidence that dystrophin-associated abnormalities are likewise detectable before the differentiated cardiac phenotype is established and within resident stem/progenitor-like populations of the postnatal myocardium. Whether abnormalities arising in these distinct developmental and postnatal contexts are mechanistically related remains to be elucidated, as does the extent to

which either contributes causally to the development or progression of dystrophin-associated cardiomyopathy.

5. BIBLIOGRAPHY

Aartsma-Rus, A., Van Deutekom, J. C. T., Fokkema, I. F., Van Ommen, G. J. B. & Den Dunnen, J. T. Entries in the Leiden Duchenne muscular dystrophy mutation database: an overview of mutation types and paradoxical cases that confirm the reading-frame rule. *Muscle Nerve* **34**, 135–144 (2006).

Allen, D. G., Whitehead, N. P. & Froehner, S. C. Absence of dystrophin disrupts skeletal muscle signaling: roles of Ca2+, reactive oxygen species, and nitric oxide in the development of muscular dystrophy. *Physiol. Rev.* **96**, 253–305 (2016). https://doi.org/10.1152/physrev.00007.2015

Beltrami, A. P. et al. Adult cardiac stem cells are multipotent and support myocardial regeneration. *Cell* **114**, 763–776 (2003). https://doi.org/10.1016/s0092-8674(03)00687-1

Birnkrant, D. J. et al. Diagnosis and management of Duchenne muscular dystrophy, part 1: diagnosis, and neuromuscular, rehabilitation, endocrine, and gastrointestinal and nutritional management. *Lancet Neurol.* **17**, 251–267 (2018). https://doi.org/10.1016/s1474-4422(18)30024-3

Bladen, C. L. et al. The TREAT-NMD DMD Global Database: analysis of more than 7,000 Duchenne muscular dystrophy mutations. *Hum. Mutat.* **36**, 395–402 (2015). https://doi.org/10.1002/humu.22758

Boyce, F. M., Beggs, A. H., Feener, C. & Kunkel, L. M. Dystrophin is transcribed in brain from a distant upstream promoter. *Proc. Natl Acad. Sci. USA* **88**, 1276–1280 (1991). https://doi.org/10.1073/pnas.88.4.1276

Brandt, E. B., Li, X. & Nelson, T. J. Activation of P53 Via Nutlin-3a Reveals Role for P53 In ROS Signaling During Cardiac Differentiation of hiPSCs. *J. Stem Cell Rep.* **3**, 101 (2021). https://doi.org/10.17303/jscr.2021.3.101

Bremner, S. B. et al. Full-length dystrophin deficiency leads to contractile and calcium transient defects in human engineered heart tissues. *J. Tissue Eng.* **13**, 20417314221119628 (2022). https://doi.org/10.1177/20417314221119628

Brenman, J. E., Chao, D. S., Xia, H., Aldape, K. & Bredt, D. S. Nitric oxide synthase complexed with dystrophin and absent from skeletal muscle sarcolemma in Duchenne muscular dystrophy. *Cell* **82**, 743–752 (1995). https://doi.org/10.1016/0092-8674(95)90471-9

Brenman, J. E. et al. Interaction of nitric oxide synthase with the postsynaptic density protein PSD-95 and α1-syntrophin mediated by PDZ domains. *Cell* **84**, 757–767 (1996). https://doi.org/10.1016/s0092-8674(00)81053-3

Byers, T. J., Lidov, H. G. W. & Kunkel, L. M. An alternative dystrophin transcript specific to peripheral nerve. *Nat. Genet.* **4**, 77–81 (1993). https://doi.org/10.1038/ng0593-77

Bylund, J. B. et al. Coordinated Proliferation and Differentiation of Human-Induced Pluripotent Stem Cell-Derived Cardiac Progenitor Cells Depend on Bone Morphogenetic Protein Signaling Regulation by GREMLIN 2. *Stem Cells Dev.* **26**, 678–693 (2017). https://doi.org/10.1089/scd.2016.0226

Cassano, M. et al. Alteration of cardiac progenitor cell potency in GRMD dogs. *Cell Transplant.* **21**, 1945–1967 (2012). https://doi.org/10.3727/096368912x638919

Chang, N. C. et al. The dystrophin glycoprotein complex regulates the epigenetic activation of muscle stem cell commitment. *Cell Stem Cell* **22**, 755–768.e6 (2018). https://doi.org/10.1016/j.stem.2018.03.022

Chong, J. J. H. et al. Progenitor cells identified by PDGFR-alpha expression in the developing and diseased human heart. *Stem Cells Dev.* **22**, 1932–1943 (2013). https://doi.org/10.1089/scd.2012.0542

Churko, J. M. et al. Defining human cardiac transcription factor hierarchies using integrated single-cell heterogeneity analysis. *Nat. Commun.* **9**, 4906 (2018). https://doi.org/10.1038/s41467-018-07333-4

Constantinou, C. et al. Human pluripotent stem cell-derived cardiomyocytes as a target platform for paracrine protection by cardiac mesenchymal stromal cells. *Sci. Rep.* **10**, 13016 (2020). https://doi.org/10.1038/s41598-020-69495-w

Cooper, L. T. et al. The role of endomyocardial biopsy in the management of cardiovascular disease. *J. Am. Coll. Cardiol.* **50**, 1914–1931 (2007). https://doi.org/10.1016/j.jacc.2007.09.008

Crisafulli, S. et al. Global epidemiology of Duchenne muscular dystrophy: an updated systematic review and meta-analysis. *Orphanet J. Rare Dis.* **15**, 141 (2020). https://doi.org/10.1186/s13023-020-01430-8

D'Souza, V. N. et al. A novel dystrophin isoform is required for normal retinal electrophysiology. *Hum. Mol. Genet.* **4**, 837–842 (1995). https://doi.org/10.1093/hmg/4.5.837

Danialou, G. et al. Dystrophin-deficient cardiomyocytes are abnormally vulnerable to mechanical stress-induced contractile failure and injury. *FASEB J.* **15**, 1655–1657 (2001). https://doi.org/10.1096/fj.01-0030fje

Den Hartogh, S. C. et al. Dual Reporter MESP1^mCherry/w^-NKX2-5^eGFP/w^ hESCs Enable Studying Early Human Cardiac Differentiation. *Stem Cells* **33**, 56–67 (2015). https://doi.org/10.1002/stem.1842

Dick, E. et al. Exon skipping and gene transfer restore dystrophin expression in human induced pluripotent stem cells-cardiomyocytes harboring DMD mutations. *Stem Cells Dev.* **22**, 2714–2724 (2013). https://doi.org/10.1089/scd.2013.0135

Duan, D., Goemans, N., Takeda, S., Mercuri, E. & Aartsma-Rus, A. Duchenne muscular dystrophy. *Nat. Rev. Dis. Primers* **7**, 13 (2021). https://doi.org/10.1038/s41572-021-00248-3

Duelen, R. et al. Human iPSC model reveals a central role for NOX4 and oxidative stress in Duchenne cardiomyopathy. *Stem Cell Reports* **17**, 352–368 (2022). https://doi.org/10.1016/j.stemcr.2021.12.019

Dumont, N. A. et al. Dystrophin expression in muscle stem cells regulates their polarity and asymmetric division. *Nat. Med.* **21**, 1455–1463 (2015). https://doi.org/10.1038/nm.3990

Eisen, B. et al. Electrophysiological abnormalities in induced pluripotent stem cell-derived cardiomyocytes generated from Duchenne muscular dystrophy patients. *J. Cell. Mol. Med.* **23**, 2125–2135 (2019). https://doi.org/10.1111/jcmm.14124

Eisen, B. & Binah, O. Modeling Duchenne muscular dystrophy cardiomyopathy with patients' induced pluripotent stem-cell-derived cardiomyocytes. *Int. J. Mol. Sci.* **24**, 8657 (2023). https://doi.org/10.3390/ijms24108657

El Harane, N. et al. Acellular therapeutic approach for heart failure: in vitro production of extracellular vesicles from human cardiovascular progenitors. *Eur. Heart J.* **39**, 1835–1847 (2018). https://doi.org/10.1093/eurheartj/ehy012

Eldridge, C. B. et al. A p53-Dependent Checkpoint Induced upon DNA Damage Alters Cell Fate during hiPSC Differentiation. *Stem Cell Reports* **15**, 827–835 (2020). https://doi.org/10.1016/j.stemcr.2020.08.003

Elliott, D. A. et al. NKX2-5^eGFP/w^ hESCs for isolation of human cardiac progenitors and cardiomyocytes. *Nat. Methods* **8**, 1037–1040 (2011). https://doi.org/10.1038/nmeth.1740

Elorbany, R. et al. Single-cell sequencing reveals lineage-specific dynamic genetic regulation of gene expression during human cardiomyocyte differentiation. *PLoS Genet.* **18**, e1009666 (2022). https://doi.org/10.1371/journal.pgen.1009666

Emery, A. E. H., Muntoni, F. & Quinlivan, R. C. M. *Duchenne Muscular Dystrophy*. 4th ed. Oxford University Press, Oxford (2015).

Ervasti, J. M. & Campbell, K. P. Membrane organization of the dystrophin-glycoprotein complex. *Cell* **66**, 1121–1131 (1991). https://doi.org/10.1016/0092-8674(91)90035-w

Ervasti, J. M. & Campbell, K. P. A role for the dystrophin-glycoprotein complex as a transmembrane linker between laminin and actin. *J. Cell Biol.* **122**, 809–823 (1993).

Fauconnier, J. et al. Leaky RyR2 trigger ventricular arrhythmias in Duchenne muscular dystrophy. *Proc. Natl Acad. Sci. USA* **107**, 1559–1564 (2010). https://doi.org/10.1073/pnas.0908540107

Feener, C. A., Koenig, M. & Kunkel, L. M. Alternative splicing of human dystrophin mRNA generates isoforms at the carboxy terminus. *Nature* **338**, 509–511 (1989). https://doi.org/10.1038/338509a0

Fojtík, P., Beckerová, D., Holomková, K., Šenfluk, M. & Rotrekl, V. Both hypoxia-inducible factor 1 and MAPK signaling pathway attenuate PI3K/AKT via suppression of reactive oxygen species in human pluripotent stem cells. *Front. Cell Dev. Biol.* **8**, 607444 (2021). https://doi.org/10.3389/fcell.2020.607444

Friedman, C. E. et al. Single-cell transcriptomic analysis of cardiac differentiation from human PSCs reveals HOPX-dependent cardiomyocyte maturation. *Cell Stem Cell* **23**, 586–598.e8 (2018). https://doi.org/10.1016/j.stem.2018.09.009

Gao, Q. Q. & McNally, E. M. The dystrophin complex: structure, function, and implications for therapy. *Compr. Physiol.* **5**, 1223–1239 (2015). https://doi.org/10.1002/cphy.c140048

Granet, J. A. et al. Muscle stem cells in Duchenne muscular dystrophy exhibit molecular impairments and altered cell fate trajectories impacting regenerative capacity. *Cell Death Dis.* **16**, 437 (2025). https://doi.org/10.1038/s41419-025-07755-1

Hoffman, E. P., Brown Jr, R. H. & Kunkel, L. M. Dystrophin: the protein product of the Duchenne muscular dystrophy locus. *Cell* **51**, 919–928 (1987). https://doi.org/10.1016/0092-8674(87)90579-4

Ieronimakis, N. et al. Coronary adventitial cells are linked to perivascular cardiac fibrosis via TGFβ1 signaling in the mdx mouse model of Duchenne muscular dystrophy. *J. Mol. Cell. Cardiol.* **63**, 122–134 (2013). https://doi.org/10.1016/j.yjmcc.2013.07.014

Jelinkova, S. et al. Generation of two Duchenne muscular dystrophy patient-specific induced pluripotent stem cell lines DMD02 and DMD03 (MUNIi001-A and MUNIi003-A). *Stem Cell Res.* **40**, 101562 (2019a). https://doi.org/10.1016/j.scr.2019.101562

Jelinkova, S. et al. Dystrophin deficiency leads to genomic instability in human pluripotent stem cells via NO synthase-induced oxidative stress. *Cells* **8**, 53 (2019b). https://doi.org/10.3390/cells8010053

Jelinkova, S. et al. DMD pluripotent stem cell derived cardiac cells recapitulate in vitro human cardiac pathophysiology. *Front. Bioeng. Biotechnol.* **8**, 535 (2020). https://doi.org/10.3389/fbioe.2020.00535

Jelinkova, S. et al. Dystrophin deficiency causes progressive depletion of cardiovascular progenitor cells in the heart. *Int. J. Mol. Sci.* **22**, 5025 (2021). https://doi.org/10.3390/ijms22095025

Ji, A. R. et al. Reactive oxygen species enhance differentiation of human embryonic stem cells into mesendodermal lineage. *Exp. Mol. Med.* **42**, 175–186 (2010). https://doi.org/10.3858/emm.2010.42.3.018

Jiang, C. et al. Notch signaling deficiency underlies age-dependent depletion of satellite cells in muscular dystrophy. *Dis. Model. Mech.* **7**, 997–1004 (2014). https://doi.org/10.1242/dmm.015917

Juan-Mateu, J. et al. DMD mutations in 576 dystrophinopathy families: a step forward in genotype-phenotype correlations. *PLoS ONE* **10**, e0135189 (2015). https://doi.org/10.1371/journal.pone.0135189

Jung, C., Martins, A. S., Niggli, E. & Shirokova, N. Dystrophic cardiomyopathy: amplification of cellular damage by Ca^{2+} signalling and reactive oxygen species-generating pathways. *Cardiovasc. Res.* **77**, 766–773 (2008). https://doi.org/10.1093/cvr/cvm089

Kamdar, F. & Garry, D. J. Dystrophin-deficient cardiomyopathy. *J. Am. Coll. Cardiol.* **67**, 2533–2546 (2016). https://doi.org/10.1016/j.jacc.2016.02.081

Kamdar, F. et al. Stem Cell-Derived Cardiomyocytes and Beta-Adrenergic Receptor Blockade in Duchenne Muscular Dystrophy Cardiomyopathy. *J. Am. Coll. Cardiol.* **75**, 1159–1174 (2020). https://doi.org/10.1016/j.jacc.2019.12.066

Kameya, S. et al. α1-Syntrophin gene disruption results in the absence of neuronal-type nitric-oxide synthase at the sarcolemma but does not induce muscle degeneration. *J. Biol. Chem.* **274**, 2193–2200 (1999). https://doi.org/10.1074/jbc.274.4.2193

Kaspar, R. W. et al. Analysis of dystrophin deletion mutations predicts age of cardiomyopathy onset in Becker muscular dystrophy. *Circ. Cardiovasc. Genet.* **2**, 544–551 (2009). https://doi.org/10.1161/circgenetics.109.867242

Kattman, S. J. et al. Stage-specific optimization of Activin/Nodal and BMP signaling promotes cardiac differentiation of mouse and human pluripotent stem cell lines. *Cell Stem Cell* **8**, 228–240 (2011). https://doi.org/10.1016/j.stem.2010.12.008

Kesari, A. et al. Integrated DNA, cDNA, and protein studies in Becker muscular dystrophy show high exception to the reading frame rule. *Hum. Mutat.* **29**, 728–737 (2008). https://doi.org/10.1002/humu.20722

Koenig, M., Monaco, A. P. & Kunkel, L. M. The complete sequence of dystrophin predicts a rod-shaped cytoskeletal protein. *Cell* **53**, 219–228 (1988). https://doi.org/10.1016/0092-8674(88)90383-2

Koenig, X. et al. Voltage-gated ion channel dysfunction precedes cardiomyopathy development in the dystrophic heart. *PLoS ONE* **6**, e20300 (2011). https://doi.org/10.1371/journal.pone.0020300

Koenig, X. et al. Enhanced currents through L-type calcium channels in cardiomyocytes disturb the electrophysiology of the dystrophic heart. *Am. J. Physiol. Heart Circ. Physiol.* **306**, H564–H573 (2014). https://doi.org/10.1152/ajpheart.00441.2013

Kyrychenko, S. et al. Pivotal role of miR-448 in the development of ROS-induced cardiomyopathy. *Cardiovasc. Res.* **108**, 324–334 (2015a). https://doi.org/10.1093/cvr/cvv238

Kyrychenko, V., Poláková, E., Janíček, R. & Shirokova, N. Mitochondrial dysfunctions during progression of dystrophic cardiomyopathy. *Cell Calcium* **58**, 186–195 (2015b). https://doi.org/10.1016/j.ceca.2015.04.006

Lai, Y. et al. Dystrophins carrying spectrin-like repeats 16 and 17 anchor nNOS to the sarcolemma and enhance exercise performance in a mouse model of muscular dystrophy. *J. Clin. Invest.* **119**, 624–635 (2009). https://doi.org/10.1172/jci36612

Landfeldt, E. et al. Predictors of cardiac disease in Duchenne muscular dystrophy: a systematic review and evidence grading. *Orphanet J. Rare Dis.* **19**, 359 (2024). https://doi.org/10.1186/s13023-024-03372-x

Laugwitz, K. L. et al. Postnatal isl1+ cardioblasts enter fully differentiated cardiomyocyte lineages. *Nature* **433**, 647–653 (2005). https://doi.org/10.1038/nature03215

Le Belle, J. E. et al. Proliferative neural stem cells have high endogenous ROS levels that regulate self-renewal and neurogenesis in a PI3K/Akt-dependent manner. *Cell Stem Cell* **8**, 59–71 (2011). https://doi.org/10.1016/j.stem.2010.11.028

Lederfein, D. et al. A 71-kilodalton protein is a major product of the Duchenne muscular dystrophy gene in brain and other nonmuscle tissues. *Proc. Natl Acad. Sci. USA* **89**, 5346–5350 (1992). https://doi.org/10.1073/pnas.89.12.5346

Lederfein, D., Yaffe, D. & Nudel, U. A housekeeping type promoter, located in the 3' region of the Duchenne muscular dystrophy gene, controls the expression of Dp71, a major product of the gene. *Hum. Mol. Genet.* **2**, 1883–1888 (1993). https://doi.org/10.1093/hmg/2.11.1883

Li, Y. et al. Genetic lineage tracing of nonmyocyte population by dual recombinases. *Circulation* **138**, 793–805 (2018). https://doi.org/10.1161/circulationaha.118.034250

Lian, X. et al. Robust cardiomyocyte differentiation from human pluripotent stem cells via temporal modulation of canonical Wnt signaling. *Proc. Natl Acad. Sci. USA* **109**, E1848–E1857 (2012). https://doi.org/10.1073/pnas.1200250109

Lidov, H. G. W., Selig, S. & Kunkel, L. M. Dp140: a novel 140 kDa CNS transcript from the dystrophin locus. *Hum. Mol. Genet.* **4**, 329–335 (1995). https://doi.org/10.1093/hmg/4.3.329

Lima Correa, B. et al. Extracellular vesicles from human cardiovascular progenitors trigger a reparative immune response in infarcted hearts. *Cardiovasc. Res.* **117**, 292–307 (2021). https://doi.org/10.1093/cvr/cvaa028

Lin, B. et al. Modeling and study of the mechanism of dilated cardiomyopathy using induced pluripotent stem cells derived from individuals with Duchenne muscular dystrophy. *Dis. Model. Mech.* **8**, 457–466 (2015). https://doi.org/10.1242/dmm.019505

Liu, Q. et al. Genetic lineage tracing identifies in situ Kit-expressing cardiomyocytes. *Cell Res.* **26**, 119–130 (2016). https://doi.org/10.1038/cr.2015.143

Mannhardt, I. et al. Human engineered heart tissue: analysis of contractile force. *Stem Cell Reports* **7**, 29–42 (2016). https://doi.org/10.1016/j.stemcr.2016.04.011

Marini, V. et al. Long-term culture of patient-derived cardiac organoids recapitulated Duchenne muscular dystrophy cardiomyopathy and disease progression. *Front. Cell Dev. Biol.* **10**, 878311 (2022). https://doi.org/10.3389/fcell.2022.878311

Markham, L. W. et al. Abnormalities of diastolic function precede dilated cardiomyopathy associated with Duchenne muscular dystrophy. *J. Am. Soc. Echocardiogr.* **19**, 865–871 (2006). https://doi.org/10.1016/j.echo.2006.02.003

Martin, C. M. et al. Persistent expression of the ATP-binding cassette transporter, Abcg2, identifies cardiac SP cells in the developing and adult heart. *Dev. Biol.* **265**, 262–275 (2004). https://doi.org/10.1016/j.ydbio.2003.09.028

Massouridès, E. et al. Dp412e: a novel human embryonic dystrophin isoform induced by BMP4 in early differentiated cells. *Skelet. Muscle* **5**, 40 (2015). https://doi.org/10.1186/s13395-015-0062-6

Mathieu, J. et al. Hypoxia induces re-entry of committed cells into pluripotency. *Stem Cells* **31**, 1737–1748 (2013). https://doi.org/10.1002/stem.1446

McNally, E. M. et al. Contemporary cardiac issues in Duchenne muscular dystrophy. *Circulation* **131**, 1590–1598 (2015). https://doi.org/10.1161/circulationaha.114.015151

Melacini, P. et al. Myocardial involvement is very frequent among patients affected with subclinical Becker's muscular dystrophy. *Circulation* **94**, 3168–3175 (1996). https://doi.org/10.1161/01.cir.94.12.3168

Meyers, T. A. & Townsend, D. Cardiac pathophysiology and the future of cardiac therapies in Duchenne muscular dystrophy. *Int. J. Mol. Sci.* **20**, 4098 (2019). https://doi.org/10.3390/ijms20174098

Monaco, A. P., Bertelson, C. J., Liechti-Gallati, S., Moser, H. & Kunkel, L. M. An explanation for the phenotypic differences between patients bearing partial deletions of the DMD locus. *Genomics* **2**, 90–95 (1988). https://doi.org/10.1016/0888-7543(88)90113-9

Moretti, A. et al. Patient-specific induced pluripotent stem-cell models for long-QT syndrome. *N. Engl. J. Med.* **363**, 1397–1409 (2010). https://doi.org/10.1056/nejmoa0908679

Mournetas, V. et al. Myogenesis modelled by human pluripotent stem cells: a multi-omic study of Duchenne myopathy early onset. *J. Cachexia Sarcopenia Muscle* **12**, 209–232 (2021). https://doi.org/10.1002/jcsm.12665

Mozin, E. et al. Dystrophin deficiency impairs cell junction formation during embryonic myogenesis from pluripotent stem cells. *iScience* **27**, 110242 (2024). https://doi.org/10.1016/j.isci.2024.110242

Nigro, G., Comi, L. I., Politano, L. & Bain, R. J. I. The incidence and evolution of cardiomyopathy in Duchenne muscular dystrophy. *Int. J. Cardiol.* **26**, 271–277 (1990). https://doi.org/10.1016/0167-5273(90)90082-g

Nigro, G. et al. Evaluation of the cardiomyopathy in Becker muscular dystrophy. *Muscle Nerve* **18**, 283–291 (1995). https://doi.org/10.1002/mus.880180304

Oh, H. et al. Cardiac progenitor cells from adult myocardium: homing, differentiation, and fusion after infarction. *Proc. Natl Acad. Sci. USA* **100**, 12313–12318 (2003). https://doi.org/10.1073/pnas.2132126100

Paige, S. L. et al. Endogenous Wnt/β-catenin signaling is required for cardiac differentiation in human embryonic stem cells. *PLoS ONE* **5**, e11134 (2010). https://doi.org/10.1371/journal.pone.0011134

Panovský, R. et al. Cardiac profile of the Czech population of Duchenne muscular dystrophy patients: a cardiovascular magnetic resonance study with T1 mapping. *Orphanet J. Rare Dis.* **14**, 10 (2019). https://doi.org/10.1186/s13023-018-0986-1

Perloff, J. K. Cardiac rhythm and conduction in Duchenne's muscular dystrophy: a prospective study of 20 patients. *J. Am. Coll. Cardiol.* **3**, 1263–1268 (1984). https://doi.org/10.1016/s0735-1097(84)80186-2

Pesl, M. et al. Atomic force microscopy combined with human pluripotent stem cell derived cardiomyocytes for biomechanical sensing. *Biosens. Bioelectron.* **85**, 751–757 (2016). https://doi.org/10.1016/j.bios.2016.05.073

Pesl, M. et al. Cardiovascular progenitor cells and tissue plasticity are reduced in a myocardium affected by Becker muscular dystrophy. *Orphanet J. Rare Dis.* **15**, 65 (2020). https://doi.org/10.1186/s13023-019-1257-4

Pioner, J. M. et al. Absence of full-length dystrophin impairs normal maturation and contraction of cardiomyocytes derived from human-induced pluripotent stem cells. *Cardiovasc. Res.* **116**, 368–382 (2020a). https://doi.org/10.1093/cvr/cvz109

Pioner, J. M. et al. Advances in stem cell modeling of dystrophin-associated disease: implications for the wider world of dilated cardiomyopathy. *Front. Physiol.* **11**, 368 (2020b). https://doi.org/10.3389/fphys.2020.00368

Puchalski, M. D. et al. Late gadolinium enhancement: precursor to cardiomyopathy in Duchenne muscular dystrophy?. *Int. J. Cardiovasc. Imaging* **25**, 57–63 (2009).

Qiu, X. X. et al. Rapamycin and CHIR99021 Coordinate Robust Cardiomyocyte Differentiation From Human Pluripotent Stem Cells Via Reducing p53-Dependent Apoptosis. *J. Am. Heart Assoc.* **6**, e005295 (2017). https://doi.org/10.1161/jaha.116.005295

Quinlan, J. G. et al. Evolution of the mdx mouse cardiomyopathy: physiological and morphological findings. *Neuromuscul. Disord.* **14**, 491–496 (2004). https://doi.org/10.1016/j.nmd.2004.04.007

Ramachandra, C. J. A. et al. ErbB Receptor Tyrosine Kinase: A Molecular Switch Between Cardiac and Neuroectoderm Specification in Human Pluripotent Stem Cells. *Stem Cells* **34**, 2461–2470 (2016). https://doi.org/10.1002/stem.2420

Ribeiro Jr, A. F. et al. Muscle satellite cells and impaired late stage regeneration in different murine models for muscular dystrophies. *Sci. Rep.* **9**, 11842 (2019). https://doi.org/10.1038/s41598-019-48156-7

Roberts, R. G., Coffey, A. J., Bobrow, M. & Bentley, D. R. Exon structure of the human dystrophin gene. *Genomics* **16**, 536–538 (1993). https://doi.org/10.1006/geno.1993.1225

Santini, M. P., Forte, E., Harvey, R. P. & Kovacic, J. C. Developmental origin and lineage plasticity of endogenous cardiac stem cells. *Development* **143**, 1242–1258 (2016). https://doi.org/10.1242/dev.111591

Schaaf, S. et al. Human engineered heart tissue as a versatile tool in basic research and preclinical toxicology. *PLoS ONE* **6**, e26397 (2011). https://doi.org/10.1371/journal.pone.0026397

Shahin, W. S. et al. Redox-dependent Igfbp2 signaling controls Brca1 DNA damage response to govern neural stem cell fate. *Nat. Commun.* **14**, 444 (2023). https://doi.org/10.1038/s41467-023-36174-z

Sharma, S. et al. A Deep Proteome Analysis Identifies the Complete Secretome as the Functional Unit of Human Cardiac Progenitor Cells. *Circ. Res.* **120**, 816–834 (2017). https://doi.org/10.1161/circresaha.116.309782

Sicinski, P. et al. The molecular basis of muscular dystrophy in the mdx mouse: a point mutation. *Science* **244**, 1578–1580 (1989). https://doi.org/10.1126/science.2662404

Smart, N. et al. Thymosin β4 induces adult epicardial progenitor mobilization and neovascularization. *Nature* **445**, 177–182 (2007). https://doi.org/10.1038/nature05383

Spurney, C. et al. Cooperative International Neuromuscular Research Group Duchenne Natural History Study demonstrates insufficient diagnosis and treatment of cardiomyopathy in Duchenne muscular dystrophy. *Muscle Nerve* **50**, 250–256 (2014). https://doi.org/10.1002/mus.24163

Sultana, N. et al. Resident c-kit+ cells in the heart are not cardiac stem cells. *Nat. Commun.* **6**, 8701 (2015). https://doi.org/10.1038/ncomms9701

Takahashi, K. et al. Induction of pluripotent stem cells from adult human fibroblasts by defined factors. *Cell* **131**, 861–872 (2007). https://doi.org/10.1016/j.cell.2007.11.019

Vagnozzi, R. J. et al. Genetic lineage tracing of Sca-1+ cells reveals endothelial but not myogenic contribution to the murine heart. *Circulation* **138**, 2931–2939 (2018). https://doi.org/10.1161/circulationaha.118.035210

van Berlo, J. H. et al. c-kit+ cells minimally contribute cardiomyocytes to the heart. *Nature* **509**, 337–341 (2014). https://doi.org/10.1038/nature13309

Veerman, C. C. et al. Immaturity of human stem-cell-derived cardiomyocytes in culture: fatal flaw or soluble problem?. *Stem Cells Dev.* **24**, 1035–1052 (2015). https://doi.org/10.1089/scd.2014.0533

Wang, W. et al. Mitochondrial DNA damage level determines neural stem cell differentiation fate. *J. Neurosci.* **31**, 9746–9751 (2011). https://doi.org/10.1523/jneurosci.0852-11.2011

Wang, Y. X. et al. EGFR-Aurka signaling rescues polarity and regeneration defects in dystrophin-deficient muscle stem cells by increasing asymmetric divisions. *Cell Stem Cell* **24**, 419–432.e6 (2019). https://doi.org/10.1016/j.stem.2019.01.002

Williams, I. A. & Allen, D. G. Intracellular calcium handling in ventricular myocytes from mdx mice. *Am. J. Physiol. Heart Circ. Physiol.* **292**, H846–H855 (2007a). https://doi.org/10.1152/ajpheart.00688.2006

Williams, I. A. & Allen, D. G. The role of reactive oxygen species in the hearts of dystrophin-deficient mdx mice. *Am. J. Physiol. Heart Circ. Physiol.* **293**, H1969–H1977 (2007b). https://doi.org/10.1152/ajpheart.00489.2007

Yang, L. et al. Human cardiovascular progenitor cells develop from a KDR^+ embryonic-stem-cell-derived population. *Nature* **453**, 524–528 (2008). https://doi.org/10.1038/nature06894

Yilmaz, A. et al. Cardiac involvement in patients with Becker muscular dystrophy: new diagnostic and pathophysiological insights by a CMR approach. *J. Cardiovasc. Magn. Reson.* **10**, 50 (2008). https://doi.org/10.1186/1532-429x-10-50

Zhang, L. et al. Cardiac Sca-1+ cells are not intrinsic stem cells for myocardial development, renewal, and repair. *Circulation* **138**, 2919–2930 (2018). https://doi.org/10.1161/circulationaha.118.035200

Zhou Z-Q et al. Derivation and validation of diagnostic models for myocardial fibrosis in Duchenne muscular dystrophy: assessed by multi-parameter cardiovascular magnetic resonance. *Orphanet J. Rare Dis.* **18**, 388 (2023). https://doi.org/10.1186/s13023-023-02931-y

6. SUPPLEMENT MATERIAL

6.1. Annex 1

Generation of two Duchenne muscular dystrophy patient-specific induced pluripotent stem cell lines DMD02 and DMD03 (MUNIi001-A and MUNIi003-A)

Jelinkova S, Markova L, Pesl M, Valaskova I, Makaturova E, Jurikova L, Vondracek P, Lacampagne A, Dvorak P, Meli AC, ***Rotrekl V***

Stem Cell Research 40 (2019) 101562

Contents lists available at ScienceDirect

Stem Cell Research

journal homepage: www.elsevier.com/locate/scr

Lab Resource: Multiple Cell Lines

Generation of two Duchenne muscular dystrophy patient-specific induced pluripotent stem cell lines DMD02 and DMD03 (MUNIi001-A and MUNIi003-A)

Sarka Jelinkova[a,b], Lenka Markova[a], Martin Pesl[a,b], Iveta Valáškova[a,c], Eva Makaturová[c], Lenka Jurikova[d], Petr Vondracek[a,d], Alain Lacampagne[e], Petr Dvorak[a,b], Albano C. Meli[a,e], Vladimir Rotrekl[a,b,*]

[a] Department of Biology, Faculty of Medicine, Masaryk University, Brno 625 00, Czech Republic
[b] International Clinical Research Center ICRC, St. Anne's University Hospital Brno, Brno 602 00, Czech Republic
[c] Department of Clinical Genetics, University hospital Brno, Brno 613 00, Czech Republic
[d] Department of Pediatric Neurology, Faculty of Medicine, Masaryk University, Brno 625 00, Czech Republic
[e] PhyMedExp, INSERM, University of Montpellier, CNRS, Montpellier 342 95, France

A B S T R A C T

Duchenne muscular dystrophy (DMD) affects 1:3500–5000 newborn boys and manifests with progressive skeletal muscle wasting, respiratory failure and eventual heart failure. Symptoms show different onset from patients' childhood to the second decade of age. We reprogrammed fibroblasts from two independent DMD patients with a complete loss of dystrophin expression, carrying deletions of exons 45–50 and 48–50. The resulting hiPSCs show expression of pluripotency markers (NANOG, OCT4, SSEA4), differentiation capacity into all three germ layers, normal karyotype, genetic identity to the originating parental fibroblasts and the patient-specific dystrophin mutation.

Resource utility

Two human induced pluripotent stem cell (hiPSC) lines carrying mutations in the *DMD* gene were generated to study the development of Duchenne muscular dystrophy (DMD) *in vitro*, from a perspective of stem cell damage and in perspective to the pathophysiology of the resulting hiPSC-derived cardiomyocytes (CMs) and skeletal myotubes.

Resource details

DMD is an X-linked muscular degenerative disease which causes progressive weakness and loss of ambulation in the early teen years (Emery et al., 2015). Despite the progress of clinical care, heart failure or respiratory failure lead to death by the end of the 2nd decade of life.

DMD is caused by mutations in the *DMD* gene coding dystrophin protein leading to destabilization of the dystrophin glycoprotein complex (DGC), with sarcolemmal instability, cell death, fibrosis and lipid expansion in skeletal and cardiac muscles. Up to date, there is no curative therapy for this condition. DMD-associated dilated cardiomyopathy (DCM) is a major cause of mortality in affected patients and requires dedicated investigation and realistic models. The most common DMD model is the mdx mouse(Sicinski et al., 1989), although the cardiac symptoms are mild and progress slowly, compared to humans relative to lifespan. Therefore, the mdx model carries major limitations in cardiac disease modelling. Similarly, large animal models like golden retriever muscular dystrophy (GRMD), canine X-linked muscular dystrophy (CXMD), genetically engineered swine model, and feline muscular dystrophy (HFMD) have severe limitations coming from the animal physiology and variable cardiac involvement(Emery et al., 2015).

To investigate the human DMD cardiac phenotype using a cellular model, we generated patient-specific hiPSCs lines that were subsequently differentiated into cardiomyocytes. The informed consent forms were obtained according to the Ethical Committee and Helsinki declaration. Skin/muscle biopsies were harvested from two independent DMD boys (10- and 14-years old). From the biopsies, we derived two hiPSC lines harbouring deletions in *DMD* gene spanning exons 45–50 (DMD02, MUNIi001-A) and exons 48–50 (DMD03, MUNIi003-A). Individual clones were chosen empirically based on morphology. Selected clones from both lines tested positive for pluripotent markers alkaline phosphatase, Nanog, Oct3/4, TRA1–81 and SSEA4 (Fig. 1 A) and their expression pattern was comparable to wild type (WT) hiPSC. Quantitative analysis of pluripotency markers' mRNAs revealed similar expression of Oct4 and Nanog in both DMD

* Corresponding author at: Department of Biology, Faculty of Medicine, Masaryk University, Kamenice 5, building A3, Brno 625 00, Czech Republic.
E-mail address: vrotrekl@med.muni.cz (V. Rotrekl).

https://doi.org/10.1016/j.scr.2019.101562
Received 7 May 2019; Received in revised form 2 July 2019; Accepted 14 July 2019
Available online 09 September 2019
1873-5061/ © 2019 The Authors. Published by Elsevier B.V. This is an open access article under the CC BY license (http://creativecommons.org/licenses/BY/4.0/).

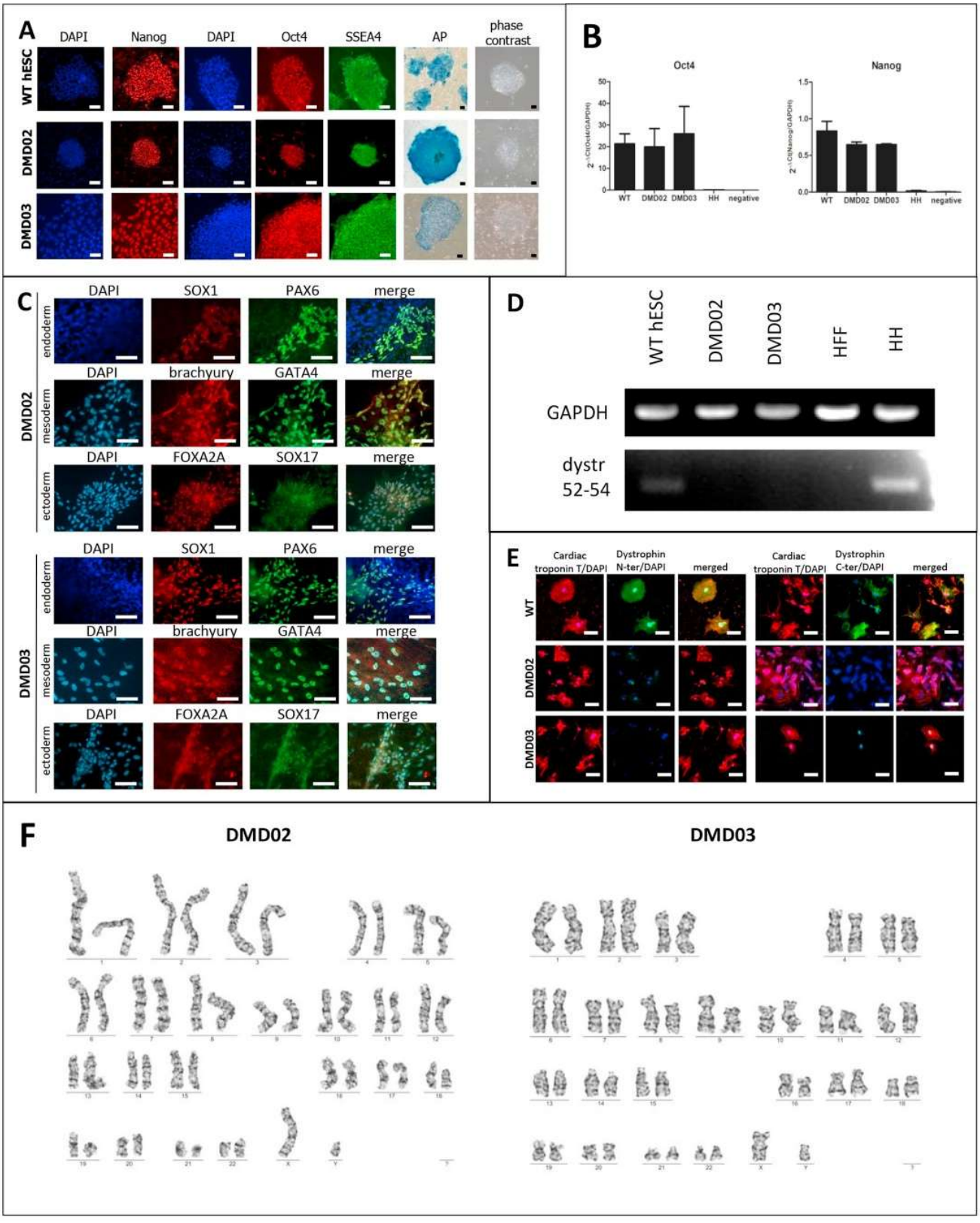
A
DAPI
Nanog
DAPI
Oct4
SSEA4
AP
phase contrast
WT hESC
DMD02
DMD03
B
Oct4
Nanog
WT
DMD02
DMD03
HH
negative
C
DAPI
SOX1
PAX6
merge
endoderm
DAPI
brachyury
GATA4
merge
mesoderm
DAPI
FOXA2A
SOX17
merge
ectoderm
DMD02
DMD03
D
WT hESC
DMD02
DMD03
HFF
HH
GAPDH
dystr 52-54
E
Cardiac troponin T/DAPI
Dystrophin N-ter/DAPI
merged
Cardiac troponin T/DAPI
Dystrophin C-ter/DAPI
merged
WT
DMD02
DMD03
F
DMD02
DMD03

Fig. 1.

Table 1
Summary of lines.

iPSC line names	Abbreviation in figures	Gender	Age	Ethnicity	Genotype of locus	Disease
MUNIi001-A	DMD02	Male	10	Caucasian	DMD	Duchenne muscular dystrophy
MUNIi003-A	DMD03	Male	14	Caucasian	DMD	Duchenne muscular dystrophy

Table 2
Characterization and validation.

Classification	Test	Result	Data
Morphology	Photography	normal	Fig. 1, panel A
Phenotype	Qualitative analysis (i.e. Immunocytochemistry)	Assess staining/expression of pluripotency markers: Oct4, Nanog, Sox2	Fig. 1 panel A
	Quantitative analysis (i.e. Immunocytochemistry counting, Flow cytometry, RT-qPCR)	Assess % of positive cells or transcripts for antigen & cell surface markers DMD03 Oct3/4: 98%, Nanog: 98%, SSEA-4: 99% DMD02: Oct3/4: 97%, Nanog: 98%, SSEA-4: 99%	Fig. 1, panel A, calculated from ICC images, Fig. 1 panel B as qPCR result
Genotype	Karyotype (G-banding) and resolution	Both 46XY, Resolution 450–500	Fig. 1 panel F
Identity	STR analysis	DNA Profiling performed with 17 sites, matched	submitted in archive with journal
Mutation analysis	MLPA	X-linked mutation on exons 45–50 (DMD02) /48–50 (DMD03)	Supplementary Table 1
Microbiology and virology	Mycoplasma	Mycoplasma testing by luminescence. Negative	Not shown, but available with authors
Differentiation potential	Directed differentiation	ectodermal markers (SOX1 and PAX6), endodermal markers (SOX17 and FOXA2A) and mesodermal markers (GATA4 and brachyury) expression showed by ICC, plus successful differentiation into CMs	Fig. 1 panel C and D
Donor screening	HIV 1 + 2 Hepatitis B, Hepatitis C	Negative	N/A
Genotype additional info	Blood group genotyping	N/A	N/A
	HLA tissue typing	HLA typed Class I and Class II	N/A

hiPSC lines and WT control, while no expression was found in differentiated human heart tissue (Fig. 2B). The ability of the generated DMD hiPSC lines to differentiate *in vitro* into all three germ layers was tested by incubation with ectodermal, endodermal or mesodermal inducing medium (Fig. 1C). We observed an expression of early differentiation markers of ectoderm (SOX1 in red, PAX6 in green), endoderm (SOX17 in green, FOXA2A in red) and mesoderm (GATA4 in green, brachyury in red) in both DMD hiPSC lines. Multiplex ligation-dependent probe amplification (MLPA) analysis showed the presence of the same mutation in the DMD hiPSC lines (patient 1: deleted exons 45–50, referred to as DMD02; and patient 2: deleted exons 48–50, referred to as DMD03; Supplementary Table 1) and short tandem repeats analysis confirmed their origin from the patient derived fibroblasts (data stored with the editors). The obtained DMD hiPSC lines presented no dystrophin mRNA expression in pluripotent state compared to the WT hiPSC (Fig. 1D, human heart sample used as positive control, human foreskin fibroblasts used as negative control). Dystrophin absence was confirmed in CMs differentiated from DMD hiPSCs by western blot (Jelinkova et al., 2019). All hiPSC derived CMs had positive signal for cardiac troponin T as CM marker (Caluori et al., 2019) (two antibodies recognizing N-terminus (N-ter) and C-terminus (C-ter) of dystrophin protein were used, Fig. 1E). All hiPSC derived CMs had positive signal for cardiac troponin T as CM marker. The generated hiPSC lines are karyotypically healthy (both 46, XY, Supplementary files).

Materials and methods

Tissue processing

The fibroblasts of two DMD patients were derived from skin/muscle (for DMD02/DMD03, respectively) biopsies. Informed consents approved by Ethics Committee (Faculty of Medicine, Masaryk University) were signed by parents of the patients beforehand. The biopsy tissues were cut into 0.5–1 mm^3 pieces, seeded onto 6 well plates (TPP) in medium containing KnockOut DMEM (Invitrogen), 10% heat-inactivated fetal bovine serum, 0,1 mM β-mercaptoethanol, 1% penicillin-streptomycin, 1% L-glutamine, 1% non-essential amino acids and layered with cover glasses. The tissue samples were kept in the incubator for 5 days without movement. The medium was further changed every 2–3 days and cells passaged at day 10 *in vitro* of cultivation using trypsin.

Pluripotent stem cell lines derivation and characterization

The hiPSC lines were obtained by reprogramming of cultivated human fibroblasts using CytoTuneTM iPS reprogramming kit (A13780–01; Life Technologies, Carlsbad, CA, USA) according to manufacturer's recommendations. DMD hiPSC lines are referred to as DMD02 (MUNIi001-A) and DMD03 (MUNIi003-A) and were further cultivated either on feeder layer of mouse embryonic fibroblasts in DMEM/F12, 15% KnockOut Serum replacement, 1% L-glutamine, 1% non-essential amino acids (all Invitrogen, Carlsbad, CA, USA), 0,1 mM β-mercaptoethanol (Sigma Aldrich, St.Louis, MO, USA) and 10 ng/ml FGF2 (Peprotech, Rocky Hill, NJ, USA)] or on Matrigel™ (Corning, New York, USA)-coated dish in feeder conditioned medium(Krutá et al., 2014). DMD hiPSCs were characterized using immunocytochemical staining of pluripotency markers (Nanog, Oct4, SSEA4, Alkaline phosphatase was tested using Blue Microwell Substrate kit AB0100 and AB0200, Sigma Aldrich) and compared with wild type (WT) human embryonic stem cell (hESC) line (Center for Cell Therapy line 14, CCTL14)(Krutá et al., 2014). The ability of the DMD hiPSC lines to differentiate *in vitro* into all three germ layers was tested by incubation for:

i) ectodermal induction: 2 days in RPMI1640, 1× B27, N2 supplement (Gibco, Thermo Fisher Scientific) plus SB431542 (Sigma Aldrich); 4 days in RPMI1640, 1× B27, N2 supplement
ii) endodermal induction: 6 days in RPMI1640 with B27, Activin A 50 ng/ml, BMP4 20 ng/ml, (both R&D)
iii) mesodermal induction: 3 days in RPMI1640 with B27, Activin A 10 ng/ml, BMP4 10 ng/ml; 1 day addition of IWP2 (Sigma Aldrich); 2 days in medium without IWP2.

Expression of early differentiation markers of ectoderm, endoderm and mesoderm were detected in both DMD hiPSC lines after 6 days of differentiation.

Immunocytochemistry

Cells were fixed with 2% paraformaldehyde for 15 min and ice-cold methanol for 5 min, then permeabilized with 0.5% Triton X-100 and blocked with 1% bovine serum albumin for 60 min. Samples were incubated overnight at 4 °C with appropriate primary antibodies and 60 min at room temperature with secondary antibodies. Nuclei were counterstained with 4′,6-diamidine-2′-phenylindole dihydrochloride (DAPI, Sigma Aldrich, St. Louis, MO, USA) and microscopic images were obtained using confocal microscope LSM700 and processed with Zen system (both Carl Zeiss, Oberkrochen, Germany).

Mutation validation

DMD hiPSCs lines were tested for the mutation presence by clinical MLPA analysis. MLPA was performed using SALSA MLPA P034 DMD mix 1 probemix and SALSA MLPA P035 DMD mix 2 probemix (LOT B1–1014, B1–0216, MRC Holland, Amsterdam, Netherlands), according to manufacturer's instructions. MLPA fragments were separated on ABI PRISM 3130 Genetic analyser (Applied Biosystems) and data were analysed using Coffalyser software (MRC Holland).

PCR

Total mRNA from cell culture and human heart samples was lysed using RNA Blue reagent (Top-Bio, Prague, Czech Republic) according to the manufacturer's instructions, and the total mRNA was isolated using the RNeasy Micro Kit (Qiagen, Hilden, Germany). mRNA concentration and purity were determined using NanoDrop (NanoDrop technologies, Wilmington, Germany). For reverse transcription PCR (rtPCR), cDNA was synthesized by Moloney Mouse Leukemia Virus (M-MLV) reverse transcriptase (Invitrogen, Carlsbad, CA, USA) at 37 °C for 1 h followed by 5 min at 85 °C. The consequent semi quantitative PCR was performed using Taq polymerase (Top-Bio, T032, Prague Czech Republic) and included denaturation at 95 °C for 10 min followed by 35 cycles of 95 °C for 10 s, annealing at 64 °C for 45 s and extension at 72 °C for 20 s; the final extension step proceeded at 72 °C for 10 min. For quantitative PCR, LightCycler® 480 SYBR Green I Master kit was used according to manufacturer's instructions. Annealing at 60 °C and 45 cycles were used for the PCR reaction on LightCycler LC480 Instrument (both Roche, Basil, Switzerland). The PCR primers (Generi-Biotech, Hradec Kralove, Czech Republic) and annealing conditions are shown in Reagent Details Table. The PCR product was then run on 1% agarose gel for 100 min/130 V/500 mA and photos were obtained using UV lamp DNR MiniBis Pro (Bio-Imaging Systems, Neve Yamin, Israel).

Line identity validation

Cell culture identity was analysed using short tandem repeat analysis using ABI PRISM 3130 Genetic analyser and PowerPlex® ESI17 Fast System (Promega) according to manufacturer's recommendations (Tables 1 and 2).

Karyotype

Karyotypes were analysed in passages P83 (DMD02) and 59 (DMD03) (number indicates passage number on feeder layer) after incubation with colchicine (2 µg/ml) for 4 h and treatment with hypotonic solution consisting of cultivation medium and water in ratio 1:3. Chromosome banding was achieved using Giemsa staining. Chromosomes from 10 mitoses in each sample evaluated in resolution 400–450 bands. BX53 microscope (Olympus, Tokio, Japan) was used with 1250× magnification and photos were taken using ProgRes MF camera (Jenoptik, Jena, Germany). Images were evaluated using LUCIA Cytogenetics 2 Karyo (Laboratory Imaging s.r.o., Prague, Czech Republic).

Key resources table

Unique stem cell lines identifier	*MUNIi001-A* *MUNIi003-A*
Alternative names of stem cell lines	*DMD02* *DMD03*
Institution	Department of Biology, Faculty of Medicine, Masaryk University, Brno 625 00, Czech Republic;
Contact information of distributor	*Vladimír Rotrekl PhD,vrotrekl@med.muni.cz*
Type of cell lines	*hiPSC*
Origin	*human*
Cell Source	*Leg skin biopsy fibroblasts*
Clonality	*mixed*
Method of reprogramming	*Sendai virus*
Multiline rationale	*Mutation in DMD gene with deletion of exons 45–50 (MUNIi001-A) or exons 48–50 (MUNIi003-A)*
Gene modification	*Yes*
Type of modification	*Hereditary*
Associated disease	*Duchenne muscular dystrophy*
Gene/locus	*Xp21*
Method of modification	*N/A*
Name of transgene or resistance	*N/A*
Inducible/constitutive system	*N/A*
Date archived/stock date	*MUNIi003-A 12.4.2015* *MUNIi001-A 16.11.2015*
Cell line repository/bank	*https://hpscreg.eu/cell-line/MUNIi001-A* *https://hpscreg.eu/cell-line/MUNIi003-A*
Ethical approval	*Faculty of Medicine, Masaryk University Ethics Committee (Brno, Czech Republic), approval number 37/2011*

Supplementary data to this article can be found online at https://doi.org/10.1016/j.scr.2019.101562.

Declaration of Competing Interest

The authors declare no conflict of interest.

Acknowledgments

This work was supported by the Ministry of Education, Youth, and Sports of the Czech Republic (7AMB13FR011, projects no. LQ1605 and no. LQ1601 from the National Program of Sustainability II), by the European Regional Development Fund - Project ENOCH (No. CZ.02.1.01/0.0/0.0/16_019/0000868) and by the Grant Agency of Masaryk University, Faculty of Medicine (no. ROZV/23/LF8/2019). We thank Dr. Peter Andrews (Department of Biomedical Science, Centre for Stem Cell Biology, University of Sheffield, Sheffield, UK) for antibody against SSEA4.

References

Caluori, G., Pribyl, J., Pesl, M., et al., 2019. Non-invasive electromechanical cell-based biosensors for improved investigation of 3D cardiac models. Biosens. Bioelectron. 124-125, 129–135. https://doi.org/10.1016/j.bios.2018.10.021.

Emery, A.E.H., Muntoni, F., Quinlivan, R.C.M., 2015. *Duchenne Muscular Dystrophy*. Fourth Edition. Oxford University Press, Oxford, New York.

Jelinkova, S., Fojtik, P., Kohutova, A., et al., 2019. Dystrophin deficiency leads to genomic instability in human pluripotent stem cells via NO synthase-induced oxidative stress. Cells. 8 (1). https://doi.org/10.3390/cells8010053.

Krutá, M., Šeneklová, M., Raška, J., et al., 2014. Mutation frequency dynamics in HPRT locus in culture-adapted human embryonic stem cells and induced pluripotent stem cells correspond to their differentiated counterparts. Stem Cells Dev. 23 (20), 2443–2454. https://doi.org/10.1089/scd.2013.0611.

Sicinski, P., Geng, Y., Ryder-Cook, A.S., Barnard, E.A., Darlison, M.G., Barnard, P.J., 1989. The molecular basis of muscular dystrophy in the mdx mouse: a point mutation. Science. 244 (4912), 1578–1580.

6.2. Annex 2

Non-invasive electromechanical cell-based biosensors for improved investigation of 3D cardiac models

Caluori G, Pribyl J, Pesl M, Jelinkova S, ***Rotrekl V****, Skladal P, Raiteri R*

Biosensors and Bioelectronics 124–125 (2019) 129–135

Contents lists available at ScienceDirect

Biosensors and Bioelectronics

journal homepage: www.elsevier.com/locate/bios

Non-invasive electromechanical cell-based biosensors for improved investigation of 3D cardiac models

Guido Caluori[a,b,c], Jan Pribyl[a], Martin Pesl[b,d,e], Sarka Jelinkova[d], Vladimir Rotrekl[d], Petr Skladal[a,*], Roberto Raiteri[c,*]

[a] Central European Institute of Technology, Masaryk University, Kamenice 5, 62500 Brno, Czech Republic
[b] International Clinical Research Centre of Saint Anne Hospital Brno, Pekarska 53, 60200 Brno, Czech Republic
[c] Department of Informatics, Bioengineering Robotics and Systems Engineering, University of Genova, Via All'Opera Pia, 13, 16145 Genova, Italy
[d] Department of Biology, Faculty of Medicine, Masaryk University, Kamenice 5, 62500 Brno, Czech Republic
[e] 1st Department of Cardiovascular Diseases, St. Anne's University Hospital and Masaryk University, Pekarska 53, Brno, Czech Republic

ARTICLE INFO

Keywords:
Excitation-contraction coupling
Human pluripotent stem cells
Cardiomyocytes
Atomic force microscopy
Microelectrode array
Drug testing

ABSTRACT

Cardiomyocytes (CM) placed on microelectrode array (MEA) were simultaneously probed with cantilever from atomic force microscope (AFM) system. This electric / nanomechanical combination in real time recorded beating force of the CMs cluster and the triggering electric events. Such "organ-on-a-chip" represents a tool for drug development and disease modeling. The human pluripotent stem cells included the WT embryonic line CCTL14 and the induced dystrophin deficient line reprogrammed from fibroblasts of a patient affected by Duchenne Muscular Dystrophy (DMD, complete loss of dystrophin expression). Both were differentiated to CMs and employed with the AFM/MEA platform for diseased CMs' drug response testing and DMD characterization. The dependence of cardiac parameters on extracellular Ca^{2+} was studied. The differential evaluation explained the observed effects despite variability of biological samples. The β-adrenergic stimulation (isoproterenol) and antagonist trials (verapamil) addressed ionotropic and chronotropic cell line-dependent features. For the first time, a distinctive beating-force relation for DMD CMs was measured on the 3D cardiac in vitro model.

1. Introduction

In the field of cell-based biosensors, cardiomyocytes (CM) are often used as models to study heart related diseases. The monitoring of electric activities of CMs is typically chosen; (multi)electrode transducers seem well established and widely available as microelectrode arrays (MEA) (Rothermel et al., 2005). The beating of CMs can be followed relatively easily (e.g. by video microscopy, Laurila et al., 2015), though in many situations the missing information on the associated beating force is of paramount importance in heart remodeling pathologies, such as dystrophinopathies and cardiomyopathies (Vatta et al., 2005). Beating force is associated with pathophysiological electro-mechanical coupling, and its alterations result often in mechanical heart failure (Pesl et al., 2016a). Such biomechanical measurements investigating the dilated cardiomyopathy were previously done on CMs using the stretcher device (Knoll et al., 2002). More detailed investigations were later done using cantilevers as nanomechanical transducers and atomic force microscope (AFM) as the evaluation system in real time with individual cardiomyocyte cells (Liu et al., 2012a,2012b) or cell clusters (Pesl et al., 2016a). Thus, combination of AFM for biomechanical changes with MEA sensing electric signals described here seems naturally promising for elucidating complex events in cardiomyocytes obtained from patient derived stem cells. This approach provides a robust and convenient example of the organ-on-a-chip system demonstrating its capabilities on disease related CMs.

Supplementary material related to this article can be found online at doi:10.1016/j.bios.2018.10.021.

The introduction of human pluripotent stem cells (hPSC, either embryonic, hESC, or induced pluripotent, hiPSC) and cardiac differentiation protocols allowed almost two decades of study on the cardiac organogenesis and functionality. In particular, patient-specific hiPSC representing a direct supply of healthy and mutation-carrying samples (Sinnecker et al., 2014) allow for description of the diseases progression involved in heart failure (Moretti et al., 2013). To improve the comparison between in vitro models, CRISPR-Cas9 technology has recently gained an outstanding popularity for its efficiency and flexibility in inducing precise mutations in cell lines, providing researchers with isogenic controls (Motta et al., 2017). hPSC-derived cardiomyocytes

* Corresponding authors.
E-mail addresses: skladal@chemi.muni.cz (P. Skladal), roberto.raiteri@unige.it (R. Raiteri).

https://doi.org/10.1016/j.bios.2018.10.021
Received 1 July 2018; Received in revised form 11 October 2018; Accepted 11 October 2018
Available online 16 October 2018
0956-5663/ © 2018 Elsevier B.V. All rights reserved.

and models recapitulate the morphological, genetic and functional characteristics of the heart muscle, specifically the subcellular cascade known as cardiac excitation-contraction coupling (cECC), responsible for heart pumping function (Bers, 2002). Cardiomyocytes from hPSC can be derived as 2D or 3D stem cell cultures. However, the 3D models seem to be superior and more physiologically relevant compared to the 2D ones (Regmi and Jeong, 2016). For monolayer culture, the multiple existing protocols with high differentiation efficiency involve modulation of the canonical Wnt/β-catenin pathway (Lian et al., 2012; Burridge et al., 2014), with high differentiation efficiency. For 3D cultures, the protocols exploit the spontaneous differentiation triggered from the aggregation of hPSC into embryoid bodies, which is driven to cardiac phenotypes using hypoxia and small molecules cocktails (Pesl et al., 2014). The efficiency of differentiation and grade of maturation can vary according to protocol and cell lines, and can be improved by physical methods, as in electro-mechanical stimulation (Bauwens et al., 2016). Purified hPSC-CMs can be further reassembled in precise geometries, such as in the engineered heart tissue (Tzatzalos et al., 2016). From gene expression to functionality, hPSC-CMs present an embryonic-like cardiac phenotype, with immature sarcomeres, sarcoplasmic reticulum and calcium cycling (Mummery et al., 2012; Acimovic et al., 2014). An immature phenotype has also been proven for embryoid body-derived cardiac models (Doevendans et al., 2000). Nevertheless, hPSC-CMs play a key role in future drug development with reduced attrition rate (Liang et al., 2013; Zheng et al., 2013), in cardiotoxicity assays (Takeda et al., 2018), disease modeling (Dell'Era et al., 2015) and in cell-based regenerative therapies (Doppler et al., 2013), and further studies to achieve cardiac maturation are ongoing. This aspect is also investigated by our proposed approach, to assess its robustness.

The hPSC-derived cardiac models can be characterized by functional (or phenotypic) properties though multiple in vitro assays, reviewed in another work from our group (Pesl et al., 2016b). Among these, atomic force microscopy has in the past three decades achieved remarkable role in the evaluation of biological samples mechanics and topography (Alonso and Goldmann, 2003; Kilpatrick et al., 2015) in native culture environment. In particular, it has been employed in important studies on single CMs (Liu et al., 2012a). A combination of AFM and 3D cardiac models has already been proposed as cell-based biosensor (CBB) in our previous work (Pesl et al., 2016a). Most AFM systems are now currently integrated with optical and confocal microscopy, which allows the implementation of combined measures of AFM and calcium imaging (Liu et al., 2012b; Caluori et al., 2018), but further systems can be included if properly miniaturized. Small biosensors, such as microelectrode arrays (MEA), can be engineered to comply with AFM and optical microscopy systems for cardiac investigation (Cogollo et al., 2011). The attractiveness of MEA-based electrophysiology resides in its ability to multiprobe extracellular field potentials (EFP) of electroactive cells in a non-destructive fashion, which allows for prolonged and complex measurements of cells and tissues (Spira and Hai, 2013).

In this work, we present an electromechanical in vitro system for the combined study of cECC on 3D cardiac models, employing both AFM and MEA platforms together. The aim of this work is to provide an improved method for cardiac models characterization and drug testing in the format of an organ (heart)-on-a-chip. For this reason, we have confronted a model of cardiac maturation with respect to its control, and employed a disease model of Duchenne muscular dystrophy (DMD), a progressively invalidating pathology of the striated muscle, including the myocardium (Finsterer and Stöllberger, 2003).

2. Materials and methods

2.1. hPSC culture and cardiac differentiation

The cardiac cells clusters were obtained using the hESC line CCTL14 (Adewumi et al., 2007) and one hiPSC line reprogrammed from fibroblasts of a patient affected by Duchenne Muscular Dystrophy (DMD). The patient carries a deletion of exons 45–50 of the DMD gene causing a complete loss of dystrophin expression. The line has been fully characterized for pluripotency markers (https://hpscreg.eu/cell-line/MUNIi001-A) and the differentiated CMs were tested for presence of striated pattern of sarcomeres labeled with cardiac troponin T (sc-8121, Santa Cruz), and cytoplasmic presence of dystrophin (NCL-DYSB, Leica) (see Supplementary material, SFig. 1). Pluripotent cells were firstly thawed and seeded on mitotically-inactivated mouse embryonic fibroblasts (feeder cells). The hPSC colonies were cultivated in DMEM-F12 (Thermofisher, Waltham, MA, USA) supplemented with 15% KnockOut fetal bovine serum Serum Replacement (FBS, Life Technologies, Carlsbad, CA, USA), 1% L-glutamine (Thermofisher), 0.5% penicillin/streptomycin (Thermofisher), 1% 2-mercaptoethanol (Thermofisher), 1% non-essential amino acids (Life Technologies), and 4 ng ml^{-1} and 10 ng ml^{-1} human fibroblast growth factor 2 (hFGF2, Peptrotech, London, UK) for hESC and hiPSC, respectively. Medium was changed daily and colonies were propagated for at least 5 passages, by manual fractioning. hESC cells were divided in a control group (CTRL) and another group (DORSO) undergoing an exposure to 500 nM of dorsomorphin (Sigma Aldrich, St. Louis, MO, USA) 4 days to the differentiation protocol, to improve cardiac commitment (Hao et al., 2008).

Cardiac differentiation was started by embryoid body formation, as described elsewhere (Pesl et al., 2013). Briefly, compact, round colonies were manually cut and scratched from the culture surface. For DMD iPSC, the colonies were kept intact, carefully detached from the culturing surface as a whole. The cell leaflets were transferred in hypoxic incubation atmosphere (5% O_2) and underwent a sequential cytokine modulation in KnockOut DMEM (Life Technologies), supplemented with 10% FBS, 1% L-glutamine, 1% PS, 1% 2-mercapthoethanol, 1% non-essential amino acids (further referred simply as culture medium). Beating cardiac clusters (BCC, Supplementary Fig. 1) were visible from day 14 and were transferred into normoxic atmosphere. After day 22, they were kept in the culture medium with 10 μg ml^{-1} ascorbic acid (Sigma Aldrich).

2.2. Microelectrode arrays cleaning and coating

Before beating CMs cluster plating, 60 channel MEAs (60MEA200/30iR-Ti/ITO, Multichannel Systems, Reutlingen, Germany) were cleaned using a 0.1% w/v solution of Tergazyme detergent (Alconox, White Plains, NY, US) in MilliQ water for at least 8 h. The culture well (i.e. the area inside the plastic ring) was then thoroughly washed with MilliQ water to remove the excess detergent. The preparation of the device was moved to a UV-sterilized clean box (Biosan, Riga, Latvia). Each MEA was placed in 100 mm sterile Petri dish (TPP, Trasadingen, Switzerland), and the MEA culture well was sterilized by filling it with 70% ethanol solution. After 30 min, the sterilizing solution was removed, the culture well on MEA was rinsed twice with 0.2 μm-filtered MilliQ water and let dry. The sensing area (i.e. the electrode array area) was then coated with 20–50 μl of 0.1 mg ml^{-1} laminin (Sigma Aldrich) and fibronectin (Sigma Aldrich) mixture, 1:1 ratio, to promote cell adhesion. The MEAs were put in a cell incubator at 37 °C, 5% CO_2, overnight. The next day, MEAs were rinsed twice with filtered MilliQ water to remove excess of adhesion factor from the surface.

2.3. BCCs plating on MEA chips

Suspended BCCs were collected and plated on MEA sensing area with 30 μl droplet of the culture medium. This amount of medium was a safe tradeoff between sample wobbling limitation and the need of hydrated environment. Samples were manually placed on top of electrode array, then put in standard cell incubator and kept in this overnight (with loosely fitted lid and additional droplets were placed separately around the well to prevent evaporation). The following day, medium

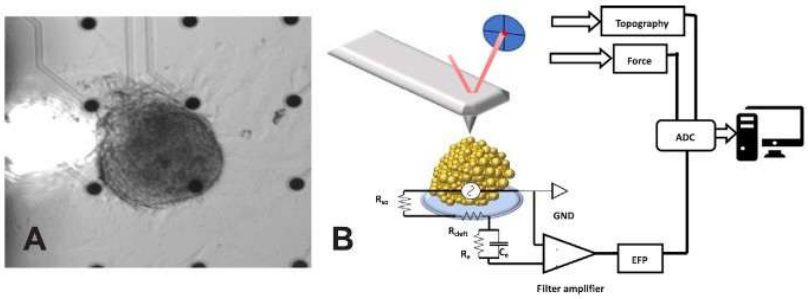

Fig. 1. Real case and schematic of the proposed electromechanical cell-based system. A) A beating cardiac cluster (BCC) placed on a microelectrode array (MEA) sensing area. The bright spot on the left side represents the AFM laser reflecting from the cantilever. Scale bar is 200 μm. B) Schematic representation of the implemented setup. The BCC acts as a periodic micro-voltage generator sensed by the planar electrode, while the AFM measures the topographical displacement and the exerted force. The synchronous acquisition is guaranteed by the common acquisition board and computer.

was gently added atop up to 1 ml. The BCCs were allowed to stabilize up to 3 days in vitro to ensure appropriate adhesion, spreading and formation of cell-electrode contacts. Fig. 1A and Supplementary Fig. 3 show typical BCCs properly placed on MEA, before beginning the experiments. Supplementary video recording presents movements of the adhered BCC clearly demonstrating the regular beating events.

2.4. Setup preparation and experimental protocols

The MEA chip containing the samples was housed in a customized holder made of an aluminum plate with adhesive heating pads and Pt100 temperature probe (RS Components, Corby, UK), and an electronic board with contacts to interface with the MEA electrodes. The electronic board was equipped with 60-channels unity-gain amplifiers to provide low impedance tracks and noise shielding. A second filtering-amplifying stage provides a pass-band of 10–3000 Hz and a total gain of 60 dB. The described holder was then fixed on the motorized stage of an inverted microscope (Olympus IX-81S1F-3, Tokyo, Japan). An AFM scanner head with 15 μm vertical range (BioAFM NanoWizard 3, JPK, Berlin, Germany) was placed above the sample. A soft silicon nitride cantilever SNL-10-D (Bruker, Billerica, MA, USA; nominal spring constant 30 pN m^{-1}) was used as nanomechanical probe to ensure stable contact without applying disruptive forces on the sample. The cantilever spring constant was calibrated before each experiment using the thermal noise method (Butt and Jaschke, 1995). A contact force of 5 nN was found optimal compromise between baseline stability and absence of visible adverse effects on the sample, as previously showed (Pesl et al., 2016a). Each experiment was performed in Tyrode solution (135 mM NaCl, 10 mM HEPES, 5.4 mM KCl, 0.9 mM $MgCl_2$, pH 7.4) supplemented with 10 mM glucose and 1.8 mM $CaCl_2$. After solution exchange, the calibrated cantilever was immersed in liquid and put in contact with the sample several times to identify the superficial center of contraction (i.e. the point with highest vertical positive displacement). Once the center of contraction was found, the drug trials started at an interval of 5 min of recording and 10 min settling time after drug administration or washout (a schematic is provided in Supplementary Fig. 4).

Calcium chloride solution was obtained in Tyrode buffer to give a stepwise increment of 1.1 mM after each addition. Isoproterenol stock solution (30 μM) was made in sterilized MilliQ water to prevent it from quenching: the selected step increment was 300 nM. Finally, Verapamil hydrochloride (Lekoptin, Lek Pharmaceuticals, Ljubljana, Slovinia) stock solutions (127.5 μM) were made in Tyrode, for a step increment of 255 nM. The added volume of drug solution never exceeded 5% of the basal volume in the MEA chip (2 ml).

2.5. Data recording and evaluation

All the presented protocols were repeated on 3 biological replicates of each cell line. Electromechanical recordings were acquired at 5 kHz sampling frequency through a LabVIEW virtual instrument and a proprietary data acquisition board PCI6071E (National Instruments, Austin, TX, USA). Fig. 1B shows a schematic of the acquisition system. Cell mechanocardiogram (MCG) comprehends the time-dependent topographical changes (i.e. the vertical displacement of the AFM piezo actuator, in μm) and the uncompensated force (in nN). The cell-cantilever contact was never lost during drug injections or medium washout. The obtained data were post-processed and analyzed using a Matlab R2016b (Natwick, MA, USA) GUI, using state of the art algorithms. From each recording, the parameters listed in Table 1 and defined in Supplementary Fig. 5 were determined. Statistical analysis was performed in Prism 5.0 (GraphPad Software, La Jolla, CA, USA) and numerical results are presented as mean ± SEM, after passing normality test. Datasets were compared for statistical significance using 1-way analysis of variance (ANOVA) with Bonferroni post-test, or repeated measures 2-way ANOVA with matching on drug concentration levels. Statistical significance was accepted with p-values below 0.05.

3. Results and discussion

3.1. Simultaneous electromechanical recording

The implemented setup allowed the simultaneous visualization, synchronous recording and coupled analysis of the electromechanical features of the cECC (Fig. 2A). The lowest observable noise level in the MEA-EP traces was 33.3 μVpp, whereas the average noise in the force and in the Z height traces were 18.3 pN and 24.5 nm respectively. Online and post-processing digital filtration allowed the analysis of

Table 1
Description of extracted parameters.

Parameter name	Description
Beating rate	Reciprocal of time distance between two adjacent events
Electro mechanical delay	Time between the electrical event and 10% of the next contraction maximum amplitude
Contraction time	Time between 10% of the peak amplitude and the peak, on the rising side
Relaxation time	Time between the event peak and the point corresponding to 10% of the peak amplitude on the falling side
Duration time	The sum of contraction and relaxation times
Average speed of contraction	Mean of the first derivative of the rising part of contraction
Time constant	Time parameter obtained by fitting the relaxation time interval with a decreasing exponential function
Force	The uncompensated force peak-to-peak during the contraction
Z height	The peak excursus of the AFM Z-piezo following the contraction

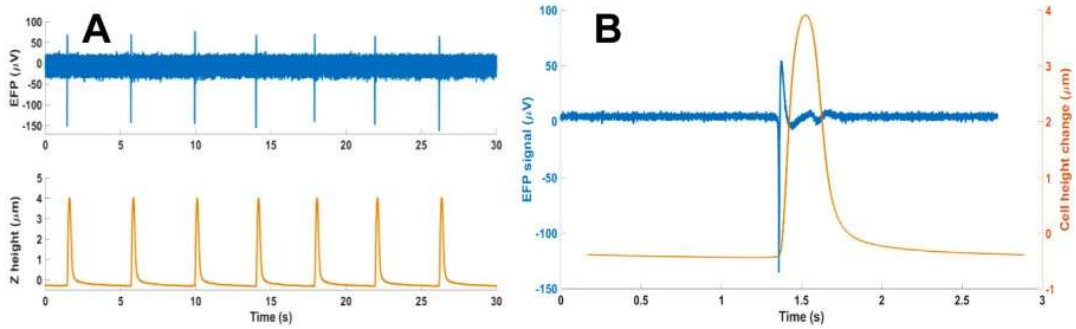

Fig. 2. Representative recording obtained with the implemented electromechanical system, and its post-processed part. A) Simultaneously and synchronously acquired extracellular field potential (top) and mechanical contraction (bottom). B) Averaged curves from the same recording; it is possible to appreciate the noise reduction due to filtering. The two traces are separated by the mean calculated delay.

EFPs with signal-to-noise ratio even close to 0 dB. Nevertheless, approximately half of the plated samples were able to produce a visible EFP trace, while mechanically beating. This issue is most probably due to scarcely-conductive coupling between the MEA planar electrodes and the BCC. Extracellular biopotentials morphology is fundamentally dependent on the conductive sample/electrode proximity and high resistance cleft (Spira and Hai, 2013). As BCC present a mixed cell population of cardiomyocytes and fibroblast-like cells (Supplementary Fig. 1A), as also previously reported (Ma et al., 2011); it is plausible that a non-conductive patch might adhere to the electrode area. In fact, fibroblast-like cells are found to be dedicated into BCC adhesion and spreading (Supplementary Fig. 2). This drawback is easily amendable, since it is possible to remove gently and re-plate BCCs in sterile conditions.

Each measurement lasted between 4 and 5 h, without any remarkable alteration of cardiac activity, if not due to drug stimulation. This can be also seen in the absence of morphological alteration between beginning and end of protocol (Supplementary Fig. 3). Although probed in not completely sterile conditions, it was found that if refilled with antibiotics-containing medium, at the end of the experiments, the samples can keep on without visible contamination up to 4 days. This is particularly useful when testing overnight or realizing several-day treatments. Such evidence shows, like previously reported, how the adopted BCC model presents an outstanding resilience. Since an applied force of 5 nN did not elicit any spontaneous change in the measured parameters, in time, one can infer that the implemented CBBs are really following alteration of cECC and not mechano-electric feedback from stretch-induced depolarization (Zhang et al., 2008).

An accurate peak detection and averaging period selection allowed the reconstruction of important physiological parameters described in Table 1, namely beating rate, contraction speed, cardiac cycle duration and, most importantly, a coupled parameter such as the electro-mechanical delay (EMD). To our best knowledge, this is the first time that such parameter is measured on 3D cardiac in vitro model. Fig. 2B shows the obtainable averaged electromechanical events, corrected by the calculated EMD.

3.2. Differential drug response and correlation analysis is indispensable to distinguish cell-type dependency of cardiac parameters

Once the feasibility and features of the implemented electromechanical CBBs were assessed, we firstly asked whether basal conditions would be sufficient to distinguish diseased and healthy hPSC derived BCC. The baseline beating frequency for all the cell lines tested was not significantly different (0.327 ± 0.023 Hz for CTRL, 0.325 ± 0.062 Hz for DORSO and 0.468 ± 0.103 Hz for DMD). The same evidence was found for other important functional parameters, such as the basal force (2.1 ± 1.9 nN for CTRL, 12.0 ± 4.7 nN for DORSO and 0.89 ± 0.46 nN for DMD) and EMD (23.0 ± 1.3 ms for CTRL, 22.0 ± 3.0 ms for DORSO and 25.6 ± 5.3 ms for DMD). Therefore, different stimulation / inhibition drug protocols were tested to validate the adopted models versus the expected cardiac response and assess the presence of cell type-dependent differences.

3.3. Calcium trials

Initially, the dependence of cardiac parameters on extracellular Ca^{2+} concentration was tested. This ion and its extracellular availability are in fact of primary importance for cECC, particularly for the hPSC-derived CMs, which possess an immature calcium handling toolkit (Keung et al., 2014) and rely mostly on membrane transport (Youm, 2016). Cell type-dependency was found by 2-way ANOVA for beating rate ($p = 0.007$), contraction duration ($p = 0.0003$), time decay ($p < 0.0001$) and EMD ($p = 0.026$). A difference close to significance was reached for the average speed of contraction ($p = 0.069$). The effect of the Ca^{2+} concentration was found significant only in relationship to the beating rate ($p < 0.0001$). All cell lines experienced a decrease in beating rate proportional to Ca^{2+} concentration. The CTRL and DORSO groups plateaued around ¾ of the basal rate (67 ± 10% and 68.6 ± 5.1%, respectively), while the DMD group decreased to 89.5 ± 3.2% of its basal rate. The beating rate phenotype of mutation-carrying cell line correlates with previously described pre-existing calcium stress impairing inward ion flux (Fanchaouy et al., 2009). This frequency decrease was paralleled by an increase of exerted force in all the cell lines (120.3 ± 9.4% for the CTRL group, 110 ± 14% for DORSO and 112 ± 19% for DMD). This phenomenon is due to the immature contractile phenotype of hPSC-derived CMs, which possess negative frequency-force relationship (Pesl et al., 2016b). The observed change of contractile events was found as an increase of the relaxation period, expressed by the decay time constant for the CTRL and DORSO groups (108.1 ± 3.5% and 110.5 ± 4.2%, respectively) and a decrease for DMD (84.3 ± 5.2%). The Ca^{2+} dependent decay time decrease in dystrophin mutation-carrying line is in correlation with previously described pre-existing calcium overload (Fanchaouy et al., 2009), which may limit the contraction dilation due to saturated sarcomere, probably resulting in limited ability of the DMD CBB to employ force imposed reaction during cluster stretch as imposed in healthy tissue by Frank Starling mechanisms. The EMD, a parameter directly connected to electromechanical coupling, did prove statistically significant for cell-type. CTRL did not show a dose-dependent relation with the Ca^{2+} concentration (109–99% variation range); DORSO showed a similar trend with only non-significant increase with respect to CTRL (142–131%), validating the CBB's robustness toward line specific variability in differentiation efficiency. Conversely, the DMD group showed a dose-dependent trend (up to 257 ± 71% of the basal delay); it is possible that increasing calcium levels are gradually

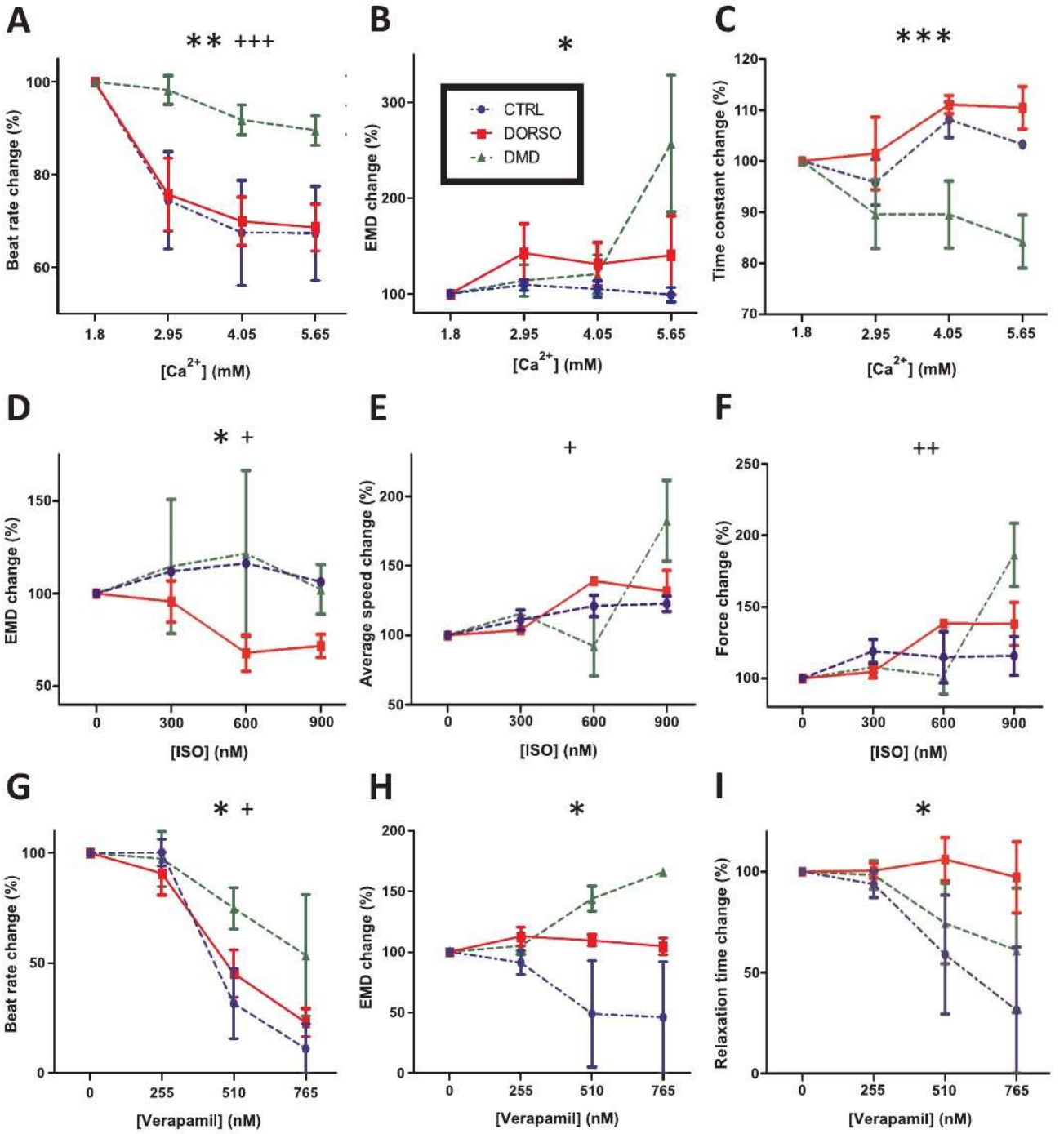

Fig. 3. Selected results of drug trials performed with the presented electrochemical cell-based biosensor. The top row (A-B-C) represents extracellular calcium concentration trials. The middle row (D-E-F) β-adrenergic stimulation trials (Isoproterenol). The bottom row (G-H-I) represent class IV antiarrhythmic / calcium channel blocker trial (Verapamil). The * symbol indicates statistically significant difference according to the beating cardiac cluster type. The + symbol indicates statistically significant difference due to the chemical concentration. One symbol indicates a p-value < 0.05, two symbols < 0.01, three symbols < 0.001. All the comparisons are carried on with repeated measurements 2-way ANOVA with row matching (drug concentration).

impairing the already elevated activity of an altered ryanodine receptor to coordinate the calcium-induced calcium release (Fauconier et al., 2010). The previous results are summarized in Fig. 3A-C.

3.4. Isoproterenol trials

The β-adrenergic stimulation was performed via increasing isoproterenol concentration to assess the ionotropic and chronotropic cell line-dependent features. Surprisingly, no extracted parameter showed significant dependency over the cell type, except for the EMD ($p = 0.0130$), which was also significantly concentration dependent ($p = 0.012$). Other concentration-dependent parameters were the average speed of contraction ($p = 0.031$) and the exerted force ($p = 0.006$), with DMD group showing marked increase at end

concentration (182 ± 29% and 186 ± 22% respectively). In contrast, DORSO experienced roughly 1/3 increase of these parameters (132 ± 15% for average speed and 138 ± 15% for force) and CTRL only 1/5 increase (122.7 ± 5.5% and 116 ± 14% respectively). Isoproterenol effect appears to have a threshold concentration between 300 and 600 nM. After this threshold, the CTRL and DMD groups slightly altered EMD (101.0 ± 6.0% and 96.6 ± 2.7%, respectively), whereas the DORSO group decreased its measured EMD to 73.0 ± 7.6% of the baseline value. This difference might be explained with better differentiation grade of dorsomorphin-treated groups, since dorsomorphin is an inhibitor of BMP signaling and promotes cardiac differentiation (Kattman et al., 2011). It is therefore plausible that an improved differentiation guarantees a better BCC syncytium, able to improve cECC timing in response to adrenergic stimulation. The notable results are shown in Fig. 3D-F. The same negative beating rate/force relationship was also noticed for all the cell lines, except when an arrhythmic behavior (e.g. multiple beating modes) was induced.

3.5. Verapamil trials

The antagonist trials were carried on L-type calcium channels to observe the reaction of different BCCs to class IV antiarrhythmics. Verapamil, as an example of this class, was shown to improve skeletal muscle force in DMD patients but led also to adverse cardiac side effect. However, no data on mechanism of such adverse effect exists (Nascimento Osorio et al., 2018). Previously, the growing CMs were coupled to RTCA impedance system, which allowed to quantify only beat rate effects of Verapamil (Wang et al., 2013). Here, the beat rate influence of drug showed to be cell type-dependent ($p = 0.019$) and dose dependent ($p = 0.001$). The EMD parameter was found to be only cell-type dependent ($p = 0.0316$), together with the relaxation time ($p = 0.030$). The measured exerted force and Z height change were found solely dose-dependent ($p = 0.015$ and $p = 0.019$ respectively). The DMD cells showed decrease in beating rate down to 53 ± 27% of baseline, compared to 11 ± 11% of CTRL and 23.0 ± 6.3% of DORSO groups. The EMD shows different trends for each cell line: for the CTRL groups, the delay drops to 46 ± 46% of the baseline; DORSO group upped to 112% of the baseline and ended the trial at 104.0 ± 7.1%; the DMD group showed an increase of 143% to finish the trial at 111 ± 55%. These distinct trends can be due to the different biological backgrounds of the BCC models: CTRL group may respond to L-type channel inhibition by referring to the inositol-3-phosphate complex, which spontaneously produces calcium influx in embryonic cardiac phenotype (Youm, 2016); dorsomorphin-treated BCC might express higher number of functional L-type calcium channels, therefore being more resilient to the same drug concentration and present delayed coupling, with stable force level. DMD samples can present calcium leaking at the membrane level (Burr and Molkentin, 2015), although cECC delay is linearly increasing, which together with the decreasing force suggests impairment of the contractile machinery (Li et al., 2014). The mentioned notable results are shown in Fig. 3G-I.

4. Conclusions

We have successfully implemented and tested the electro-mechanical cell-based biosensor for the simultaneous and synchronous probing of cardiac excitation-contraction coupling. The system allows the characterization of cardiac models through differential drug trials and sample-type discrimination. For the first time, to our knowledge, a distinctive beating-force relation was shown for Duchenne muscular dystrophy cardiac models. The bioelectromechanical parameters derived from the cardiomyocyte cluster based models provide important insights into heart pathologies and sometimes (such as in β-adrenergic stimulation assays) serve as the only discriminant between different models.

Current limitations of the systems regard the non-sterility of the measurement environment, and the localized probing of a 3D model with a single MEA electrode and AFM cantilever. The system also suffers from a substantial biological sample variability, which requires more experimental repetitions to achieve better accuracy of results; this can be overcome by suitable choice of drug treatment regimens to focus the data collection toward the desired disease phenotype. Future improvement with higher-density electrode arrays and tip-less cantilevers providing a wider surface contact should provide a higher information content and improve stability of models, respectively.

Acknowledgments

This research has been financially supported by the Ministry of Education, Youth and Sports of the Czech Republic under the project CEITEC 2020 (LQ1601) and ICRC (LQ1605), the CIISB research infrastructure project LM2015043 supported the AFM measurements at the Core Facility Nanobiotechnology, and the Grant Agency of the Czech Republic (GACR) provided support through grant no. P302/12/G157.

Conflict of interest

The authors declare no conflict of interest.

Appendix A. Supporting information

Supplementary data associated with this article can be found in the online version at doi:10.1016/j.bios.2018.10.021.

References

Acimovic, I., Vilotic, A., Pesl, M., Lacampagne, A., Dvorak, P., Rotrekl, V., Meli, A.C., 2014. Biomed. Res. Int. 2014, 512831.
Adewumi, O., Aflatoonian, B., Ahrlund-Richter, L., Amit, M., Andrews, P.W., Beighton, G., Bello, P.A., Benvenisty, N., Berry, L.S., et al., 2007. International stem cell initiative. Nat. Biotechnol. 25, 803–816.
Alonso, L., Goldmann, W.H., 2003. Life Sci. 72, 2553–2560.
Bauwens, C.L., Toms, D., Ungrin, M., 2016. J. Vis. Exp. 115, e54308.
Bers, D.M., 2002. Cardiac excitation–contraction coupling. Nature 415, 198–205.
Burr, A.R., Molkentin, J.D., 2015. Cell Death Differ. 22, 1402–1412.
Burridge, P.W., Matsa, E., Shukla, P., Lin, Z.C., Churko, J.M., Ebert, A.D., Lan, F., Diecke, S., Huber, B., Mordwinkin, N.M., Plews, J.R., Abilez, O.J., Cui, B., Gold, J.D., Wu, J.C., 2014. Nat. Methods 11, 855–860.
Butt, H.-J., Jaschke, M., 1995. Nanotechnology 6, 1–7.
Caluori, G., Pribyl, J., Cmiel, V., Pesl, M., Potocnak, T., Provaznik, I., Skladal, P., Rotrekl, V., 2018. Simultaneous study of mechanobiology and calcium dynamics on hESC-derived cardiomyocytes clusters. J. Mol. Recognit. e2760.
Cogollo, J.F.S., Tedesco, M., Martinoia, S., Raiteri, R., 2011. Biomed. Microdevice 13, 613–621.
Dell'Era, P., Benzoni, P., Crescini, E., Valle, M., Xia, E., Consiglio, A., Memo, M., 2015. World J. Stem Cells 7, 329–342.
Doevendans, P.A., Kubalak, S.W., An, R.-H., Becker, D.K., Chien, K.R., Kass, R.S., 2000. J. Mol. Cell. Cardiol. 32, 839–851.
Doppler, S.A., Deutsch, M.A., Lange, R., Krane, M., 2013. J. Thorac. Dis. 5, 683–697.
Fanchaouy, M., Polakova, E., Jung, C., Ogrodnik, J., Shirokova, N., Niggli, E., 2009. Cell Calcium 46, 114–121.
Finsterer, J., Stöllberger, C., 2003. Cardiology 99, 1–19.
Hao, J., Daleo, M.A., Murphy, C.K., Yu, P.B., Ho, J.N., Hu, J., Peterson, R.T., Hatzopoulos, A.K., Hong, C.C., 2008. PLOS One 3, e2904.
Kattman, S.J., Witty, A.D., Gagliardi, M., Dubois, N.C., Niapour, M., Hotta, A., Ellis, J., Keller, G., 2011. Cell Stem Cell 18, 228–240.
Keung, W., Boheler, K.R., Li, R.A., 2014. Stem Cell Res. Ther. 5, 17.
Kilpatrick, J.I., Revenko, I., Rodriguez, B.J., 2015. Adv. Healthc. Mater. 4, 2456–2474.
Knoll, R., Hoshijima, M., Hoffman, H.M., Person, V., Lorenzen-Schmidt, I., Bang, M.L., Hayashi, T., Shiga, N., Yasukawa, H., Schaper, W., McKenna, W., Yokoyama, M., Schork, N.J., Omens, J.H., McCulloch, A.D., Kimura, A., Gregorio, C.C., Poller, W., Schultheiss, P., Chien, K.R., 2002. Cell 111, 943–955.
Laurila, E., Ahola, A., Hyttinen, J., Aalto-Setälä, K., 2015. Biochim Biophys. Acta 1863-7B, 1864–1872.
Lian, X., Zhang, J., Azarin, S.M., Zhu, K., Hazeltine, L.B., Bao, X., Hsiao, C., Kamp, T.J., Palecek, S.P., 2012. Nat. Protoc. 8, 162–175.
Li, Y., Zhang, S., Zhang, X., Li, J., Ai, X., Zhang, L., Yu, D., Yu, D., Ge, S., Peng, Y., Chen, X., 2014. Cardiovasc. Res. 103, 60–71.
Liang, P., Lan, F., Lee, A.S., Gong, T., Sanchez-Freire, V., Wang, Y., Diecke, S., Sallam, K., Knowles, J.W., Wang, P.J., Nguyen, P.K., Bers, D.M., Robbins, R.C., Wu, J.C., 2013. Circulation 127, 1677–1691.
Liu, J., Sun, N., Bruce, M.A., Wu, J.C., Butte, M.J., 2012a. PLoS One 7, e37559.

Liu, Y., Feng, J., Shi, L., Niu, R., Sun, Q., Liu, H., Li, J., Guo, J., Zhu, J., Han, D., 2012b. Nanoscale 4, 99–102.
Ma, J., Guo, L., Fiene, S.J., Anson, B.D., Thomson, J.A., Kamp, T.J., Kolaja, K.L., Swanson, B.J., January, C.T., 2011. Am. J. Physiol. Hear. Circ. Physiol 301, H2006–H2017. https://doi.org/10.1152/ajpheart.00694.2011.
Moretti, A., Laugwitz, K.L., Dorn, T., Sinnecker, D., Mummery, C., 2013. Cold Spring Harb. Perspect. Med. 3.
Motta, B.M., Pramstaller, P.P., Hicks, A.A., Rossini, A., 2017. Stem Cells Int. 2017, 8960236.
Mummery, C.L., Zhang, J., Ng, E.S., Elliott, D.A., Elefanty, A.G., Kamp, T.J., 2012. Circ. Res. 111, 344–358.
Nascimento Osorio, A., Medina Cantillo, J., Camacho Salas, A., Madruga Garrido, M., Vilchez Padill, J.J., 2018. Neurologia. https://doi.org/10.1016/j.nrleng.2018.01.001. (In press).
Pesl, M., Acimovic, I., Pribyl, J., Hezova, R., Vilotic, A., Fauconnier, J., Vrbsky, J., Kruzliak, P., Skladal, P., Kara, T., Rotrekl, V., Lacampagne, A., Dvorak, P., Meli, A.C., Fauconnier, J., Vrbsky, J., Kruzliak, P., Skladal, P., Kara, T., Rotrekl, V., Lacampagne, A., Dvorak, P., Meli, A.C., 2013. Heart Vessels 29, 834–846.
Pesl, M., Ivana, A., Pribyl, J., Hezova, R., Vilotic, A., Aimond, F., Fauconnier, J., Vrbsky, J., Kruzliak, P., Skladal, P., Kara, T., Rotrekl, V., Lacampagne, A., Dvorak, P., Meli, A.C., 2014. Biophys. J. 106 (565A–565A).
Pesl, M., Pribyl, J., Acimovic, I., Vilotic, A.A., Jelinkova, S., Salykin, A., Lacampagne, A., Dvorak, P., Meli, A.C., Skladal, P., Rotrekl, V., 2016a. Biosens. Bioelectron. 85, 751–757.
Pesl, M., Pribyl, J., Caluori, G., Cmiel, V., Acimovic, I., Jelinkova, S., Dvorak, P., Starek, Z., Skladal, P., Rotrekl, V., 2016b. J. Mol. Recognit. 30, e2602.
Regmi, S., Jeong, J.H., 2016. Macromol. Res. 24, 1037–1046.
Rothermel, A., Kurz, R., Ruffer, M., Weigel, W., Jahnke, H.G., Sedello, A.K., Stepan, H., Faber, R., Schulze-Forster, K., Robitzki, A.A., 2005. Cell. Physiol. Biochem. 16, 51–58.
Sinnecker, D., Laugwitz, K.-L.L., Moretti, A., 2014. Pharmacol. Ther. 143, 246–252.
Spira, M.E., Hai, A., 2013. Nat. Nanotechnol. 8, 83–94.
Takeda, M., Miyagawa, S., Fukushima, S., Saito, A., Ito, E., Harada, A., Sawa, Y., 2018. Tissue Eng. C Meth. 24, 56–67.
Tzatzalos, E., Abilez, O.J., Shukla, P., Wu, J.C., 2016. Adv. Drug Deliv. Rev. 96, 234–244.
Vatta, M., Sinagra, G., Brunelli, L., Faulkner, G., 2005. J. Cardiovasc. Med. 10, 149–156.
Wang, T., Hu, N., Cao, J., Wu, J., Su, K., Wang, P., 2013. Biosens. Bioelectron. 49, 9–13.
Youm, J.B., 2016. Integr. Med. Res. 5, 3–10.
Zhang, Y., Sekar, R.B., McCulloch, A.D., Tung, L., 2008. Prog. Biophys. Mol. Biol. 97, 367–382.
Zheng, W., Thorne, N., McKew, J.C., 2013. Drug Discov. Today 18, 1067–1073.

6.3. Annex 3

DMD Pluripotent Stem Cell Derived Cardiac Cells Recapitulate *in vitro* Human Cardiac Pathophysiology

Jelinkova S, Vilotic A, Pribyl J, Aimond F, Salykin A, Acimovic I, Pesl M, Caluori G, Klimovic S, Urban T, Dobrovolna H, Soska V, Skladal P, Lacampagne A, Dvorak P, Meli AC, ***Rotrekl V***

frontiers in Bioengineering and Biotechnology

ORIGINAL RESEARCH
published: 19 June 2020
doi: 10.3389/fbioe.2020.00535

DMD Pluripotent Stem Cell Derived Cardiac Cells Recapitulate *in vitro* Human Cardiac Pathophysiology

Sarka Jelinkova[1,2], Aleksandra Vilotic[1], Jan Pribyl[3], Franck Aimond[4], Anton Salykin[1], Ivana Acimovic[1], Martin Pesl[1,2,5], Guido Caluori[2,5], Simon Klimovic[6], Tomas Urban[1], Hana Dobrovolna[7], Vladimir Soska[7,8], Petr Skladal[5,6], Alain Lacampagne[4], Petr Dvorak[1,2], Albano C. Meli[1,4†] and Vladimir Rotrekl[1,2*†]*

[1] Department of Biology, Faculty of Medicine, Masaryk University, Brno, Czechia, [2] International Clinical Research Center ICRC, St. Anne's University Hospital Brno, Brno, Czechia, [3] CEITEC, Masaryk University, Brno, Czechia, [4] PhyMedExp, University of Montpellier, INSERM, CNRS, Montpellier, France, [5] First Department of Internal Medicine—Cardioangiology, Faculty of Medicine, Masaryk University, Brno, Czechia, [6] Department of Biochemistry, Faculty of Science, Masaryk University, Brno, Czechia, [7] Department of Clinical Biochemistry, St. Anne's University Hospital of Brno, Brno, Czechia, [8] Second Clinic of Internal Medicine, Masaryk University of Brno, Brno, Czechia

OPEN ACCESS

Edited by:
Monica Boffito,
Politecnico di Torino, Italy

Reviewed by:
Monica Mattioli-Belmonte,
Marche Polytechnic University, Italy
Hannes Todt,
Medical University of Vienna, Austria

***Correspondence:**
Albano C. Meli
albano.meli@inserm.fr
Vladimir Rotrekl
vrotrekl@med.muni.cz

[†] These authors have contributed equally to this work

Specialty section:
This article was submitted to Biomaterials, a section of the journal Frontiers in Bioengineering and Biotechnology

Received: 15 December 2019
Accepted: 04 May 2020
Published: 19 June 2020

Citation:
Jelinkova S, Vilotic A, Pribyl J, Aimond F, Salykin A, Acimovic I, Pesl M, Caluori G, Klimovic S, Urban T, Dobrovolna H, Soska V, Skladal P, Lacampagne A, Dvorak P, Meli AC and Rotrekl V (2020) DMD Pluripotent Stem Cell Derived Cardiac Cells Recapitulate in vitro Human Cardiac Pathophysiology. Front. Bioeng. Biotechnol. 8:535. doi: 10.3389/fbioe.2020.00535

Duchenne muscular dystrophy (DMD) is a severe genetic disorder characterized by the lack of functional dystrophin. DMD is associated with progressive dilated cardiomyopathy, eventually leading to heart failure as the main cause of death in DMD patients. Although several molecular mechanisms leading to the DMD cardiomyocyte (DMD-CM) death were described, mostly in mouse model, no suitable human CM model was until recently available together with proper clarification of the DMD-CM phenotype and delay in cardiac symptoms manifestation. We obtained several independent dystrophin-deficient human pluripotent stem cell (hPSC) lines from DMD patients and CRISPR/Cas9-generated DMD gene mutation. We differentiated DMD-hPSC into cardiac cells (CC) creating a human DMD-CC disease model. We observed that mutation-carrying cells were less prone to differentiate into CCs. DMD-CCs demonstrated an enhanced cell death rate in time. Furthermore, ion channel expression was altered in terms of potassium (Kir2.1 overexpression) and calcium handling (dihydropyridine receptor overexpression). DMD-CCs exhibited increased time of calcium transient rising compared to aged-matched control, suggesting mishandling of calcium release. We observed mechanical impairment (hypocontractility), bradycardia, increased heart rate variability, and blunted β-adrenergic response connected with remodeling of β-adrenergic receptors expression in DMD-CCs. Overall, these results indicated that our DMD-CC models are functionally affected by dystrophin-deficiency associated and recapitulate functional defects and cardiac wasting observed in the disease. It offers an accurate tool to study human cardiomyopathy progression and test therapies *in vitro*.

Keywords: duchenne muscular dystrophy, DMD, human pluripotent stem cells, cardiomyocytes, intracellular calcium, excitation-contraction coupling, adrenergic response, cardiomyocyte death

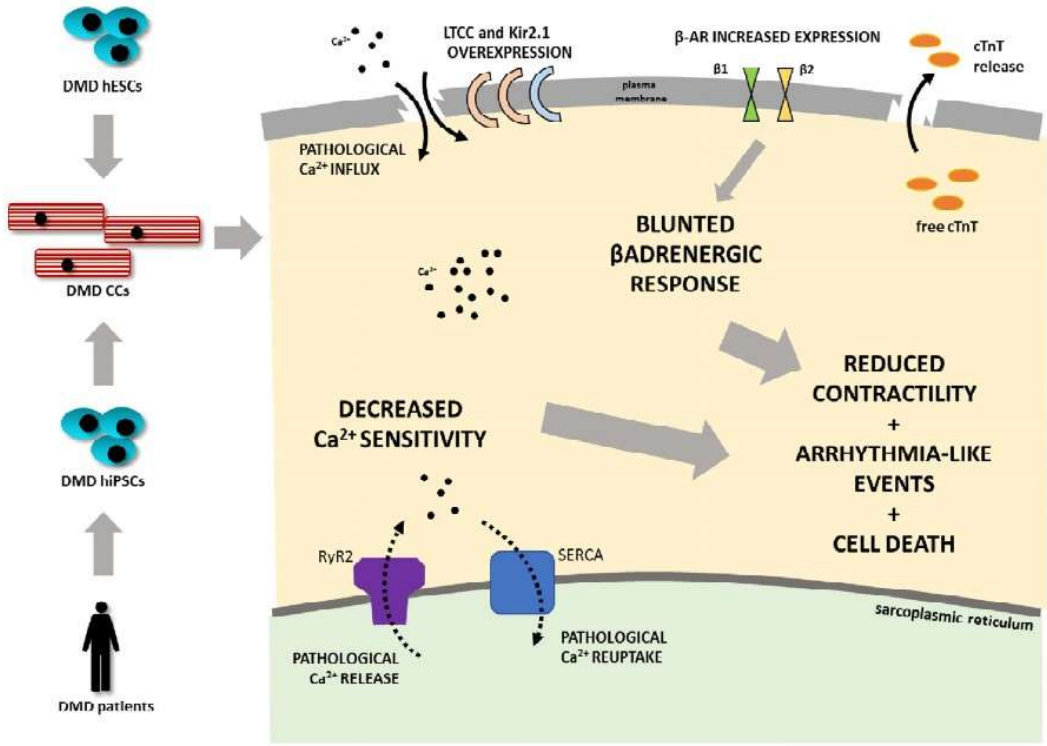

GRAPHICAL ABSTRACT | Duchenne muscular dystrophy (DMD) is associated with progressive dilated cardiomyopathy eventually leading to heart failure as the main cause of death in DMD patients. A human cardiomyocyte (CM) model was developed from several independent dystrophin-deficient human pluripotent stem cell (hPSC) lines from DMD patients and hESC line with deletion of DMD gene generated by CRISPR/Cas9 technology. DMD hPSC were differentiated into CMs. DMD mutation-carrying cells are less prone to differentiate into CMs. DMD CMs further demonstrate an enhanced cell death rate. Ion channel expression was altered in terms of potassium (Kir2.1 overexpression) and calcium handling (DHPR overexpression). DMD-CMs exhibited mishandling of calcium demonstrated by increased time of calcium release. Further mechanical impairment (hypocontractility), bradycardia, increased beat rate variability, and blunted β-adrenergic response connected with remodeling of β-adrenergic receptors' expression was found in DMD-CMs (LTCC L-type calcium channel, cTnT - cardiac troponin T, Kir2.1 - potassium channel).

Abbreviations: ACTC1, cardiac muscle alpha actin; AFM, atomic force microscopy; AP, action potential; APD, action potential duration; AR, adrenergic receptor; BMP4, bone morphogenic factor 4; CC, cardiac cell; cDMD, CRISPR/Cas9 generated DMD-hESC line; cl4, control hiPSC line; CM, cardiomyocyte; cTNT, cardiac troponin T; DAD, delayed after depolarization; DAPI, 4′,6-Diamidine-2′-phenylindole dihydrochloride; DCM, dilated cardiomyopathy; DHPR, dihydropyridine receptor; DMD, Duchenne muscular dystrophy; EB, embryonic body; ECC, excitation-contraction coupling; FGF2, fibroblast growth factor (basic, or 2); FKBP12. 6, calstabin 2; GJA1, connexin43; hESC, human embryonic stem cells; hiPSC, human induced pluripotent stem cells; hPSC, human pluripotent stem cells; IBI, inter-beat variability; ISO, isoproterenol; Kir2.1, Kir2.2, Kir2.3, potassium channels encoded by KCNJ2, KCNJ4, and KCNJ12 genes respectively; LTCC, L-type calcium channel; mdx; mdx:utr, muscular dystrophy on X chromosome, mouse model lacking dystrophin; utrophin and dystrophin lacking mouse model; mEF, mouse embryonic fibroblasts; METO, metoprolol; MYH6, myosin heavy chain α; MYH7, myosin heavy chain β; MYL2, myosin light chain 2; MYL7, myosin light chain 7; NKX2.5, NK homeobox 5; NOS, nitric oxide synthase, inducible (iNOS), neuronal (nNOS); qRT-PCR, quantitative real-time PCR; ROS, reactive oxygen species; RyR2, ryanodine receptor 2; SAC, stretch activated channels; SERCA (ATP2A), Sarcoplasmic/endoplasmic reticulum calcium ATPase 1; SR, sarcoplasmic reticulum; VEGF, vascular endothelial growth factor; WT, wild type control.

INTRODUCTION

Duchenne muscular dystrophy (DMD, prevalence 1/3,500–6,000 boys) is an X-linked genetic disorder which impairs striated muscles and results in severe disability and premature death in young men (Mah et al., 2014; Vry et al., 2016; Stehlíková et al., 2017). DMD is often associated with dilated cardiomyopathy (Manzur et al., 2008), which develops in affected patients during their teenage years. It is represented by a slowly progressing decline in diastolic function, systolic ejection fraction, and fractional shortening (Markham et al., 2006). Mechanical degeneration is associated with progressive cardiomyocyte (CM) wasting and spreading of fibrosis throughout the ventricular wall (Finsterer and Stöllberger, 2003; Panovský et al., 2019), which leads to intracardiac conduction disturbances, inducing atrial and life-threatening ventricular arrhythmias (Chenard et al., 1993; Himmrich et al., 2000). Gradual dilatation of the ventricle, thinning of the wall (Wagner et al., 2007), and consequent loss of contractility lead to repeated episodes of heart failure, which

recently became the most frequent mortality cause in DMD patients worldwide (Finsterer and Stöllberger, 2003; Fayssoil et al., 2010).

DMD is caused by mutations in the dystrophin gene (*DMD*), which can result in a total lack of functional dystrophin or presence of a truncated inactive form of the protein (Blake et al., 2002). Dystrophin plays a major role in the organization of dystrophin glycoprotein complex (Clarac et al., 2009) responsible for sarcolemmal adhesion to the basal lamina and intracellular pathway regulations. Whereas, skeletal muscle degeneration is extensively studied, the cellular mechanisms of the cardiac pathophysiology are still unclear. Available studies point out the role of oxidative stress and DMD-induced Ca^{2+} mismanagement (Williams and Allen, 2007; Jung et al., 2008; Caluori et al., 2019), with subsequent cytosolic imbalance and cell damage (Gerke et al., 2005).

In DMD (muscular dystrophy on X chromosome, *mdx)* mice, we have shown that dystrophin deficiency caused post-translational remodeling of the cardiac ryanodine receptor (RyR2) macromolecular complex, due to S-nitrosylation and Calstabin2 (FKBP12.6) depletion, which leads to intracellular diastolic Ca^{2+} leak and ventricular arrhythmias (Fauconnier et al., 2010).

Intracellular Ca^{2+} leak from the sarcoplasmic reticulum (SR) was also associated with deregulation of stretch-activated channels (SAC) though reactive oxygen species (ROS)-mediated hyperactivity (Jung et al., 2008).

Further studies in animal models showed misregulation of other ion channels such as voltage-gated Nav1.5 and L-type calcium channel (LTCC) hyperactivation (Koenig et al., 2011), as well as upregulation of inflammation-related induced nitric oxide synthase (iNOS) (Fauconnier et al., 2010; Peterson et al., 2018). Such observations remain to be validated in human DMD. Furthermore, to this day, there are only limited studies of human DMD cardiac cell (CC) models, describing some of the discrepancies eventually leading to DMD-CM damage (Eisen et al., 2019; Pioner et al., 2020). In the present study, we thus focused, for the first time, on evaluating the impact of dystrophin-deficiency on some molecular properties of the excitation-contraction coupling (ECC) and flight-or-fight response in some patient-specific DMD human pluripotent stem cell-derived cardiac cells (DMD-hPSC-CCs) as well as in CRISPR/Cas9 engineered hPSC-CCs (summarized in **Graphical abstract**).

MATERIALS AND METHODS

A wide selection of methods was used for analysis of the model starting from generation of the hPSC lines to analysis of 3D contracting clusters and dissociated CCs; thus, the methodological approach has been summarized in **Figure 1**.

Cell Lines, Cultivation, Reprogramming, and hPSC Differentiation Into Cardiomyocytes via Embryoid Bodies

Patient-specific DMD human induced pluripotent stem cell (hiPSC) lines (DMD02 and DMD03) and CRISPR/Cas9 dystrophin-deficient human embryonic stem cell (hESC) line (cDMD) were used (described in Jelinkova et al., 2019a,b). The fibroblasts of two DMD patients were derived from skin/muscle (for DMD02/DMD03, respectively) biopsies. Informed consents approved by Ethics Committee (Faculty of Medicine, Masaryk University) were signed by parents of the patients beforehand and the investigation conformed to the principles outlined in the Declaration of Helsinki.

Control human embryonic stem cell (hESC) line CCTL14 (serving as isogenic control for cDMD) as well as CCTL12 hESC line (further referred to as WT hESC) derived in Masaryk University, Brno, and previously characterized (International Stem Cell Initiative et al., 2007), were used. hiPSC control line UEFhfiPS1.4 (Qu et al., 2013) and cl.4 obtained from Majlinda Lako (NewCastle, UK) (further called WT-hiPSC) were used for comparison with DMD-hiPSC to reduce the effect of reprogramming on the CC phenotype.

All human pluripotent stem cell (hPSC) lines were routinely maintained on feeder layer of mitotically inactivated mouse embryonic fibroblasts (mEF) as previously described (Dvorak et al., 2005; Krutá et al., 2014; Jelinkova et al., 2019a).

Cardiac differentiation and eventual subsequent dissociation of hPSC-CCs were performed for confocal fluorescent intracellular Ca^{2+} measurements, patch-clamp, atomic force microscopy (AFM), and immunocytochemistry as previously described (Pesl et al., 2014) with minor modifications. Briefly, grown colonies were cut into pieces with a pipette tip and clumps were transferred into differentiating embryonic body (EB) medium (86% KnockOut Dulbecco modified eagle medium, 10% fetal bovine serum, 1% L-glutamine, 1% penicillin/streptomycin, 1% nonessential amino acids, 0,1mM 2-mercaptoethanol) with 10 ng/ml bone morphogenic protein 4 (BMP4, R&D) and 10 μg/ml ascorbic acid (Sigma Aldrich) where they formed EBs. After 2 days, the medium was changed into EB medium with 5 ng/ml basic fibroblast growth factor (FGF2, Peprotech), 10 ng/ml BMP4, 6 ng/ml Activin A (R&D) and 10 μg/ml ascorbic acid (Sigma Aldrich) and incubated for 4 days. The next 3 days consisted of EB medium supplemented with 10 ng/ml vascular endothelial growth factor (VEGF, R&D), 10 μM IWR1 (Sigma Aldrich), and 10 μg/ml ascorbic acid. The EBs were further cultivated in EB medium with 10 μg/ml ascorbic acid, 10 ng/ml VEGF, and 5 ng/ml FGF2 for 12 days with medium changed every 4 days, and then with EB medium with 10 μg/ml ascorbic acid until further analysis. The differentiation procedure was performed for 13 days in hypoxic conditions (5% oxygen). Then, the EBs were moved into normoxic conditions (20% oxygen) for further cultivation.

Immunodetection

Immunocytological analyses utilized [antibody specific against N-terminal (1:50 ICC/1:50-1:300 WB, Cat# NCL-DYSB, Leica Biosystems), and antibody specific against C-terminal (1:100 ICC/1:1000 WB, Abcam, Cat# ab15277)], for cardiac markers cardiac troponin T (cTnT; SantaCruz, Cat# sc-8121, 1:200) α-actinin (SigmaAldrich, Cat# A7180, 1:500) L-type channel (LTCC, dihydropyridine receptor DHPR alpha 2 subunit/CACNA2D1 antibody abcam, Cat# ab2864, 1:200),

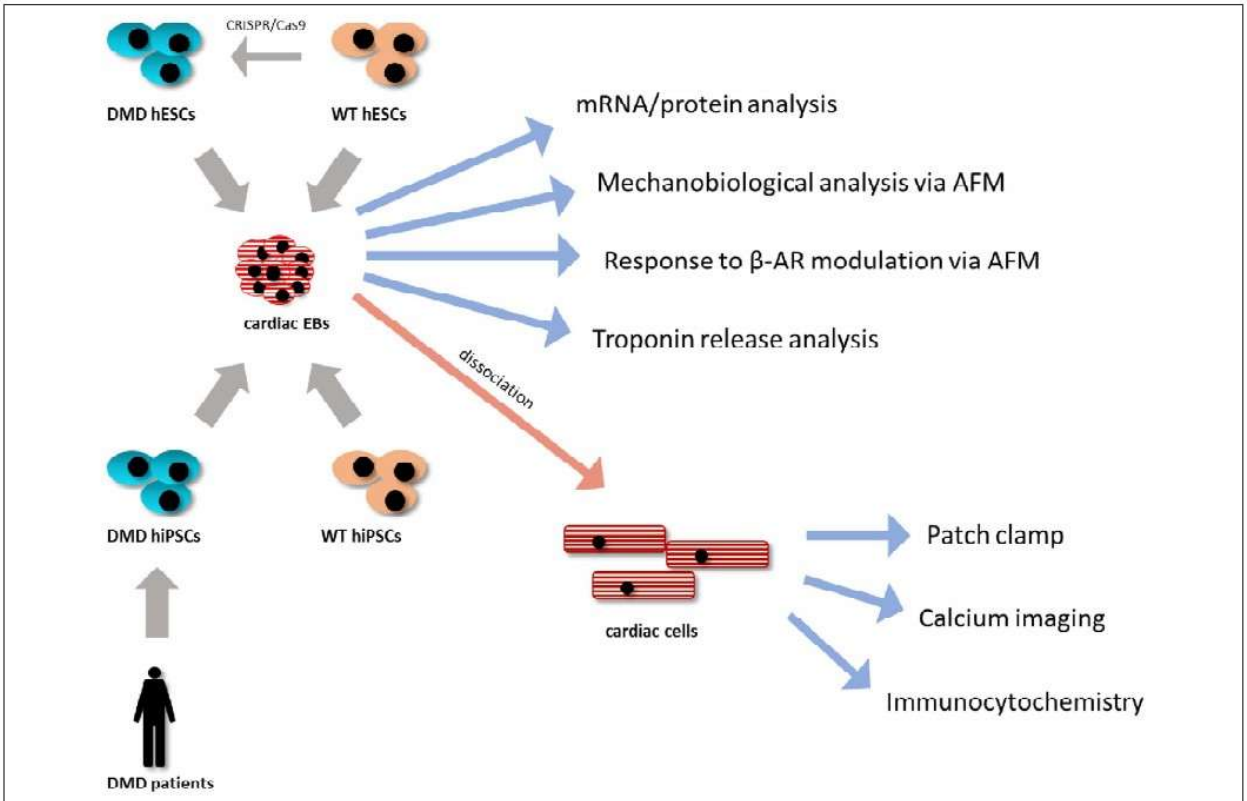

FIGURE 1 | Methodological approach. DMD-hiPSC lines from two Duchenne muscular dystrophy (DMD) patients were generated and analyzed compared to WT-hiPSC lines. DMD-hESC line was generated using CRISPR/Cas9 technology by targetted deletion of the DMD gene from a healthy WT hESC line serving as isogenic control. All hPSC lines were differentiated using 3D cell aggregates (embryonic bodies, EBs). These EBs were then used for molecular and mechanobiological analysis methods or were enzymatically dissociated into isolated cardiac cells, which were further analyzed using single cell specific analysis as protein localization and ion fluxes analyses.

assays were performed as described previously (Krutá et al., 2013). For cTnT and α-actinin, cells were fixed using 4% paraformaldehyde at room temperature for 10-15 min. Cells for dystrophin labeling were fixed with 2% paraformaldehyde for 10 min at room temperature, then with ice cold methanol for 5 min, and incubated with pre-extraction buffer (25 mM HEPES, 50 mM NaCl, 1 mM EDTA, 3 mM MgCl2, 200 mM sucrose, 0.5% Triton X-100) before continuing to blocking steps.

The cells were permeabilized and blocked with blocking solution 1 (1% bovine serum albumin, BSA, 0.2% Triton X-100 in phosphate buffer saline, PBS, 15 min on ice) and blocking solution 2 (1% BSA, 1% NaN3, 0.05% Tween 20 in PBS, 60 min on ice). Primary antibodies were diluted in PBS/Tween (0.05%) and incubated overnight at 4°C. Samples were extensively washed with PBS/Tween (0.05%) and incubated with appropriate fluorescent secondary antibody for 1 h at room temperature. For nuclear counterstain, 4′,6-Diamidine-2′-phenylindole dihydrochloride (DAPI) was used. All fluorescent and confocal microscopy experiments were performed using Confocal LSM700 microscope and processed using Zen software (both Carl Zeiss, Oberkochen, Germany).

For dystrophin immunoblots, protein samples from cell lysates were run in 4–12% gradient polyacrylamide gel for 70 min/170V/400mA, blotted at 100 V/300 mA for 2 h, and labeled with antibody against dystrophin protein. After dystrophin detection, the membrane was incubated with antibody against lamin B as loading control (1:1000, Santa Cruz, sc6217). Adrenergic receptors (AR) were analyzed using β1 specific (Thermo Fisher, PA5-28808, 1:500) and β2 specific (abcam, ab137494, 1:500) antibody. Human heart atrial tissue was obtained as procedural surplus material, available during bicaval orthotopic heart transplantation from donor organs and was used as positive control as previously described (Pesl et al., 2020).

Quantitative Real-Time PCR

Cardiac EBs 30–50 days old and human heart samples (obtained as surplus material from donor hearts during cardiac transplantations) were lysed using RNA Blue reagent (Top-Bio, Prague, Czech Republic) according to the manufacturer's instructions, and the total mRNA was isolated using the RNeasy Micro Kit (Qiagen, Hilden, Germany). RNA concentration and purity were determined using NanoDrop (NanoDrop

technologies, Wilmington, DE, USA). cDNA was synthesized by Moloney Mouse Leukemia Virus (M-MLV) reverse transcriptase (Invitrogen, Carlsbad, CA, USA) at 37°C for 1 h followed by 5 min at 85°C. For quantitative real-time PCR (qRT-PCR), LightCycler® 480 SYBR Green Master kit (Roche, Basel, Switzerland) was used according to manufacturer's instructions, and PCR was performed, with annealing temperature 60°C and 55 cycles on LightCycler LC480 Instrument (Roche). The PCR primers (Generi-Biotech, Hradec Kralove, Czech Republic) are shown in **Supplementary Table 1**.

Measurements of Intracellular Cytosolic Ca^{2+} Variations by Fluorescent Confocal Microscopy

The contracting EBs were dissociated to single CCs by incubation in Ca^{2+}-free solution [120 mM NaCl, 5.4 mM KCl, 5 mM $MgSO_4$, 5 mM sodium pyruvate, 20 mM glucose, 20 mM taurine, 10 mM HEPES (all Sigma Aldrich), pH6.9] at room temperature and enzymatically treated with 0.8 mg/ml type II collagenase (Gibco) and 0.037 mg/ml type XIV proteinase (Sigma Aldrich) in the same solution for 3 min at 37°C. The clusters were then incubated in dissociating solution (85 mM KCl, 30 mM K_2HPO_4, 5 mM $MgSO_4$, 1 mM EGTA, 5 mM sodium pyruvate, 5 mM creatine, 20 mM taurine, 20 mM glucose, 2 mM disodium pyruvate, pH = 7.4) for 20 min at 37°C and plated on gelatin coated 35 mm glass bottom culture dishes (MatTek) in EB medium until the next day. On the day of measurements, cells were incubated in a Tyrode's solution (140 mM NaCl, 5 mM HEPES, 4 mM KCl, 1 mM $MgCl_2$, 1.8 mM $CaCl_2$, 10 mM glucose, pH 7.4) with 3 μM Fluo4-AM (Invitrogen, Carlsbad, CA, USA) for 20 min at room temperature. After the incubation with Fluo4-AM, the solution was replaced with the fresh Tyrode's solution and the cells were placed on the stage of an inverted microscope. Ca^{2+} images in line-scan mode were recorded with a laser scanning confocal microscope Zeiss LSM Exciter (Carl Zeiss), with 40x water immersion objective, in x–y mode, 1 image/0.495 s. Electrical pacing was set up with frequency 0.5, 1 Hz (20 V, 0.5 ms duration and 1 ms delay). The kinetic properties of intracellular Ca^{2+} variations including Ca^{2+} transients and diastolic events were analyzed by in-house developed PeakInspector software (https://asalykin.github.io/PeakInspector/) as previously described (Acimovic et al., 2018).

Electrophysiological Recordings Through Patch-Clamp

Electrophysiological recordings were obtained using whole-cell patch-clamp technique on an Axopatch 200B (Axon Instruments, Foster City, CA) at room temperature (22–24°C). The recording pipettes contained: 120 mM KCl, 8 mM EGTA, 10 mM HEPES, 6.8 mM $MgCl_2$, 3 mM $CaCl_2$, 4 mM $ATPNa_2$, 0.4 mM $GTPNa_2$ (pH 7.2). The bath solution contained: 130 mmol/L NaCl, 4 mM/L KCl, 1.8 mM/L $MgCl_2$, 1.8 mM/L $CaCl_2$, 10 mM/L HEPES, 11 mM/L glucose (pH 7.4). Action potentials (APs) were measured in the current-clamp configuration in response to brief (1–2 ms) depolarizing current injections at 1 Hz. The resting membrane potential, the amplitude and duration (APDs) at 20, 50, and 90% repolarization of the APs were measured (respectively indicated as APD_{20}, APD_{50}, and APD_{90}). 7 DMD-hPSC-derived CCs (DMD-CCs) and 18 WT-hPSC-derived CCs (WT-CCs) were analyzed. Cells arrhythmogenicity was tested using application of successive 10 s runs in the current clamp configuration defined by 5 brief (1 ms) depolarizing current injections at 2 Hz followed by a resting period. Data were analyzed using the Clampfit 10.0 (Axon Instruments) software.

Atomic Force Microscopy Measurements

Atomic force microscope (JPK NanoWizard 3, JPK, Berlin, Germany), combined with an inverted light microscope (IX-81S1F-3, Olympus, Tokyo, Japan), was used to obtain mechanocardiograms of beating EBs as previously described (Pesl et al., 2014; Caluori et al., 2019; Pribyl et al., 2019). Drug response tests were performed after initial equilibration in Tyrode's solution, followed by addition of 70 μM metoprolol, 10 min of stabilization time, and then 10 min of measurement. Isoproterenol (1 μM) was subsequently added into the solution, and mechanocardiograms were measured after 20 min of stabilization. The mechanical properties of beating EBs were expressed as force of contraction in nN as previously described (Pesl et al., 2014); however, the values were relativized for final comparison.

Free Troponin Analysis

The EBs were formed and cardiac induction was initiated as described above. On day 18, individual EBs homogenous in size and shape were separated onto 12 well plate coated with gelatin and 1ml of proper induction medium was added. From day 21 to 51 with frequency of 4 days, medium sample was collected, spun, and the supernatant frozen in −20°C until all samples were harvested. The samples were then analyzed for free troponin T concentration using two epitopes based immunochemical system Cobas e602 (Basel, Switzerland) specifically high sensitive short turnaround time (STAT) kit Elecsys Tropo T hs STAT 100 (Roche diagnostics, Basel, Switzerland; Hess et al., 2008) according to the manufacturer's instructions.

Statistical Analysis

Statistical evaluation was carried out in GraphPad Prism 8.3 software (GraphPad Software, Inc., La Jolla, CA, USA). Available normality tests were performed for the obtained data, and Student's two-tailed *t*-test or ANOVA was used to assess statistically significant differences on normally distributed group pairs. Where normality tests failed, non-parametric tests were used. Individual statistical test used was specified in individual figure legends.

RESULTS

DMD-CCs Do Not Express Full-Length Dystrophin Protein

Three previously described patient-specific DMD-hiPSC and one CRISPR/Cas9-mediated DMD-hESC lines (Jelinkova et al., 2019a,b) were differentiated into CMs (Pesl et al., 2014). WT hESC [hESC CCTL12 (hPSCreg name MUNIe005-A, passages

15–61) and CCTL14 (hPSCreg name MUNIe007-A, passages 15–63) derived in Masaryk University, Brno, and characterized previously (International Stem Cell Initiative et al., 2007)] and WT-hiPSC [cl.4 (passages 43–84) obtained from Dr. Majlinda Lako (Newcastle University, UK) (Armstrong et al., 2010) and hfiPSC (passages 20–52) (Qu et al., 2013)] were used as controls. The obtained DMD-CCs were evaluated for dystrophin presence. The strategy for antibody detection is illustrated in **Figure 2A**. Dystrophin expression was evaluated using immunocytology with specific antibodies against high molecular weight isoform of dystrophin (antibody specific to N-terminus detecting the full-length 427 kDa isoform, **Figure 2B**, left panel), as well as shorter isoforms (antibody specific to C-terminus, which is present in various lower molecular weight dystrophin isoforms, **Figure 2B**, right panel). Dystrophin expression was observed with both antibodies in WT-CCs as membranous signal of the antibody (**Supplementary Figure 2**). No membranous/cytoplasmic protein signal was detected in any DMD-CCs (**Figure 2B**). Nuclear signal of dystrophin was detected by C-ter antibody (which can detect shorter dystrophin isoforms, most likely the Dp71 isoform), and no cytoplasmic/membranous signal was observed in CCs derived from either DMD-hPSC lines. Furthermore, western blot analysis with N-ter and C-ter antibodies showed expression of some shorter dystrophin isoforms (Dp140, Dp116, and Dp71) in the DMD cell lines, but none in the full high molecular band (Dp427) (**Figure 2C**, full membranes in **Supplementary Figure 2**).

Dystrophin Deficiency Leads to Cardiac Differentiation With Lower Yield of Spontaneously Beating EBs

Next, we aimed at characterizing the impact of dystrophin deficiency on the cardiac differentiation of hPSCs through the EB-based method as previously published (Pesl et al., 2014). We compared the yield of beating EBs upon differentiation of all DMD and WT-hPSC lines. First of all, we used the spontaneous beat in 3D EB clusters as a criterion to evaluate the cardiac differentiation success. The differentiation efficacy represented by the fraction of spontaneously beating EBs (detected at day 29 after cardiac differentiation start) was decreased in DMD-EBs compared to WT-EBs (**Figure 3A**, statistical evaluation in **Supplementary Table 2**). At the cellular level, the beating EBs from all tested cell lines contained CCs (**Figure 3B**) with striated pattern of cardiac troponin T (cTnT) and α-actinin. The differentiation efficacy was also measured in age-matched groups of DMD- and WT-EBs aged 25–29 days by qRT-PCR of well-known cardiac markers [*NKX2.5* ($p = 0.42$), myosin heavy chain α (*MYH6*, $p = 0.71$), myosin heavy chain β (*MYH7*, $p = 0.82$), myosin light chain 2 (*MYL2*, $p = 0.17$), myosin light chain 7 (*MYL7*, $p = 0.42$), ryanodine receptor 2 (*RYR2*, $p = 0.61$), cardiac muscle alpha actin (*ACTC1*, $p = 0.78$), connexin43 (*GJA1*, $p = 0.36$)], showing no significant difference in relative mRNA expression. However, a tendency for lower yield of most of the markers in the obtained DMD clusters was observed, with the exception for *MYH7* and *GJA1* (**Figure 3C**). Inward rectifier potassium channels Kir2.1, Kir2.2, and Kir2.3 were also tested (*KCNJ2*, *KCNJ4*, and *KCNJ12*, respectively) with significant increase in Kir2.1 expression ($p = 0.004$); SERCA (*ATP2A*) shows no difference in mRNA expression.

DMD-CCs Display Altered Electrophysiological Properties

Next, we tested whether dystrophin deficiency alters the cardiac electrophysiological properties and arrhythmogenicity of single hPSC-derived CCs. Action potential (AP) properties (resting membrane potential (RP), amplitude, and duration (APD) in DMD- (26–46 days old) and WT-CCs (36–41 days old) were recorded using the patch clamp technique. Age matching of the CCss was not possible in this instance due to technical reasons as only a limited number of CCs were analyzed. Both DMD- and WT-CCs mostly exhibited triangular-shaped APs with various APD90 durations ranging from 20 to 380 ms (**Figures 4A,B**) similarly to WT with measured APD90 ranging from 20 to 520 ms. More occasionally, plateau-shaped APs with longer (>300 ms) APD90 durations were observed (**Figures 4A,B**, **Supplementary Figure 7**). No significant difference was observed in RP, amplitude, and durations between DMD- ($n = 7$) and WT-CCs ($n = 18$) APs (**Figure 4B**). Occurrence of fast pacing induced delayed afterdepolarization (DAD) events was observed and quantified. No difference ($p = 0.25$) between DMD-CCs (50%; 1.2 ± 0.3 events/10 s, $n = 7$) and WT-CCs (35%; 1.9 ± 0.4 events/10 s, $n = 18$) in the occurrence of DAD was observed (**Figure 4C**).

DMD-CCs Exhibit Abnormal Intracellular Ca^{2+} Handling

Intracellular SR Ca^{2+} handling has been shown to be affected in several DMD models, in particular through RyR2 mediated Ca^{2+} leak (Andersson and Marks, 2010; Fauconnier et al., 2010; Andersson et al., 2012). Using confocal fluorescent microscopy as we previously showed in hPSC-CCs (Pesl et al., 2014; Acimovic et al., 2018), we investigated the enzymatically dissociated single cell Ca^{2+} handling in DMD and WT-CCs matched between 40 and 50 days after differentiation. We chose this age as a safe timepoint to interpret the eventual differences as prevalently caused by the DMD mutation: it is in fact reported that calcium machinery in hPSC-CCs reaches a "stationary state" between 21 and 30 days after induction (Hwang et al., 2015). We acquired intracellular Ca^{2+} transients in resting state and under physiological pacing conditions (0.5 and 1 Hz). We analyzed spontaneous frequency of calcium transients, together with their time parameters, and occurrence of secondary small diastolic calcium events possibly triggering increased automaticity.

A lower frequency was observed in the major Ca^{2+} transients in DMD- compared to WT-CCs in resting conditions (1.262 ± 1.608 Hz vs. 2.416 ± 3.441 Hz respectively, $p < 0.0001$). Ca^{2+} transient dynamics resulted altered in DMD single CCs: either in resting or in paced conditions, the time to peak, dependent on the SR Ca^{2+} release properties, was significantly elongated in dystrophin deficient cells ($p < 0.0001$, **Figure 5A**). Ca^{2+} transient

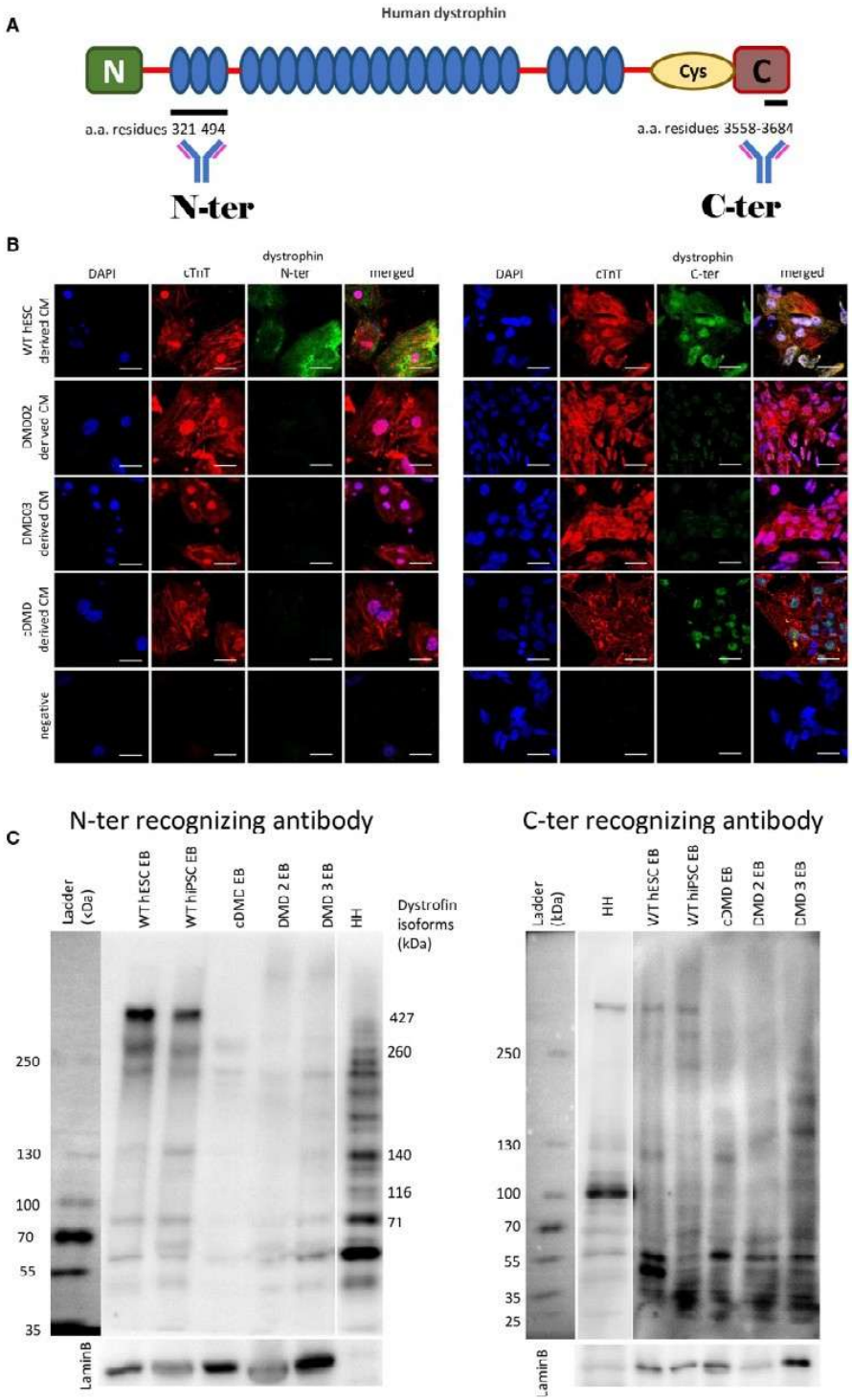

FIGURE 2 | DMD-hPSC differentiate into cardiac cells (CCs), which do not express dystrophin. **(A)** Antibodies against dystrophin N-terminal (N) aminoacid (a.a.) residues 321–494 and C-terminal aminoacid residues 3558–3684 were used. **(B)** hPSC derived CCs were analyzed for presence of dystrophin (in green). WT hESC

(Continued)

FIGURE 2 | derived CCs dissociated from spontaneously beating EBs presenting with positive signal for cardiac troponin T (red) showed positive signal for dystrophin labeled by N-terminus specific antibody as well as by C-terminus specific antibody. None of the DMD-hPSC lines (DMD02, DMD03, and cDMD) derived CCs showed any signal for dystrophin. DAPI was used for nuclear counterstain. Ruler represents 50 μm. **(C)** The differentiated EBs were lyzed and western blot analysis was performed to identify the individual isoforms expressed. Both used WT-hPSC derived EBs show expression of various dystrophin isoforms including Dp427, Dp260, Dp140, and Dp71. The CRISPR/Cas9 generated cDMD-EBs show no expression of either isoform, while only shorter isoforms were identified in patient DMD-hiPSC-EBs with promoters downstream of the patient's mutations. Human heart tissue (HH) was used as positive control. LaminB was used as loading control.

decay time, expression of the features of calcium reuptake, was increased in DMD in resting state (+59.24 ms average increase, $p = 0.013$, **Figure 5B**); this prolongation was non-significant in pacing conditions. Transient duration, which determines the contraction cycle and possible Ca^{2+}-induced arrhythmogenicity, was also elongated in DMD-CCs (**Figure 5C**; 63.53 ms in resting state, $p = 0.002$, and 71.51 ms under 0.5 Hz pacing, $p = 0.025$). These data suggest that the lack of dystrophin affects DMD-CCs during spontaneous and triggered SR Ca^{2+} release, affecting overall calcium dynamic.

We then observed and quantified the occurrence of secondary small-amplitude Ca^{2+} release events occurring after a main transient during diastole (relaxation and baseline, **Figure 5D**) and found significantly increased frequency of these events in DMD-CCs ($p = 0.0172$, **Figure 5E**).

Aberrant L-Type Voltage-Dependent Ca^{2+} Channel Expression in DMD-CCs

To further understand how dystrophin deficiency affects Ca^{2+} homeostasis and ECC in DMD-CCs, we verified the expression pattern of LTCCs using dihydropyridine receptor (DHPR) α2 subunit/CACNA2D1 antibody. At the protein level, DHPR α2 subunit expression was increased in patient-specific DMD-CCs (DMD02 and 03, **Figure 5F**). No difference was observed on the mRNA level of the CACNA1C (encoding Cav1.2) or CACNA1D (encoding Cav1.3) between the WT and DMD groups (**Figure 5G**). We then tested the cellular localization of the L-type channels using DHPR immunostaining. In line with previous protein analysis, DMD-CCs (detected by cTnT labeling) showed stronger signal of the LTCC, and no other difference was detected (**Figure 5H**).

DMD-EBs Display Hypocontractility, Bradycardia, and Higher Heart Rate Variability

DMD-associated dilated cardiomyopathies is characterized by thinner left ventricle, reduced cardiac output, and hypo-contractility of the heart (Hajjar et al., 1993; Bondue et al., 2018; Amedro et al., 2019). We thus tested whether DMD-CCs contained in 3D cardiac clusters (EBs) exhibit weaker contractile properties by measuring the contraction force and beat rate by AFM as we previously published (Pesl et al., 2014, 2016; Acimovic et al., 2018). We observed weaker spontaneous contraction force in DMD-EBs (**Figure 6A**, $p < 0.0001$) while they exhibited similar overall beat rate compared to WT-EBs (**Figure 6B**, $p = 0.139$; for separate data of each line, see **Supplementary Figure 6**). We noticed a peculiar variability in the inter-beat interval (IBI, **Figure 6C**, $p = 0.0039$) (examples of AFM curves are shown in **Supplementary Figure 6A**) across the different samples. While WT-EBs showed consistent IBI with few exceptions, DMD-EBs showed high heterogeneity (**Figure 6C**, **Supplementary Figures 5B–D**). We observed not only different variability in recorded IBI but also prevalence in shorter IBI in WT-EBs compared to DMD-EBs (1 ± 1.0 s, and 0.96 ± 0.35 s for WT-hESC- and hiPSC-EBs respectively, $2.4 \pm 1{,}6$ s for DMD02-EBs, 2.1 ± 1.2 s for DMD03-EBs and 1.9 ± 1.2 s for cDMD-EBs, p-values in **Supplementary Table 3**) (**Figures 6D–G**).

Moreover, DMD-EBs displayed more dispersed IBI scatter plot and histogram than WT-EBs (**Figures 6H,I**). Using representative Poincaré plots, a quantitative measure of the evolvement in time of the IBI, we found more scattered inter-contraction pattern in DMD-EBs compared to WT-EBs (**Figures 6J,K**) showing a higher beat rate variability.

Loss of Dystrophin Leads to β-Adrenergic Remodeling and Cardiomyocyte Wasting

Dystrophin-deficient mouse CMs have been shown to display aberrant response to β-AR stimulation (Li et al., 2014). Thus, we evaluated the β-adrenergic response in DMD-EBs to investigate the effect of stress. We monitored the mechanobiological properties of the contracting clusters upon a selective β1-AR inhibitor (metoprolol, METO) followed by a non-selective β-AR activator (isoproterenol, ISO). In presence of METO, the WT-hPSC-EBs exhibited a significant decrease in contraction force ($p = 0.0042$ for WT hESC, $p = 0.0156$ for WT-hiPSC) and beat rate ($p = 0.0051$ for WT hESC, **Figures 7A,B**). DMD-hiPSC-EBs showed no response in beat rate nor contraction force to modulation by ISO nor METO. cDMD-EBs showed a response in contraction force to METO application similarly to its isogenic control ($p = 0.0003$ for contraction force and $p = 0.103$ for beat rate). WT-EBs responded to subsequent β-adrenergic stimulation by ISO application (partially competing with METO) through marginally significant increase in relative contraction force ($p = 0.0596$ for WT hESC, $p = 0.03$ for WT hiPSC, **Figure 7A**), DMD-EBs did not show statistically significant responses to ISO nor METO. cDMD-hESC line, however, responded similarly to its isogenic WT control in contraction force increase (with significant change in response to modulation, $p = 0.0039$). The pharmacokinetic answer to ISO has been additionally tested by exclusion of METO response using division of Tyrode and ISO value still showing response in WT-EBs ($p = 0.0021$) with no significant change in DMD-EBs ($p = 0.1309$) (as shown in **Supplementary Figure 4C**).

These mechanobiological data suggest that the DMD-EBs exhibit much weaker response to stress conditions in presence of β-AR modulation. Thus, we compared the expression of the β1, β2, and β3 AR at the protein level between DMD- and

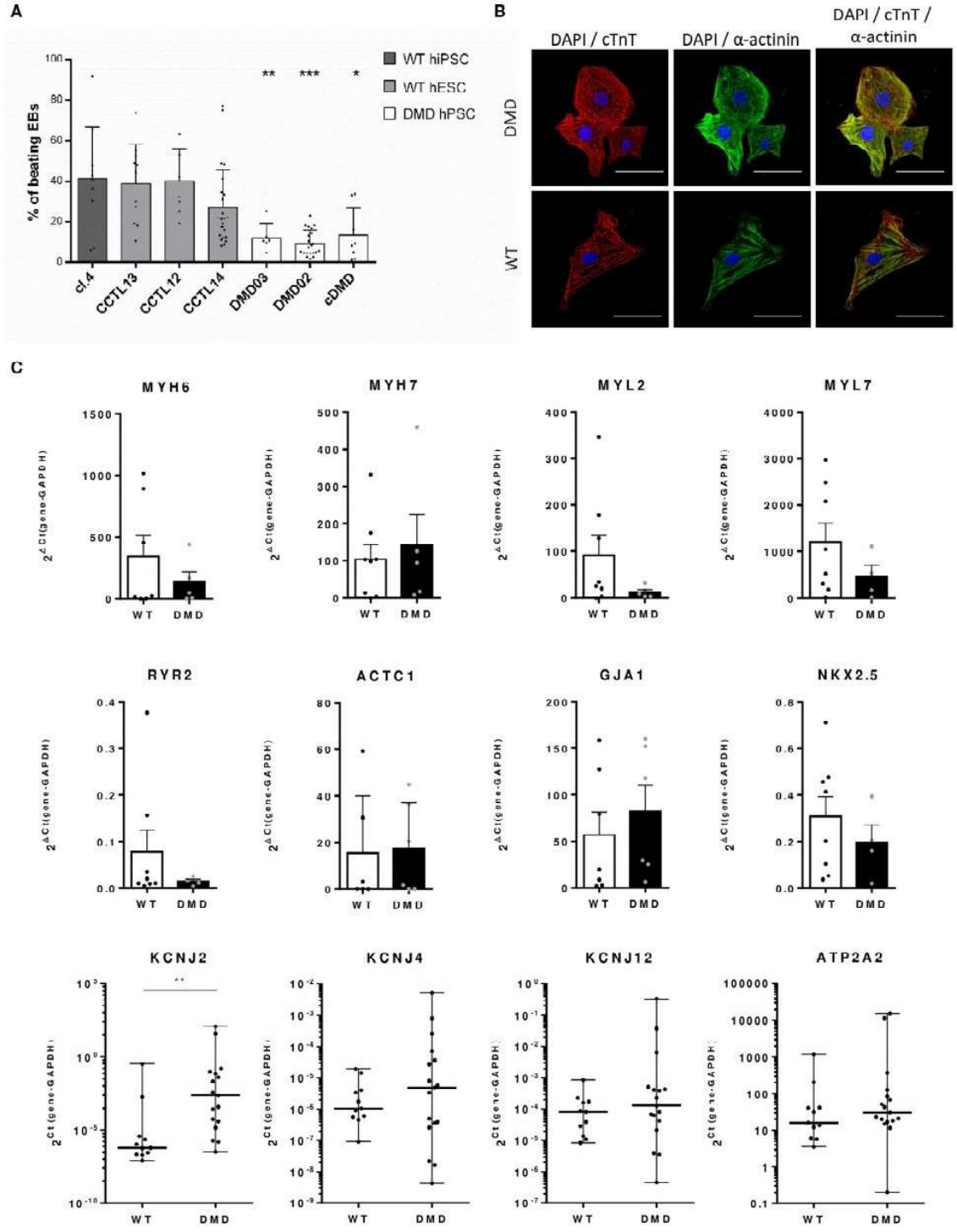

FIGURE 3 | Differentiation efficacy is lower in DMD-hPSC lines. **(A)** All DMD-hPSC and WT-hPSC lines were differentiated into spontaneously contracting EBs containing cardiomyocytes and cardiac cells. The ratio of these spontaneously contracting clusters was evaluated and compared to wild-type (WT) controls ($n = 36$

(Continued)

FIGURE 3 | for CCTL14 EBs, $n = 8$ for CCTL12 EBs, $n = 13$ for CCTL13, $n = 12$ for cl.4 EBs, $n = 25$ for DMD02 EBs, $n = 6$ for DMD03 EBs, $n = 19$ for cDMD-EBs). Lesser yields of beating EBs were identified in all DMD-hPSC lines. Statistical difference was calculated by one-way ANOVA and multiple comparison with Dunn's test. Significance ($^*p < 0.05$, $^{**}p < 0.01$, $^{***}p < 0.01$) is visualized as asterisks for the lowest values; for individual p-values, see **Supplementary Table 1. (B)** EBs were dissociated and cells labeled for cardiac markers α-actinin (in green) and cardiac troponin T (cTnT, in red) (DAPI is labeling the nuclei). WT and DMD-CCs presented similar level of typical striated pattern of sarcomeres. Line represents 50 μm. **(C)** Differentiation efficacy was evaluated by rt qPCR on mRNA levels of cardiac markers showing only non-significant differences in expression of various markers (MYH6, $n = 7$ for WT and $n = 5$ for DMD; MYL2, $n = 8$ for WT and $n = 4$ for DMD; MYL7, $n = 8$ for WT and $n = 4$ for DMD; RYR2, $n = 8$ for WT and $n = 4$ for DMD; ACTC1 $n = 6$ for WT and $n = 5$ for DMD; NKX2.5, $n = 8$ for WT and $n = 4$ for DMD, ATP2A2, $n = 11$ for WT and $n = 17$ for DMD) and non-significant increase in MYH7 ($n = 8$ for WT and $n = 5$ for DMD) and GJA1 ($n = 7$ for WT and $n = 6$ for DMD). Potassium channels were analyzed using Kir2.x isoforms mRNA expression (KCNJ2 – Kir2.1, KCNJ4 – Kir2.2 and KCNJ12 – Kir2.3, for all $n = 11$ for WT and $n = 17$ for DMD). Statistical significance on pooled DMD and pooled WT data sets was calculated using Mann–Whitney test; exact value for each is represented by • in each graph.

WT-EBs. While DMD-EBs derived from patient hiPSC showed increased β1 ($p = 0.0103$) and β2 AR expression ($p = 0.0162$) compared to isogenic WT-EBs, cDMD-EBs show similar or lower expression of both (**Figures 7C–E**). β3 expression was analyzed by quantitative rt qPCR showing no significant differences in between WT- and DMD-EBs (**Supplementary Figure 4D**).

A pathological overexpression of β-AR together with the blunted drug response and hypocontractility above described lead us to ask whether our derived CCs are already undergoing complex changes leading to their death, with consequential depletion and mechanical function deterioration in our 3D model. Thus, CC death was quantified, over time after differentiation, via cTnT concentration in the culture medium, originating from the dying CCs in the EBs. DMD lines showed from day 35 a significantly increased free cTnT level in their medium, compared to WT samples (**Figure 7F**, statistical evaluation in **Supplementary Table 4**). Interestingly, the DMD-EB kept beating even late after cardiac induction, even over the observed increased CM death (**Supplementary Video 1**).

DISCUSSION

Dilated cardiomyopathy, ultimately leading to heart failure, is the most common outcome in patients with dystrophin mutations (Kamdar and Garry, 2016; Papa et al., 2017), and it develops in DMD patients due to muscle wasting, but remains mostly unexplained in its dynamics. The DMD (*mdx*) mouse model has critical limitations since it develops only mild symptoms of heart failure with slow progression and unaffected lifespan compared to control mice (Carnwath and Shotton, 1987; Coulton et al., 1988; Shirokova and Niggli, 2013). In the present study, we provided a detailed description of patient-specific hiPSC-CCs and CRISPR/Cas9 engineered hESC-CCs. DMD-CC exhibited several molecular and functional abnormalities including an altered Ca^{2+} handling, irregular bradycardic beating, hypocontractility, and remodeling processes such as βAR alteration and CMs wasting. Our evidences on the alteration of ECC are in agreement with symptoms described in DMD patients.

Our results showed that dystrophin deficiency leads to lower efficacy in differentiating hPSCs into CCs. Interestingly, DMD-CCs exhibited a similar relative expression of known cardiac markers, and with trending increased Connexin 43 expression, similarly observed in *mdx* and *mdx:utr* CMs as a remodeling mechanism following functional dystrophin absence, with potential fatal arrhythmias in presence of β adrenergic stimulation (Patrick Gonzalez et al., 2015). Lower differentiation efficacy can point to cell fate errors: these can result from increased DNA damage caused by deregulated NOS activity (Jelinkova et al., 2019a). This process can lead to loss of stemness both at the commitment and self-renewal level (Rossi et al., 2007; Inomata et al., 2009). DNA damage can also affect multipotent stem cells division, rendering muscular differentiation ineffective (Dumont et al., 2015). Dystrophin loss was recently associated, in advanced CM *in vitro* models, with delayed contractile machinery formation, suggesting a mutation-derived impairment even at the latest stage of CM development (Pioner et al., 2020).

Then, we inquired whether and to what extent the mutation affected the single cell and EB ECC. We measured the electrophysiological properties and found similar AP features between DMD- and WT-CCs. While most of the recorded AP displayed atrial-like AP properties, our results suggested that dystrophin deficiency does not alter the electrophysiological properties of the derived hPSC-CCs. The AP durations we obtained indicate mixed population of various type of excitable cells from ventricular-like CMs (APD90 $\geq$ 300 ms), through atrial- and nodal-like CMs (APD90 $\geq$ 160 ms) and undefined/immature cardiomyocyte-like cells (APD90 $<$ 100 ms) similarly to what others previously found (He et al., 2003; Zhu et al., 2016). Nevertheless, a significant increase of Kir2.1 mRNA expression level point to a possible alteration of APD, which results in reduced effective refractory period during diastole *in vivo*. Furthermore, regarding the voltage-gated ion channels expression, DMD-CCs exhibited increased expression of DHPRα subunit of L-type Ca^{2+} channels but no difference in Cav1.2 and Cav1.3 isoform expression. L-type Ca^{2+} channels presenting gain-of-function mechanism was reported in dystrophic hearts (Koenig et al., 2014). In a recently published work (Eisen et al., 2019), it was shown that prolongation of APD in DMD-CMs was caused by increased $I_{Ca,L}$ density, which can be matched to prolonged diastole in DMD patients (Panovský et al., 2019). APD alterations, both at the potassium and calcium current levels, can lead to ventricular tachycardia (Choi et al., 2002; McNally et al., 2015), or premature ventricular beats, possibly degenerating into Torsades-de-Pointes ventricular fibrillations (Weiss et al., 2010).

Correlated with the mentioned calcium channels alterations, we measured the intracellular Ca^{2+} transients on dissociated CCs and observed a reduced spontaneous firing in DMD-CCs, with a significantly higher occurrence of small Ca^{2+} events in diastolic phase. For Ca^{2+} dynamics, DMD-CCs presented

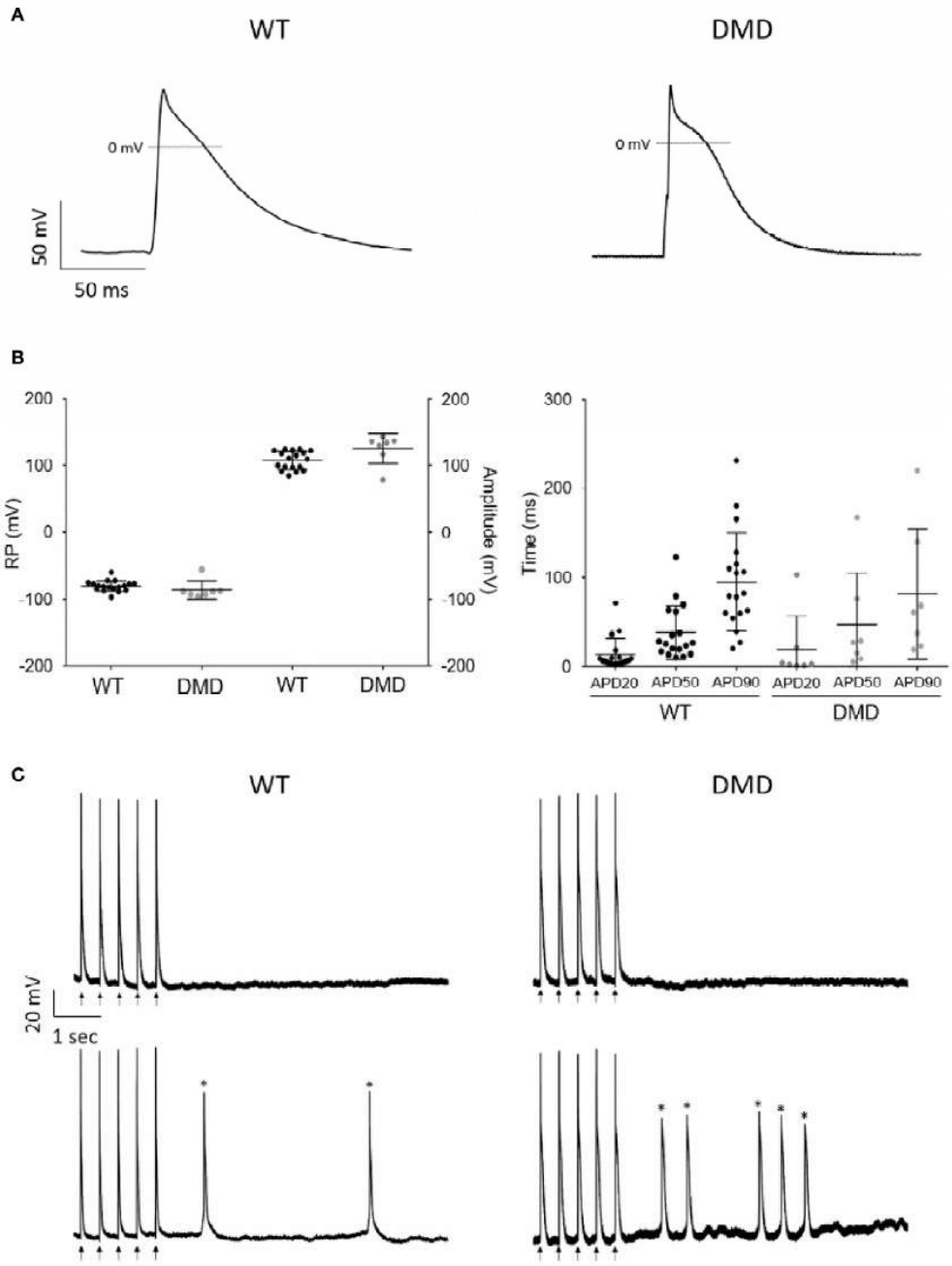

FIGURE 4 | AP recordings showed no difference in WT and DMD-CCs. **(A)** Representative AP recordings obtained from WT and DMD-hiPSC derived CCs, under current clamp configuration. **(B)** Scatter plot of RP (mV) and amplitude (mV) (left) and APD 20, 50, and 90 durations (right) of WT ($n = 18$) and DMD ($n = 7$) hPSC-CCs are represented. No significant difference was observed among these parameters between WT and DMD-hPSC-CCs. Exact n value for each is represented by • in each graph. Mean ± SEM are represented. **(C)** Representative arrhythmic events recorded in WT-CCs (left) and DMD-CCs (right). Upper panels show representative recordings of non-arrhythmogenic cells from WT-CCs and DMD-CCs and bottom panels show representative recordings of arrhythmogenic cells showing extra events, such as DAD (Asterisks).

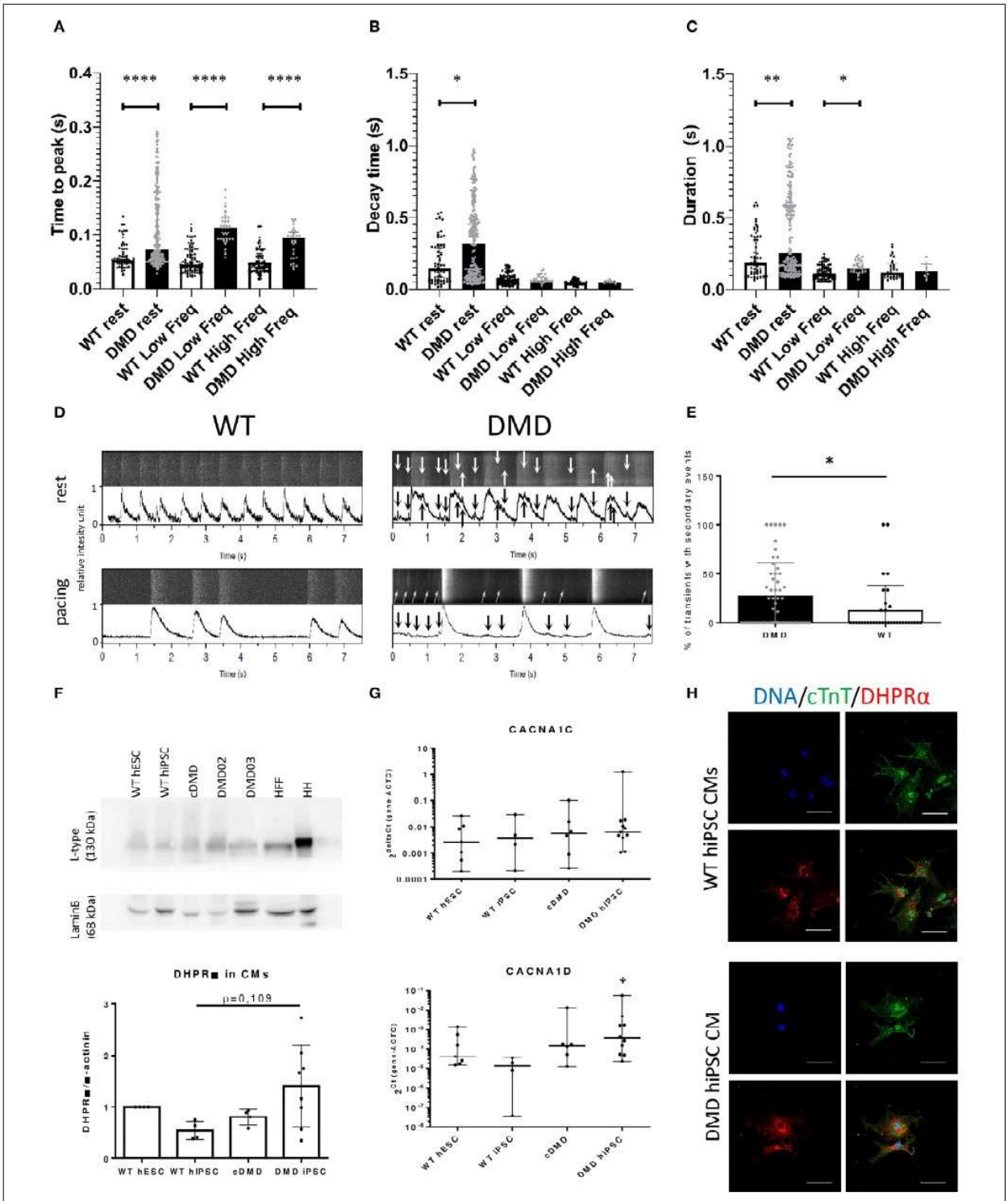

FIGURE 5 | The dynamics of Ca^{2+} release and re-pumping is affected by dystrophin deficiency. Release of Ca^{2+} transients was measured using Fluo4 dyes in enzymatically dissociated DMD (91 cells and $n = 278$ transients were analyzed for resting conditions; 20 cells and $n = 83$ transients were analyzed for low frequency

(Continued)

FIGURE 5 | paced at 0.5 Hz) and WT-CCs (30 cells and $n = 262$ transients were analyzed for resting conditions; 15 cells and $n = 128$ transients were analyzed for low frequency paced at 0.5 Hz) in the age 40–50 days of differentiation. **(A)** Time to peak, **(B)** decay time, and **(C)** contraction duration time were analyzed for the main Ca^{2+} transients. The DMD-CMs showed significantly higher Ca^{2+} amplitude and longer time to release and repump/extrude the Ca^{2+} back into the SR/out of the cell in comparison to WT. The exact values are plotted in the graphs; red line represents the median. Significance (*$p < 0.05$) is visualized as asterisks as calculated by Mann–Whitney one-sided test (*$p < 0.05$, **$p < 0.01$, ****$p < 0.0001$). The Ca^{2+} leakage is demonstrated by Ca^{2+} events of low-amplitude (arrows) among the main Ca^{2+} transients [**D**—the obtained data from microscope with line scanning (upper bar) and transferred into peak graph by PeakInspector (lower bar) with and without electrical pacing of 0.5 Hz]. The occurrence of these small events is increased in DMD-CCs transients **(E)** as analyzed by Mann–Whitney test ($n = 54$ and $n = 35$ analyzed cells, for DMD and WT, respectively). **(F)** L-type channel (DHPR subunit) expression was characterized, showing non-significant increase in protein expression in DMD-hiPSC compared to WT-EBs as calculated by one-way ANOVA ($n = 4$, $n = 4$, $n = 4$ and $n = 8$ for WT hESC, WT-hiPSC, cDMD, and DMD-hiPSC-EBs). HH was used as positive control, HFF (human foreskin fibroblasts) as non-CM cell sample. **(G)** CaV isoform's (CACNA1C and CACNA1D) mRNA expression of LTCC subunits were analyzed using rt qPCR showing no difference between the groups. The values were calculated for CMs using ACTC for normalization. At least three biological repetitions were used for the analysis with exact value for each represented by • in the graph. Statistical difference was calculated using one-way ANOVA. **(H)** ICC analysis showed stronger signal for LTCC (in red) in DMD-hiPSC CCs recognized by cTnT labeling (in green). Line represents 50 μm.

prolonged rising time under resting and paced conditions with high variability. The Ca^{2+} transient decay time mean was significantly longer in resting conditions for DMD-CCs, even if this difference was abolished during pacing. This led to a measured prolonged duration of the transients, except under the 1 Hz physiological pacing.

Altered Ca^{2+} transients dynamics correlate with cellular alteration of ECC, as previously shown in our work and others (Sato et al., 2007; Caluori et al., 2019; Pioner et al., 2020). In particular, longer rising time might be correlated to a state of calcium overload, derived from sarcolemmal tears (Danialou et al., 2001) and SR leakage by remodeling of RyR2 by S-nitrosylation (Fauconnier et al., 2010; Oda et al., 2015) or loss of the closed-state stabilizer calstabin2 (Fauconnier et al., 2010). RyR2 misregulation can explain also that the presence of small Ca^{2+} amplitude events by random firing is a state of overload. Prolonged cytosolic Ca^{2+}, as expressed by increased duration of the transients, can contribute to arrhythmic events via inverse Na^{+}-Ca^{2+}-exchange activation (Voigt et al., 2012) and electromechanical dissociation. However, it should be noted that young DMD boys rarely exhibit arrhythmias (Villa Chet et al., 2015). We performed patch-clamp experiments and observed no difference in the number of arrhythmic events in WT- and DMD-CCs. In our previous work, we have shown how DMD-EBs are insensitive to positive chronotropic effect of high extracellular Ca^{2+} concentration, most likely due to low diffusion gradients in case of constant cytosolic overload (Caluori et al., 2019). Nevertheless, WT-EBs tolerated high levels of extracellular Ca^{2+} by modulating their contractile activity, while DMD-EBs presented an increased and erratic electromechanical coupling delay, together with an increased calcium reuptake time. In accordance with the presented evidences, we have previously shown how DMD-EBs are less sensitive to Verapamil L-type channels inhibition.

From the single cell electrochemical experiments, and previous results in the DMD-EB electromechanical alterations, we focused on the study of 3D mechanical behavior and its modulation. EBs showed that the overall spontaneous beat rate of WT and DMD groups did not differ at rest. However, we identified an increased heart rate variability though IBI analysis and its time-dependent correlation, similarly to Eisen et al.'s observations (Eisen et al., 2019), which also showed high heterogeneity in beat rate variability in dissociated DMD-hiPSC-CCs. Heart rate variability via L-type inactivation can be increased and even become pro-arrhythmogenic in case of spontaneous SR leakage (Johnson et al., 2013), a condition proven in the case of DMD models. The measured contraction force in DMD-EBs was significantly lowered compared to WT-EBs, as previously shown in single cell models (Pioner et al., 2020) and correlated to the ejection fraction decrease in reported patient's hearts (Corrado et al., 2002; Villa Chet et al., 2015; Panovský et al., 2019). Both lower contraction force and arrhythmic events occur in DMD patient's heart from a very young age and before dilated cardiomyopathy onset. In fact, 25% of pediatric DMD patients under 10 years old already showed decreased ejection fraction and have developed sinus tachycardia (Sadek et al., 2017). Overall, our model presents functional alterations of an early-stage cardiac manifestation of DMD.

For the first time, we further evaluated the ECC modulation abilities by pharmacological response in DMD-CCs through the β-AR response. We found an impaired response in DMD-EBs through lack of contraction force and beat rate modulation similarly to *mdx* hearts (Meyers et al., 2019). Our data showed visible changes in contraction force and beat rate in WT-EBs in the presence of isoproterenol (non-selective β adrenergic agonist) or metoprolol (β1 receptor inhibitor) but no change of both parameters in DMD-EBs. Surprisingly, the CRISPR/Cas9-induced cDMD-EBs reacted to β adrenergic modulation similarly to WT-EBs. The response might involve an unknown compensatory mechanism proper of the engineered line. As further confirmation, cDMD-CCs presented similar levels of β-AR with respect to its isogenic hESC-derived WT-CCs. In contrast, patient-specific DMD-EBs showed an increased expression in β1 and β2 receptors compared to WT-EBs. It has been previously shown that *mdx* CMs present lowered density of β1-AR (Li et al., 2014) with blunted β-adrenergic signaling pathway (Lu and Hoey, 2000; Li et al., 2014). Here, patient-specific DMD-CCs showed increased protein expression level of both, still with blunted response to adrenergic modulation.

That is also similar to non-DMD heart failure, where β1 overexpression is quite common (Engelhardt et al., 1999); trying to compensate for the weak contractility of the organ and the overactivation of the receptors then leads to receptor dysfunction in signaling, thus their insensitivity (Bristow et al., 1982; Rengo et al., 2009; de Lucia et al., 2018). The impaired contraction

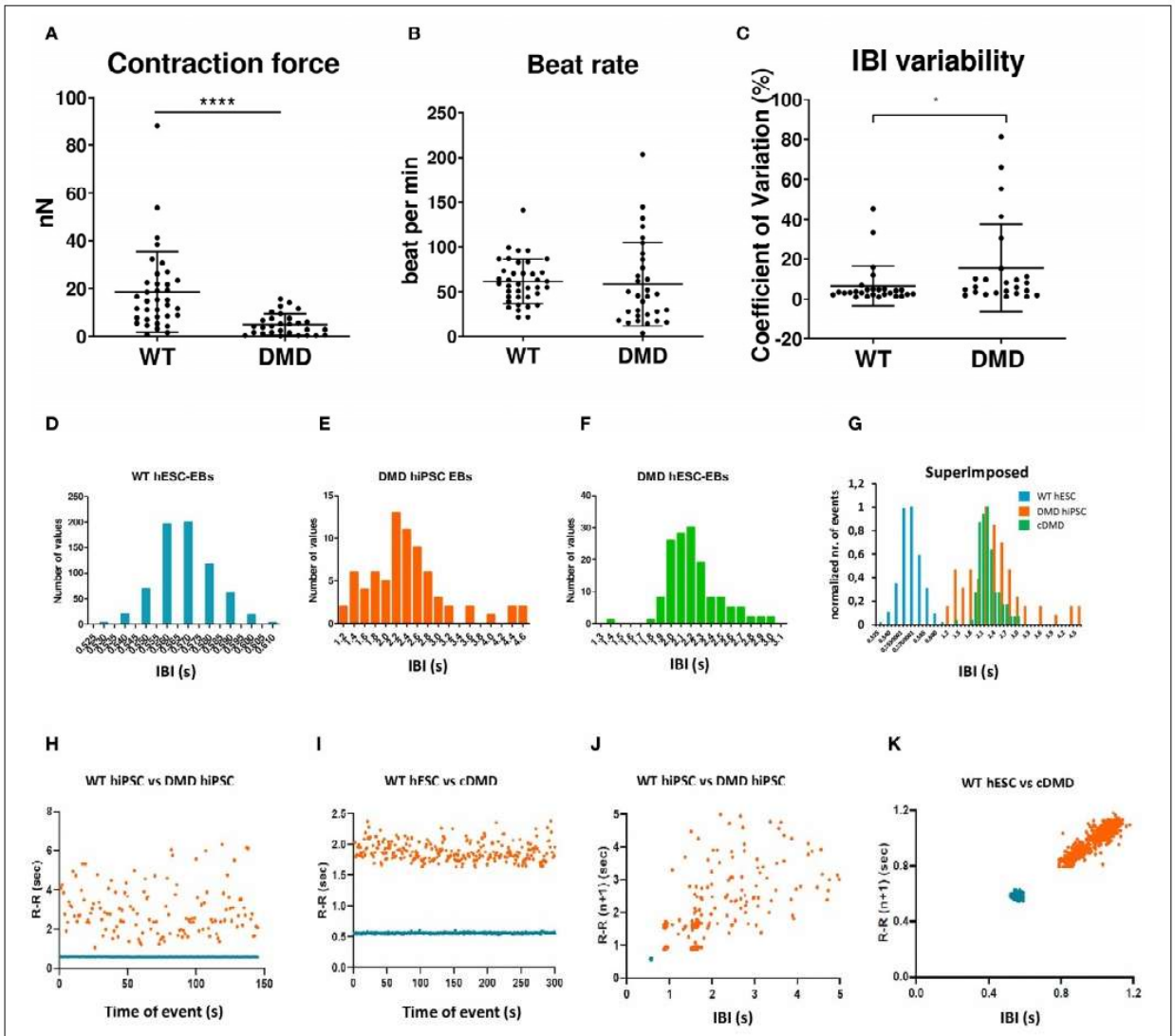

FIGURE 6 | The spontaneously contracting EBs lacking dystrophin showed weaker contraction force and signs of arrhythmias. The EBs were analyzed by AFM-based methods. **(A,B)** Contraction force is decreased in DMD-hPSC derived EBs ($n = 36$ for WT, $n = 29$ for DMD-EBs), beat rate is not affected by DMD mutation ($n = 38$ for WT, $n = 31$ for DMD-EBs). The statistical difference was calculated by Mann-Whitney test ($^*p < 0.05$, $^{****}p < 0.0001$). At least five biological repetitions were used in each differentiated line; exact value for each is represented by • in each graph. Beat rate variability was identified in DMD-EBs. Graph shows coefficient of variation analysis **(C)** of pooled control and DMD groups. The data were cleaned of outliers by ROUT test ($q = 1\%$), and normality was tested by available tests showing non-normal distribution. Statistical difference was calculated using Mann–Whitney test. Representative IBI histograms of control (**D**, $n = 712$ peaks of the representative EB analyzed), DMD-hiPSC (**E**, $n = 76$ peaks of the representative EB analyzed), and DMD-hESC (**F**, $n = 165$ peaks of the representative EB analyzed) EBs and superimposed example of all three groups with normalized values **(G)**. Superimposed representative inter-beat-interval (IBI) scatter plots of control hiPSC with DMD-hiPSC-EBs ($n = 145$ time points for each EB) **(H)** and control hESC with DMD-hESC-EBs ($n = 334$ time points for each EB) **(I)**. Superimposed Poincaré plots of control hiPSC with DMD-hiPSC-EBs (**J**, same representative EBs as in **H**) and control hESC with DMD-hESC-EBs (**K**, same representative EBs as in **I**).

force observed in DMD-EBs can also be caused by β3 inhibitory function (Skeberdis, 2004). β3 normally acts as β-adrenergic break, but has been also shown to temper with mechanical properties of skeletal muscle together with nNOS expression increase leading to elevated ROS production (Puzzo et al., 2016). However, our results indicated that β3 expression was unchanged in DMD-CCs although we cannot exclude difference in β3 cellular distribution. The use of β-AR modulators has been shown to be challenging in management of cardiomyopathy in DMD patients due to severe hypotension events (McNally et al., 2015). Investigations using β blockers in DMD cardiomyopathy have turned up mixed results, with some studies demonstrating a

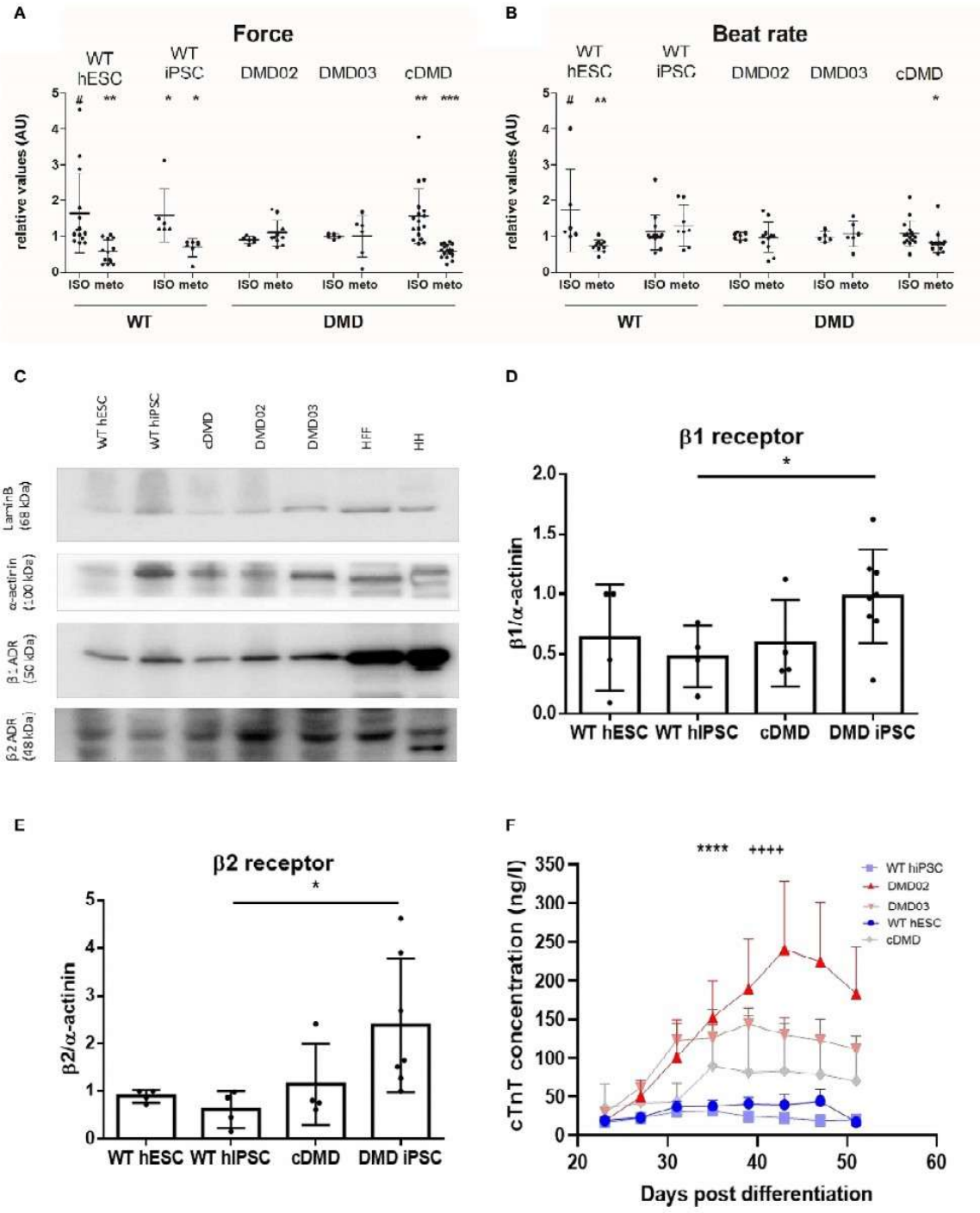

FIGURE 7 | DMD-CCs show remodeled β-adrenergic response and increased death. The contraction force and beat rate were measured using an AFM-based method and tested for β adrenergic response with isoproterenol (ISO, activator) and metoprolol (METO, inhibitor) **(A)**. WT-CMs show increase in contraction force (n = ISO/METO: n = 14/13 for WT hESC, n = 6/7 for WT-hiPSC-EBs, n = 6/10 for DMD02 EBs, n = 5/6 for DMD03 EBs, n = 17/17 for cDMD-EBs, exact value for each is represented by • in each graph) and **(B)** beat rate (n = ISO/METO: n = 6/11 for WT hESC, n = 14/8 for WT-hiPSC-EBs, n = 7/11 for DMD02 EBs, n = 5/6 for DMD03 EBs, n = 15/15 for cDMD-EBs, exact value for each is represented by • in each graph) after ISO treatment and decrease in both parameters under METO

(Continued)

FIGURE 7 | treatment. The DMD-hiPSC-EBs remained unresponsive to any of these stimulations. cDMD derived EBs show similar response in contraction force to its isogenic WT control. The red line represents the ratio of 1 for better orientation in change. Significance calculated by Wilcoxon test (*$p < 0.05$, **$p < 0.01$, ***$p < 0.01$, #$p < 0.1$) is visualized as asterisks. **(C–E)** Western blot analysis of β receptors shows higher expression of β1 in DMD-hiPSC derived EBs compared to WT-EBs; cDMD line shows similar expression to its isogenic WT control (calculates as β1 signal/actinin signal). β2 receptor showed increased levels in DMD-hiPSC-EBs. Human heart (HH) sample was used as positive control, human foreskin fibroblasts (HFF) as CM negative sample. Lamin B was used as loading control. Exact value for each is represented by • in each graph. Statistical difference was calculated by Mann-Whitney test for both β1 and β2 receptor expression. **(F)** CM death in the EBs was evaluated using free troponin level analysis in the medium. All DMD-EBs show significantly increased free cTnT levels compared to WT-EBs. Statistical difference was calculated using two-way ANOVA with uncorrected Fisher's post hoc test. ****$p < 0.0001$ according to cell line factor (WT vs. DMD) and $++++p < 0.0001$ according to day of differentiation factor.

clear benefit while others showed little effect of β-AR blockade on outcomes signaling lack of response to the modulation (Kajimoto et al., 2006; Matsumura et al., 2010; Viollet et al., 2012). The β-AR responsiveness might as well be linked to the type of mutation of the *DMD* gene, which might explain why one of our models lacked dystrophin expression yet was responsive to adrenergic modulation. Nevertheless, the beat rate and contraction force response to adrenergic modulation in patient-specific DMD-EBs suggested that the human DMD phenotype is accompanied by altered density of the β-AR on the sarcolemma and less sensitive β-AR pathway. The latter can involve a hampered lusitropic effect, resulting in a hypocontractile Ca^{2+}-saturated sarcomere (Culligan et al., 2002; Asp et al., 2013).

As a further original contribution, we finally investigated whether ECC alterations and regulatory pathways remodeling were associated in the dish with CCs wasting. Serum concentration of cTnT is a routinely used marker of CMs death, especially for acute myocardial infarction, although with high sensitivity assays it is also a prognostic marker of non-ischemic cardiac diseases (Park et al., 2017). We have indeed observed how even *in vitro* early stage models of DMD undergo progressive CMs injury, with detected levels of free cTnT up to 10 times the one of age-matched control lines. Dystrophin mutations, with severe symptomatology like in Duchenne's or milder like in Becker's, are all characterized with progressive cardiac symptoms stemming from loss of CMs, remodeling of the cardiac tissue with substitutive fibrosis, and ventricular dilation leading to heart failure accompanied by non-CM cell population depletion (Pesl et al., 2020). CM death can be indirectly caused by high levels of cytosolic Ca^{2+}, reportedly present in DMD through several mechanisms, which increases proteolysis and triggers mitochondrial dysfunctions with consequent ATP exhaustion (Meyers and Townsend, 2019; Tsurumi et al., 2019). Despite the fact that troponin levels measured by immunoassay methods in the media cannot define the mechanisms of cardiomyocyte injury, nor prove if the cell remains viable after such injury or became apoptotic, our findings confirmed that clinical assays can be used together with our model to follow subclinical stages of DMD cardiac involvement. Remarkably, this progressive CCs death is not correlated with loss of contractility. Pioner at al. demonstrated how up to 100 days of cultivation DMD models preserved their contractile function assuming a hypertrophic phenotype (Pioner et al., 2020). A similar mechanism could explain the similar evidence we observed in our 3D model, where CM depletion might be compensated by surviving CM hypertrophy. This evidence opens further uses of our presented model to study progressive cellular adaptation at different stages of the diseases.

LIMITATIONS OF THE STUDY

The reported study presents several limitations. The electrophysiological analysis via patch clamp lacks a proper age matching; therefore, the highly variable parameters might have masked mutation-related changes. Furthermore, no channel-specific study was performed to make a causative link between the presented channels overexpression to the calcium handling and contractile alterations observed. We did not directly characterize the age effect on calcium handling and contractility on hPSC-CC. However, we have relied on existent information on the topic to exclude a significant contribution of incomplete maturation to the reported differences.

CONCLUSIONS

The purpose of this work was to model some key cardiac molecular properties in DMD cardiomyopathy using DMD patient-specific and engineered CRISPR/Cas9 isogenic hPSC derived cardiac cells. Our results indicated that our DMD models in the dish are functionally affected by dystrophin deficiency and recapitulate functional defects and cardiac wasting observed in the disease. This work contributes to determine cardiac defects in DMD patients. It offers an accurate tool to study human cardiomyopathy progression and test therapies in the dish.

DATA AVAILABILITY STATEMENT

The datasets generated for this study are available on request to the corresponding author.

ETHICS STATEMENT

The fibroblasts of two DMD patients were derived from skin/muscle biopsies with the patients informed consent and St. Anne's University Hospital (Brno, Czech Republic) Ethics Committee approval under the number 37/2011. Written informed consent to participate in this study was provided by the patient/participants legal guardian.

AUTHOR CONTRIBUTIONS

All the authors have contributed to the manuscript writing and corrections and were included substantially in the project preparation, conception, and evaluation. SJ has differentiated the cardiomyocytes, ran ICC, PCR, and western blot analyses, evaluated obtained data and interpreted them, prepared the figures, and wrote the draft of the manuscript. AV was included in the experimental design, differentiated cardiomyocytes and performed Ca^{2+} imaging and ICC staining, and helped interpret the data. JP performed the AFM measurements and initial evaluation of the data. FA performed the electrophysiological measurements and interpreted them. MP performed AFM measurement of the EBs. GC participated in AFM measurements and interpretation of the results. AS performed AFM and Ca^{2+} imaging data analysis. IA performed Ca^{2+} imaging of the WT cells and helped interpret the data. VS and HD performed cTnT assays. SK evaluated AFM data. TU performed dystrophin western blot. PS, AL, PD, AM, and VR supervised the project, interpreted the obtained results, and corrected the manuscript. AM and VR were responsible for the experimental design of the project, coordination, and supervision in equal matter.

FUNDING

This work was supported by the Ministry of Education, Youth, and Sports of the Czech Republic (7AMB13FR011, No. CZ.02.1.01/0.0/0.0/16_013/0001776, No. CZ.02.1.01/0.0/0.0/16_019/0000868), CIISB research infrastructure LM2018127 and supported by funds from the Faculty of Medicine MU to junior researchers SJ and MP. This work was also supported by grants of the European Regional Development Fund (CIISB4HEALTH No. CZ.02.1.01/0.0/0.0/16_013/0001776), South Moravian Centre for International Mobility (SoMoPro No. 2SGA2744), and the European Society of Cardiology (ESC; R12042FF). The French Muscular Dystrophy Association (AFM; project 16073, MNM2 2012, and 20225), the Fondation pour la Recherche Médicale (FRM; SPF20130526710), the PHC Barrande (Duchenstem No. 28379TE), the Institut National pour la Santé et la Recherche Médicale (INSERM) also supported this work.

SUPPLEMENTARY MATERIAL

The Supplementary Material for this article can be found online at: https://www.frontiersin.org/articles/10.3389/fbioe.2020.00535/full#supplementary-material

REFERENCES

Acimovic, I., Refaat, M. M., Moreau, A., Salykin, A., Reiken, S., Sleiman, Y., et al. (2018). Post-translational modifications and diastolic calcium leak associated to the novel RyR2-D3638A mutation lead to CPVT in patient-specific hiPSC-derived cardiomyocytes. *J. Clin. Med.* 7:423. doi: 10.3390/jcm7110423

Amedro, P., Vincenti, M., De La Villeon, G., Lavastre, K., Barrea, C., Guillaumont, S., et al. (2019). Speckle-tracking echocardiography in children with duchenne muscular dystrophy: a prospective multicenter controlled cross-sectional study. *J. Am. Soc. Echocardiogr.* 32, 412–422. doi: 10.1016/j.echo.2018.10.017

Andersson, D. C., and Marks, A. R. (2010). Fixing ryanodine receptor Ca leak - a novel therapeutic strategy for contractile failure in heart and skeletal muscle. *Drug Discov. Today Dis. Mech.* 7, e151–e157. doi: 10.1016/j.ddmec.2010.09.009

Andersson, D. C., Meli, A. C., Reiken, S., Betzenhauser, M. J., Umanskaya, A., Shiomi, T., et al. (2012). Leaky ryanodine receptors in β sarcoglycan deficient mice: a potential common defect in muscular dystrophy. *Skelet. Muscle* 2:9. doi: 10.1186/2044-5040-2-9

Armstrong, L., Tilgner, K., Saretzki, G., Atkinson, S. P., Stojkovic, M., Moreno, R., et al. (2010). Human induced pluripotent stem cell lines show stress defense mechanisms and mitochondrial regulation similar to those of human embryonic stem cells. *Stem Cells* 28, 661–673. doi: 10.1002/stem.307

Asp, M. L., Martindale, J. J., Heinis, F. I., Wang, W., and Metzger, J. M. (2013). Calcium mishandling in diastolic dysfunction: mechanisms and potential therapies. *Biochim. Biophys. Acta* 1833, 895–900. doi: 10.1016/j.bbamcr.2012.09.007

Blake, D. J., Weir, A., Newey, S. E., and Davies, K. E. (2002). Function and genetics of dystrophin and dystrophin-related proteins in muscle. *Physiol. Rev.* 82, 291–329. doi: 10.1152/physrev.00028.2001

Bondue, A., Arbustini, E., Bianco, A., Ciccarelli, M., Dawson, D., De Rosa, M., et al. (2018). Complex roads from genotype to phenotype in dilated cardiomyopathy: scientific update from the working group of myocardial function of the european society of cardiology. *Cardiovasc. Res.* 114, 1287–1303. doi: 10.1093/cvr/cvy122

Bristow, M. R., Ginsburg, R., Minobe, W., Cubicciotti, R. S., Sageman, W. S., Lurie, K., et al. (1982). Decreased catecholamine sensitivity and beta-adrenergic-receptor density in failing human hearts. *N. Engl. J. Med.* 307, 205–211. doi: 10.1056/NEJM198207223070401

Caluori, G., Pribyl, J., Pesl, M., Jelinkova, S., Rotrekl, V., Skladal, P., et al. (2019). Non-invasive electromechanical cell-based biosensors for improved investigation of 3D cardiac models. *Biosens. Bioelectron.* 124–125, 129–135. doi: 10.1016/j.bios.2018.10.021

Carnwath, J. W., and Shotton, D. M. (1987). Muscular dystrophy in the mdx mouse: histopathology of the soleus and extensor digitorum longus muscles. *J. Neurol. Sci.* 80, 39–54. doi: 10.1016/0022-510X(87)90219-X

Chenard, A. A., Becane, H. M., Tertrain, F., de Kermadec, J. M., and Weiss, Y. A. (1993). Ventricular arrhythmia in duchenne muscular dystrophy: prevalence, significance and prognosis. *Neuromuscul. Disord.* 3, 201–206. doi: 10.1016/0960-8966(93)90060-W

Choi, B.-R., Burton, F., and Salama, G. (2002). Cytosolic Ca^{2+} triggers early afterdepolarizations and torsade de pointes in rabbit hearts with type 2 long QT syndrome. *J. Physiol.* 543, 615–631. doi: 10.1113/jphysiol.2002.024570

Clarac, F., Massion, J., and Smith, A. M. (2009). Duchenne, charcot and babinski, three neurologists of la salpetrière hospital, and their contribution to concepts of the central organization of motor synergy. *J. Physiol. Paris* 103, 361–376. doi: 10.1016/j.jphysparis.2009.09.001

Corrado, G., Lissoni, A., Beretta, S., Terenghi, L., Tadeo, G., Foglia-Manzillo, G., et al. (2002). Prognostic value of electrocardiograms, ventricular late potentials, ventricular arrhythmias, and left ventricular systolic dysfunction in patients with Duchenne muscular dystrophy. *Am. J. Cardiol.* 89, 838–841. doi: 10.1016/S0002-9149(02)02195-1

Coulton, G. R., Morgan, J. E., Partridge, T. A., and Sloper, J. C. (1988). The mdx mouse skeletal muscle myopathy: I. A histological, morphometric and biochemical investigation. *Neuropathol. Appl. Neurobiol.* 14, 53–70. doi: 10.1111/j.1365-2990.1988.tb00866.x

Culligan, K., Banville, N., Dowling, P., and Ohlendieck, K. (2002). Drastic reduction of calsequestrin-like proteins and impaired calcium binding in dystrophic mdx muscle. *J. Appl. Physiol.* 92, 435–445. doi: 10.1152/japplphysiol.00903.2001

Danialou, G., Comtois, A. S., Dudley, R., Karpati, G., Vincent, G., Des Rosiers, C., et al. (2001). Dystrophin-deficient cardiomyocytes are abnormally vulnerable

to mechanical stress-induced contractile failure and injury. *FASEB J.* 15, 1655–1657. doi: 10.1096/fj.01-0030fje

de Lucia, C., Eguchi, A., and Koch, W. J. (2018). New insights in cardiac β-adrenergic signaling during heart failure and aging. *Front. Pharmacol.* 9:904. doi: 10.3389/fphar.2018.00904

Dumont, N. A., Wang, Y. X., von Maltzahn, J., Pasut, A., Bentzinger, C. F., Brun, C. E., et al. (2015). Dystrophin expression in muscle stem cells regulates their polarity and asymmetric division. *Nat. Med.* 21, 1455–1463. doi: 10.1038/nm.3990

Dvorak, P., Dvorakova, D., Koskova, S., Vodinska, M., Najvirtova, M., Krekac, D., et al. (2005). Expression and potential role of fibroblast growth factor 2 and its receptors in human embryonic stem cells. *Stem Cells* 23, 1200–1211. doi: 10.1634/stemcells.2004-0303

Eisen, B., Ben Jehuda, R., Cuttitta, A. J., Mekies, L. N., Shemer, Y., Baskin, P., et al. (2019). Electrophysiological abnormalities in induced pluripotent stem cell-derived cardiomyocytes generated from duchenne muscular dystrophy patients. *J. Cell. Mol. Med.* 23, 2125–2135. doi: 10.1111/jcmm.14124

Engelhardt, S., Hein, L., Wiesmann, F., and Lohse, M. J. (1999). Progressive hypertrophy and heart failure in beta1-adrenergic receptor transgenic mice. *Proc. Natl. Acad. Sci. U.S.A.* 96, 7059–7064. doi: 10.1073/pnas.96.12.7059

Fauconnier, J., Thireau, J., Reiken, S., Cassan, C., Richard, S., Matecki, S., et al. (2010). Leaky RyR2 trigger ventricular arrhythmias in duchenne muscular dystrophy. *Proc. Natl. Acad. Sci. U.S.A.* 107, 1559–1564. doi: 10.1073/pnas.0908540107

Fayssoil, A., Nardi, O., Orlikowski, D., and Annane, D. (2010). Cardiomyopathy in duchenne muscular dystrophy: pathogenesis and therapeutics. *Heart Fail Rev.* 15, 103–107. doi: 10.1007/s10741-009-9156-8

Finsterer, J., and Stöllberger, C. (2003). The heart in human dystrophinopathies. *Cardiology* 99, 1–19. doi: 10.1159/000068446

Gerke, V., Creutz, C. E., and Moss, S. E. (2005). Annexins: linking Ca^{2+} signalling to membrane dynamics. *Nat. Rev. Mol. Cell Biol.* 6, 449–461. doi: 10.1038/nrm1661

Hajjar, R. J., Liao, R., Young, J. B., Fuleihan, F., Glass, M. G., and Gwathmey, J. K. (1993). Pathophysiological and biochemical characterisation of an avian model of dilated cardiomyopathy: comparison to findings in human dilated cardiomyopathy. *Cardiovasc. Res.* 27, 2212–2221. doi: 10.1093/cvr/27.12.2212

He, J.-Q., Ma, Y., Lee, Y., Thomson, J. A., and Kamp, T. J. (2003). Human embryonic stem cells develop into multiple types of cardiac myocytes: action potential characterization. *Circ. Res.* 93, 32–39. doi: 10.1161/01.RES.0000080317.92718.99

Hess, G. P. D., Horsch, A. D., and Zdunek, D. D. (2008). *Means and Methods for Optimization of Diagnostic and Therapeutic Approaches in Chronic Artery Disease Based on the Detection of Troponin T and NT-proBNP*. Available online at: https://patents.google.com/patent/EP1925943A1/en/en22 (accessed December 14, 2019).

Himmrich, E., Popov, S., Liebrich, A., Rosocha, S., Zellerhoff, C., Nowak, B., et al. (2000). [Hidden intracardiac conduction disturbances and their spontaneous course in patients with progressive muscular dystrophy]. *Z Kardiol.* 89, 592–598. doi: 10.1007/s003920070208

Hwang, H. S., Kryshtal, D. O., Feaster, T. K., Sánchez-Freire, V., Zhang, J., Kamp, T. J., et al. (2015). Comparable calcium handling of human iPSC-derived cardiomyocytes generated by multiple laboratories. *J. Mol. Cell. Cardiol.* 85, 79–88. doi: 10.1016/j.yjmcc.2015.05.003

Inomata, K., Aoto, T., Binh, N. T., Okamoto, N., Tanimura, S., Wakayama, T., et al. (2009). Genotoxic stress abrogates renewal of melanocyte stem cells by triggering their differentiation. *Cell* 137, 1088–1099. doi: 10.1016/j.cell.2009.03.037

International Stem Cell Initiative, Adewumi, O., Aflatoonian, B., Ahrlund-Richter, L., Amit, M., Andrews, P. W., et al. (2007). Characterization of human embryonic stem cell lines by the international stem cell initiative. *Nat. Biotechnol.* 25, 803–816. doi: 10.1038/nbt1318

Jelinkova, S., Fojtik, P., Kohutova, A., Vilotic, A., Marková, L., Pesl, M., et al. (2019a). Dystrophin deficiency leads to genomic instability in human pluripotent stem cells via NO synthase-induced oxidative stress. *Cells* 8:53. doi: 10.3390/cells8010053

Jelinkova, S., Markova, L., Pesl, M., Valáškova, I., Makaturová, E., Jurikova, L., et al. (2019b). Generation of two duchenne muscular dystrophy patient-specific induced pluripotent stem cell lines DMD02 and DMD03 (MUNIi001-A and MUNIi003-A). *Stem Cell Res.* 40:101562. doi: 10.1016/j.scr.2019.101562

Johnson, D. M., Heijman, J., Bode, E. F., Greensmith, D. J., van der Linde, H., Abi-Gerges, N., et al. (2013). Diastolic spontaneous calcium release from the sarcoplasmic reticulum increases beat-to-beat variability of repolarization in canine ventricular myocytes after β-adrenergic stimulation. *Circ. Res.* 112, 246–256. doi: 10.1161/CIRCRESAHA.112.275735

Jung, C., Martins, A. S., Niggli, E., and Shirokova, N. (2008). Dystrophic cardiomyopathy: amplification of cellular damage by Ca^{2+} signalling and reactive oxygen species-generating pathways. *Cardiovasc. Res.* 77, 766–773. doi: 10.1093/cvr/cvm089

Kajimoto, H., Ishigaki, K., Okumura, K., Tomimatsu, H., Nakazawa, M., Saito, K., et al. (2006). Beta-blocker therapy for cardiac dysfunction in patients with muscular dystrophy. *Circ. J.* 70, 991–994. doi: 10.1253/circj.70.991

Kamdar, F., and Garry, D. J. (2016). Dystrophin-deficient cardiomyopathy. *J. Am. Coll. Cardiol.* 67, 2533–2546. doi: 10.1016/j.jacc.2016.02.081

Koenig, X., Dysek, S., Kimbacher, S., Mike, A. K., Cervenka, R., Lukacs, P., et al. (2011). Voltage-gated ion channel dysfunction precedes cardiomyopathy development in the dystrophic heart. *PLoS ONE* 6:e20300. doi: 10.1371/journal.pone.0020300

Koenig, X., Rubi, L., Obermair, G. J., Cervenka, R., Dang, X. B., Lukacs, P., et al. (2014). Enhanced currents through L-type calcium channels in cardiomyocytes disturb the electrophysiology of the dystrophic heart. *Am. J. Physiol. Heart Circ. Physiol.* 306, H564–H573. doi: 10.1152/ajpheart.00441.2013

Krutá, M., Bálek, L., Hejnová, R., Dobšáková, Z., Eiselleová, L., Matulka, K., et al. (2013). Decrease in abundance of apurinic/apyrimidinic endonuclease causes failure of base excision repair in culture-adapted human embryonic stem cells. *Stem Cells* 31, 693–702. doi: 10.1002/stem.1312

Krutá, M., Šeneklová, M., Raška, J., Salykin, A., Zerzánková, L., Pešl, M., et al. (2014). Mutation frequency dynamics in HPRT locus in culture-adapted human embryonic stem cells and induced pluripotent stem cells correspond to their differentiated counterparts. *Stem Cells Dev.* 23, 2443–2454. doi: 10.1089/scd.2013.0611

Li, Y., Zhang, S., Zhang, X., Li, J., Ai, X., Zhang, L., et al. (2014). Blunted cardiac beta-adrenergic response as an early indication of cardiac dysfunction in duchenne muscular dystrophy. *Cardiovasc. Res.* 103, 60–71. doi: 10.1093/cvr/cvu119

Lu, S., and Hoey, A. (2000). Changes in function of cardiac receptors mediating the effects of the autonomic nervous system in the muscular dystrophy (MDX) mouse. *J. Mol. Cell. Cardiol.* 32, 143–152. doi: 10.1006/jmcc.1999.1063

Mah, J. K., Korngut, L., Dykeman, J., Day, L., Pringsheim, T., and Jette, N. (2014). A systematic review and meta-analysis on the epidemiology of duchenne and becker muscular dystrophy. *Neuromuscul. Disord.* 24, 482–491. doi: 10.1016/j.nmd.2014.03.008

Manzur, A. Y., Kinali, M., and Muntoni, F. (2008). Update on the management of duchenne muscular dystrophy. *Arch. Dis. Child.* 93, 986–990. doi: 10.1136/adc.2007.118141

Markham, L. W., Michelfelder, E. C., Border, W. L., Khoury, P. R., Spicer, R. L., Wong, B. L., et al. (2006). Abnormalities of diastolic function precede dilated cardiomyopathy associated with Duchenne muscular dystrophy. *J. Am. Soc. Echocardiogr.* 19, 865–871. doi: 10.1016/j.echo.2006.02.003

Matsumura, T., Tamura, T., Kuru, S., Kikuchi, Y., and Kawai, M. (2010). Carvedilol can prevent cardiac events in duchenne muscular dystrophy. *Intern. Med.* 49, 1357–1363. doi: 10.2169/internalmedicine.49.3259

McNally, E. M., Kaltman, J. R., Benson, D. W., Canter, C. E., Cripe, L. H., Duan, D., et al. (2015). Contemporary cardiac issues in duchenne muscular dystrophy. *Circulation* 131, 1590–1598. doi: 10.1161/CIRCULATIONAHA.114.015151

Meyers, T. A., Heitzman, J. A., Krebsbach, A. M., Aufdembrink, L. M., Hughes, R., Bartolomucci, A., et al. (2019). Acute AT1R blockade prevents isoproterenol-induced injury in mdx hearts. *J. Mol. Cell. Cardiol.* 128, 51–61. doi: 10.1016/j.yjmcc.2019.01.013

Meyers, T. A., and Townsend, D. (2019). Cardiac pathophysiology and the future of cardiac therapies in duchenne muscular dystrophy. *Int. J. Mol. Sci.* 20:4098. doi: 10.3390/ijms20174098

Oda, T., Yang, Y., Uchinoumi, H., Thomas, D. D., Chen-Izu, Y., Kato, T., et al. (2015). Oxidation of ryanodine receptor (RyR) and calmodulin enhance Ca release and pathologically alter, RyR structure and calmodulin affinity. *J. Mol. Cell. Cardiol.* 85, 240–248. doi: 10.1016/j.yjmcc.2015.06.009

Panovský, R., Pešl, M., Holeček, T., Máchal, J., Feitová, V., Mrázová, L., et al. (2019). Cardiac profile of the czech population of duchenne muscular dystrophy patients: a cardiovascular magnetic resonance study with T1 mapping. *Orphanet J. Rare Dis.* 14:10. doi: 10.1186/s13023-018-0986-0

Papa, A. A., D'Ambrosio, P., Petillo, R., Palladino, A., and Politano, L. (2017). Heart transplantation in patients with dystrophinopathic cardiomyopathy: review of the literature and personal series. *Intractable Rare Dis Res.* 6, 95–101. doi: 10.5582/irdr.2017.01024

Park, K. C., Gaze, D. C., Collinson, P. O., and Marber, M. S. (2017). Cardiac troponins: from myocardial infarction to chronic disease. *Cardiovasc. Res.* 113, 1708–1718. doi: 10.1093/cvr/cvx183

Patrick Gonzalez, J., Ramachandran, J., Xie, L.-H., Contreras, J. E., and Fraidenraich, D. (2015). Selective connexin43 inhibition prevents isoproterenol-induced arrhythmias and lethality in muscular dystrophy mice. *Sci. Rep.* 5:13490. doi: 10.1038/srep13490

Pesl, M., Acimovic, I., Pribyl, J., Hezova, R., Vilotic, A., Fauconnier, J., et al. (2014). Forced aggregation and defined factors allow highly uniform-sized embryoid bodies and functional cardiomyocytes from human embryonic and induced pluripotent stem cells. *Heart Vessels* 29, 834–846. doi: 10.1007/s00380-013-0436-9

Pesl, M., Jelinkova, S., Caluori, G., Holicka, M., Krejci, J., Nemec, P., et al. (2020). Cardiovascular progenitor cells and tissue plasticity are reduced in a myocardium affected by Becker muscular dystrophy. *Orphanet J. Rare Dis.* 15:65. doi: 10.1186/s13023-019-1257-4

Pesl, M., Pribyl, J., Acimovic, I., Vilotic, A., Jelinkova, S., Salykin, A., et al. (2016). Atomic force microscopy combined with human pluripotent stem cell derived cardiomyocytes for biomechanical sensing. *Biosens. Bioelectron.* 85, 751–757. doi: 10.1016/j.bios.2016.05.073

Peterson, J. M., Wang, D. J., Shettigar, V., Roof, S. R., Canan, B. D., Bakkar, N., et al. (2018). NF-κB inhibition rescues cardiac function by remodeling calcium genes in a duchenne muscular dystrophy model. *Nat. Commun.* 9:3431. doi: 10.1038/s41467-018-05910-1

Pioner, J. M., Guan, X., Klaiman, J. M., Racca, A. W., Pabon, L., Muskheli, V., et al. (2020). Absence of full-length dystrophin impairs normal maturation and contraction of cardiomyocytes derived from human-induced pluripotent stem cells. *Cardiovasc. Res.* 116, 368–382.

Pribyl, J., Pešl, M., Caluori, G., Acimovic, I., Jelinkova, S., Dvorak, P., et al. (2019). Biomechanical characterization of human pluripotent stem cell-derived cardiomyocytes by use of atomic force microscopy. *Methods Mol. Biol.* 1886, 343–353. doi: 10.1007/978-1-4939-8894-5_20

Puzzo, D., Raiteri, R., Castaldo, C., Capasso, R., Pagano, E., Tedesco, M., et al. (2016). CL316,243, a β3-adrenergic receptor agonist, induces muscle hypertrophy and increased strength. *Sci. Rep.* 5:37504. doi: 10.1038/srep37504

Qu, C., Puttonen, K. A., Lindeberg, H., Ruponen, M., Hovatta, O., Koistinaho, J., et al. (2013). Chondrogenic differentiation of human pluripotent stem cells in chondrocyte co-culture. *Int. J. Biochem. Cell Biol.* 45, 1802–1812. doi: 10.1016/j.biocel.2013.05.029

Rengo, G., Lymperopoulos, A., and Koch, W. J. (2009). Future g protein-coupled receptor targets for treatment of heart failure. *Curr. Treat. Options Cardiovasc. Med.* 11, 328–338. doi: 10.1007/s11936-009-0033-5

Rossi, D. J., Bryder, D., Seita, J., Nussenzweig, A., Hoeijmakers, J., and Weissman, I. L. (2007). Deficiencies in DNA damage repair limit the function of haematopoietic stem cells with age. *Nature* 447, 725–729. doi: 10.1038/nature05862

Sadek, A. A., Mahmoud, S. M., El-Aal, M. A., Allam, A. A., and El-Halim, W. I. A. (2017). Evaluation of cardiac functions in children with duchenne muscular dystrophy: a prospective case-control study. *Electron. Physician.* 9, 5732–5739. doi: 10.19082/5732

Sato, H., Shiraishi, I., Takamatsu, T., and Hamaoka, K. (2007). Detection of TUNEL-positive cardiomyocytes and c-kit-positive progenitor cells in children with congenital heart disease. *J. Mol. Cell. Cardiol.* 43, 254–261. doi: 10.1016/j.yjmcc.2007.05.011

Shirokova, N., and Niggli, E. (2013). Cardiac phenotype of duchenne muscular dystrophy: insights from cellular studies. *J. Mol. Cell. Cardiol.* 58, 217–224. doi: 10.1016/j.yjmcc.2012.12.009

Skeberdis, V. A. (2004). Structure and function of beta3-adrenergic receptors. *Medicina (Kaunas).* 40, 407–413.

Stehlíková, K., Skálová, D., Zídková, J., Haberlová, J., Vohánka, S., Mazanec, R., et al. (2017). Muscular dystrophies and myopathies: the spectrum of mutated genes in the czech republic. *Clin. Genet.* 91, 463–469. doi: 10.1111/cge.12839

Tsurumi, F., Baba, S., Yoshinaga, D., Umeda, K., Hirata, T., Takita, J., et al. (2019). The intracellular Ca^{2+} concentration is elevated in cardiomyocytes differentiated from hiPSCs derived from a duchenne muscular dystrophy patient. *PLoS ONE* 14:e0213768. doi: 10.1371/journal.pone.0213768

Villa Chet, R., Czosek Richard, J., Ahmed, H., Khoury Philip, R., Anderson Jeffrey, B., Knilans Timothy, K., et al. (2015). Ambulatory monitoring and arrhythmic outcomes in pediatric and adolescent patients with duchenne muscular dystrophy. *J. Am. Heart Assoc.* 5:e002620. doi: 10.1161/JAHA.115.002620

Viollet, L., Thrush, P. T., Flanigan, K. M., Mendell, J. R., and Allen, H. D. (2012). Effects of angiotensin-converting enzyme inhibitors and/or beta blockers on the cardiomyopathy in duchenne muscular dystrophy. *Am. J. Cardiol.* 110, 98–102. doi: 10.1016/j.amjcard.2012.02.064

Voigt, N., Li, N., Wang, Q., Wang, W., Trafford, A. W., Abu-Taha, I., et al. (2012). Enhanced sarcoplasmic reticulum Ca^{2+}-leak and increased Na+-Ca2+-exchanger function underlie delayed afterdepolarizations in patients with chronic atrial fibrillation. *Circulation* 125, 2059–2070. doi: 10.1161/CIRCULATIONAHA.111.067306

Vry, J., Gramsch, K., Rodger, S., Thompson, R., Steffensen, B. F., Rahbek, J., et al. (2016). European cross-sectional survey of current care practices for duchenne muscular dystrophy reveals regional and age-dependent differences. *J. Neuromuscul. Dis.* 3, 517–527. doi: 10.3233/JND-160185

Wagner, K. R., Lechtzin, N., and Judge, D. P. (2007). Current treatment of adult duchenne muscular dystrophy. *Biochim. Biophys. Acta* 1772, 229–237. doi: 10.1016/j.bbadis.2006.06.009

Weiss, J. N., Garfinkel, A., Karagueuzian, H. S., Chen, P.-S., and Qu, Z. (2010). Early afterdepolarizations and cardiac arrhythmias. *Heart Rhythm.* 7, 1891–1899. doi: 10.1016/j.hrthm.2010.09.017

Williams, I. A., and Allen, D. G. (2007). Intracellular calcium handling in ventricular myocytes from mdx mice. *Am. J. Physiol. Heart Circ. Physiol.* 292, H846–H855. doi: 10.1152/ajpheart.00688.2006

Zhu, R., Millrod, M. A., Zambidis, E. T., and Tung, L. (2016). Variability of action potentials within and among cardiac cell clusters derived from human embryonic stem cells. *Sci. Rep.* 6:18544. doi: 10.1038/srep18544

Conflict of Interest: The authors declare that the research was conducted in the absence of any commercial or financial relationships that could be construed as a potential conflict of interest.

Copyright © 2020 Jelinkova, Vilotic, Pribyl, Aimond, Salykin, Acimovic, Pesl, Caluori, Klimovic, Urban, Dobrovolna, Soska, Skladal, Lacampagne, Dvorak, Meli and Rotrekl. This is an open-access article distributed under the terms of the Creative Commons Attribution License (CC BY). The use, distribution or reproduction in other forums is permitted, provided the original author(s) and the copyright owner(s) are credited and that the original publication in this journal is cited, in accordance with accepted academic practice. No use, distribution or reproduction is permitted which does not comply with these terms.

6.4. Annex 4

Dystrophin Deficiency Leads to Genomic Instability in Human Pluripotent Stem Cells via NO Synthase-Induced Oxidative Stress

Jelinkova S, Fojtik P, Kohutova A, Vilotic A, Markova L, Pesl M, Jurakova T, Kruta M, Vrbsky J, Gaillyova R, Valaskova I, Frak I, Lacampagne A, Forte G, Dvorak P, Meli AC, ***Rotrekl V***

cells

MDPI

Article

Dystrophin Deficiency Leads to Genomic Instability in Human Pluripotent Stem Cells via NO Synthase-Induced Oxidative Stress

Sarka Jelinkova [1,2], Petr Fojtik [1,†], Aneta Kohutova [1,2,†], Aleksandra Vilotic [1], Lenka Marková [1], Martin Pesl [1,2,3], Tereza Jurakova [1], Miriama Kruta [1], Jan Vrbsky [2], Renata Gaillyova [1,4], Iveta Valášková [1,4], Ivan Frák [1], Alain Lacampagne [5], Giancarlo Forte [2], Petr Dvorak [1,2], Albano C. Meli [1,5,*,‡] and Vladimir Rotrekl [1,2,*,‡]

1 Department of Biology, Faculty of Medicine, Masaryk University, 625 00 Brno, Czech Republic; sarka.jelinkova89@gmail.com (S.J.); petrfoj@hotmail.com (P.F.); aneta.baumeisterova@gmail.com (A.K.); aleksandra.vilotic@gmail.com (A.V.); zerzankova.lenka@gmail.com (L.M.); peslmartin@gmail.com (M.P.); t.jurakova@gmail.com (T.J.); kruta.miriama@gmail.com (M.K.); gaillyova.renata@fnbrno.cz (R.G.); Valaskova.Iveta@fnbrno.cz (I.V.); ivan.frak@gmail.com (I.F.); petr.dvorak@rect.muni.cz (P.D.)

2 International Clinical Research Center ICRC, St. Anne's University Hospital Brno, 602 00 Brno, Czech Republic; vrbsky.jan@fnusa.cz (J.V.); giaforte@gmail.com (G.F.)

3 1st Department of Internal Medicine—Cardioangiology, Faculty of Medicine, Masaryk University, 602 00 Brno, Czech Republic

4 Department of Clinical Genetics, University hospital Brno, 613 00 Brno, Czech Republic

5 PhyMedExp, INSERM, University of Montpellier, CNRS, 342 95 Montpellier CEDEX 5, France; alain.lacampagne@inserm.fr

* Correspondence: albano.meli@inserm.fr (A.C.M.); vrotrekl@med.muni.cz (V.R.); Tel.: +334-67-41-52-44 (A.C.M.); +420-549-498-002 (V.R.)

† Both authors contributed equally.

‡ Both authors contributed equally as supervising researchers.

Received: 17 October 2018; Accepted: 11 January 2019; Published: 15 January 2019



Abstract: Recent data on Duchenne muscular dystrophy (DMD) show myocyte progenitor's involvement in the disease pathology often leading to the DMD patient's death. The molecular mechanism underlying stem cell impairment in DMD has not been described. We created dystrophin-deficient human pluripotent stem cell (hPSC) lines by reprogramming cells from two DMD patients, and also by introducing dystrophin mutation into human embryonic stem cells via CRISPR/Cas9. While dystrophin is expressed in healthy hPSC, its deficiency in DMD hPSC lines induces the release of reactive oxygen species (ROS) through dysregulated activity of all three isoforms of nitric oxide synthase (further abrev. as, NOS). NOS-induced ROS release leads to DNA damage and genomic instability in DMD hPSC. We were able to reduce both the ROS release as well as DNA damage to the level of wild-type hPSC by inhibiting NOS activity.

Keywords: DMD; dystrophin; pluripotent stem cells; genome stability; ROS; NO synthases

1. Introduction

Duchenne muscular dystrophy (DMD) is an X-linked rare genetic disorder which impairs muscles and results in severe disability and premature death in young men [1]. Initially, DMD starts to develop in skeletal muscles causing muscle weakness and atrophy due to fibrosis [2], preceded by the presence of apoptotic myocytes [3,4]. During teenage years, fibrosis affects also the cardiac muscle [5]. It is further exacerbated by intracardiac conduction disturbances, and it induces atrial and ventricular arrhythmias [6,7] leading to the development of dilated cardiomyopathy [8], and ultimately, to heart

failure in DMD patients [5,9]. Disease progression and muscle degeneration leading to skeletal muscle wasting was recently also linked to satellite cell depletion [10,11].

DMD is caused by mutations in the dystrophin gene, resulting in truncated inactive or missing forms of dystrophin [12], which is a part of dystrophin glycoprotein complex (DGC) [13]. DGC in myocytes binds the sarcolemma to the extracellular matrix [14] and stabilizes the plasma membrane of striated muscle cells [15]. Even though a specific dystrophin isoform (Dp412) [16] and several others [17] were previously shown to be expressed in stem cells, the role of dystrophin or DGC is still unknown. DGC consists of multiple proteins, including nitric oxide synthase (NOS) isoforms [18], [19–21]. NOS produces NO by conversion of L-arginine to L-citruline. In low L-arginine concentration, NOS produces O_2 or H_2O_2 e.g., [22,23] that acts as reactive oxygen species (ROS), or can react with NO and form ONOO, a reactive nitrogen species (RNS) that quickly decomposes to a strong oxidant $HO^{\cdot}$ [24]. Due to $ONOO^{\cdot}$ quick conversion to ROS and common strong oxidative properties, the ROS/RNS are further referenced only as ROS. The deregulation of nNOS was shown to be one of the intracellular sources of oxidative stress in the DMD animal model (*mdx*) myocytes [21]. In DMD myocytes, neuronal NOS (nNOS) loses its localization to DGC, which leads to a decrease in muscle force that can be restored by downregulation of nNOS [20]. iNOS was shown to be overexpressed in *mdx* myocytes, and this increase further regulates the expression of eNOS [25]. Increased oxidative stress in DMD myocytes was also attributed to mitochondrial complex I insufficiency [26], or changed expression of NADPH oxidase 2 (NOX2) [27]. Oxidative stress in turn leads to further interleukin-6 mediated ROS release [28,29], that initiates a vicious ROS cycle in DMD myocytes, leading to cell death and eventual myocyte replacement by scar tissue [3,4]. These pathological features resemble clinically-observed skeletal muscle and myocardial fibrosis (e.g., [30]), suggesting that myocyte depletion is associated with DMD.

Different mechanisms are proposed and still discussed to explain the discrepancy between functional impairment with premature death of DMD cardiomyocytes (CMs) [31] and the later onset of myocardial fibrosis and heart failure compared to skeletal muscle, usually diagnosed in the second decade of the patients' lives [13]. Tissue remodeling was attributed to inflammatory response induced by the cardiomyocyte death, mediated mostly by T and B lymphocytes [32,33] and increased oxidative stress [34].

The skeletal muscle pathophysiological changes in DMD mouse models have been recently connected to satellite cell depletion [35]. The proliferation, resistance to oxidative stress, and multilineage differentiation capacities decreased rapidly in a period of weeks in mdx mice satellite cells [35], thus pointing at progenitors' premature depletion either by cell death, differentiation or loss of self-renewal [36–39]. Insufficient data are available so far concerning the expression and function of dystrophin in stem cells [40–43], mostly due to the limited accessibility of tissue specific stem cells from patients, while animal models only partially resemble the human DMD phenotype [44]. Thus, we considered that it was of utmost importance to dissect the molecular mechanisms using a human pluripotent stem cell (hPSC) model of DMD.

2. Materials and Methods

2.1. Control Cell Lines and Cultivation

As control lines for standard model of pluripotent stem cells, we employed hESC CCTL12 (hPSCreg name MUNIe005-A, passages 39–61)) and CCTL14 (hPSCreg name MUNIe007-A, passages 23–63) derived in Masaryk University, Brno, and characterized previously [45]. hiPSC control lines are used in key experiments as additional control to limit the effect of the genetic variability of the source material. Used lines are AM13 (previously described in [46], passages 22–78), clone (cl.)1 (passages 40–89) and cl.4 (passages 62–84) obtained from Dr. Majlinda Lako (Newcastle University, UK) [47] and episomaly reprogrammed hiPSC (CBIA1, passages 44–50)) obtained from Irena Koutná (Centre for Biomedical Image Analysis, Masaryk University, Brno, Czech Republic) (described in [48]). All human pluripotent stem cell lines were routinely maintained on feeder layer of mitotically inactivated mouse

embryonic fibroblasts (mEF) as described previously [46,49]. For CM differentiation, an embryoid body protocol was used as described in [50] with small modifications. For comparison of fibroblasts before reprogramming (for DMD passages 8–11), human foreskin fibroblast lines from newborns, SCRC-1041 and SCRC-1043 (passages 11–15) [obtained from the American Type Culture Collection (Manassas, VA, USA), described in [51] were used.

2.2. Tissue Processing, Reprogramming and Identification

The fibroblasts of two DMD patients were derived from skin/muscle biopsies with the patients informed consent and St. Anne' University Hospital (Brno, Czech Republic) Ethics Committee approval, as previously described [52]. Briefly, the biopsy tissue was cut into 0.5–1 mm^3 pieces and seeded onto 6 well plates in medium containing KnockOut DMEM (Invitrogen, Carlsbad, CA, USA), 10% heat-inactivated fetal bovine serum, 0.1 mM β-mercaptoethanol, 1% penicillin-streptomycin, 1% L-glutamine, 1% non-essential amino acids and layered with cover glasses. The dishes were left in the incubator for 5 days with no movement. The medium was then changed every 2–3 days and passaged first at day 10 of cultivation using trypsin.

Two DMD patient-specific human induced pluripotent stem cell lines were obtained by the reprogramming of cultivated human fibroblasts using a CytoTuneTM iPS reprogramming kit (A13780-01; Life Technologies, Carlsbad, CA, USA), according to manufacturer's recommendations. DMD hiPSC lines are referred to as DMD02 (hPSCreg name MUNIi001-A, passages 24–85) and DMD03 (hPSCreg name MUNIi003-A, passages 17–80). DMD hiPSCs were characterized using immunocytochemical staining of pluripotency markers (Nanog, Oct4, SSEA4, TRA-1-81, for antibodies details, see Supplementary Table S10) and compared with WT hESC and WT hiPSC line. Derived mutation-carrying lines of DMD hiPSCs were verified for the mutation presence by clinical multiplex ligation-dependent probe amplification (MLPA) analysis. Analysis was performed using SALSA MLPA P034 DMD mix 1 probemix and SALSA MLPA P035 DMD mix 2 probemix (LOT B1-1014, B1-0216, MRC Holland, Amsterdam, The Netherlands), according to manufacturer's instructions. ABI PRISM 3130 Genetic analyzer (Applied Biosystems, Foster City, CA, USA) was used to perform the experiment and data were analyzed using Coffalyser (MRC Holland, version v.140721.1958, Amsterdam, The Netherlands) software.

Short Tandem Repetition analysis for cell culture identity was performed using ABI PRISM 3130 Genetic analyzer and PowerPlex® ESI17 Fast System (Promega, Madison, WI, USA) according to manufacturer's recommendations. Karyotypes were analyzed after colchicine (2 μg/mL) incubation for 4 h, hypotonic solution treatment consisting of cultivation medium and water in ratio 1:3, bands were labeled using Giemsa staining. FISH analysis was performed using Cambio WCP 8 (SO); WCP 12 (SG) DNA Probe (Kreatech, Leica, Wetzlar, Germany). For off-target analysis, WGS libraries were prepared using NEBNext® Ultra™ II FS DNA Library Prep kit for Illumina (New Eengland Biolabs, Ipswich, MA, USA). Samples were sequenced at low coverage using Illumina NextSeq 500 (pair-end 2× 250 bp, with median coverage 2×). Sequences were aligned to reference genome using bwa [53] and CNVs were analyzed with Control-FREEC [54].

2.3. CRISPR/Cas9 DMD hESC Clone Generation

Dystrophin-deficient hESC lines were produced by CRISPR/Cas9 technology from WT hESC line CCTL14. Guiding RNA was designed to hit exon 51 of dystrophin gene. Set of complementary single-stranded DNA oligonucleotides—gRNA (DMD1_R1: 5′-CACCGCTTGGACAGAACTTACCGAC-3′, DMD1_R2: 5′-AAACGTCGGTAAGTTCTGTCCAAGC-3′) were cloned into pSpCas9(BB)-2A-GFP (PX458) (pSpCas9(BB)-2A-GFP (PX458), a gift from Feng Zhang (Addgene, Cambridge, MA, USA, plasmid # 48138) [55] and transfected into hESC line CCTL14 using FuGENE HD transfection reagent (Promega Corporation, Madison, WI, USA) according to manufacturer's instructions. The next day, green fluorescent protein (GFP)-positive cells were FACS-sorted (MoFlo Astrios, Beckman Coulter, Brea, CA, USA) as single cells into 96-well plate and clonally propagated. 54 clones were recovered and screened for the mutation in dystrophin gene by reverse transcription PCR on mRNA level. Appropriately selected

clones without signal for dystrophin were screened using MLPA analysis, which resulted in obtaining CRISPR DMD (cDMD) hESC line (for analysis used in passages 114–159).

2.4. Fluorescent Labeling

For detection of reactive oxygen and reactive nitrogen species (ROS/RNS), the DMD hPSC and WT hPSC cells were incubated with CellROX Green reagent (Life Technologies) for 1 h. Cells were then fixed with 4% paraformaldehyde (PFA) for 15 min at room temperature. Microscopic data were analyzed as signal intensity per area using FIJI/ImageJ [56]. All other fluorescent labeling was conducted with cells fixed by 4% PFA for 15 min in room temperature, then permeabilized with 0.5% Triton X-100 and blocked with 1% bovine serum albumin. Immunocytological analyses for pluripotent markers (Nanog, Oct4, SSEA4, TRA1-81) and cardiac markers (NOS, dystrophin, PCNA and laminB) were performed (for a complete list of antibodies and dilutions, see Supplementary Table S10). For dystrophin detection, the cells were fixed with 2% PFA and ice-cold methanol, and then incubated with preextraction buffer (25 mM HEPES, 50 mM NaCl, 1 mM EDTA, 3 mM $MgCl_2$, 200 mM sucrose, 0.5% Triton X-100) prior to standard protocol for immunodetection by fluorescent labels. For nuclear counterstain, 4′,6-diamidine-2′-phenylindole dihydrochloride (DAPI, Sigma Aldrich, St. Louis, MO, USA) was used. The DNA damage was analyzed using γH2AX detection with incubation in pre-extraction buffer (25 mM HEPES, 50 mM NaCl, 1 mM EDTA, 3 mM $MgCl_2$, 200 mM sucrose, 0.5% Triton X-100) for 10 min on ice prior to permeabilization. For analysis of DSB, the total number of foci per image was divided by the nuclei count per image. For double labeling of γH2AX and nNOS/iNOS/eNOS, the cells were fixed with 2% PFA and ice-cold methanol and then incubated with pre-extraction buffer. All fluorescent and confocal microscopy was performed using LSM700 confocal microscope (Carl Zeiss, Oberkochen, Germany).

2.5. Inhibition Conditions

To assess the influence of ROS on the formation of γH2AX foci, cells were treated for 24 h + 2 h with the ROS scavenger *N*-Acetyl-L-cysteine (NAC) at 5 mM concentration, the ″+″ indicating a medium change containing fresh NAC. To assess the effect of NOS on ROS release, cells were treated for 3 days with the NOS inhibitor Nω-nitro-L-arginine methyl ester hydrochloride (L-NAME) at a 0.1 μM concentration (N5751, Sigma Aldrich), prior to ROS/γH2AX foci analysis. For specific inhibition, L-canavanine (CAN, 100 μM, Sigma Aldrich, for iNOS), N(5)-(1-Iminoethyl)-L-ornithine HCl (L-NIO, 100 μM, Santa Cruz, for eNOS), spermine and spermidine (SM and SMD, 0,5 μM, both Sigma Aldrich, for nNOS) were used 3 days prior to γH2AX foci analysis. Silencing of each NOS isoform was performed using X-tremeGENE™ siRNA Transfection Reagent (Sigma Aldrich) and siRNA against NOS1 (nNOS, sc-29416, Santa Cruz), NOS2 (iNOS, sc-29417, Santa Cruz) or NOS3 (eNOS, sc-36093, Santa Cruz) in 250 nM concentration 48 h prior to γH2AX foci analysis. DNA damage analysis evaluation using γH2AX foci was then performed only on such colonies that showed an expression decrease compared to the non-silenced control.

2.6. Mutation Frequency

Mutation frequency (MF) experiments were performed on feeder-free cultures described in [46,57]. Hypoxanthine phosphoribosyltransferase (HPRT) based assays were performed to evaluate MF as described in [46] with minor modifications. Cells were seeded into media containing 2.5 μg/mL 6-thioguanine (TG; Sigma-Aldrich). The concentration of TG was increased to 8μg/mL 8 days after seeding. Mutants were selected after 3–4 weeks. MF was calculated as ratio of the number of selected mutant colonies to plating efficiency of cells in nonselective media. For induced MF, cells were irradiated by ionizing radiation (IR: 0.5 Gy/min; 137Cs; total of 3 Gy) 24 h after the initial plating. The medium was replaced every 1–2 days during a selection period of 3–4 weeks until clearly bordered colonies were manually counted. The final MFs were calculated as the ratio of the number of mutant colonies to the plating efficiency of cells in the nonselective medium at the beginning of the experiment.

For MF analysis in human fibroblasts, the cells were seeded in a medium consisting of KockOut DMEM with 10% FBS, 1% L-glutamine, 1% Penicilin/streptomycin and 7 µg/mL TG and replaced every 3–4 days. Mutants were selected after 5–7 weeks.

2.7. Western Blot

For dystrophin immunoblots, denaturated protein samples from cell lysates were run in 4–10% gradient polyacrylamide gel for 70 min/170 V/400 mA, blotted at 100 V/300 mA for 2 h and labeled with antibody against N terminal (NCL-DYSB, Leica) and C terminal (ab15277, abcam) of dystrophin protein. As a loading control, tubulin or laminB were used. Human heart atrial tissue was obtained as procedural surplus material, available during bicaval orthotopic heart transplantation from donor organs. For western blot analysis, the sample was homogenized and dissolved in RIPA buffer (10 mM Tris-Cl (pH 8.0), 1 mM EDTA, 0.5 mM EGTA, 1% Triton X-100, 0.1% sodium deoxycholate, 0.1% SDS, 140 mM NaCl, 1 mM phenylmethanesulfonyl fluoride) and the supernatant was used.

For DNA repair protein expression, 10% polyacrylamide gel was run for 60 min/170 V/400 mA and blotted for 1 h. Proteins were labeled with antibodies against ligase1, ligase 3, ligase 4, NBS1, Rad51 and APE1 in dilution as stated in Supplementary material (Table S10).

2.8. Reverse Transcription PCR

Total mRNA from cell samples, human heart samples, hPSC derived hepatocytes (obtained from Tereza Váňová Ph.D) and RPMI myeloma cells (obtained from Sabina Ševčíková) was isolated using RNA Blue reagent (Top-Bio, Prague, Czech republic) according to the manufacturer's instructions, and the total mRNA was isolated using the RNeasy Micro Kit (Qiagen, Hilden, Germany). mRNA concentration and purity was determined using NanoDrop (NanoDrop technologies, Wilmington, Germany). For reverse transcription PCR (rtPCR), cDNA was synthesized by Moloney Mouse Leukemia Virus (M-MLV) reverse transcriptase (Invitrogen, Carlsbad, CA, USA) at 37 °C for 1 h followed by 5 min at 85 °C. The consequent PCR using Taq polymerase (Top-Bio, T032) included denaturation at 94 °C for 10 min followed by cycles of 94 °C for 30 s, annealing step and extension at 72 °C for 1 min; the final extension step proceeded at 72 °C for 10 min. The PCR primers (Generi-Biotech, Hradec Kralove, Czech Republic) and annealing conditions are shown in Supplementary Table S11. The PCR product was then run in 1% agarose gel for 45 min/130 V/500 mA and photos were obtained using UV lamp DNR MiniBis Pro (Bio-Imaging Systems, Neve Yamin, Israel).

2.9. Statistical Analysis

Statistical evaluation was carried out in GraphPad Prism 6 software (GraphPad Software, Inc., La Jolla, CA, USA). At least 3 biological repetitions were used in each experiment, exact value for each is represented by • in each graph. Then n value, mean and standard deviation are stated in Supplementary Tables. Kolmogorov-Smirnov normality test was performed for obtained data. Student's t test, one-way ANOVA with appropriate multiple comparison post hoc test or two-way ANOVA with a Tukey's post hoc test was applied as appropriate. $p < 0.05$ was considered statistically significant. Individual test use is specified in figure legends. All measured data underwent post-hoc statistical power analysis [58] with appropriate α value (according to p-value determination in each experiment set) with all the power values result above 74%.

3. Results

3.1. Model DMD hPSC Cell Lines Harboring Dystrophin Mutation Are Pluripotent

Two independent DMD human induced pluripotent stem cell (hiPSC) lines DMD02 and DMD03 were derived from two patients harboring a mutation in the dystrophin gene, and individual clones were chosen empirically based on morphology (for patient data, see Supplementary Material). Both clones tested positively for pluripotent markers Nanog, Oct3/4, TRA1-81 and SSEA4 (Figure 1a) and the expression pattern was comparable to wild type (WT) hiPSC and WT human embryonic stem

cell (hESC). For a complete cell line description and identification (karyotype Figure S1, STR matching Tables S1 and S2), see Cell line description and identification (Supplementary material).

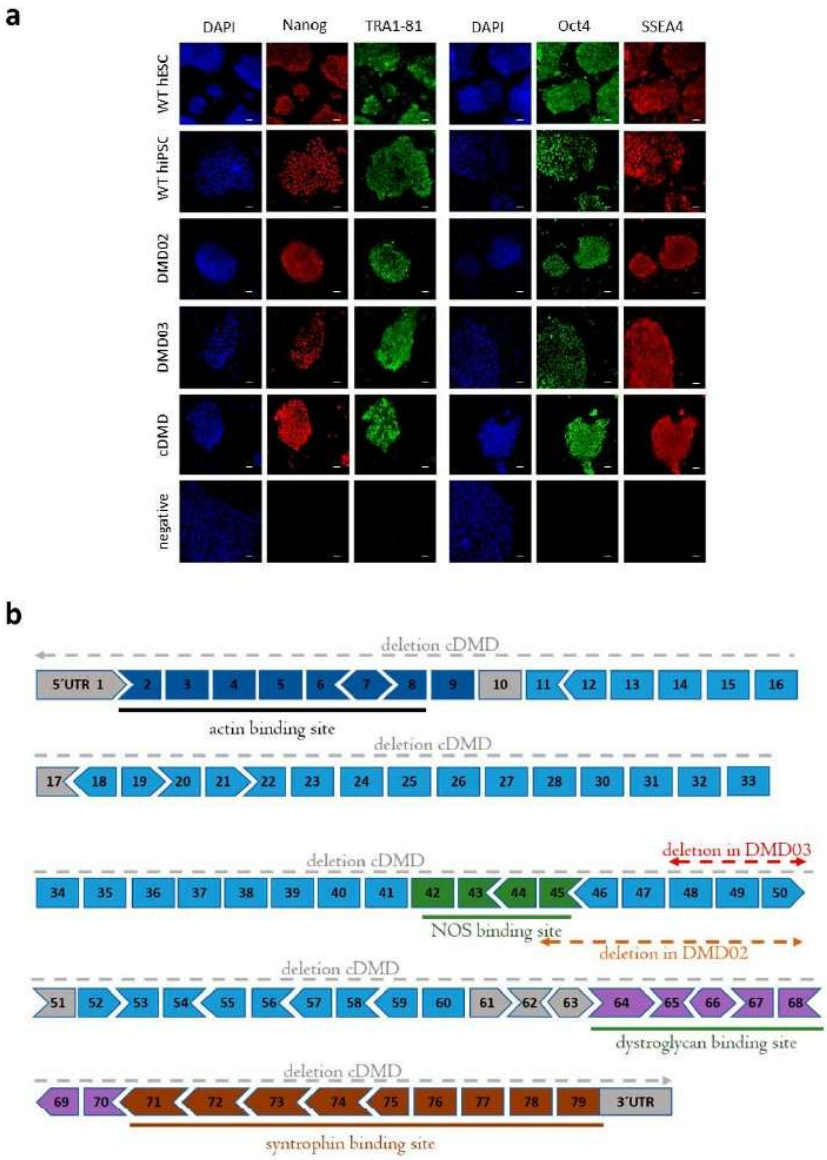

Figure 1. DMD hPSC lines are pluripotent. (**a**) Two patients derived (DMD02 and DMD03) and hESC derived (cDMD) DMD stem cell lines were analyzed for presence of pluripotency markers (Nanog (red on the left), TRA1-81 (green on the left) with their corresponding DAPI staining, and Oct4 (green on the right), SSEA4 (red on the right) with their corresponding DAPI staining). All DMD hiPSC and cDMD lines present comparable expression to WT (WT hESC and WT hiPSC). Nuclei are counterstained with DAPI (blue). Ruler represents 50 µm. (**b**) Structure of the DMD gene and positions of mutations in each DMD hPSC line. Locations of binding sites for actin, NOS, dystroglycans and syntrophins are shown. The diagram shows how the 79 exons fit together in terms of the normal open reading frame. Exons are colored according to the domain they encode: N-terminus (dark blue), rod domain (light blue dark green with hinge regions in grey), cysteine-rich domain (purple) and C-terminus (brown). NOS binding site is visualized in green. DMD02 line carries deletion of exons 45–50 (red line), DMD03 deletion of exons 48–50 (orange line) and cDMD lacks a whole allele and all exons are deleted from the chromosome (grey line).

The ability of DMD hiPSC to spontaneously differentiate in vitro into embryoid bodies (EBs) containing all three germ layers 15 days post aggregation was shown using reverse transcription PCR (Figure S3) and compared to WT hESC, serving as a standard of pluripotency. A similar pattern of expression change of early differentiation markers ectoderm (NEUROD1, PAX6), and mesoderm (GATA6, VIM) were found in EBs from both DMD hiPSC and WT hESC lines. Endodermal markers (AFP and GATA4) were also present in both DMD hiPSC and WT hESC lines, but AFP expression level was higher in DMD hiPSC.

The hESC line with a complete loss of one allele of DMD gene (cDMD) was obtained by CRISPR/Cas9 technology (MLPA analysis, Figures S4 and S5). The cDMD line was tested for pluripotency marker expression with positive labeling for Nanog, Oct3/4, Tra1-81 and SSEA4 (Figure 1a). For further description of the line (karyotype Figure S1, sequencing Figure S2, STR matching, and MLPA Figures S4 and S5), see Supplementary material (Cell line description and identification, Figures S1 and S2).

A complete characterization of mutation localization in each DMD hPSC line is illustrated in Figure 1b.

3.2. WT hPSC, But Not DMD hPSC, Express High Molecular Weight Isoform of Dystrophin

mRNA analysis of exons 52–54 (downstream of the patient's mutation) revealed that all tested WT hiPSC and WT hESC expressed dystrophin mRNA (Figure 2a,b), although the expression was weaker compared to adult healthy human heart biopsy (for human heart biopsy details, see Materials) or beating cardiac EBs differentiated from hPSC.

All tested WT hPSC also expressed the high molecular weight dystrophin protein, as shown by western blot protein analysis (427 kDa; Figure 2c and Supplementary Figure S6). The DMD hiPSC derived from both patients and cDMD presented a complete loss of dystrophin expression on mRNA levels (Figure 2b) and protein levels (Figure 2c) compared to the corresponding control hPSC.

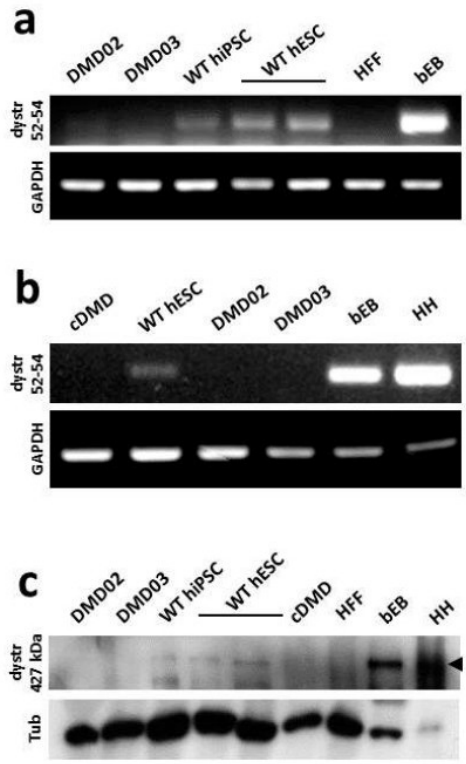

Figure 2. WT hPSC, but not DMD hPSC, express dystrophin. (**a**) Dystrophin mRNA exons 52–54 were detected by rtPCR in both WT hiPSC and hESC lines and in CM containing beating embryonic bodies (bEB). No signal was detected in DMD hiPSC lines. GAPDH was used as a loading control. Human foreskin fibroblasts (HFF) were used as negative control. (**b**) demonstrates the absence of expression of dystrophin mRNA exons 52–54 in cDMD line. For positive control, bEB and human heart (HH) sample were used. DMD02 and DMD03 hiPSC lines were used for lack of expression comparison. (**c**) High molecular weight dystrophin (dystr) protein (Dp427 isoform; antibody against N-terminal part) is expressed in pluripotent stem cells as shown by immunoblot of dystrophin expression in WT hiPSC and two WT hESC lines, while all DMD hPSC lines show complete lack 427 kDa form of dystrophin. As a positive control, human heart (HH) biopsy of non-dystrophic patient was used together with WT hESC derived bEB. HFF were used as a negative control. Tubulin (Tu) was used as a loading control. Loading of bEB and HH was adjusted not to overload dystrophin due to its high expression. DMD hPSC lines are pluripotent.

3.3. Dystrophin Defect Leads to Elevated Oxidative Stress in DMD hPSC

Based on the observation of dystrophin expression in pluripotent stem cells and its loss due to the mutation, we asked whether dysfunctions associated with DMD muscle cells such as ROS elevation [28,34] were also present at the pluripotent state. We analyzed production of ROS in the DMD hPSC lines (DMD02, DMD03 and cDMD) using CellROX dye (Figure 3a), (detects both, ROS and RNS). All DMD hPSC lines presented significantly increased ROS production (normalized values evaluated by one sample *t* test to relative value of WT controls) (Figure 3b, Table S1). Even though a significant change in ROS presence was identified, the mRNA expression of antioxidant enzymes is not changed with the exclusion of GPX3, whose expression was elevated in all DMD lines compared to WT hPSC (Supplementary material Figure S7). Treatment with ROS scavenger N-acetyl-L-cysteine (NAC) led to a significant reduction in ROS level in DMD hiPSC lines (Figure 3c, Table S1) comparable to WT hPSC (Figure S8) while no change after NAC treatment was detected in WT hESC (Figure 3c). In order to eliminate the genetic variability of the individual cell lines from specific effect of NAC, all WT and all DMD hPSC lines were pooled together, showing that significantly elevated ROS level in

DMD hPSC ($p < 0.0001$) can be reduced to the level of WT hPSC by the application of NAC ($p = 0.6270$ as evaluated by Wilcoxon test comparing control values from WT iPSC and WT hESC to corresponding NAC treated DMD lines, Figure S8, Supplementary Table S2).

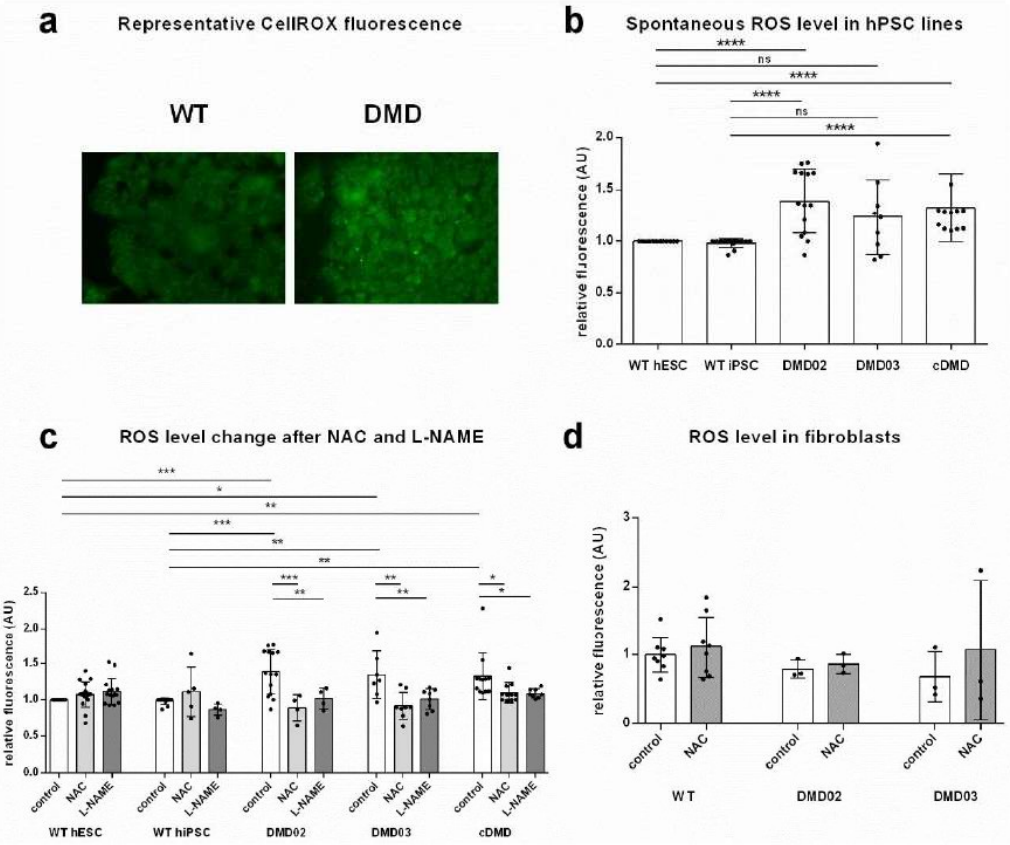

Figure 3. Elevated spontaneous NOS induced ROS release in DMD hPSC. (**a**) Representative example of ROS level in hiPSC line DMD03 compared to WT hESC. Fluorescence intensity per area (Image J) was normalized to WT hESC. (**b**) Spontaneous level of ROS measured by CellROX Green dye fluorescent signal in DMD hPSC lines is elevated compared to the WT hESC. Statistical significance was evaluated by One sample *t*-test comparing the values to normalized relative control in WT hESC and WT hiPSC (* $p < 0.05$, ** $p < 0.01$, *** $p < 0.001$). Error bars show standard deviation. (**c**) ROS production with ROS scavenger N-acetyl-L-cysteine (NAC) treatment was significantly decreased in all tested DMD hPSC lines but not WT hPSC lines compared to the cells with no treatment. ROS production with NOS inhibitor L-NAME decreased significantly in all DMD hPSC lines. Graph shows change in fluorescent intensity per area expressed as percentual value of untreated controls of corresponding hPSC line. Statistical difference was evaluated by two-way ANOVA comparing the NAC/L-NAME treated cells to non-treated control cells as well as WT cells compared to DMD cells. (**d**) ROS levels in DMD fibroblasts from both DMD patients used for reprogramming do not differ from three independent WT foreskin fibroblasts from newborn boys at similar passage number. Statistical difference was evaluated by one-way ANOVA. At least 3 biological repetitions were used in each experiment, exact value for each is represented by • in each graph.

In order to exclude genetic bias, DMD patient specific primary fibroblast cultures, which were used to reprogram the DMD hiPSC lines, were also tested for ROS level together with two different WT primary cell lines of human foreskin fibroblasts as controls. No differences in the ROS levels between DMD and WT fibroblasts were observed ($p = 0.2$) which corresponds to the absence of high molecular

weight dystrophin expression in fibroblasts. Similarly, the NAC treatment did not have effect on ROS accumulation in WT or DMD fibroblasts ($p = 0.7$) (Figure 3d, Supplementary Table S3).

3.4. Inhibition of NOS Activity Led to Decrease in ROS Production in DMD hPSC But Not in WT hPSC

In order to evaluate the contribution of DGC-associated NOS on the oxidative stress in hPSC, we analyzed the ROS release in DMD hPSC lines and WT hPSC in presence and absence of Nω-nitro-L-arginine methyl ester hydrochloride (L-NAME), a non-specific NOS inhibitor (Figure 3c, Table S1). The inhibition of NOS led to significant decrease of ROS release in DMD hPSC. The resulting level of ROS in DMD hPSC with L-NAME inhibited NOS matched the level found in WT hPSC ($p = 0.1207$ as evaluated by Wilcoxon test comparing control values from WT iPSC and WT hESC to corresponding L-NAME treated DMD lines, Figure S8, Table S2). In contrast, the WT hESC showed no difference under L-NAME treatment ($p = 0.1926$), WT hiPSC showed a decrease by 10% of ROS level (Figure 3c and Figure S8).

3.5. NOS Activity Is Elevated in DMD hPSC Lines

To examine if the increased ROS are caused by increased expression, or increased activity of NOS, the RNA expression and NOS activity were analyzed. The NOS activity assay showed significant increase in NOS activity in all DMD hPSC lines compared to WT hPSC lines (Figure 4a). ($p = 0.0023$). At the same time, all NOS isoforms' (nNOS, iNOS and eNOS) mRNAs were expressed in WT and DMD hPSC (Figure 4b) without any quantitative change in expression levels (Supplementary Table S4). It ought to be said that a known ROS producer in DMD CMs, NADPH oxidase (NOX2), is not expressed in pluripotent state at all as determined by rtPCR (Figure 4c).

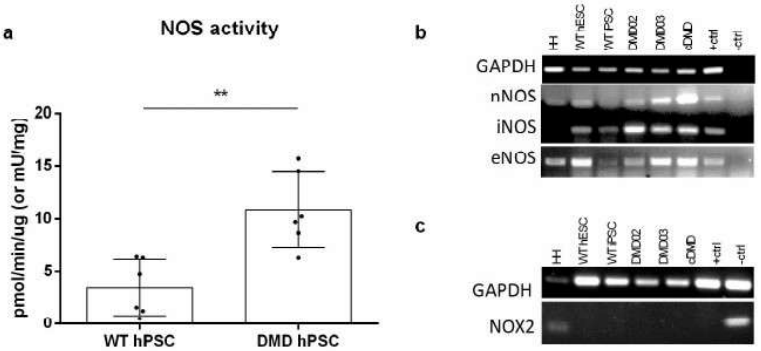

Figure 4. Enzymatic NOS activity is increased in DMD hPSC lines. (**a**) NOS activity assay showed increased production of NO (in pmol/min/μg) in DMD hPSC lines when compared to WT hPSC. 6 independent repetitions (for each WT and DMD hPSC) were used for the analysis. Student *t*-test was used for statistical evaluation of significance (** $p < 0.01$). Errorbars show standard deviation. (**b**) All three NOS isoforms (nNOS, iNOS and eNOS) are expressed in WT as well as in DMD hPSC. For a positive control (+ctrl), HH (for NOX and nNOS), hepatocytes (for iNOS) or RPMI myeloma cells (for eNOS) were used. Water instead of cDNA was used for negative control (−ctrl). GAPDH was used as loading control. (**c**) mRNA analysis revealed that NOX2, is not expressed in pluripotent state. Human heart tissue (HH) was used as positive control, GAPDH was used as loading control. At least 3 biological repetitions were used in each experiment, exact value for each is represented by • in each graph.

3.6. Elevated ROS Leads to Elevated DNA Damage in DMD hPSC

Our next step was to investigate the DNA damage in response to elevated ROS in DMD hPSC. We analyzed the presence of foci of histone H2A phosphorylated on serine 139 (γH2AX) associated with DNA double stranded breaks (DSB) in cell nuclei in hPSC lines (Figure 5a,b). We found a significantly elevated number of γH2AX foci per nuclei in both DMD hiPSC lines and cDMD compared to WT hPSC (for exact values, see Supplementary Table S3). Similar to ROS levels, no elevation in γH2AX foci formation was observed in the source DMD fibroblasts from the patients compared to

WT fibroblasts (Figure 5c) showing that elevated γH2AX foci formation is associated with DMD hPSC cellular physiology. We also show that expression of none of the DNA repair proteins representing the major DNA repair pathways decreases specifically in DMD clones compared to WT (Supplementary Material Figure S9), suggesting that DNA repair failure does not participate on the elevated DNA damage in DMD hPSC. In order to determine the actual contribution of oxidative stress to oxidative DNA damage and the DSB formation, we analyzed the γH2AX foci in presence of ROS scavenger NAC (Figure 5a). The NAC treatment resulted in significant decrease of the γH2AX foci in DMD hPSC, while no change of γH2AX foci number was detected in WT hPSC line (Figure 5a).

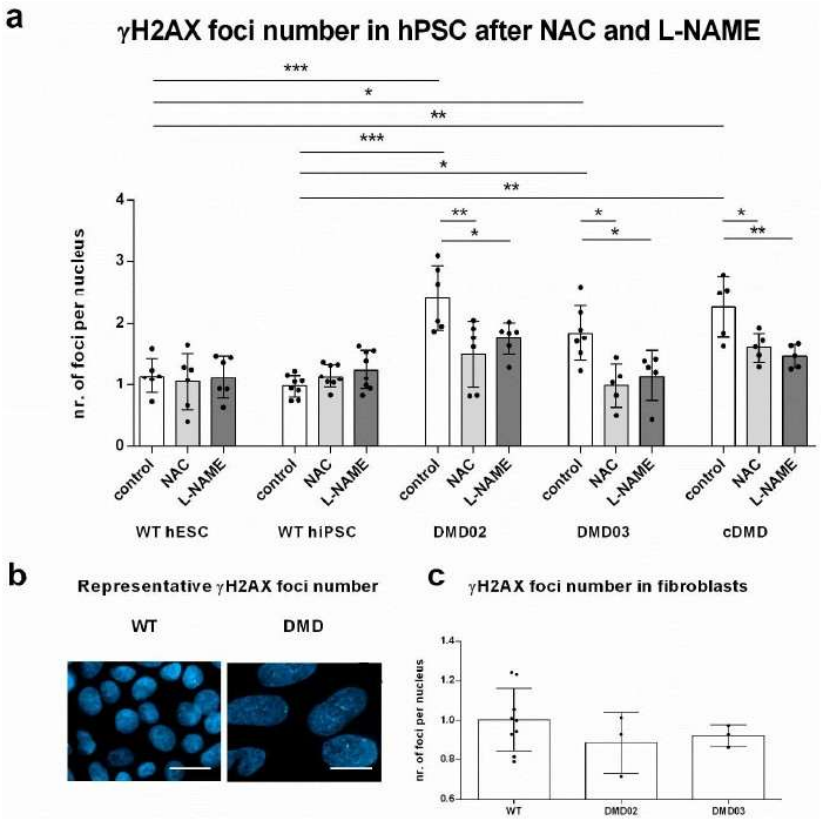

Figure 5. Elevated ROS level in DMD hPSC leads to DNA damage. (**a**) Numbers of γH2AX foci representing the spontaneous DNA damage in DMD02, DMD03 and cDMD hPSC lines were significantly elevated compared to WT hESC and WT hiPSC. Spontaneous formation of γH2AX foci in all DMD hPSC lines significantly decreased after the NAC treatment to the level of WT hPSC. No effect of NAC on the WT hPSC lines was observed. All DMD lines show significant decrease in γH2AX foci formation after treatment with L-NAME corresponding to the decrease detected after NAC treatment. WT hiPSC show increase after L-NAME treatment. Statistical difference was evaluated by one-way ANOVA and Sidak's multiple comparison test (* $p < 0.05$, ** $p < 0.01$, *** $p < 0.001$) for γH2AX foci number in between different lines, and unpaired Student's *t*-test comparing the NAC/L/NAME treated cells to corresponding untreated control cells. Error bars represent standard deviation. (**b**) Representative image of γH2AX foci staining in CCTL14 (WT) and DMD02 (DMD) hiPSC showing higher number of γH2AX foci number in DMD nuclei compared to WT nuclei. γH2AX foci are stained in green, nuclei in blue with DAPI. Line represents 20 μm. (**c**) DNA damage is not increased in DMD fibroblasts before reprogramming. γH2AX foci number per nucleus in DMD fibroblasts from both DMD patients used for reprogramming does not differ from WT foreskin fibroblasts. Statistical difference was evaluated by one-way ANOVA. The errorbars show standard deviation. At least 3 biological repetitions were used in each experiment, exact value for each is represented by • in each graph.

3.7. NOS Activity Causes ROS Release Which Leads to DNA Damage in DMD hPSC

In order to establish the upstream role of NOS activity in the induction of the DNA damage in DMD hPSC, γH2AX foci formation was analyzed after L-NAME treatment (Figure 5a, exact values in Supplementary Table S3). Inhibition of NOS resulted in significant decrease in the γH2AX foci level in all tested DMD hPSC lines. Similar to NAC treatment, the WT cells did not respond to the L-NAME treatment by decrease in the γH2AX foci formation; instead, the WT hiPSC, but not WT hESC, accumulated a significantly increased number of γH2AX foci. In summary, these data show that dystrophin deficiency in hPSC leads to the production of ROS associated with NOS activity, and that this mechanism significantly contributes to the DNA DSB formation in hPSC.

3.8. DNA Damage Increase in DMD hPSC Is Caused by nNOS, iNOS and eNOS Isoforms of NOS

In order to determine which NOS isoform is responsible for ROS-induced DNA damage, all cell lines underwent treatment with siRNA against nNOS, iNOS or eNOS (Figure S10). While silencing of any of the NOS isoform in WT hPSC did not result in detectable response in γH2AX foci number, all DMD hPSC lines showed significant decrease in γH2AX foci formation after individual silencing of separate NOS isoforms (Figure 6a and Figure S11, Supplementary Tables S8–S10). All WT and DMD hPSC lines were then treated with a set of selective inhibitors prior to γH2AX foci analysis. iNOS inhibitor L-canavanine (CAN), eNOS inhibitor N(5)-(1-Iminoethyl)-L-ornithine HCl (L-NIO) and two selective inhibitors of nNOS spermine (SM) and spermidine (SMD) were used. In DMD hPSC, all inhibitors showed a decreasing trend in γH2AX foci formation with L-NIO and SM presenting a significant decrease in DMD02 and cDMD, respectively (Figure S12, Supplementary Table S7), but only CAN presented a significant change in all DMD hPSC lines (Figure 6b and Figure S12, for exact values see Supplementary Tables S9 and S10). In WT hPSC, only SM showed an increase in γH2AX foci formation in separate lines (Figure S12, Supplementary Table S7), but with no significant change overall when data from WT hPSC were pooled (Figure 6b, Supplementary Table S6).

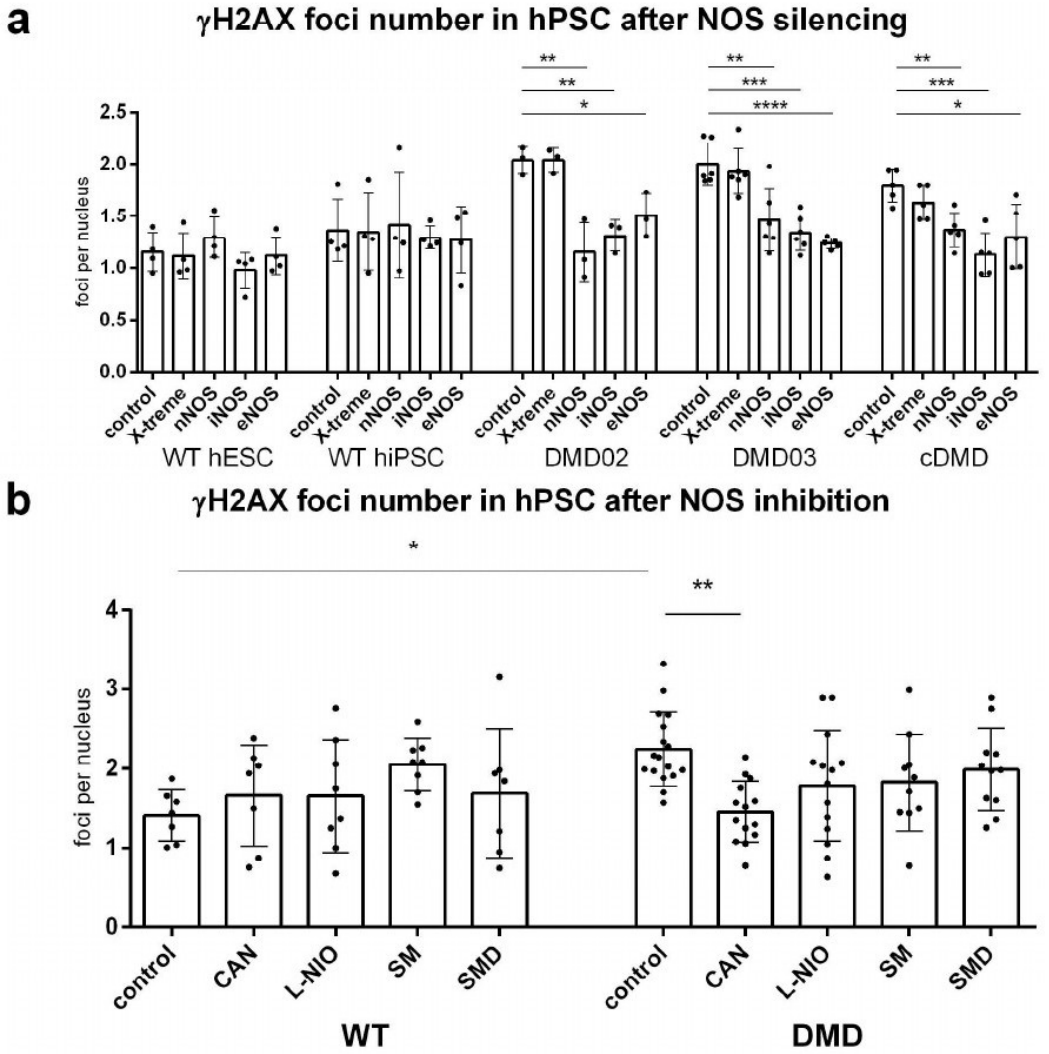

Figure 6. All isoforms of NOS are responsible for increased DNA damage in DMD hPSC. (**a**) DNA damage analysis after downregulation of each individual NOS isoform's expression show significant decrease in γH2AX foci formation in DMD hPSC while no significant effect was observed in WT hPSC. Graph shows γH2AX foci per nucleus for each individual hPSC line in untreated samples (control), after application of transfection reagent (X-treme) and with application of individual siRNA (nNOS, iNOS and eNOS). Statistical difference was evaluated by two-way ANOVA and Tukey's multiple comparison test using the mutation and treatment presence as evaluation criteria (* $p < 0.05$, ** $p < 0.01$, *** $p < 0.001$, **** $p < 0.0001$). The error bars represent standard deviation. (**b**) DNA damage analysis after application of specific inhibitors to individual NOS isoforms (CAN = L-canavanine, L-NIO = (N(5)-(1-Iminoethyl)-L-ornithine HCl), SM = spermine, SMD = spermidine) show decreasing trend in γH2AX foci presence in DMD hPSC. CAN suppressed significantly DNA damage formation in DMD hPSC cell lines while no significant effect was observed in WT hPSC. Graph shows pooled data from WT hESC and hiPSC (WT) and all 3 DMD hPSC lines (DMD). Statistical difference was evaluated by one-way ANOVA and Sidak's multiple comparisons test; ** $p < 0.01$, the error bars represent standard deviation. At least 3 biological repetitions were used in each experiment, exact value for each is represented by • in each graph.

3.9. Dystrophin Defect Leads to Compromised Genomic Stability of hPSC

We analyzed the mutation frequency (MF) of all DMD hPSC lines and compared it to that of WT hPSC using our HPRT based assay, developed previously [46]. We found that the MF in DMD hPSC was significantly elevated, differing approximately one order of magnitude from both WT hPSC (Figure 7). Induction of DNA damage with ionizing radiation (3 Gy) increased MF in all tested cell lines, preserving the difference between the DMD hPSC and WT hPSC, suggesting a cumulative effect of ROS and IR induced DNA damage on the MF (Figure S13, Supplementary Table S8). No elevation in MF was observed in the source DMD fibroblasts from the patients compared to WT fibroblasts ($p = 0.49$) (Figure 7b), showing that elevated mutagenesis is specifically associated with stem cells, presumably because fibroblasts do not express high molecular mass isoforms of dystrophin as visible in immunoblots. In summary, we show that NOS activity in dystrophin deficient DMD hPSC leads to elevated ROS and DNA damage, which eventually leads to the deterioration of genomic stability in DMD hPSC.

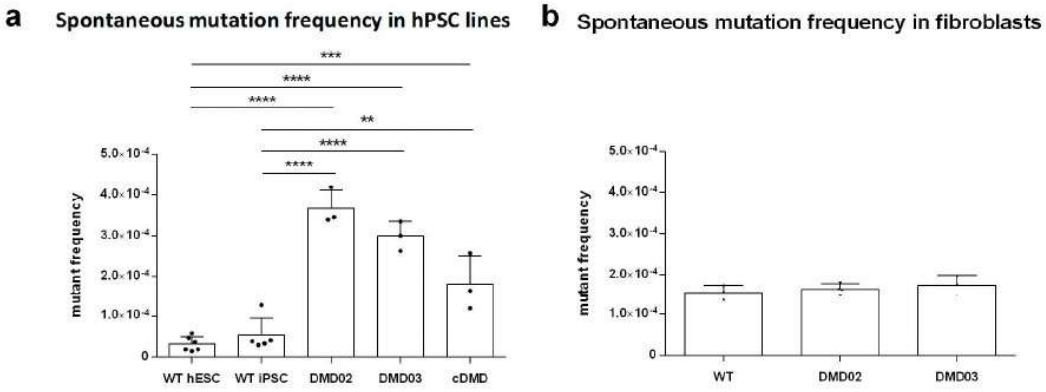

Figure 7. DMD hPSC lines present increased mutation frequency (MF). (**a**) MF of both patient specific hiPSC lines (DMD02 and DMD03), cDMD line and WT hESC and hiPSC line were measured using HPRT reporter assay. The graph shows significantly elevated spontaneous MF in all DMD hPSC lines compared to both WT hPSC lines. (**b**) The parental patient specific fibroblasts (DMD02 and DMD03) were compared to WT human foreskin fibroblasts of similar passage to exclude artificial effect of present MF before the reprogramming. No statistical difference was found in between all analyzed fibroblast lines. Statistical difference was evaluated by one-way ANOVA and Sidak's multiple comparison test (* $p < 0.05$, ** $p < 0.01$, *** $p < 0.001$, **** $p < 0.0001$). The error bars represent standard deviation. At least 3 biological repetitions were used in each experiment, exact value for each is represented by • in each graph.

4. Discussion

A few cellular models of human DMD hiPSC have been introduced recently [59,60] and reviewed in [61], and their features with regard to dystrophin deficiency have not been properly explored so far. We have obtained two independent DMD iPSC lines derived from two DMD patients which were compared to unrelated WT hiPSC and WT hESC line. We further generated cDMD hESC line by introducing DMD gene deletion in healthy hESC line using CRISPR/Cas9 strategy in order to provide a pair of isogenic cell lines, where one of them lacks dystrophin expression to eliminate the bias of varying genetic background. Our findings demonstrate for the first time aberrant phenotype of the DMD hiPSC lines and cDMD compared to WT cell lines associating the described phenotype to dystrophin expression, rather than to varying genetic background [62] or heterogeneity of different hiPSC lines [63].

Even though the molecular mechanisms causing the DMD CM death are somewhat described, no sufficient explanation on delayed myopathy development leading to muscle wasting has been offered. Recently, the skeletal muscle progenitor satellite cells [36] were also shown to express

dystrophin. The absence of dystrophin expression in mice led to defects in asymmetric division [36], and skeletal muscle degeneration was shown to be a consequence of satellite cell depletion [35]. Impaired self-renewal, earlier senescence, differentiation and homing defects were also reported for cardiac progenitors in GRMD dog model [64].

For the first time, we show that hPSC expresses various forms of dystrophin, including the high molecular weight isoform, which was previously associated with myocytes [36]. These data suggest that dystrophin might play a crucial role in the stem or progenitor cell pool, long before definite differentiation into skeletal myotubes or CMs. Data on the dystrophic progenitor phenotype together with expression of dystrophin in hPSC suggest that the general stem cell population might be vulnerable to DMD-related damage, and that hPSC lacking dystrophin might serve as valid model for molecular mechanisms leading to DMD related stem cell phenotype. The depletion of *mdx* mouse satellite cells has been connected to up-regulation of Notch and pro-inflammatory signaling molecules in skeletal muscle [65]. The effect of Notch signaling on the progenitor fate decision was shown to be associated with elevated level of ROS, such as that in lamellocytes [66]. ROS were shown to induce loss of stemness [67] and cell fate change [68] via increased DNA damage and the activation of checkpoint mechanisms [67]. ROS were also shown to contribute to the pathophysiology of muscular dystrophies [3], as well as to DMD [69,70]. We extend this knowledge by showing that not only CMs [28,71–73], but already DMD hPSC suffer from elevated ROS levels due to increased NOS activity. ROS readily induces DNA mutations [74] via oxidative DNA damage [75,76]. The ROS-induced DNA base damage is readily converted by base excision repair to DSB in hPSC [77], triggering histone H2A phosphorylation (γH2AX) and compromising the genomic stability of hPSC [46]. Our data show elevated DNA DSB (detected by γH2AX) in DMD hPSC. The ability of antioxidant NAC to downregulate the DNA DSB in DMD hPSC indicates that DSBs originate from ROS-induced DNA damage. We further show that ROS-induced DNA damage is reflected by elevated MF in DMD hPSC, which is in agreement with the concept of oxidative DNA damage mutagenicity [78]. The NOS-induced, ROS-mediated stem cell genome destabilization might also help to explain increased susceptibility of DMD patients to malignant sarcoma [79], which was previously also associated with elevated DNA damage [80]. DNA damage was shown in hematopoietic stem cells to drive their differentiation into terminally-differentiated cells [38]. We suggest that the DNA damage and mutagenesis shown in DMD hPSC might lead to diminished stem cell potential and stem cells' ageing (reviewed e.g., [81]), and subsequent stem cell depletion.

Mitochondrial damage [82] due to ROS production in the *mdx* murine myocytes was in the past attributed to mitochondrial ROS release [26]. In this context, all three isoforms of NOS seem to have a physiological role in myocytes, including CMs [73]. All three isoforms seem to be capable of interaction with DGC via 16–17 spectrin-like repeat of dystrophin (coded by exons 42–45,) but also via PDZ domain on α1-syntrophin [83] or through caveolin interaction [84]. The loss of dystrophin results in the increase of NOS activity, as shown by comparing the NOS activity in WT and DMD hPSC. Further inhibition of NOS was shown to block the synergistic effect of mechanical and oxidative stress on sarcolemmal damage in *mdx* mice [85], implicating NOS in oxidative stress regulation. Active endothelial NOS (eNOS) has been previously shown to be associated with attenuated superoxide production [86]. nNOS or inducible NOS (iNOS) deregulation were also shown to be associated with elevated ROS levels in myocytes [21,73,87]. iNOS has been previously shown to be overexpressed in myocytes in response to DMD pathophysiology [88]. We showed that inhibiting the general NOS activity in DMD hPSC leads to decreased ROS level, and consequently, to decreased DNA damage level. The effect was dystrophin specific and not caused by genetic variability or reprogramming, as it was neither detected in the WT hPSC nor in the donor fibroblasts. Only in WT hiPSC, the L-NAME treatment lowered ROS level and significantly increased the detected DNA damage. This might have only limited biological relevance, because the change is small (up to 30%) compared to DMD cell lines, and WT hESC did not respond to the treatment at all. Individual silencing of all NOS isoforms using specific siRNA led in all

three cases to a significant decrease in γH2AX foci formation in DMD hPSC, proving that each of the NOS isoform plays a role in regulation of ROS production and consequent DNA damage.

Inhibition of individual NOS isoforms by specific inhibitors also resulted in a decrease in ROS production, as well as γH2AX foci formation specific to DMD cell lines; however, except for CAN on γH2AX foci formation, these results did not reach significance. This can be explained by the incomplete inhibition or incomplete penetration of the inhibitors to the cells, but also by their off-target effect, such as, for example, the capacity of L-NIO/SM and SMD to regulate processes such as cell proliferation and differentiation [89,90] or DNA binding [91]. It has been shown that nNOS is bound to dystrophin through its PDZ domain [83,92], and eNOS is binding to DGC through caveolin [93]. Also, higher activity of eNOS has been shown when dissociated from caveolin [94,95], and changed nNOS activity in *mdx* CMs has been reported [19]. Our work shows that a lack of dystrophin leads to the loss of dystrophin-associated regulatory function on nNOS, eNOS and iNOS activity triggering ROS release and consecutive DNA damage. ROS and DNA damage increase in DMD hPSC. But the expression of antioxidant enzymes with an exception in GPX3, that is increased in DMD hPSC, did not decrease. Also the expression of the major DNA repair proteins was unaltered in DMD hPSC. It is thus unlikely that these processes participate in the oxidative DNA damage observed in DMD hPSC. This suggests that the failure of dystrophin to organize the dystrophin-associated proteins binding NOS deregulates ROS producing activities in hPSC similarly to dystrophic CMs [21,73]. These results also explain the failure of an attempt to compensate the nNOS by nitrate supplementation, which had detrimental effect on *mdx* mice muscle, presumably by even further elevating oxidative stress [96]. It must be noted that the NOS-mediated ROS production may be just part of total ROS release, which was previously associated also with mitochondrial complex-I insufficiency [26], but it might also lead to a ROS vicious cycle mediated by NF-kB induction [28], shown in *mdx* mice skeletal muscle. Since we showed that hPSCs do not express any NOX2, a main ROS producer in myocytes and CMs in DMD [27,28], it is unlikely that NOX2 would be responsible for the ROS production in pluripotent state.

In summary, our results suggest, for the first time, that dystrophin deficiency in DMD affects the genomic stability of human DMD hPSC. We propose that the absence of dystrophin in stem cells leads to the deregulation of NOS, which leads to ROS upregulation, DNA damage and mutagenesis. That, in turn, can be reflected by genomic instability-driven differentiation of the progenitors similar to human mammary epithelial cells [97], mice hematopoietic stem cells [38,98] or hair follicle [37] stem cells. However, while it is not clear whether the DMD-associated hPSC phenotype will be mimicked by tissue stem cells/progenitor impairment, we hypothesize, that progressive DNA damage/mutagenesis-driven depletion of stem cell population would explain the development of delayed muscle impairment associated with Duchenne muscular dystrophy.

Supplementary Materials: The following are available online. Patient data and diagnosis; Cell line description and identification; Figure S1: Karyotypes of used DMD lines and their parental source cells. Figure S2: Analysis of mutations induced by off target cleavage by DMD targeted CRISPR/Cas9 by whole genome sequencing and subsequent alignment; Figure S3: DMD hPSC do not differ in their differentiation capacity from WT hESC in in vitro spontaneous differentiation assay.; Figures S4 and S5: MLPA analysis of DMD patients derived hiPSC and cDMD; Figure S6: hPSC express various isoforms of dystrophin; Figure S7: Antioxidant enzyme expression level is not changed; Figure S8: The spontaneous level of ROS in DMD hPSC lines was significantly elevated compared to the WT hPSC; Figure S9: Protein expression of DNA repair proteins does not change in DMD hPSC; Figure S10: Expression downregulation efficiency of iNOS, nNOS and eNOS using siRNA; Figure S11: Individual downregulation if iNOS, nNOS and eNOS using siRNA leads to decreased DNA damage. Figure S12: Use of nNOS, iNOS and eNOS specific inhibitors decreases DNA damage in DMD hPSC only partially. Figure S13: Spontaneous and IR induced mutation frequency (MF) is elevated in DMD hPSC; Table S1: Relative fluorescence of ROS analyzed by CellROX labeling and image analysis; Table S2: Pooled data for WT and DMD hPSC with relative fluorescence by CellROX labeling and image analysis; Table S3: Exact values of γH2AX foci per nuclei with N-acetyl cysteine and L-NAME treatment; Table S4: Quantification of NOS isoforms expression; Table S5: Exact values of γH2AX foci per nuclei after specific NOS silencing; Table S6: Exact values of γH2AX foci per nuclei after specific NOS silencing, pooled data for WT and DMD hPSC; Table S7: Pooled data for WT and DMD hPSC with γH2AX foci per nuclei with specific NOS inhibitors; Table S8: Exact values of γH2AX foci per nuclei with specific NOS inhibitors; Table S9: Mean values of mutation frequencies in separate lines; Table S10: Antibodies; Table S11: PCR primers and cycling conditions.

Author Contributions: S.J. was responsible for writing of the manuscript, cell cultivation and differentiation, ROS and γH2AX analysis, pluripotency markers analysis (ICC and RT-PCR, including in vitro differentiation assay), detection of dystrophin by rtPCR and ICC. P.F. contributed by immunoblot analysis of dystrophin presence, ROS and γH2AX analysis, A.K. to cell cultivation, HPRT mutation assay and A.V. to cell cultivation. L.M. derived patient specific iPSC lines and cultivated the obtained cells, provided of pluripotency labeling and cryopreservation. M.P. was in charge of patient coordination and manuscript revision. T.J. contributed with cell cultivation and γH2AX analysis, M.K. helped with cell cultivation and HPRT mutation assay. J.V. together with I.F. generated the CRISPR/Cas9 cDMD line, I.F. also helped with cell cultivation, γH2AX and ROS analysis. R.G. and I.V. provided of MLPA analysis. G.F., A.L., P.D. revised the manuscript. A.C.M. and V.R. were in charge of manuscript revision, experiment supervision and are the responsible authors.

Funding: This work was supported by the Grant Agency of the Czech Republic (grant no.: P302/12/G157) and by the Ministry of Education, Youth, and Sports of the Czech Republic (7AMB13FR011), supported by the project no. LQ1605 from the National Program of Sustainability II (Ministry of Education, Youth, and Sports of the Czech Republic) and by the project FNUSA-ICRC no. CZ.1.05/1.1.00/02.0123 (OP VaVpI). Petr Fojtik (grant PHD talent 2015) and Tereza Jurakova were supported by The South Moravian Center for International Mobility and Sarka Jelinkova was supported by Campus France/PHC Barrande (grant nr. 843886B, Duchenstem 28379TE and 35662WG). This work also obtained financial contribution from the European Community within the Seventh Framework Program (FP/2007-2013) under Grant Agreement No. 229603. Albano C. Meli was supported by The French Muscular Dystrophy Association (AFM; project 16073, MNM2 2012 and 20225), the "Fondation de la Recherche Médicale" (FRM; SPF20130526710), the "Institut National pour la Santé et la Recherche Médicale" (INSERM) and SoMoPro—Marie Curie Actions—South Moravian Region and by the European Society of Cardiology (ESC) (R12042FF).

Acknowledgments: We thank Petr Vondracek (Department of Neurology, University hospital Brno, Brno, Czech Republic), Lenka Mrazova (Department of Neurology, University hospital Brno, Brno, Czech Republic) for the access to the patient databases, patients' and their relatives' biopsies. We also thank Irena Koutna and Pavel Simara (both Faculty of Informatics, Masaryk University, Brno, Czech Republic) for providing us with the control WT hiPSC line epi, Majlinda Lako (Institute of Genetic Medicine, Newcastle University) for providing us with cl1 hiPSC line. We thank Sabina Ševčíková and Tereza Váňová (both Faculty of Medicine, Masaryk University, Brno) for the samples of RPMI myeloma cells and hPSC derived hepatocytes. We thank Peter Andrews (Department of Biomedical Science, Centre for Stem Cell Biology, University of Sheffield, Sheffield, UK) for antibody against SSEA4. We also thank Pavel Zak for help with graphics and design of the figures. We acknowledge the CF Genomics CEITEC MU supported by the NCMG research infrastructure (LM2015091 funded by MEYS CR) for their support with obtaining scientific data presented in this paper.

Conflicts of Interest: The authors declare no conflict of interest.

References

1. Mah, J.K.; Korngut, L.; Dykeman, J.; Day, L.; Pringsheim, T.; Jette, N. A systematic review and meta-analysis on the epidemiology of Duchenne and Becker muscular dystrophy. *Neuromuscul. Disord.* **2014**, *24*, 482–491. [CrossRef] [PubMed]
2. Emery, A.E.H. The muscular dystrophies. *Lancet* **2002**, *359*, 687–695. [CrossRef]
3. Tidball, J.G.; Albrecht, D.E.; Lokensgard, B.E.; Spencer, M.J. Apoptosis precedes necrosis of dystrophin-deficient muscle. *J. Cell Sci.* **1995**, *108 (Pt 6)*, 2197–2204. [PubMed]
4. Mikhaĭlov, V.M.; Komarov, S.A.; Nilova, V.K.; Shteĭn, G.I.; Baranov, V.S. Ultrastructural and morphometrical analysis of apoptosis stages in cardiomyocytes of MDX mice. *Tsitologiia* **2001**, *43*, 729–737. [PubMed]
5. Finsterer, J.; Stöllberger, C. The heart in human dystrophinopathies. *Cardiology* **2003**, *99*, 1–19. [CrossRef] [PubMed]
6. Chenard, A.A.; Becane, H.M.; Tertrain, F.; de Kermadec, J.M.; Weiss, Y.A. Ventricular arrhythmia in Duchenne muscular dystrophy: Prevalence, significance and prognosis. *Neuromuscul. Disord.* **1993**, *3*, 201–206. [CrossRef]
7. Himmrich, E.; Popov, S.; Liebrich, A.; Rosocha, S.; Zellerhoff, C.; Nowak, B.; Przibille, O. Hidden intracardiac conduction disturbances and their spontaneous course in patients with progressive muscular dystrophy. *Z. Kardiol.* **2000**, *89*, 592–598. [CrossRef]
8. Manzur, A.Y.; Kinali, M.; Muntoni, F. Update on the management of Duchenne muscular dystrophy. *Arch. Dis. Child.* **2008**, *93*, 986–990. [CrossRef]
9. Fayssoil, A.; Nardi, O.; Orlikowski, D.; Annane, D. Cardiomyopathy in Duchenne muscular dystrophy: Pathogenesis and therapeutics. *Heart Fail. Rev.* **2010**, *15*, 103–107. [CrossRef]
10. Heslop, L.; Morgan, J.E.; Partridge, T.A. Evidence for a myogenic stem cell that is exhausted in dystrophic muscle. *J. Cell Sci.* **2000**, *113 Pt 12*, 2299–2308.

11. Webster, C.; Blau, H.M. Accelerated age-related decline in replicative life-span of Duchenne muscular dystrophy myoblasts: Implications for cell and gene therapy. *Somat. Cell Mol. Genet.* **1990**, *16*, 557–565. [CrossRef] [PubMed]
12. Blake, D.J.; Weir, A.; Newey, S.E.; Davies, K.E. Function and genetics of dystrophin and dystrophin-related proteins in muscle. *Physiol. Rev.* **2002**, *82*, 291–329. [CrossRef] [PubMed]
13. Clarac, F.; Massion, J.; Smith, A.M. Duchenne, Charcot and Babinski, three neurologists of La Salpetrière Hospital, and their contribution to concepts of the central organization of motor synergy. *J. Physiol. Paris* **2009**, *103*, 361–376. [CrossRef] [PubMed]
14. Danialou, G.; Comtois, A.S.; Dudley, R.; Karpati, G.; Vincent, G.; Des Rosiers, C.; Petrof, B.J. Dystrophin-deficient cardiomyocytes are abnormally vulnerable to mechanical stress-induced contractile failure and injury. *FASEB J.* **2001**, *15*, 1655–1657. [CrossRef] [PubMed]
15. Gao, Q.; McNally, E.M. The Dystrophin Complex: Structure, function and implications for therapy. *Compr. Physiol.* **2015**, *5*, 1223–1239. [PubMed]
16. Massouridès, E.; Polentes, J.; Mangeot, P.-E.; Mournetas, V.; Nectoux, J.; Deburgrave, N.; Nusbaum, P.; Leturcq, F.; Popplewell, L.; Dickson, G.; et al. Dp412e: A novel human embryonic dystrophin isoform induced by BMP4 in early differentiated cells. *Skelet Muscle* **2015**, *5*, 40. [CrossRef]
17. Dick, E.; Kalra, S.; Anderson, D.; George, V.; Ritso, M.; Laval, S.H.; Barresi, R.; Aartsma-Rus, A.; Lochmüller, H.; Denning, C. Exon skipping and gene transfer restore dystrophin expression in human induced pluripotent stem cells-cardiomyocytes harboring DMD mutations. *Stem Cells Dev.* **2013**, *22*, 2714–2724. [CrossRef]
18. Janke, A.; Upadhaya, R.; Snow, W.M.; Anderson, J.E. A new look at cytoskeletal NOS-1 and β-dystroglycan changes in developing muscle and brain in control and mdx dystrophic mice. *Dev. Dyn.* **2013**, *242*, 1369–1381. [CrossRef]
19. Ramachandran, J.; Schneider, J.S.; Crassous, P.-A.; Zheng, R.; Gonzalez, J.P.; Xie, L.-H.; Beuve, A.; Fraidenraich, D.; Peluffo, R.D. Nitric Oxide Signaling Pathway in Duchenne Muscular Dystrophy Mice: Upregulation of L-arginine Transporters. *Biochem. J.* **2013**, *449*, 133–142. [CrossRef]
20. Li, D.; Yue, Y.; Lai, Y.; Hakim, C.H.; Duan, D. Nitrosative stress elicited by nNOSμ delocalization inhibits muscle force in dystrophin-null mice. *J. Pathol.* **2011**, *223*, 88–98. [CrossRef]
21. Chang, W.J.; Iannaccone, S.T.; Lau, K.S.; Masters, B.S.; McCabe, T.J.; McMillan, K.; Padre, R.C.; Spencer, M.J.; Tidball, J.G.; Stull, J.T. Neuronal nitric oxide synthase and dystrophin-deficient muscular dystrophy. *Proc. Natl. Acad. Sci. USA* **1996**, *93*, 9142–9147. [CrossRef] [PubMed]
22. Heinzel, B.; John, M.; Klatt, P.; Böhme, E.; Mayer, B. Ca^{2+}/calmodulin-dependent formation of hydrogen peroxide by brain nitric oxide synthase. *Biochem. J.* **1992**, *281*, 627–630. [CrossRef] [PubMed]
23. Xia, Y.; Zweier, J.L. Superoxide and peroxynitrite generation from inducible nitric oxide synthase in macrophages. *Proc. Natl. Acad. Sci. USA* **1997**, *94*, 6954–6958. [CrossRef] [PubMed]
24. Beckman, J.S.; Beckman, T.W.; Chen, J.; Marshall, P.A.; Freeman, B.A. Apparent hydroxyl radical production by peroxynitrite: Implications for endothelial injury from nitric oxide and superoxide. *Proc. Natl. Acad. Sci. USA* **1990**, *87*, 1620–1624. [CrossRef] [PubMed]
25. Mosqueira, M.; Zeiger, U.; Förderer, M.; Brinkmeier, H.; Fink, R.H.A. Cardiac and respiratory dysfunction in Duchenne muscular dystrophy and the role of second messengers. *Med. Res. Rev.* **2013**, *33*, 1174–1213. [CrossRef] [PubMed]
26. Rybalka, E.; Timpani, C.A.; Cooke, M.B.; Williams, A.D.; Hayes, A. Defects in mitochondrial ATP synthesis in dystrophin-deficient mdx skeletal muscles may be caused by complex I insufficiency. *PLoS ONE* **2014**, *9*, e115763. [CrossRef] [PubMed]
27. Kyrychenko, S.; Kyrychenko, V.; Badr, M.A.; Ikeda, Y.; Sadoshima, J.; Shirokova, N. Pivotal role of miR-448 in the development of ROS-induced cardiomyopathy. *Cardiovasc. Res.* **2015**, *108*, 324–334. [CrossRef] [PubMed]
28. Henríquez-Olguín, C.; Altamirano, F.; Valladares, D.; López, J.R.; Allen, P.D.; Jaimovich, E. Altered ROS production, NF-κB activation and interleukin-6 gene expression induced by electrical stimulation in dystrophic mdx skeletal muscle cells. *Biochim. Biophys. Acta* **2015**, *1852*, 1410–1419. [CrossRef] [PubMed]
29. Kozakowska, M.; Pietraszek-Gremplewicz, K.; Jozkowicz, A.; Dulak, J. The role of oxidative stress in skeletal muscle injury and regeneration: Focus on antioxidant enzymes. *J. Muscle Res. Cell. Motil.* **2015**, *36*, 377–393. [CrossRef] [PubMed]

30. Sciorati, C.; Staszewsky, L.; Zambelli, V.; Russo, I.; Salio, M.; Novelli, D.; Di Grigoli, G.; Moresco, R.M.; Clementi, E.; Latini, R. Ibuprofen plus isosorbide dinitrate treatment in the mdx mice ameliorates dystrophic heart structure. *Pharmacol. Res.* **2013**, *73*, 35–43. [CrossRef]
31. Straub, V.; Rafael, J.A.; Chamberlain, J.S.; Campbell, K.P. Animal models for muscular dystrophy show different patterns of sarcolemmal disruption. *J. Cell Biol.* **1997**, *139*, 375–385. [CrossRef]
32. Farini, A.; Meregalli, M.; Belicchi, M.; Battistelli, M.; Parolini, D.; D'Antona, G.; Gavina, M.; Ottoboni, L.; Constantin, G.; Bottinelli, R.; et al. T and B lymphocyte depletion has a marked effect on the fibrosis of dystrophic skeletal muscles in the scid/mdx mouse. *J. Pathol.* **2007**, *213*, 229–238. [CrossRef] [PubMed]
33. Morrison, J.; Lu, Q.L.; Pastoret, C.; Partridge, T.; Bou-Gharios, G. T-cell-dependent fibrosis in the mdx dystrophic mouse. *Lab. Investig.* **2000**, *80*, 881–891. [CrossRef] [PubMed]
34. Messina, S.; Vita, G.L.; Aguennouz, M.; Sframeli, M.; Romeo, S.; Rodolico, C.; Vita, G. Activation of NF-kB pathway in Duchenne muscular dystrophy: Relation to age. *Acta Myol.* **2011**, *30*, 16–23. [PubMed]
35. Lu, A.; Poddar, M.; Tang, Y.; Proto, J.D.; Sohn, J.; Mu, X.; Oyster, N.; Wang, B.; Huard, J. Rapid depletion of muscle progenitor cells in dystrophic mdx/utrophin-/- mice. *Hum. Mol. Genet.* **2014**, *23*, 4786–4800. [CrossRef]
36. Dumont, N.A.; Wang, Y.X.; von Maltzahn, J.; Pasut, A.; Bentzinger, C.F.; Brun, C.E.; Rudnicki, M.A. Dystrophin expression in muscle stem cells regulates their polarity and asymmetric division. *Nat. Med.* **2015**, *21*, 1455–1463. [CrossRef] [PubMed]
37. Inomata, K.; Aoto, T.; Binh, N.T.; Okamoto, N.; Tanimura, S.; Wakayama, T.; Iseki, S.; Hara, E.; Masunaga, T.; Shimizu, H.; et al. Genotoxic stress abrogates renewal of melanocyte stem cells by triggering their differentiation. *Cell* **2009**, *137*, 1088–1099. [CrossRef]
38. Rossi, D.J.; Bryder, D.; Seita, J.; Nussenzweig, A.; Hoeijmakers, J.; Weissman, I.L. Deficiencies in DNA damage repair limit the function of haematopoietic stem cells with age. *Nature* **2007**, *447*, 725–729. [CrossRef]
39. Rübe, C.E.; Fricke, A.; Widmann, T.A.; Fürst, T.; Madry, H.; Pfreundschuh, M.; Rübe, C. Accumulation of DNA damage in hematopoietic stem and progenitor cells during human aging. *PLoS ONE* **2011**, *6*, e17487. [CrossRef]
40. Miyagoe-Suzuki, Y.; Nishiyama, T.; Nakamura, M.; Narita, A.; Takemura, F.; Masuda, S.; Minami, N.; Murayama, K.; Komaki, H.; Goto, Y.-I.; et al. Induction of Pluripotent Stem Cells from a Manifesting Carrier of Duchenne Muscular Dystrophy and Characterization of Their X-Inactivation Status. *Stem Cells Int.* **2017**, *2017*, 7906843. [CrossRef]
41. Choi, I.Y.; Lim, H.; Estrellas, K.; Mula, J.; Cohen, T.V.; Zhang, Y.; Donnelly, C.J.; Richard, J.-P.; Kim, Y.J.; Kim, H.; et al. Concordant but Varied Phenotypes among Duchenne Muscular Dystrophy Patient-Specific Myoblasts Derived using a Human iPSC-Based Model. *Cell Rep.* **2016**, *15*, 2301–2312. [CrossRef] [PubMed]
42. Hashimoto, A.; Naito, A.T.; Lee, J.-K.; Kitazume-Taneike, R.; Ito, M.; Yamaguchi, T.; Nakata, R.; Sumida, T.; Okada, K.; Nakagawa, A.; et al. Generation of Induced Pluripotent Stem Cells From Patients With Duchenne Muscular Dystrophy and Their Induction to Cardiomyocytes. *Int. Heart J.* **2016**, *57*, 112–117. [CrossRef] [PubMed]
43. Spaltro, G.; Vigorelli, V.; Casalnuovo, F.; Spinelli, P.; Castiglioni, E.; Rovina, D.; Paganini, S.; Di Segni, M.; Nigro, P.; Gervasini, C.; et al. Derivation of the Duchenne muscular dystrophy patient-derived induced pluripotent stem cell line lacking DMD exons 49 and 50 (CCMi001DMD-A-3, Δ49, Δ50). *Stem Cell Res.* **2017**, *25*, 128–131. [CrossRef] [PubMed]
44. McGreevy, J.W.; Hakim, C.H.; McIntosh, M.A.; Duan, D. Animal models of Duchenne muscular dystrophy: From basic mechanisms to gene therapy. *Dis. Model Mech.* **2015**, *8*, 195–213. [CrossRef] [PubMed]
45. International Stem Cell Initiative; Adewumi, O.; Aflatoonian, B.; Ahrlund-Richter, L.; Amit, M.; Andrews, P.W.; Beighton, G.; Bello, P.A.; Benvenisty, N.; Berry, L.S.; et al. Characterization of human embryonic stem cell lines by the International Stem Cell Initiative. *Nat. Biotechnol.* **2007**, *25*, 803–816. [PubMed]
46. Krutá, M.; Šeneklová, M.; Raška, J.; Salykin, A.; Zerzánková, L.; Pešl, M.; Bártová, E.; Franek, M.; Baumeisterová, A.; Košková, S.; et al. Mutation frequency dynamics in HPRT locus in culture-adapted human embryonic stem cells and induced pluripotent stem cells correspond to their differentiated counterparts. *Stem Cells Dev.* **2014**, *23*, 2443–2454. [CrossRef]

47. Armstrong, L.; Tilgner, K.; Saretzki, G.; Atkinson, S.P.; Stojkovic, M.; Moreno, R.; Przyborski, S.; Lako, M. Human induced pluripotent stem cell lines show stress defense mechanisms and mitochondrial regulation similar to those of human embryonic stem cells. *Stem Cells* **2010**, *28*, 661–673. [CrossRef]
48. Šimara, P.; Tesařová, L.; Padourová, S.; Koutná, I. Generation of human induced pluripotent stem cells using genome integrating or non-integrating methods. *Folia Biol. (Praha)* **2014**, *60* (Suppl. 1), 85–89.
49. Dvorak, P.; Dvorakova, D.; Koskova, S.; Vodinska, M.; Najvirtova, M.; Krekac, D.; Hampl, A. Expression and potential role of fibroblast growth factor 2 and its receptors in human embryonic stem cells. *Stem Cells* **2005**, *23*, 1200–1211. [CrossRef]
50. Pesl, M.; Acimovic, I.; Pribyl, J.; Hezova, R.; Vilotic, A.; Fauconnier, J.; Vrbsky, J.; Kruzliak, P.; Skladal, P.; Kara, T.; et al. Forced aggregation and defined factors allow highly uniform-sized embryoid bodies and functional cardiomyocytes from human embryonic and induced pluripotent stem cells. *Heart Vessels* **2014**, *29*, 834–846. [CrossRef]
51. Eiselleova, L.; Peterkova, I.; Neradil, J.; Slaninova, I.; Hampl, A.; Dvorak, P. Comparative study of mouse and human feeder cells for human embryonic stem cells. *Int. J. Dev. Biol.* **2008**, *52*, 353–363. [CrossRef] [PubMed]
52. Park, I.-H.; Lerou, P.H.; Zhao, R.; Huo, H.; Daley, G.Q. Generation of human-induced pluripotent stem cells. *Nat. Protoc.* **2008**, *3*, 1180–1186. [CrossRef] [PubMed]
53. Li, H.; Durbin, R. Fast and accurate short read alignment with Burrows-Wheeler transform. *Bioinformatics* **2009**, *25*, 1754–1760. [CrossRef] [PubMed]
54. Boeva, V.; Popova, T.; Bleakley, K.; Chiche, P.; Cappo, J.; Schleiermacher, G.; Janoueix-Lerosey, I.; Delattre, O.; Barillot, E. Control-FREEC: A tool for assessing copy number and allelic content using next-generation sequencing data. *Bioinformatics* **2012**, *28*, 423–425. [CrossRef] [PubMed]
55. Ran, F.A.; Hsu, P.D.; Wright, J.; Agarwala, V.; Scott, D.A.; Zhang, F. Genome engineering using the CRISPR-Cas9 system. *Nat. Protoc.* **2013**, *8*, 2281–2308. [CrossRef] [PubMed]
56. Schneider, C.A.; Rasband, W.S.; Eliceiri, K.W. NIH Image to ImageJ: 25 Years of Image Analysis. Available online: https://www.nature.com/articles/nmeth.2089 (accessed on 27 June 2018).
57. Kunova, M.; Matulka, K.; Eiselleova, L.; Salykin, A.; Kubikova, I.; Kyrylenko, S.; Hampl, A.; Dvorak, P. Adaptation to robust monolayer expansion produces human pluripotent stem cells with improved viability. *Stem Cells Transl. Med.* **2013**, *2*, 246–254. [CrossRef] [PubMed]
58. Post-hoc Power Calculator. Available online: http://clincalc.com/Stats/Power.aspx (accessed on 22 August 2018).
59. Lin, B.; Li, Y.; Han, L.; Kaplan, A.D.; Ao, Y.; Kalra, S.; Bett, G.C.L.; Rasmusson, R.L.; Denning, C.; Yang, L. Modeling and study of the mechanism of dilated cardiomyopathy using induced pluripotent stem cells derived from individuals with Duchenne muscular dystrophy. *Dis. Model Mech.* **2015**, *8*, 457–466. [CrossRef] [PubMed]
60. Guan, X.; Mack, D.L.; Moreno, C.M.; Strande, J.L.; Mathieu, J.; Shi, Y.; Markert, C.D.; Wang, Z.; Liu, G.; Lawlor, M.W.; et al. Dystrophin-deficient cardiomyocytes derived from human urine: New biologic reagents for drug discovery. *Stem Cell Res.* **2014**, *12*, 467–480. [CrossRef]
61. Acimovic, I.; Vilotic, A.; Pesl, M.; Lacampagne, A.; Dvorak, P.; Rotrekl, V.; Meli, A.C. Human Pluripotent Stem Cell-Derived Cardiomyocytes as Research and Therapeutic Tools. Available online: https://www.hindawi.com/journals/bmri/2014/512831/ (accessed on 18 June 2018).
62. Hockemeyer, D.; Jaenisch, R. Induced pluripotent stem cells meet genome editing. *Cell Stem Cell* **2016**, *18*, 573–586. [CrossRef] [PubMed]
63. Narsinh, K.H.; Sun, N.; Sanchez-Freire, V.; Lee, A.S.; Almeida, P.; Hu, S.; Jan, T.; Wilson, K.D.; Leong, D.; Rosenberg, J.; et al. Single cell transcriptional profiling reveals heterogeneity of human induced pluripotent stem cells. *J. Clin. Investig.* **2011**, *121*, 1217–1221. [CrossRef]
64. Cassano, M.; Berardi, E.; Crippa, S.; Toelen, J.; Barthelemy, I.; Micheletti, R.; Chuah, M.; Vandendriessche, T.; Debyser, Z.; Blot, S.; et al. Alteration of cardiac progenitor cell potency in GRMD dogs. *Cell Transplant.* **2012**, *21*, 1945–1967. [CrossRef] [PubMed]
65. Mu, X.; Tang, Y.; Lu, A.; Takayama, K.; Usas, A.; Wang, B.; Weiss, K.; Huard, J. The role of Notch signaling in muscle progenitor cell depletion and the rapid onset of histopathology in muscular dystrophy. *Hum. Mol. Genet.* **2015**, *24*, 2923–2937. [CrossRef] [PubMed]
66. Small, C.; Ramroop, J.; Otazo, M.; Huang, L.H.; Saleque, S.; Govind, S. An Unexpected Link Between Notch Signaling and ROS in Restricting the Differentiation of Hematopoietic Progenitors in *Drosophila*. *Genetics* **2014**, *197*, 471–483. [CrossRef] [PubMed]

67. Wang, J.; Sun, Q.; Morita, Y.; Jiang, H.; Gross, A.; Lechel, A.; Hildner, K.; Guachalla, L.M.; Gompf, A.; Hartmann, D.; et al. A differentiation checkpoint limits hematopoietic stem cell self-renewal in response to DNA damage. *Cell* **2012**, *148*, 1001–1014. [CrossRef] [PubMed]
68. Mandal, P.K.; Rossi, D.J. DNA-damage-induced differentiation in hematopoietic stem cells. *Cell* **2012**, *148*, 847–848. [CrossRef] [PubMed]
69. Williams, I.A.; Allen, D.G. Intracellular calcium handling in ventricular myocytes from mdx mice. *Am. J. Physiol. Heart Circ. Physiol.* **2007**, *292*, H846–H855. [CrossRef] [PubMed]
70. Whitehead, N.P.; Pham, C.; Gervasio, O.L.; Allen, D.G. N-Acetylcysteine ameliorates skeletal muscle pathophysiology in mdx mice. *J. Physiol. (Lond.)* **2008**, *586*, 2003–2014. [CrossRef]
71. Fauconnier, J.; Thireau, J.; Reiken, S.; Cassan, C.; Richard, S.; Matecki, S.; Marks, A.R.; Lacampagne, A. Leaky RyR2 trigger ventricular arrhythmias in Duchenne muscular dystrophy. *Proc. Natl. Acad. Sci. USA* **2010**, *107*, 1559–1564. [CrossRef]
72. Messina, S.; Altavilla, D.; Aguennouz, M.; Seminara, P.; Minutoli, L.; Monici, M.C.; Bitto, A.; Mazzeo, A.; Marini, H.; Squadrito, F.; et al. Lipid peroxidation inhibition blunts nuclear factor-kappaB activation, reduces skeletal muscle degeneration, and enhances muscle function in mdx mice. *Am. J. Pathol.* **2006**, *168*, 918–926. [CrossRef]
73. Davidson, S.M.; Duchen, M.R. Effects of NO on mitochondrial function in cardiomyocytes: Pathophysiological relevance. *Cardiovasc. Res.* **2006**, *71*, 10–21. [CrossRef]
74. Hsie, A.W.; Recio, L.; Katz, D.S.; Lee, C.Q.; Wagner, M.; Schenley, R.L. Evidence for reactive oxygen species inducing mutations in mammalian cells. *Proc. Natl. Acad. Sci. USA* **1986**, *83*, 9616–9620. [CrossRef] [PubMed]
75. Sohal, R.S.; Mockett, R.J.; Orr, W.C. Mechanisms of aging: An appraisal of the oxidative stress hypothesis. *Free Radic. Biol. Med.* **2002**, *33*, 575–586. [CrossRef]
76. Douki, T.; Rivière, J.; Cadet, J. DNA tandem lesions containing 8-oxo-7,8-dihydroguanine and formamido residues arise from intramolecular addition of thymine peroxyl radical to guanine. *Chem. Res. Toxicol.* **2002**, *15*, 445–454. [CrossRef] [PubMed]
77. Krutá, M.; Bálek, L.; Hejnová, R.; Dobšáková, Z.; Eiselleová, L.; Matulka, K.; Bárta, T.; Fojtík, P.; Fajkus, J.; Hampl, A.; et al. Decrease in abundance of apurinic/apyrimidinic endonuclease causes failure of base excision repair in culture-adapted human embryonic stem cells. *Stem Cells* **2013**, *31*, 693–702. [CrossRef] [PubMed]
78. Wang, D.; Kreutzer, D.A.; Essigmann, J.M. Mutagenicity and repair of oxidative DNA damage: Insights from studies using defined lesions. *Mutat. Res. Fundam. Mol. Mech. Mutagen.* **1998**, *400*, 99–115. [CrossRef]
79. Wang, Y.; Marino-Enriquez, A.; Bennett, R.R.; Zhu, M.; Shen, Y.; Eilers, G.; Lee, J.-C.; Henze, J.; Fletcher, B.S.; Gu, Z.; et al. Dystrophin Is a Tumor Suppressor in Human Cancers with Myogenic Programs. *Nat. Genet.* **2014**, *46*, 601–606. [CrossRef] [PubMed]
80. Schmidt, W.M.; Uddin, M.H.; Dysek, S.; Moser-Thier, K.; Pirker, C.; Höger, H.; Ambros, I.M.; Ambros, P.F.; Berger, W.; Bittner, R.E. DNA Damage, Somatic Aneuploidy, and Malignant Sarcoma Susceptibility in Muscular Dystrophies. *PLoS Genet* **2011**, *7*, e1002042. [CrossRef]
81. Burkhalter, M.D.; Rudolph, K.L.; Sperka, T. Genome instability of ageing stem cells—Induction and defence mechanisms. *Ageing Res. Rev.* **2015**, *23*, 29–36. [CrossRef]
82. Kyrychenko, V.; Poláková, E.; Janíček, R.; Shirokova, N. Mitochondrial dysfunctions during progression of dystrophic cardiomyopathy. *Cell Calcium* **2015**, *58*, 186–195. [CrossRef]
83. Brenman, J.E.; Chao, D.S.; Gee, S.H.; McGee, A.W.; Craven, S.E.; Santillano, D.R.; Wu, Z.; Huang, F.; Xia, H.; Peters, M.F.; et al. Interaction of nitric oxide synthase with the postsynaptic density protein PSD-95 and alpha1-syntrophin mediated by PDZ domains. *Cell* **1996**, *84*, 757–767. [CrossRef]
84. Feron, O.; Belhassen, L.; Kobzik, L.; Smith, T.W.; Kelly, R.A.; Michel, T. Endothelial nitric oxide synthase targeting to caveolae. Specific interactions with caveolin isoforms in cardiac myocytes and endothelial cells. *J. Biol. Chem.* **1996**, *271*, 22810–22814. [CrossRef] [PubMed]
85. Dudley, R.W.R.; Danialou, G.; Govindaraju, K.; Lands, L.; Eidelman, D.E.; Petrof, B.J. Sarcolemmal damage in dystrophin deficiency is modulated by synergistic interactions between mechanical and oxidative/nitrosative stresses. *Am. J. Pathol.* **2006**, *168*, 1276–1287. [CrossRef] [PubMed]

86. Kinugawa, S.; Huang, H.; Wang, Z.; Kaminski, P.M.; Wolin, M.S.; Hintze, T.H. A defect of neuronal nitric oxide synthase increases xanthine oxidase-derived superoxide anion and attenuates the control of myocardial oxygen consumption by nitric oxide derived from endothelial nitric oxide synthase. *Circ. Res.* **2005**, *96*, 355–362. [CrossRef] [PubMed]
87. Kyrychenko, S.; Poláková, E.; Kang, C.; Pocsai, K.; Ullrich, N.D.; Niggli, E.; Shirokova, N. Hierarchical accumulation of RyR post-translational modifications drives disease progression in dystrophic cardiomyopathy. *Cardiovasc. Res.* **2013**, *97*, 666–675. [CrossRef] [PubMed]
88. Villalta, S.A.; Nguyen, H.X.; Deng, B.; Gotoh, T.; Tidball, J.G. Shifts in macrophage phenotypes and macrophage competition for arginine metabolism affect the severity of muscle pathology in muscular dystrophy. *Hum. Mol. Genet.* **2009**, *18*, 482–496. [CrossRef] [PubMed]
89. Altun, A.; Temiz, T.K.; Balcı, E.; Polat, Z.A.; Turan, M. Effects of tyrosine kinase inhibitor E7080 and eNOS inhibitor L-NIO on colorectal cancer alone and in combination. *Chin. J. Cancer Res.* **2013**, *25*, 572–584. [PubMed]
90. Díaz-Troya, S.; Najib, S.; Sánchez-Margalet, V. eNOS, nNOS, cGMP and protein kinase G mediate the inhibitory effect of pancreastatin, a chromogranin A-derived peptide, on growth and proliferation of hepatoma cells. *Regul. Pept.* **2005**, *125*, 41–46. [CrossRef]
91. Ouameur, A.A.; Tajmir-Riahi, H.-A. Structural Analysis of DNA Interactions with Biogenic Polyamines and Cobalt(III)hexamine Studied by Fourier Transform Infrared and Capillary Electrophoresis. *J. Biol. Chem.* **2004**, *279*, 42041–42054. [CrossRef]
92. Lai, Y.; Thomas, G.D.; Yue, Y.; Yang, H.T.; Li, D.; Long, C.; Judge, L.; Bostick, B.; Chamberlain, J.S.; Terjung, R.L.; et al. Dystrophins carrying spectrin-like repeats 16 and 17 anchor nNOS to the sarcolemma and enhance exercise performance in a mouse model of muscular dystrophy. *J. Clin. Investig.* **2009**, *119*, 624–635. [CrossRef]
93. Gratton, J.-P.; Bernatchez, P.; Sessa, W.C. Caveolae and caveolins in the cardiovascular system. *Circ. Res.* **2004**, *94*, 1408–1417. [CrossRef]
94. Michel, J.B.; Feron, O.; Sacks, D.; Michel, T. Reciprocal regulation of endothelial nitric-oxide synthase by Ca^{2+}-calmodulin and caveolin. *J. Biol. Chem.* **1997**, *272*, 15583–15586. [CrossRef] [PubMed]
95. Schilling, K.; Opitz, N.; Wiesenthal, A.; Oess, S.; Tikkanen, R.; Müller-Esterl, W.; Icking, A. Translocation of endothelial nitric-oxide synthase involves a ternary complex with caveolin-1 and NOSTRIN. *Mol. Biol. Cell* **2006**, *17*, 3870–3880. [CrossRef] [PubMed]
96. Timpani, C.A.; Trewin, A.J.; Stojanovska, V.; Robinson, A.; Goodman, C.A.; Nurgali, K.; Betik, A.C.; Stepto, N.; Hayes, A.; McConell, G.K.; et al. Attempting to Compensate for Reduced Neuronal Nitric Oxide Synthase Protein with Nitrate Supplementation Cannot Overcome Metabolic Dysfunction but Rather Has Detrimental Effects in Dystrophin-Deficient mdx Muscle. *Neurotherapeutics* **2017**, *14*, 429–446. [CrossRef] [PubMed]
97. Wang, H.; Bierie, B.; Li, A.G.; Pathania, S.; Toomire, K.; Dimitrov, S.D.; Liu, B.; Gelman, R.; Giobbie-Hurder, A.; Feunteun, J.; et al. BRCA1/FANCD2/BRG1-Driven DNA Repair Stabilizes the Differentiation State of Human Mammary Epithelial Cells. *Mol. Cell* **2016**, *63*, 277–292. [CrossRef] [PubMed]
98. Pilzecker, B.; Buoninfante, O.A.; van den Berk, P.; Lancini, C.; Song, J.-Y.; Citterio, E.; Jacobs, H. DNA damage tolerance in hematopoietic stem and progenitor cells in mice. *Proc. Natl. Acad. Sci. USA* **2017**, *114*, E6875–E6883. [CrossRef] [PubMed]



© 2019 by the authors. Licensee MDPI, Basel, Switzerland. This article is an open access article distributed under the terms and conditions of the Creative Commons Attribution (CC BY) license (http://creativecommons.org/licenses/by/4.0/).

6.5. Annex 5

Both Hypoxia-Inducible Factor 1 and MAPK Signaling Pathway Attenuate PI3K/AKT via Suppression of Reactive Oxygen Species in Human Pluripotent Stem Cells

Fojtik P, Beckerova D, Holomkova K, Senfluk M, ***Rotrekl V***

frontiers in Cell and Developmental Biology

ORIGINAL RESEARCH
published: 21 January 2021
doi: 10.3389/fcell.2020.607444

Both Hypoxia-Inducible Factor 1 and MAPK Signaling Pathway Attenuate PI3K/AKT via Suppression of Reactive Oxygen Species in Human Pluripotent Stem Cells

Petr Fojtík[1,2], *Deborah Beckerová*[1,2], *Katerina Holomková*[1], *Martin Šenfluk*[1,2] *and Vladimir Rotrekl*[1,2]*

[1] Department of Biology, Faculty of Medicine, Masaryk University, Brno, Czechia, [2] International Clinical Research Center (ICRC), St. Anne's University Hospital, Brno, Czechia

OPEN ACCESS

Edited by:
Emmanuel S. Tzanakakis,
Tufts University, United States

Reviewed by:
Michal Kacper Stachowiak,
University at Buffalo, United States
Yuhua Sun,
Chinese Academy of Sciences, China
Baicheng He,
Chongqing Medical University, China

***Correspondence:**
Vladimir Rotrekl
vrotrekl@med.muni.cz

Specialty section:
This article was submitted to Stem Cell Research, a section of the journal Frontiers in Cell and Developmental Biology

Received: 17 September 2020
Accepted: 15 December 2020
Published: 21 January 2021

Citation:
Fojtík P, Beckerová D, Holomková K, Šenfluk M and Rotrekl V (2021) Both Hypoxia-Inducible Factor 1 and MAPK Signaling Pathway Attenuate PI3K/AKT via Suppression of Reactive Oxygen Species in Human Pluripotent Stem Cells.
Front. Cell Dev. Biol. 8:607444.
doi: 10.3389/fcell.2020.607444

Mild hypoxia (5% O_2) as well as FGFR1-induced activation of phosphatidylinositol-4,5-bisphosphate 3-kinase/protein kinase B (PI3K/AKT) and MAPK signaling pathways markedly support pluripotency in human pluripotent stem cells (hPSCs). This study demonstrates that the pluripotency-promoting PI3K/AKT signaling pathway is surprisingly attenuated in mild hypoxia compared to the 21% O_2 environment. Hypoxia is known to be associated with lower levels of reactive oxygen species (ROS), which are recognized as intracellular second messengers capable of upregulating the PI3K/AKT signaling pathway. Our data denote that ROS downregulation results in pluripotency upregulation and PI3K/AKT attenuation in a hypoxia-inducible factor 1 (HIF-1)-dependent manner in hPSCs. Using specific MAPK inhibitors, we show that the MAPK pathway also downregulates ROS and therefore attenuates the PI3K/AKT signaling—this represents a novel interaction between these signaling pathways. This inhibition of ROS initiated by MEK1/2–ERK1/2 may serve as a negative feedback loop from the MAPK pathway toward FGFR1 and PI3K/AKT activation. We further describe the molecular mechanism resulting in PI3K/AKT upregulation in hPSCs—ROS inhibit the PI3K's primary antagonist PTEN and upregulate FGFR1 phosphorylation. These novel regulatory circuits utilizing ROS as second messengers may contribute to the development of enhanced cultivation and differentiation protocols for hPSCs. Since the PI3K/AKT pathway often undergoes an oncogenic transformation, our data could also provide new insights into the regulation of cancer stem cell signaling.

Keywords: PI3K/AKT, MAPK, reactive oxygen species, hPSCs, HIF-1, hypoxia

INTRODUCTION

Human pluripotent stem cells (hPSCs) hold great promise for disease modeling, development of cell replacement therapies, and human embryology research due to their unique properties such as self-renewal and pluripotency. Traditionally, pluripotent stem cells can be divided into two distinct categories with very similar gene expression profiles: embryonic stem cells

(ESCs) and induced pluripotent stem cells (iPSCs). While ESCs can be derived directly from preimplantation blastocysts, iPSCs are created by reprogramming somatic cells (Takahashi et al., 2007). Preimplantation blastocysts used for the preparation of ESCs naturally reside in a low oxygen environment (Fischer and Bavister, 1993; Okazaki and Maltepe, 2006). It has been shown that low oxygen conditions prevent differentiation and support pluripotency in various stem cell populations (Ezashi et al., 2005; Forristal et al., 2010) and enhance the generation of human iPSCs from fibroblasts (Yoshida et al., 2009). Mathieu et al. (2013) have reported that the transition of committed cells to hypoxic conditions can reverse the differentiation commitment back to full pluripotency. Despite these findings, hPSCs are commonly maintained in a 21% O_2 (atmospheric oxygen concentration), although hypoxic conditions would seem more physiological (for the purposes of this publication, we will further refer to 5% O_2 as mild hypoxia). In order to maintain hPSCs self-renewal and pluripotency *in vitro*, fibroblast growth factor 2 (FGF2) is commonly used (Xu et al., 2005b; Levenstein et al., 2006; Eiselleova et al., 2009). Upon binding to fibroblast growth factor receptor (FGFR), FGF2 activates MAPK, phosphatidylinositol-4,5-bisphosphate 3-kinase/protein kinase B (PI3K/AKT), phospholipase Cγ as well as the Janus kinase/signal transducers and activators of transcription pathways.

Two of these pathways, MAPK and PI3K/AKT, have been implicated to play a role in pluripotency maintenance, self-renewal, reprogramming, and cell fate decision (Armstrong et al., 2006; Li et al., 2007; Yu et al., 2011; Wang et al., 2017; Haghighi et al., 2018), and their context-dependent crosstalk (Mendoza et al., 2011; Aksamitiene et al., 2012) contribute to the regulation of these processes (Dalton, 2013). The hypoxic environment was shown to enhance MAPK (Miyamoto et al., 2015) and PI3K/AKT pathway activity in many cell types and therefore contributes to angiogenesis (Shiojima and Walsh, 2002; Hung et al., 2007; Zhang et al., 2011), promotes survival/prevents apoptosis (Alvarez-Tejado et al., 2001; Lee et al., 2013), and stimulates glycolytic enzyme upregulation as part of the cell's adaptation process to the hypoxic conditions (Ward and Thompson, 2012; Zeng et al., 2016). A recent study performed on mouse ESCs (mESCs) showed that hypoxic conditions lead to downregulation of both the MAPK and the PI3K/AKT signaling and suggested that this effect is secured by hypoxia-mediated downregulation of reactive oxygen species (ROS) (Kučera et al., 2017). At physiological levels, ROS act as signaling molecules capable of regulating various intracellular pathways. ROS-mediated changes in cellular signaling have also been described to affect cell fate decision (Rhee, 2006; Genestra, 2007; Zhang and Yang, 2013; Khacho et al., 2016; Zhang et al., 2016; Kim et al., 2018). It should be noted that ROS levels have been described to be pathologically elevated in some of the iPSCs disease models, where they could affect differentiation (Jelinkova et al., 2019).

To fully utilize the hPSCs potential of self-renewal and differentiation into the desired cell types, it is essential to understand the signaling pathways driving cell fate decision. Since hypoxic conditions support pluripotency maintenance (Mathieu et al., 2013), we investigated whether mild hypoxia modulates FGF2 signaling pathways and their crosstalk in hPSCs. Our data suggest that ROS serve as second messengers activating PI3K/AKT. To the best of our knowledge, we are the first to report that ROS downregulation caused by mild hypoxia and MAPK activation attenuates the pluripotency-maintaining PI3K/AKT signaling in hPSCs.

Abbreviations: AKT, protein kinase B; AS19, AS1938909; CM–, conditioned human embryonic stem cell media without FGF2 supplementation; CM+, conditioned human embryonic stem cell media with FGF2 supplementation; Ctrl, control; ERK1/2, extracellular signal-regulated kinase 1 and 2; ESCs, embryonic stem cells; esiRNA, endoribonuclease-prepared short-interfering RNA; FGF2, fibroblast growth factor 2; FGFR1, fibroblast growth factor receptor 1; GAPDH, glyceraldehyde 3-phosphate dehydrogenase; GSH, glutathione; hES media, human embryonic stem cell media; hESCs, human embryonic stem cells; HIF-1, hypoxia-inducible factor 1; HIFs, hypoxia-inducible factors; hPSCs, human pluripotent stem cells; INFS, integrative nuclear FGFR1 signaling; iPSCs, induced pluripotent stem cells; MAPK, mitogen mitogen-activated protein kinase; Matrigel, Matrigel hESC-qualified Matrix; MEK1/2, mitogen mitogen-activated protein kinase kinase 1 and 2; mESCs, mouse embryonic stem cells; OKA, okadaic acid; pAKT, phosphorylated protein kinase B; PBS, phosphate buffered saline; PCNA, proliferating cell nuclear antigen; PD03, PD0325901; PD18, PD184161; PIP_3, phosphatidylinositol 3,4,5-triphosphate; PPP, pentose phosphate pathway; pERK, phosphorylated extracellular signal-regulated kinase 1 and 2; pFGFR1, phosphorylated fibroblast growth factor 1; PI3K, phosphatydylinositol-4,5-bisphosphate 3-kinase; PI3K p85, p85 subunit of phosphatydylinositol-4,5-bisphosphate 3-kinase; PP1, protein phosphatase 1; PP2A, protein phosphatase 2A; pPI3K p85, phosphorylated p85 subunit of phosphatydylinositol-4,5-bisphosphate 3-kinase; pPTEN, phosphorylated phosphatase and tensin homolog deleted on chromosome 10; PTEN, phosphatase and tensin homolog deleted on chromosome 10; ROS, reactive oxygen species; RTKs, receptor tyrosine kinases; Scr, non-targeting short-interfering RNA; SHIP2, SH2 domain-containing inositol-5′-phosphatase 2; TBS-T, tris buffered saline with Tween 20; qRT-PCR, quantitative real-time PCR; Vin, vinculin; WB, Western blot; αTu, alpha tubulin.

MATERIALS AND METHODS

Culture

Experiments were performed using human hESCs line CCTL12 and CCTL14 and human iPSCs line AM13, previously characterized by Adewumi et al. (2007) and Krutá et al. (2014). Long-term cultivation of hPSCs was performed on mitotically inactivated mouse embryonic fibroblast (MEF) from the CD1 and CF1 mouse strain in human embryonic stem cell media (hES) containing Dulbecco's modified Eagle medium (DMEM)/F12 (Thermo Fisher Scientific, Waltham, MA, USA, 21331-020) supplemented with 15% (vol/vol) knockout serum replacement (Thermo Fisher Scientific, 10828-028), non-essential amino acids (Thermo Fisher Scientific, 11140-035), 4 ng/ml FGF-2 (PeproTech, Cranbury, NJ, USA, 100-18B), L-glutamine, 0.5% (vol/vol; Biosera, Boussens, France, XC-T1715), penicillin–streptomycin (Biosera, XC-A4122), and 2-mercaptoethanol (Sigma-Aldrich, St. Louis, MO, USA, M3148) in a colony type culture. For experimental procedures, hPSCs were cultured feeder free on Matrigel hESC-qualified Matrix (Matrigel; Corning, NY, USA, 354277) coated dishes and cultivated in MEF-conditioned hES media (CM+) supplemented with FGF2 (10 ng/ml) in a monolayer-type culture. hES media was conditioned on mitotically inactivated MEF for 24 h, and the same dish containing MEF was used seven times; then, all seven batches were mixed, supplemented with L-glutamine (0.5% vol/vol) and FGF2 (10 ng/ml) and filtered. MEF-conditioned

media without FGF2 (CM–) was prepared using hES media missing FGF2, and the CM– was not further supplemented with FGF2. hPSCs maintained on Matrigel-coated dishes were cultivated for a maximum of seven passages. For cultivation in 5% O_2, cells were kept in the MCO-18M multigas incubator (Sanyo, Moriguchi, Osaka, Japan). PD184352 (PD18; 25 μM; Sigma-Aldrich, PZ0181) and PD0325901 (PD03; 0.2 μM; Sigma-Aldrich, PZ0162) were used to inhibit MEK1/2. Wortmannin (WRT; 1 μM; Sigma-Aldrich, W1628) was used to inhibit PI3K; $CoCl_2$ (50 μM; Sigma-Aldrich, 60818) was used to stabilize α subunits of hypoxia-inducible factors. AS1938909 (AS19; 10 mM; Calbiochem, San Diego, CA, USA, 565840) was used to inhibit SHIP2. Okadaic acid (OKA; 0.5 and 10 nM; Sigma-Aldrich, O9381) was used to inhibit PP2A. GSH (10 mM; Sigma-Aldrich, G6013) was used to downregulate ROS, and H_2O_2 (0.5 mM; Sigma-Aldrich, H1009) was used to induce ROS. Endoribonuclease-prepared short-interfering RNAs (esiRNAs) against hypoxia-inducible factor 1α (HIF-1α; 50 pmol; Sigma-Aldrich, EHU151981) and PTEN (50 pmol; Sigma-Aldrich, EHU106441) were introduced into the cells using Lipofectamine 2000 Transfection Reagent (Thermo Fisher Scientific, 11668-037) according to the manufacturer's manual to downregulate HIF-1α (an oxygen-sensitive subunit of HIF1) and PTEN (antagonist of PI3K). Successful downregulation (48 h after transfection) was confirmed using Western blot (WB).

Western Blotting

hPSCs cultivated on Matrigel-coated dishes to the maximum of 70% confluence were washed three times with 1× phosphate-buffered saline (PBS) and lysed on ice with 1% sodium dodecyl sulfate (SDS) lysis buffer (50 mM Tris–HCl, 1% SDS, pH 6.8). Protein concentrations were quantified using the DC Protein Assay (Bio-Rad, Hercules, CA, USA, 5000111) measured in triplicates on DTX 880 Multimode Detector (Beckman Coulter, Brea, CA, USA). Protein concentrations were then adjusted to 1 mg/ml, 10× Laemmli buffer was added, and the lysates were briefly boiled. In cases where protein concentration adjustment was unnecessary, hPSCs were lysed directly with 2× Laemmli buffer after the 1× PBS wash. SDS–polyacrylamide gel electrophoresis (SDS-PAGE) was performed using either 8 or 10% polyacrylamide gels, 10–20 μg of total protein was loaded, and gel electrophoresis was ran at 140 V/70 min. Proteins were then transferred to Immobilon-P polyvinylidene fluoride (PVDF) membrane (Merck Millipore, Burlington, MA, USA, IPVH00010) 100 V/60 min.

The membranes were blocked in 5% dried milk or bovine serum albumin in Tris-buffered saline containing 0.1% Tween-20 (TBS-T) for 1 h and incubated overnight with antibodies diluted in the respective blocking solutions at 4°C. The following day, membranes were washed 3 × 15 min with TBS-T and incubated with secondary antibodies diluted in respective blocking solution for 1 h at room temperature followed by 5 × 10 min washes with TBS-T. Immobilon Western Chemiluminescent HRP Substrate (Merck Millipore, P90720) was used as a substrate for the luminescence reaction. Developing was done in G:Box Chemi (SYNGENE, Bangalore, India). Obtained images were adjusted using the GIMP2 software and analyzed in ImageJ. Uncropped blots with molecular markers are shown in **Raw Images 1**.

For the detection of PTEN, redox state cells were harvested in native lysis buffer [100 mM Tris pH 7, 150 mM NaCl, 1 mM ethylenediaminetetraacetic acid (EDTA), 0.1% Triton X-100] supplemented with the cOmplete Mini Protease Inhibitor Cocktail (Roche, Basel, Switzerland; 11836153001) and 50 mM N-ethylmaleimide (Sigma-Aldrich; 04259). Samples were sonicated, mixed with a non-reducing loading buffer, and resolved using 8% SDS-PAGE at 4°C. Protein transfer and detection were performed as described above.

WB quantification analysis was performed using the ImageJ software. Mean gray values for individual proteins were measured using rectangle selection with a diameter fitted tightly to the largest band of that specific protein in a given WB. The same-sized rectangle selection was used for the measurement of all specific protein bands in the lane. Eventual background was subtracted using the same selection rectangle next to the specific protein band. Proteins of interest were then normalized to a loading control. Values chosen for relativization are indicated in the individual figure legends.

The following primary antibodies were used for WB: anti-ERK1/2 (9102), anti-pERK1/2 (9101S), anti-AKT (9272), anti-pAKT (9271), anti-HIF-1α (3716), anti-β-actin (3700), anti-FGFR1 (9740), anti-pFGFR1 (3476), anti-PTEN (9188), anti-pPTEN (9554), anti-PI3K p85 (4292), anti-pPI3K p85/55 (4228) (Cell Signaling Technology, Danvers, MA, USA), anti-α-Tubulin (Exbio, Prague, Czech Republic, 11-250-C100), anti-Lamin B1 (Santa Cruz Biotechnology, Dallas, TX, USA, sc-374015), and anti-PCNA (Sigma-Aldrich, HPA030522). We used the following secondary antibodies: antirabbit immunoglobulin G–horse radish peroxidase (IgG-HRP) (Cell Signaling Technology, 7074) and goat antimouse IgG-HRP (Merck Millipore, 12-349).

Analysis of Reactive Oxygen Species Generation

Cells grown on Matrigel-coated coverslips were treated with the above-described substances. Fifty minutes before the end of the treatment, CellROX Green (5 mM; Thermo Fisher Scientific, C10444) was added. Afterward, the cells were washed three times in PBS on ice and fixed with 4% paraformaldehyde (Sigma-Aldrich, 158127) for 30 min. Snapshots of the approximately same-sized cell clusters were taken with constant exposure time using a fluorescent LSM700 microscope (×40 1.3 oil differential interference contrast objective; Carl Zeiss, Oberkochen, Germany) within 6 h of fixation. ROS levels were determined as fluorescence divided by the fluorescence area in raw images using the ImageJ software.

ICC Analysis

Cells cultivated on Matrigel-coated coverslips were washed three times with PBS, fixed with 4% paraformaldehyde (Sigma-Aldrich, 158127) for 30 min, and blocked with 1% bovine serum albumin (BSA) in 0.1% Triton X-100 in PBS for 1 h. Coverslips were then incubated with a rabbit polyclonal anti-Nanog antibody (Santa Cruz Biotechnology, sc-33759) and a mouse polyclonal anti-Oct-3/4 (Santa Cruz Biotechnology, sc-5279) at a dilution

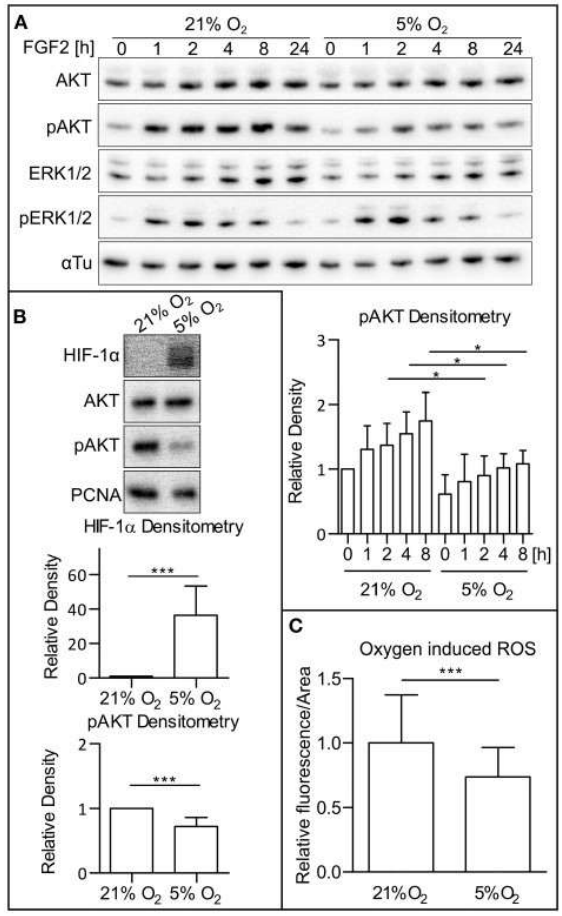

FIGURE 1 | Low O_2 (5%) decreases AKT phosphorylation and ROS levels. **(A)** WB analysis of AKT and ERK1/2 phosphorylation in 21 and 5% O_2 in CCTL14 hESCs and pAKT quantification. Cells kept in 21 or 5% O_2 were starved for 24 h and subsequently treated with FGF2 (10 ng/ml); samples were then collected at different time points. Alpha tubulin was used as a loading control. Data in the graph are presented as mean ± SD (21% O_2: 0 h, 1 ± 0, n = 4; 1 h, 1.307 ± 0.364, n = 4; 2 h, 1.373 ± 0.338, n = 4; 4 h, 1.548 ± 0.340, n = 4; 8 h, 1.747 ± 0.444, n = 4; 5% O_2: 0 h, 0.611 ± 0.301, n = 4; 1 h, 0.809 ± 0.421, n = 4; 2 h, 0.9 ± 0.306, n = 4; 4 h, 1.019 ± 0.220, n = 4; 8 h, 1.082 ± 0.208, n = 4). Statistical analysis was conducted using paired two-tailed t-test with statistical significance taken where $^{*}p < 0.05$. **(B)** Analysis of HIF-1α and pAKT levels in 21 and 5% O_2 in hPSCs. Cells cultivated for 24 h in 21 and 5% O_2 were collected 1–2 h after the treatment with FGF2. PCNA was used as a loading control. Data in graphs are presented as mean ± SD (HIF-1α: 21% O_2, 1 ± 0, n = 11; 5% O_2, 36.26 ± 17.09, n = 11; pAKT: 21% O_2, 1 ± 0, n = 26; 5% O_2, 0.721 ± 0.141, n = 26). Statistical analysis was conducted using one sample t-test (theoretical mean = 1) with statistical significance taken where $^{***}p < 0.0001$. **(C)** Analysis of ROS level in CCTL14 kept in 21 and 5% O_2 environment. Cells were cultivated in respective oxygen concentrations for 24 h, followed by a change of media and additional 2-h cultivation. Normalized data from five different experiments (with at least 10 measurements in each) are presented as mean ± SD (21% O_2, 1 ± 0.0491, n = 58; 5% O_2, 0.7411 ± 0.0299, n = 58). Statistical significance was calculated using a two-tailed Mann–Whitney test ($^{***}p < 0.0001$). Please refer to **Raw Images 1** for uncropped WB and to **Supplementary Data 1** for source data used to generate the graph shown in the figure. WB, western blot; *(Continued)*

FIGURE 1 | ROS, reactive oxygen species; CM+, conditioned media with FGF2 (10 ng/ml); FGF2, fibroblast growth factor 2; AKT, protein kinase B; pAKT, phosphorylated protein kinase B; ERK1/2, extracellular signal-regulated kinase 1 and 2; pERK1/2, phosphorylated extracellular signal-regulated kinase 1 and 2; αTu, alpha tubulin.

of 1:200 overnight at 4°C. Donkey antirabbit Alexa 594 (Thermo Fisher Scientific, A21207) and donkey antimouse Alexa 488 (Thermo Fisher Scientific, A21202) were used as secondary antibodies at a dilution of 1:500 at room temperature for 1 h. Nuclei were counterstained using 4′,6-diamidino-2-phenylindole (DAPI). Snapshots were taken with constant exposure time for individual channels using a fluorescent LSM700 microscope (×63 oil immersion objective; Carl Zeiss). Signal density per area was calculated for individual nuclei from raw images using ImageJ, and mitotic, overlapping, or otherwise irregular nuclei were left out of the analysis.

RNA Isolation and Quantitative Real-Time PCR

Total RNA was isolated using the RNA Blue reagent (Top-Bio, Czech Republic) according to the manufacturer's protocol. Messenger RNA (mRNA) concentration and purity were determined using NanoDrop (NanoDrop Technologies, Wilmington, Germany). Two micrograms of total RNA were transcribed into complementary DNA (cDNA) using the Moloney Mouse Leukemia Virus (M-MLV) reverse transcriptase (Invitrogen, Carlsbad, CA, USA) and Oligo(dT) primers (Thermo Fisher Scientific Inc., USA) at 37°C for 1 h followed by 5 min at 85°C. Quantitative real-time PCR (qRT-PCR) was performed using the LightCycler®480 DNA SYBR Green I Master (Roche) in a Light Cycler 480 instrument. The obtained data were normalized to glyceraldehyde 3-phosphate dehydrogenase (GAPDH) mRNA expression and are presented as 2−Δcq. Sequences of the primers used were as follows: GAPDH (forward: AGCCACATCGCTCAGACACC; reverse: GTACTCAGCGCCAGCATCG), POU5F1 (forward: GCAAAGCAGAAACCCTCGT; reverse: ACACTCGGACC ACATCCTTC), Sox2 (forward: ATGCACCGCTACGACGTGA; reverse: CTTTTGCACCCCTCCCATTT), and Nanog (forward: CCTATGCCTGTGATTTGTGG, reverse: CTGGGACCTTGT CTTCCTTT).

Statistical Analysis

The number of independent experiments is indicated in the figure legends. Arithmetical means and SEM/SD were calculated using the GraphPad Prism 8 software (GraphPad Software, La Jolla, CA, USA). Statistical significance was determined using a two-tailed Mann–Whitney test, one-sample Student's t-test, or a paired two-tailed Student's t-test. Asterisks denote a significant difference as follows: $^{*}p < 0.05$; $^{**}p < 0.01$; $^{***}p < 0.0001$. Source data used to generate the graphs are shown in **Supplementary Data 1**.

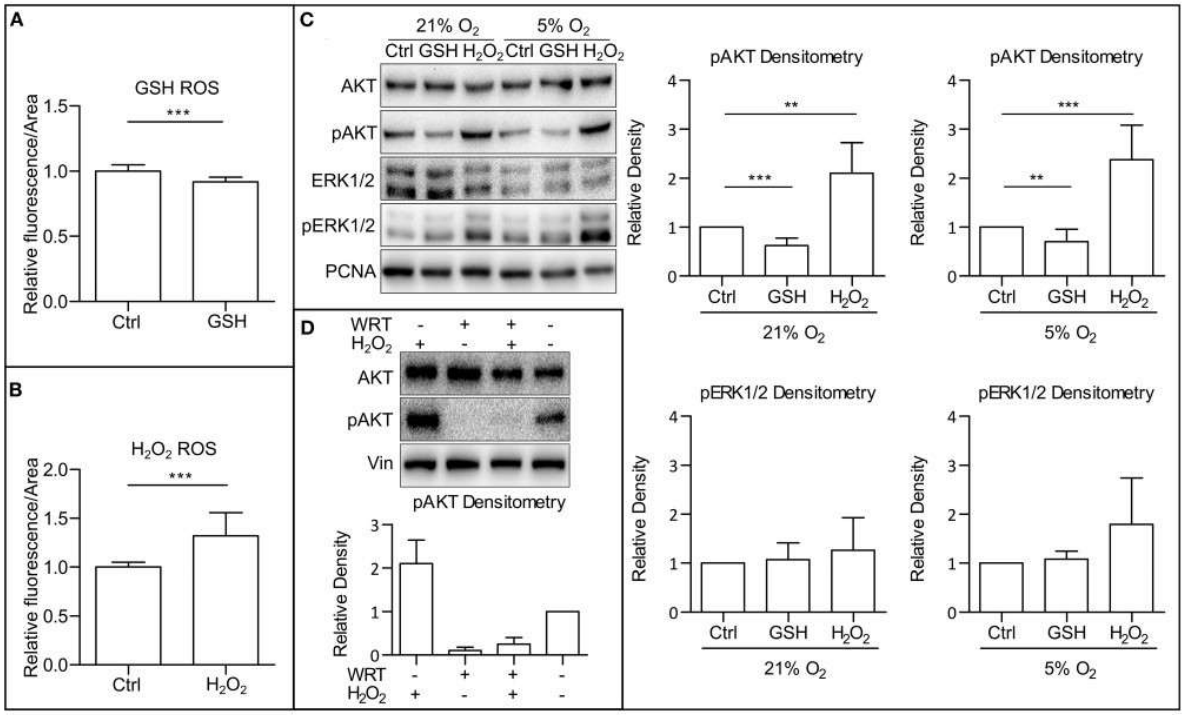

FIGURE 2 | ROS upregulate AKT phosphorylation. **(A)** Downregulation of ROS by GSH in CCTL14 hESCs. Cells in CM+ were treated for 1 h with 10 mM GSH in 5% O_2 after media change. Normalized data from three different experiments (with at least 10 individual measurements in each) are presented as mean ± SD (Ctrl, 1 ± 0.0490, $n = 33$; GSH, 0.9187 ± 0.0349, $n = 31$). Statistical significance was calculated using a two-tailed Mann–Whitney test (***$p < 0.0001$). **(B)** Upregulation of ROS by H_2O_2 in CCTL14 hESCs. Cells in CM+ were treated for 1 h with 0.5 mM H_2O_2 in 5% O_2 after media change. Normalized data from three different experiments (with at least 10 individual measurements in each) are presented as mean ± SD (Ctrl, 1 ± 0.0088, $n = 32$; H_2O_2, 1.321 ± 0.0404, $n = 34$). Statistical significance was calculated using a two-tailed Mann–Whitney test (***$p < 0.0001$). **(C)** WB analysis of ROS-induced changes in AKT and ERK1/2 phosphorylation and their quantification in hPSCs. Cells were cultivated in CM+ for 24 h in 21 and 5% O_2, respectively, then treated with 10 mM GSH and 0.5 mM H_2O_2 for 1 h in fresh media. PCNA was used as a loading control. Data in graphs are presented as mean ± SD (pAKT in 21% O_2: Ctrl, 1 ± 0; GSH, 0.622 ± 0.155, $n = 10$; H_2O_2, 2.105 ± 0.621, $n = 6$; pAKT in 5% O_2: Ctrl, 1 ± 0; GSH, 0.703 ± 0.257, $n = 9$; H_2O_2, 2.379 ± 0.703, $n = 8$; pERK1/2 in 21% O_2: Ctrl, 1 ± 0; GSH, 1.069 ± 0.344, $n = 8$; H_2O_2, 1.260 ± 0.667, $n = 6$; pERK1/2 in 5% O_2: Ctrl, 1 ± 0; GSH, 1.083 ± 0.160, $n = 8$; H_2O_2, 1.793 ± 0.952, $n = 6$). Statistical analysis was conducted using one sample *t*-test (theoretical mean = 1) with statistical significance taken where **$p < 0.01$, ***$p < 0.001$. **(D)** WB analysis of PI3K-independent effect of ROS on AKT phosphorylation. PI3K activity was inhibited using wortmannin (WRT, 1 μM/1 h) and ROS were induced using H_2O_2 (1 mM/1 h). Data in graph are presented as mean ± SEM (–/H_2O_2, 2.10 ± 0.54, $n = 4$; WRT/–, 0.107 ± 0.071, $n = 4$; WRT/H_2O_2, 0.149 ± 0.299, $n = 4$; –/–, 1 ± 0). Please refer to **Raw Images 1** for uncropped WB and to **Supplementary Data 1** for source data used to generate the graphs shown in the figure. WB, western blot; ROS, reactive oxygen species; GSH, glutathione; Ctrl, control; CM+, conditioned media with FGF2 (10 ng/ml); AKT, protein kinase B; pAKT, phosphorylated protein kinase B; ERK1/2, extracellular signal-regulated kinase 1 and 2; pERK1/2, phosphorylated extracellular signal-regulated kinase 1 and 2; PCNA, proliferating cell nuclear antigen; WRT, wortmannin.

RESULTS

Mild Hypoxia Downregulates PI3K/AKT via ROS Attenuation

To determine the dependency of PI3K/AKT and MAPK signaling dynamics on oxygen level, hPSCs were cultivated under both atmospheric oxygen (21% O_2) and mild hypoxic (5% O_2) conditions. Western blot analysis of cell lysates revealed that the amount of active (phosphorylated) AKT is downregulated upon FGF2 administration (10 ng/ml) under mildly hypoxic conditions when compared to 21% O_2 conditions and that this effect persists in time. It ought to be noted that no difference was observed under FGF2 deprivation. We also did not observe a significant difference in extracellular signal-regulated kinase 1 and 2 (ERK1/2) phosphorylation when comparing cells cultivated under 21% O_2 and 5% O_2 over the 24-h period (**Figure 1A**). This effect was observed in two hESC lines (CCTL14 and CCTL12; **Figure 1A** and **Supplementary Figure 1A**) and one iPSC line (AM13; **Supplementary Figure 1B**). Based on these results, further experiments were conducted 1 or 2 h after the FGF2 treatment. We noted a significant decrease in AKT phosphorylation and stabilization of HIF-1α in 5% O_2 (**Figure 1B**).

It has been previously established that hypoxic conditions lead to lower ROS levels in mammalian cultures (Maddalena et al., 2017). To confirm this observation in our model, we cultivated hPSCs in 21 and 5% O_2 and compared ROS levels using a ROS-sensitive fluorescent probe in combination with cell

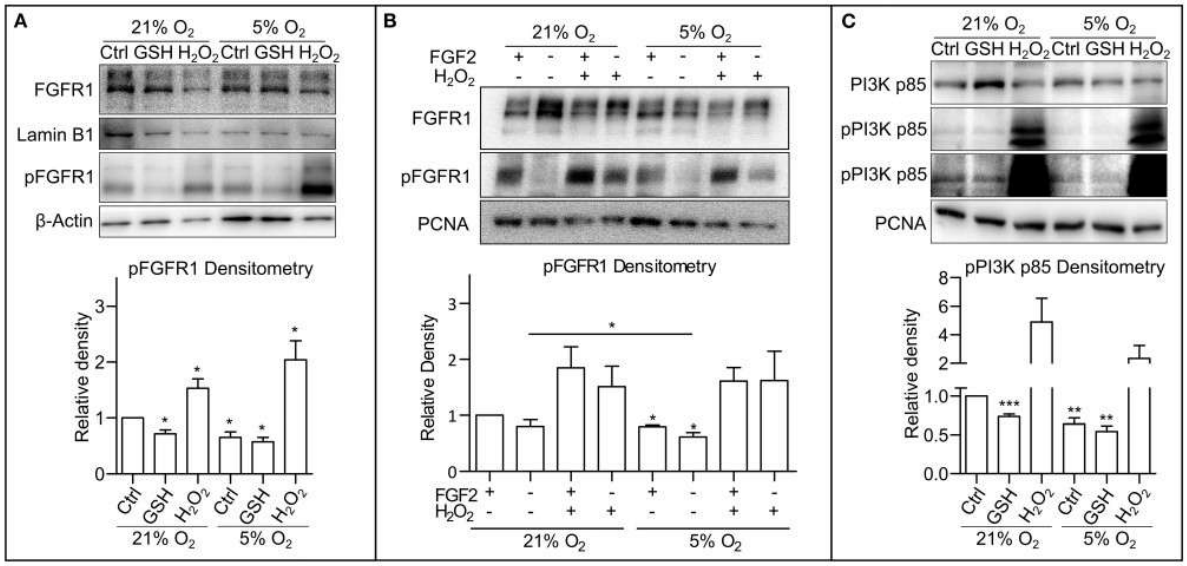

FIGURE 3 | Oxygen-induced ROS upregulate phosphorylation of FGFR1 and PI3K p85. **(A)** Representative WB analysis and quantification of ROS-induced changes in FGFR1 phosphorylation. Cells were cultivated in CM+ for 24 h in 21 and 5% O_2, respectively, then treated with 10 mM GSH and 0.5 mM H_2O_2 for 1 h in fresh media. β-Actin was used as a loading control for pFGFR1 and Lamin B1 for FGFR1. Data obtained on CCTL12, CCTL14, and AM13 hPSCs were used in the densitometry analysis. Data are presented as mean ± SEM (21% O_2: Ctrl, 1 ± 0, $n = 7$; GSH, 0.7211 ± 0.0690, $n = 6$; H_2O_2, 1.530 ± 0.1669, $n = 5$; 5% O_2: Ctrl, 0.6562 ± 0.0977, $n = 7$; GSH, 0.5748 ± 0.0801, $n = 5$; H_2O_2, 2.2038 ± 0.3416, $n = 5$). Statistical analysis was conducted using one sample *t*-test (theoretical mean = 1) with statistical significance taken where $^*p < 0.05$. **(B)** WB analysis of exogenous FGF2-independent ROS-induced FGFR1 phosphorylation. Cells kept in 21 or 5% O_2 were starved for 24 h and subsequently treated with FGF2 (10 ng/ml) and H_2O_2 (1 mM) for 1 h. PCNA was used as a loading control. Data in graph are presented as mean ± SEM (21% O_2: FGF2/–, 1 ± 0; –/–, 0.803 ± 0.199, $n = 3$; FGF2/H_2O_2, 1.845 ± 0.379, $n = 3$; –/H_2O_2, 1.511 ± 0.365, $n = 3$; 5% O_2: FGF2/–, 0.797 ± 0.033, $n = 3$; –/–, 0.617 ± 0.075, $n = 3$; FGF2/H_2O_2, 1.608 ± 0.243, $n = 3$; –/H_2O_2, 1.621 ± 0.524, $n = 3$). Statistical analysis was conducted using paired one-tailed *t*-test with significance taken where $^*p < 0.05$. **(C)** Representative WB analysis of ROS-induced changes in PI3K p85 phosphorylation in CCTL14 hESCs. Cells were cultivated in CM+ for 24 h in 21 and 5% O_2, respectively, then treated with 10 mM GSH and 0.5 mM H_2O_2 for 1 h in fresh media. PCNA was used as a loading control. Data obtained on CCTL12, CCTL14, and AM13 hPSCs were used in the densitometry analysis. Data are presented as mean ± SEM (21% O_2: Ctrl, 1 ± 0, $n = 7$; GSH, 0.7335 ± 0.0323, $n = 6$; H_2O_2, 4.907 ± 1.657, $n = 7$; 5% O_2: Ctrl, 0.6401 ± 0.0787, $n = 6$, GSH, 0.5416 ± 0.0731, $n = 6$; H_2O_2, 2.335 ± 0.9237, $n = 5$). Statistical analysis was conducted using one sample *t*-test (theoretical mean $n = 1$) with statistical significance taken where $^{**}p < 0.01$ and $^{***}p < 0.001$. Please refer to **Raw Images 1** for uncropped WB and to **Supplementary Data 1** for source data used to generate the graphs shown in the figure. WB, western blot; hESCs, human embryonic stem cells; ROS, reactive oxygen species; GSH, glutathione; Ctrl, control; hPSCs, human pluripotent stem cells; CM+, conditioned media with FGF2 (10 ng/ml); PCNA, proliferating cell nuclear antigen; FGFR1, fibroblast growth factor receptor 1; pFGFR1, phosphorylated fibroblast growth factor receptor 1; PI3K p85, p85 subunit of phosphatydylinositol-4,5-bisphosphate 3-kinase; pPI3K p85, phosphorylated p85 subunit of phosphatydylinositol-4,5-bisphosphate 3-kinase.

imaging. Compared to 21% O_2, the levels of ROS in CCTL14 cells cultivated in mild hypoxia were significantly decreased (**Figure 1C**).

ROS are known to directly affect signaling pathways (Zhang et al., 2016). Reports describe positive effects of ROS on the activity of PI3K/AKT (Okoh et al., 2013; Zhang and Yang, 2013). After establishing that mild hypoxia modulates both ROS levels (**Figure 1C**) and AKT phosphorylation (**Figures 1A,B** and **Supplementary Figures 1A,B**) in hPSCs, we wanted to study whether it is ROS that mediate AKT phosphorylation. To study this hypothesis, we used 10 mM GSH to downregulate and 0.5 mM H_2O_2 to upregulate ROS levels (**Figures 2A,B**) and analyzed their effect on AKT and ERK1/2 phosphorylation in different oxygen concentrations. Both treatments were applied 1 h prior to sample collection. GSH managed to downregulate the levels of phosphorylated AKT in hPSCs grown in 21% O_2 to levels similar to mild hypoxia, while no effect on ERK1/2 phosphorylation was observed (**Figure 2C**). The upregulation of ROS by H_2O_2 led to an increase in both AKT and statistically insignificantly in ERK1/2 phosphorylation (**Figure 2C**) under mildly hypoxic as well as atmospheric oxygen concentrations. The effect of ROS modulation on AKT phosphorylation was also observed in the CCTL12 hESC line (**Supplementary Figure 2A**) and AM13 iPSC line (**Supplementary Figure 2B**). The correlation between ROS levels (driven by oxygen tension or induced by H_2O_2) and AKT phosphorylation suggests that mild hypoxia downregulates AKT phosphorylation and thus PI3K/AKT pathway activity *via* modulation of ROS as second messengers in hPSCs. To determine whether ROS can induce AKT phosphorylation independently of PI3K, the cells were treated with a combination of compounds—H_2O_2 and a PI3K inhibitor wortmannin (WRT). The results confirm that ROS-mediated increase in AKT phosphorylation is dependent on PI3K activity (**Figure 2D**).

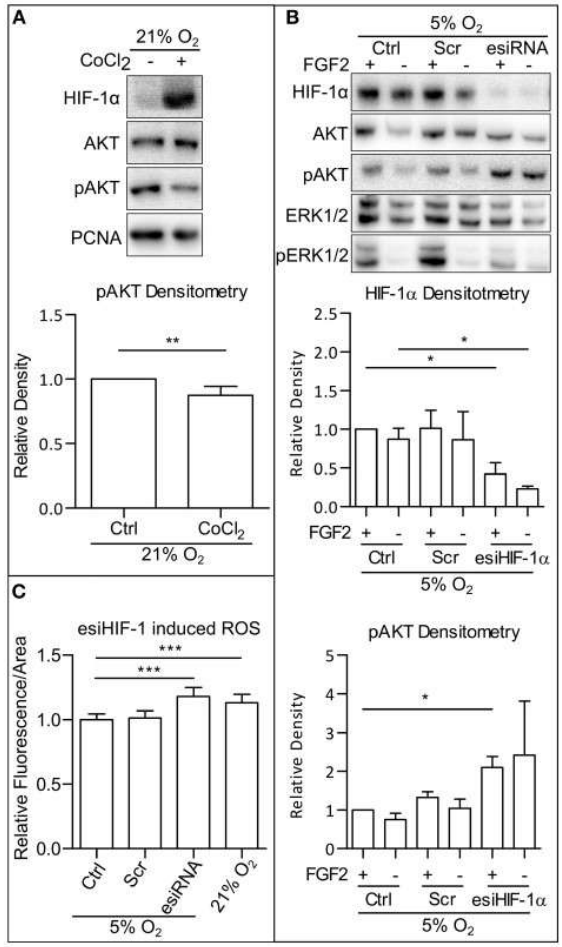

FIGURE 4 | HIF-1 downregulate AKT phosphorylation via downregulation of ROS. **(A)** WB analysis of $CoCl_2$-induced HIF-1α stabilization and decrease in AKT phosphorylation in 21% O_2. Cells were cultivated in CM+ with or without 50 mM $CoCl_2$; samples were collected 1 h after fresh media change. PCNA was used as a loading control. Graph represents mean ± SEM (Ctrl, 1 ± 0; $CoCl_2$, 0.874 ± 0.028, $n = 6$). Statistical analysis was performed using one samples *t*-test (theoretical mean = 1) with statistical significance taken where $^{**}p < 0.01$. **(B)** WB analysis of HIF-1α knockdown effect on AKT phosphorylation in 5% O_2. Cells kept in 21% O_2 in CM+ were transfected with an esiRNA targeting HIF-1α for 48 h and then transferred to 5% O_2 and further cultivated with CM- for 24 h. Subsequently, fresh CM– was added, and respective samples were treated with FGF2 (10 ng/ml) for 2 h. Total AKT and ERK1/2 were used as loading controls. Graphs represent mean ± SEM (HIF-1α: Ctrl/+, 1 ± 0; Ctrl/–, 0.87 ± 0.141, $n = 3$; Scr/+, 1.011 ± 0.235, $n = 4$; Scr/–, 0.864 ± 0.362, $n = 3$; esiHIF/+, 0.422 ± 0.143, $n = 4$; esiHIF/–, 0.233 ± 0.034, $n = 3$; pAKT: Ctrl/+, 1 ± 0; Ctrl/–, 0.75 ± 0.162, $n = 3$; Scr/+, 1.324 ± 0.15, $n = 4$; Scr/–, 1.042 ± 0.243, $n = 3$; esiHIF/+, 2.1 ± 0.284, $n = 4$; esiHIF/–, 2.419 ± 1.394, $n = 3$). Statistical analysis was performed using one sample *t*-test (theoretical mean = 1) and paired one-tailed *t*-test with statistical significance taken where $^{*}p < 0.05$. **(C)** Analysis of HIF-1α knockdown induced ROS in CCTL14 hESCs. Normalized data from three different experiments (with at least 10 individual measurements in each) are expressed as mean ± SD (Ctrl, 1 ± 0.0455, $n = 36$; Scr, 1.013 ± 0.0563, $n = 43$; esiRNA, 1.179 ± 0.0709, $n = 44$; 21% O_2, 1.131 ± 0.0644, *(Continued)*

FIGURE 4 | $n = 42$). Statistical significance was calculated using a two-tailed Mann–Whitney test ($^{***}p < 0.0001$). Please refer to **Raw Images 1** for uncropped WB and to **Supplementary Data 1** for source data used to generate the graphs shown in the figure. WB, western blot; ROS, reactive oxygen species; GSH, glutathione; Ctrl, control; hPSCs, human pluripotent stem cells; CM+, conditioned media with FGF2 (10 ng/ml); Scr, scrambled short-interfering RNA; esiRNA, endoribonuclease-prepared short-interfering RNA; AKT, protein kinase B; pAKT, phosphorylated protein kinase B; ERK1/2, extracellular signal-regulated kinase 1 and 2; pERK1/2, phosphorylated extracellular signal-regulated kinase 1 and 2; PCNA, proliferating cell nuclear antigen; HIF-1α, hypoxia-inducible factor 1α.

It has been previously described that ROS are able to activate receptor tyrosine kinases (RTKs), either directly causing their autophosphorylation (Chiarugi and Buricchi, 2007) or by inhibition of protein tyrosine phosphatases (Chiarugi and Cirri, 2003; Östman et al., 2011). Thus, to pinpoint the particular mechanism by which ROS modulate PI3K/AKT signaling in hPSCs, we looked upstream of AKT at FGF receptor 1 (FGFR1), the most abundantly expressed FGF receptor in hESCs (Dvorak et al., 2005). Using Western blot, we observed a significantly lower level of FGFR1 Tyr653/654 activating phosphorylation in mild hypoxia compared to 21% O_2. The treatment with H_2O_2 (0.5 mM/1 h) led to upregulation of FGFR1 phosphorylation in both 21 and 5% O_2, while the GSH treatment (10 mM/1 h) led to a significant downregulation of FGFR1 phosphorylation only in 21% O_2, in a fashion similar to AKT phosphorylation (**Figure 3A**). This was also observed in the CCTL12 hESC (**Supplementary Figure 3A**) and AM13 iPSCs (**Supplementary Figure 3B**). To elucidate the role of ROS-induced FGFR1 dimerization and autophosphorylation under different oxygen concentrations, we compared FGFR1 phosphorylation with and without exogenous stimulation by FGF2 in 21% O_2, 5% O_2, and in H_2O_2 (1 mM/1 h)-treated cells. Our results show that H_2O_2-mediated ROS induction is sufficient to induce FGFR1 phosphorylation regardless of the exogenous stimulation by FGF2. ROS, therefore, seem to induce dimerization and autophosphorylation of FGFR1 in hPSCs (**Figure 3B**). Moreover, a stronger FGFR1 phosphorylation was detected in cells in 21% O_2 compared to 5% O_2 without FGF2 stimulation (**Figure 3B**), indicating that the difference in ROS concentration between 21% O_2 and 5% O_2 environment (**Figure 1C**) is sufficient to promote FGFR autophosphorylation independent of exogenous stimuli.

When inhibited, the PI3K's regulatory subunit p55/85 is bound to the p110 catalytic subunit. Upon phosphorylation, p55/85 releases p110, which then catalyzes the conversion of phosphatidylinositol 4,5-diphosphate to phosphatidylinositol 3,4,5-triphosphate (PIP_3). **Figure 3C** shows that PI3K p85 phosphorylation was upregulated in 21% O_2 when compared to mild hypoxia, and H_2O_2 led to a massive upregulation of PI3K p85 phosphorylation under both conditions. Treatment with GSH resulted in a significant downregulation of PI3K p85 phosphorylation (**Figure 3C**) corresponding with the GSH-induced changes in FGFR1 (**Figure 3A** and **Supplementary Figures 3A,B**) and AKT

phosphorylation (**Figure 2C** and **Supplementary Figures 2A,B**). These observations were also made in CCTL12 hESCs (**Supplementary Figure 3C**) and AM13 iPSCs (**Supplementary Figure 3D**). Taken together, these findings suggest that ROS upregulate FGFR1 phosphorylation either directly or via inhibition of phosphatases, which subsequently leads to PI3K and AKT phosphorylation.

ROS Are Attenuated in HIF-1-Dependent Manner

To understand what contributes to the ROS downregulation in mild hypoxia, we looked at the effect of HIFs, the main facilitators of cellular adaptation to hypoxic conditions (Semenza, 2001; Keith et al., 2012). First, we employed $CoCl_2$ (50 mM), a hypoxia mimetic capable of stabilizing the alpha subunits of HIFs in 21% O_2 (**Figure 4A**). In our cells, $CoCl_2$ treatment led to a decrease in AKT phosphorylation, comparable to the decrease observed in mild hypoxia (**Figures 1A,B** and **Supplementary Figures 1A,B**). It has been previously established that $CoCl_2$ stabilizes alpha subunits of all HIFs, but only HIF-1α is transcriptionally active under $CoCl_2$ treatment (Befani et al., 2013). Next, we silenced HIF-1α expression using endoribonuclease-prepared short-interfering RNA (esiRNA). This caused a decrease in ERK1/2 phosphorylation and an increase in AKT phosphorylation independent of FGF2 presence (**Figure 4B**), which was also observed in AM13 iPSCs (**Supplementary Figure 4A**). To determine if HIF-1α-mediated phospho-AKT downregulation is also associated with the changing levels of ROS, we compared ROS levels in cells maintained in 5% O_2, in hESCs treated and untreated with esiRNA targeting HIF-1α, and in cells grown in 21% O_2. The silencing of HIF-1α expression induced a significant increase in ROS in 5% O_2, an amount comparable to that observed in 21% O_2 (**Figure 4C**). These results suggest that the upregulation of AKT phosphorylation observed in hPSCs following HIF-1α silencing is associated with ROS upregulation.

MAPK Downregulate PI3K/AKT via ROS Attenuation

Since we observed a simultaneous increase in AKT phosphorylation and a decrease in ERK1/2 phosphorylation following the HIF-1α knockdown by esiRNA, we wondered whether MAPK could play a role in PI3K/AKT regulation in hPSCs. Crosstalk between the MAPK and PI3K/AKT pathway was previously described (Aksamitiene et al., 2012). In order to analyze the effect of MAPK on PI3K/AKT, we used two small molecule inhibitors of mitogen-activated protein kinase kinase 1 and 2 (MEK1/2), PD184161 (PD18), and PD0325901 (PD03) to treat cells cultivated either in 21% O_2 or 5% O_2. Comparing the results, it can be seen that the downregulation of ERK1/2 phosphorylation leads to the upregulation of AKT phosphorylation in 21% O_2 in the presence of FGF2 in CCTL14 and CCTL12 hESCs and AM13 iPSCs (**Figure 5A** and **Supplementary Figures 5A,B**). These results suggest a negative impact of FGF2-induced MAPK signaling on PI3K/AKT pathway activation in hPSCs.

To assess whether MAPK signaling modulates ROS, we analyzed ROS levels in hESC line CCTL14 treated with a MEK1/2 inhibitor PD03 under both 21 and 5% O_2. MEK1/2 inhibition leads to a statistically insignificant ($p = 0.145$) upregulation of ROS in 21% O_2 and a significant upregulation of ROS in 5% O_2 (**Figure 5B**) compared to untreated cells maintained in corresponding O_2 concentrations. Considering that both the maintenance of cells in 21% O_2 and MEK1/2 inhibition in mild hypoxia were sufficient to raise ROS and elevated ROS are associated with increased AKT phosphorylation, it is possible that MAPK suppresses PI3K/AKT signaling via modulation of ROS levels as second messengers.

We, therefore, combined the ROS scavenger GSH (10 mM) and MEK1/2 inhibitor PD03 in 21% O_2. This led to a rescue of the PD03-induced AKT phosphorylation (**Figure 5C**), implicating that MAPK downregulates AKT phosphorylation via modulation of ROS. Same results were acquired in CCTL12 hESCs (**Supplementary Figure 5C**) and AM13 iPSCs (**Supplementary Figure 5D**). To further validate this hypothesis, we also looked at FGFR1 Tyr653/654-activating phosphorylation, which we previously detected to be upregulated by ROS (**Figures 3A,B** and **Supplementary Figures 3C,D**). Our results show that FGFR1 phosphorylation is also upregulated by MEK1/2 inhibition, and the addition of GSH rescues this effect in 21% O_2 in all three hPSCs lines used in this study (**Figure 5D** and **Supplementary Figures 5C,E**). In summary, our results suggest that MAPK can downregulate PI3K/AKT phosphorylation via the downregulation of second messengers—intracellular ROS.

ROS Downregulate PI3K/AKT via PTEN Inhibition

To establish the molecular mechanism by which MAPK and oxygen-induced ROS modulation leads to the AKT phosphorylation changes, we analyzed a set of candidate phosphatases possibly involved in the regulation of AKT phosphorylation: the phosphatase and tensin homolog protein deleted on chromosome 10 (PTEN), SH2-domain containing inositol-5′-phosphatase 2 (SHIP2), and protein phosphatase 2A (PP2A). PTEN, a primary antagonist of PI3K, has been described to be regulated in several ways: by its total amount, its phosphorylation (Vazquez et al., 2001), or by the formation of reversible ROS-induced disulfide bridges (Lee et al., 2002; Covey et al., 2007; Kim et al., 2018). We observed that the total amount of PTEN, as well as the extent of its phosphorylation, did not differ in 5 and 21% O_2 in CCTL14 and CCTL12 hESCs and AM13 iPSCs (**Figure 6A** and **Supplementary Figures 6A,B**). We also did not observe any changes in the total amount of PTEN and PTEN phosphorylation after direct modulation of ROS levels by H_2O_2 (0.5 mM/1 h) and GSH (10 mM/1 h) in these cell lines (**Figure 6B** and **Supplementary Figures 6C,D**). Interestingly, after silencing PTEN expression by esiRNA and comparing the levels of phosphorylated AKT, we noted a slight increase in AKT phosphorylation in 21% O_2 and a significant upregulation in 5% O_2 in all three hPSCs lines used in this study (**Figure 6C** and **Supplementary Figures 6E,G**). Moreover, when we combined PTEN silencing with a GSH treatment to

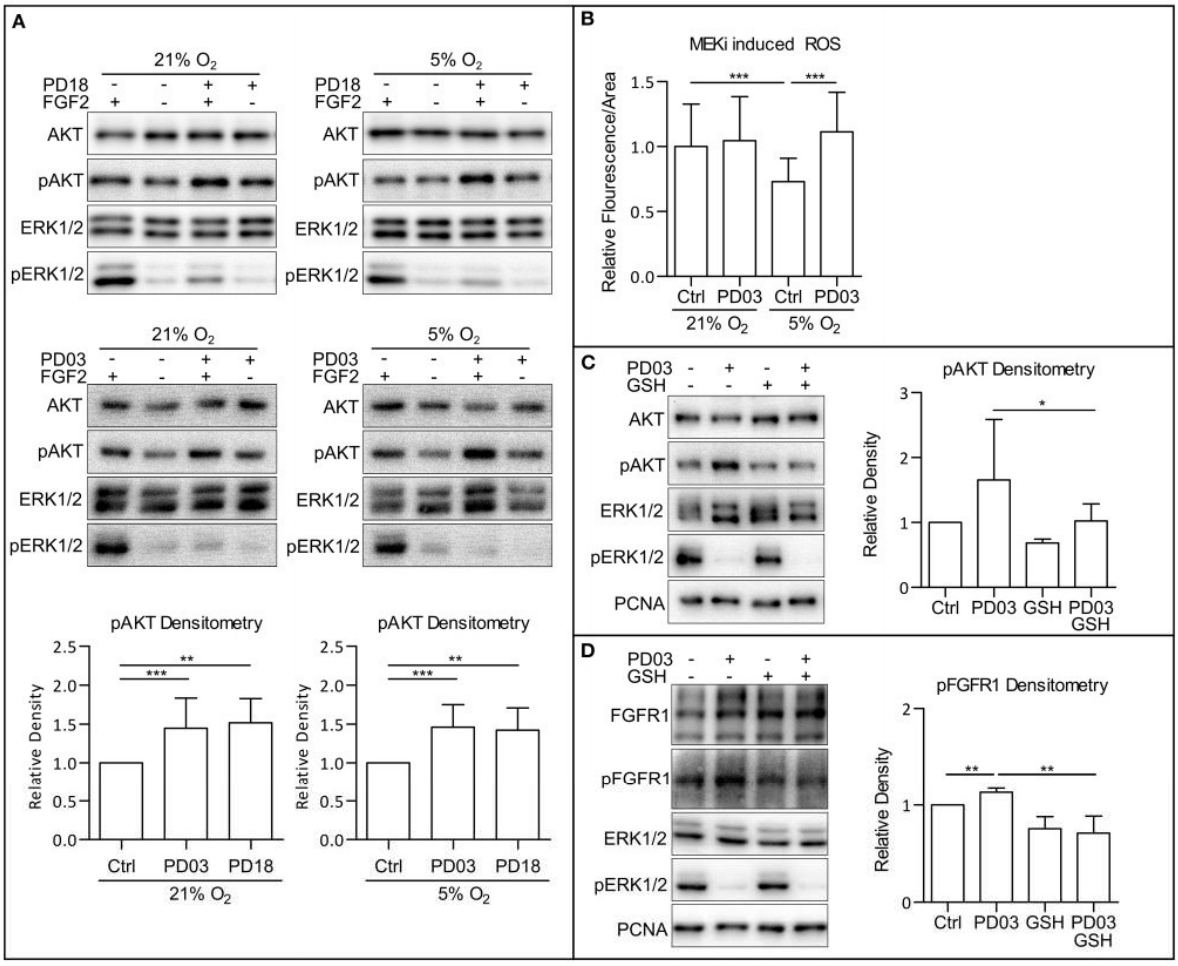

FIGURE 5 | MAPK pathway downregulates PI3K/AKT via downregulation of ROS. **(A)** WB analysis of MEK1/2 inhibition-induced upregulation of AKT phosphorylation. Cells were cultivated in 21 and 5% O_2 in CM– 24 h prior the experiment; then, respective cells were treated with FGF2 (10 ng/ml), PD184352 (PD18, 25 μM), and PD0325901 (PD03, 0.2 μM) for 2 h in respective oxygen concentrations. Total AKT and ERK1/2 were used as loading controls. Graphs represent mean ± SD (21% O_2: Ctrl, 1 ± 0; PD03, 1.447 ± 0.386, $n = 18$; PD18, 1.517 ± 0.312, $n = 6$; 5% O_2: Ctrl, 1 ± 0; PD03, 1.459 ± 0.292, $n = 16$; PD18, 1.422 ± 0.285, $n = 9$). Statistical significance was calculated using one sample *t*-test (theoretical mean = 1) with statistical significance taken where $^{**}p < 0.01$ and $^{***}p < 0.001$. **(B)** MEK1/2 inhibition upregulates ROS in 5% O_2 in CCTL14 hESCs. Cells were cultivated in CM+ in respective oxygen concentrations for 24 h and additional 2 h after media change and treatment with PD03 (0.2 μM) the next day. Normalized data from three different experiments (with at least 10 measurements in each) are presented as mean ± SD (21% O_2, 1 ± 0.3268, $n = 36$; 21% O_2 PD03, 1.045 ± 0.3406, $n = 37$; 5% O_2, 0.7304 ± 0.1785, $n = 36$; 5% O_2 PD03, 1.113 ± 0.3059, $n = 41$). Statistical significance was calculated using a two-tailed Mann–Whitney test ($^{***}p < 0.0001$). **(C)** GSH reverts MEK1/2-inhibition induced phosphorylation of AKT. Cells were cultivated in 21% O_2 in CM+. Respective samples were treated with GSH (10 mM) and PD03 (0.2 μM) for 1 h. PCNA was used as a loading control. Graph represents mean ± SD (Ctrl, 1 ± 0; PD03, 1.654 ± 0.933, $n = 6$; GSH, 0.686 ± 0.139, $n = 6$; PD03/GSH, 0.954 ± 0.29, $n = 6$). Statistical significance was calculated using one sample *t*-test (theoretical mean = 1) with statistical significance taken where $^{*}p < 0.05$. **(D)** GSH reverts MEK1/2-inhibition induced phosphorylation of FGFR1. Cells were cultivated in 21% O_2 in CM+. Respective samples were treated with GSH (10 mM) and PD03 (0.2 μM) for 1 h. PCNA was used as a loading control. Graph represents mean ± SD (Ctrl, 1 ± 0; PD03, 1.131 ± 0.042, $n = 5$; GSH, 0.754 ± 0.125, $n = 5$; PD03/GSH, 0.709 ± 0.178, $n = 5$). Statistical significance was calculated using one sample *t*-test (theoretical mean = 1) and paired two-tailed *t*-test with statistical significance taken where $^{**}p < 0.05$. Please refer to **Raw Images 1** for uncropped WB and to **Supplementary Data 1** for source data used to generate the graphs shown in the figure. WB, western blot; ROS, reactive oxygen species; GSH, glutathione; Ctrl, control; CM+, conditioned media with FGF2 (10 ng/ml); CM–, conditioned media without FGF2; PD18, PD184161; PD03, PD0325901; AKT, protein kinase B; pAKT, phosphorylated protein kinase B; ERK1/2, extracellular signal-regulated kinase 1 and 2; pERK1/2, phosphorylated extracellular signal-regulated kinase 1 and 2; MEK1/2, mitogen activated protein kinase kinase 1 and 2; PCNA, proliferating cell nuclear antigen; FGFR1, fibroblast growth factor receptor 1; pFGFR1, phosphorylated fibroblast growth factor receptor 1.

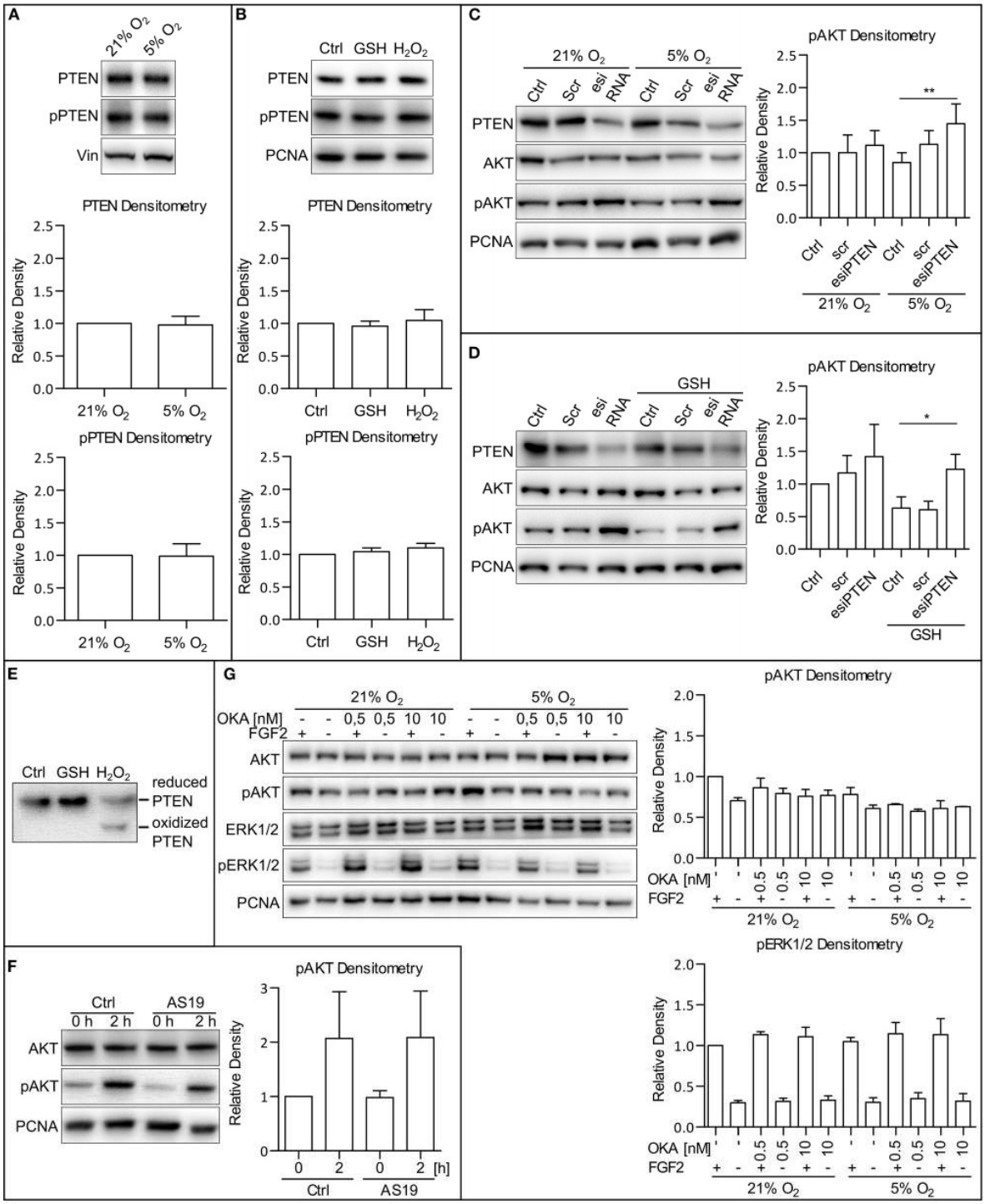

FIGURE 6 | PTEN activity is downregulated by ROS. **(A)** WB analysis of PTEN expression and phosphorylation dependent on oxygen concentration. Cells were cultivated in CM+ and respective oxygen concentrations for 24 h and additional 2 h after fresh CM+ change. Vinculin (Vin) was used as a loading control. Graphs

(Continued)

FIGURE 6 | represent mean ± SD (PTEN: 21% O_2, 1 ± 0; 5% O_2, 0.977 ± 0.134, $n = 10$; pPTEN: 21% O_2, 1 ± 0; 5% O_2, 0.988 ± 0.189, $n = 10$). Statistical significance was calculated using one sample *t*-test (theoretical mean = 1). **(B)** WB analysis of the impact of ROS on PTEN expression and phosphorylation. Cells were cultivated in CM+ for 24 h and an additional hour after fresh CM+ change and GSH (10 mM) and H_2O_2 (0.5 mM) treatment. PCNA was used as a loading control. Graphs represent mean ± SEM (PTEN: Ctrl, 1 ± 0; GSH, 0.958 ± 0.078, $n = 4$; H_2O_2, 1.046 ± 0.167, $n = 4$; pPTEN: Ctrl, 1 ± 0; GSH, 1.042 ± 0.058, $n = 4$; H_2O_2, 1.099 ± 0.071, $n = 4$). Statistical significance was calculated using one sample *t*-test (theoretical mean = 1). **(C)** The silencing of PTEN expression upregulates AKT phosphorylation more substantially in 5% compared to the 21% O_2 environment. Cells cultivated in 21% O_2 in CM+ were transfected with an esiRNA targeting PTEN for 48 h, and respective cells were transferred to 5% O_2 24 h before the harvesting. PCNA was used as a loading control. Graph represents mean ± SD (21% O_2: Ctrl, 1 ± 0; Scr, 1 ± 0.274, $n = 6$; esiPTEN, 1.116 ± 0.225, $n = 6$; 5% O_2: Ctrl, 0.851 ± 0.15, $n = 6$; Scr, 1.129 ± 0.211, $n = 6$; esiPTEN, 1.445 ± 0.305, $n = 6$). Statistical significance was calculated using paired two-tailed *t*-test with significance taken where $^{**}p < 0.01$. **(D)** AKT phosphorylation after PTEN silencing is more pronounced in GSH-treated cells compared to the control in CCTL14 hESCs. Cells cultivated in 21% O_2 in CM+ were transfected with esiRNA targeting PTEN. Respective cells were treated with GSH (10 mM) 1 h prior to harvesting. PCNA was used as a loading control. Graph represents mean ± SD (21% O_2: Ctrl, 1 ± 0; Scr, 1.166 ± 0.268, $n = 5$; esiPTEN, 1.416 ± 0.495, $n = 5$; GSH: Ctrl, 0.63 ± 0.172, $n = 5$; Scr, 0.605 ± 0.131, $n = 5$; esiPTEN, 1.225 ± 0.229, $n = 5$). Statistical significance was calculated using paired two-tailed *t*-test with significance taken where $^{*}p < 0.05$. **(E)** WB analysis of PTEN oxidation in hPSCs. Cells were treated with 10 mM GSH and 0.5 mM H_2O_2 for 1 h and harvested in native lysis buffer. Oxidized PTEN migrated faster on 8% gel due to H_2O_2-induced disulfides. **(F)** WB analysis of cells treated with SHIP2 inhibitor. Cells were cultivated in CM+ in 21% O_2. Twenty-four hours prior to the treatment, CM– was administered, and the cells were transferred to 5% O_2. The next day, fresh CM– was administered, and the cells were treated with FGF2 (10 ng/ml) and AS1938909 (AS19, 10 μM) for 0 or 2 h. PCNA was used as a loading control. Graph represents mean ± SD (21% O_2: 0 h, 1 ± 0; 2 h, 2.069 ± 0.86, $n = 4$; 5% O_2: 0 h, 0.979 ± 0.314, $n = 6$; 2 h, 2.089 ± 0.853, $n = 4$). Statistical significance was calculated using one sample *t*-test (theoretical mean = 1). **(G)** WB analysis of PP2A and PP1 inhibition with okadaic acid in CCTL14 hESCs. Cells were cultivated in CM+ in 21% O_2 for 24 h; then, CM– was administered, and the cells were transferred to 5% O_2. The following day, fresh CM– was administered once again, and the cells were treated for 2 h with FGF2 (10 ng/ml) and okadaic acid (OKA) in 0.5 and 10 nM concentrations, specific for PP2A and PP1 inhibition, respectively. PCNA was used as a loading control. Graphs represent mean ± SEM (pAKT: 21% O_2: FGF2/–, 1 ± 0; –/–, 0.704 ± 0.037, $n = 3$; FGF2/0.5, 0.862 ± 0.120, $n = 3$; –/0.5, 0.793 ± 0.064, $n = 3$; FGF2/10, 0.759 ± 0.083, $n = 3$; –/10, 0.77 ± 0.064; 5% O_2: FGF2/–, 0.781 ± 0.086, $n = 3$; –/–, 0.61 ± 0.039, $n = 3$; FGF2/0.5, 0.656 ± 0.12, $n = 3$; –/0.5, 0.576 ± 0.024, $n = 3$; FGF2/10, 0.609 ± 0.96, $n = 3$; –/10, 0.633 ± 0.001; pERK1/2: 21% O_2: FGF2/–, 1 ± 0; –/– 0.299 ± 0.028, $n = 3$; FGF2/0.5, 1.136 ± 0.034, $n = 3$; –/0.5, 0.315 ± 0.039, $n = 3$; FGF2/10, 1.109 ± 0.116, $n = 3$; –/10, 0.328 ± 0.053; 5% O_2: FGF2/–, 1.05 ± 0.051, $n = 3$; –/–, 0.304 ± 0.056, $n = 3$; FGF2/0.5, 1.146 ± 0.138, $n = 3$; –/0.5 0.348 ± 0.075, $n = 3$; FGF2/10, 1.134 ± 0.198, $n = 3$; –/10, 0.316 ± 0.094). Statistical significance was calculated using one sample *t*-test (theoretical mean = 1). Please refer to **Raw Images 1** for uncropped WB and to **Supplementary Data 1** for source data used to generate the graphs shown in the figure. WB, western blot; ROS, reactive oxygen species; GSH, glutathione; Ctrl, control; CM+, conditioned media with FGF2 (10 ng/ml); scr, scrambled short interfering RNA; esiRNA, endoribonuclease-prepared short interfering RNA; AKT, protein kinase B; pAKT, phosphorylated protein kinase B; ERK1/2, extracellular signal-regulated kinase 1 and 2; pERK1/2, phosphorylated extracellular signal-regulated kinase 1 and 2; PCNA, proliferating cell nuclear antigen; PTEN, phosphatase and tensin homolog deleted on chromosome 10; pPTEN, phosphorylated phosphatase and tensin homolog deleted on chromosome 10; Vin, Vinculin; PP1, protein phosphatase 1; PP2A, protein phosphatase 2A; AS19, AS1938909; OKA, okadaic acid.

induce ROS downregulation in 21% O_2, AKT phosphorylation appeared to be significantly elevated in GSH-treated hPSCs with downregulated PTEN compared to GSH-free cells (**Figure 6D** and **Supplementary Figures 6F,G**). To analyze whether PTEN can undergo oxidization in hPSCs, we collected native lysates of H_2O_2-treated and control cells and performed 8% SDS-PAGE to detect an oxidation-induced shift in PTEN mobility (Lee et al., 2002; Covey et al., 2007). The results show that ROS-induced PTEN oxidation takes place in hPSCs as well (**Figure 6E**). Overall, these data indicate that PTEN is more active in a low ROS environment, which could partially contribute to lower levels of AKT phosphorylation observed in mild hypoxia. Although we did not detect oxygen or ROS-mediated changes in PTEN total amount or its phosphorylation, our data suggest that it is the ROS-regulated PTEN activity that contributes to the ROS-mediated upregulation of AKT phosphorylation.

SHIP2 and PP2A Are Not Involved in the Immediate Mild Hypoxia-Induced Downregulation of AKT Phosphorylation

SHIP2 is an antagonist of PI3K functionally similar to PTEN that is described to be regulated by ROS (Zhang et al., 2007). To analyze whether SHIP2 facilitates the downregulation of AKT phosphorylation in mild hypoxia, we treated hPSCs in 5% O_2 with a specific SHIP2 inhibitor AS1938909 (AS19, 10 μM/2 h). hPSCs treated with AS19 did not display a significantly elevated AKT phosphorylation than untreated control (**Figure 6F** and **Supplementary Figures 7A,B**), suggesting that SHIP2 is not involved in the observed downregulation of PI3K/AKT in mild hypoxia.

PP2A directly regulates AKT and ERK1/2 phosphorylation and is also described to be regulated by ROS (Rao and Clayton, 2002; Raman and Pervaiz, 2019). To analyze its role in the regulation of AKT in hPSCs, we used a 2-h okadaic acid (OKA) treatment in the 0.5 nM concentration specific for PP2A and in the 10 nM concentration specific for protein phosphatase 1 (PP1). Treatment with OKA in both concentrations did not significantly enhance AKT or ERK1/2 phosphorylation in hPSCs regardless of O_2 concentration (**Figure 6G** and **Supplementary Figures 7C,D**). This, together with the fact that PP2A targets both AKT and ERK1/2 and that we did not see ERK1/2 downregulation in mild hypoxia, suggests that it has no role in the observed hypoxia-mediated downregulation of AKT phosphorylation in hPSCs.

ROS Attenuation Upregulates Pluripotency Markers

Since we were able to describe a link between attenuated ROS levels in mild hypoxia and a decrease in PI3K/AKT signaling, we proceeded to study the effect of ROS levels on pluripotency maintenance. Using immunocytochemistry (ICC), we compared the amount of two well-established pluripotency markers Oct-3/4 and Nanog in hPSCs in 21% O_2, in hPSCs with ROS scavenged by GSH (10 mM/24 h), and in hPSCs in 5% O_2. It has been shown that the effect of hypoxia on the levels of pluripotency markers

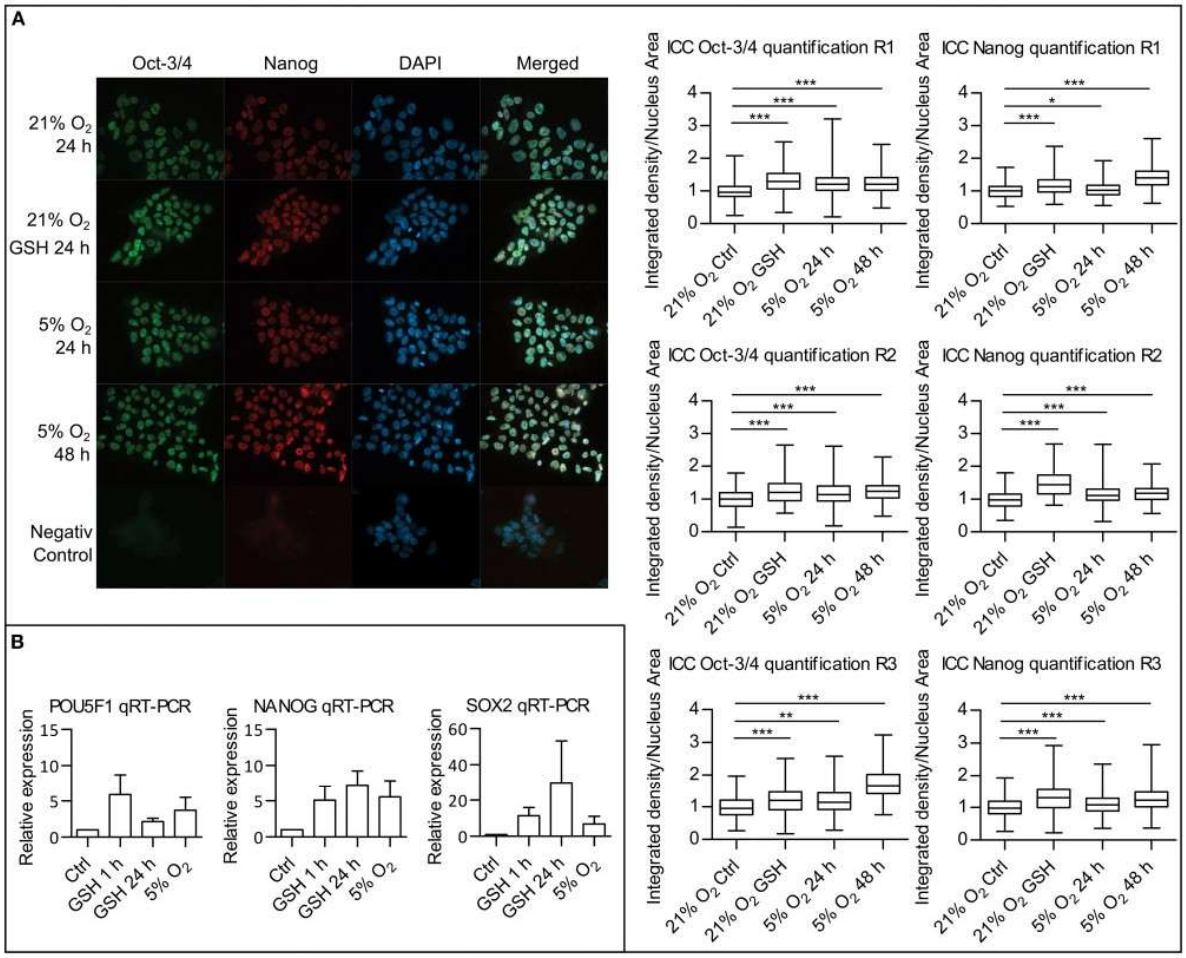

FIGURE 7 | ROS scavenging by GSH increases pluripotency markers expression. **(A)** ICC analysis of Oct-3/4 and Nanog proteins amounts with quantification. hPSCs in 21% O_2 with and without GSH (10 mM) were stained and fixed after 24 h together with hPSCs, which were in 5% O_2 for 24 and 48 h. Representative snapshots are presented. Graphs on the right show relative quantification of signal density per nuclear area for individual nuclei from three repetitions (R1–3). Box plots show mean, 25–75% percentile range, and whiskers show minimal and maximal value range. Mean values and standard deviations for Oct-3/4: R1: 21% O_2, 1 ± 0.241, $n = 364$; 21% O_2 GSH, 1.306 ± 0.332, $n = 397$; 5% O_2 24 h, 1.235 ± 0.317, $n = 465$; 5% O_2 48 h, 1.225 ± 0.295, $n = 647$; R2: 21% O_2, 1 ± 0.280, $n = 230$; 21% O_2 GSH, 1.240 ± 0.408, $n = 68$; 5% O_2 24 h, 1.202 ± 0.407, $n = 231$; 5% O_2 48 h, 1.249 ± 0.316, $n = 230$; R3: 21% O_2, 1 ± 0.311, $n = 267$; 21% O_2 GSH, 1.197 ± 0.423, $n = 135$; 5% O_2 24 h, 1.197 ± 0.396, $n = 231$; 5% O_2 48 h, 1.715 ± 0.436, $n = 356$. Mean values and standard deviations for Nanog: R1: 21% O_2, 1 ± 0.223, $n = 376$; 21% O_2 GSH, 1.173 ± 0.280, $n = 392$; 5% O_2 24 h, 1.038 ± 0.217, $n = 463$; 5% O_2 48 h, 1.421 ± 0.323, $n = 645$; R2: 21% O_2, 1 ± 0.264, $n = 249$; 21% O_2 GSH, 1.465 ± 0.376, $n = 69$; 5% O_2 24 h, 1.144 ± 0.303, $n = 232$; 5% O_2 48 h, 1.18 ± 0.261, $n = 217$; R3: 21% O_2, 1 ± 0.299, $n = 279$; 21% O_2 GSH, 1.309 ± 0.421, $n = 132$; 5% O_2 24 h, 1.086 ± 0.305, $n = 251$; 5% O_2 48 h, 1.268 ± 0.339, $n = 309$. Statistical significance was calculated using unpaired two-tailed *t*-test with significance taken where $^*p < 0.05$, $^{**}p < 0.01$, and $^{***}p < 0.0001$. **(B)** Quantitative real-time PCR analysis of pluripotency genes POU5F1, NANOG, and SOX2 expression. Graphs show relative expression of pluripotency genes in untreated hPSCs controls, hPSCs treated with GSH (10 mM) for 1 and 24 h, and hPSCs maintained in 5% O_2 for 24 h. Graphs represent mean ± SEM (POU5F1: Ctrl, 1 ± 0; GSH 1 h, 5.880 ± 2.834, $n = 4$; GSH 24 h, 2.158 ± 0.453, $n = 4$; 5% O_2, 3.740 ± 1.770, $n = 4$; NANOG: Ctrl, 1 ± 0; GSH 1 h, 5.110 ± 2.008, $n = 5$; GSH 24 h, 7.260 ± 1.983, $n = 4$; 5% O_2, 5.572 ± 2.322, $n = 5$; SOX2: Ctrl, 1 ± 0; GSH 1 h, 11.38 ± 4.618, $n = 4$; GSH 24 h, 29.98 ± 23.30, $n = 4$; 5% O_2, 6.848 ± 4.147, $n = 4$). GSH, reduced glutathione; hPSCs, human pluripotent stem cells; ICC, immunocytochemistry; R1–3, repetitions 1–3; ROS, reactive oxygen species; SEM, standard error of mean.

requires longer incubation times (Forristal et al., 2010; Mathieu et al., 2014). We, therefore, analyzed the Oct-3/4 and Nanog levels after 24 and 48 h in the 5% O_2 environment. Upon nuclear signal quantification, we observed a significant increase in the nuclear Oct-3/4 and Nanog signal in 5% O_2 after 24 and 48 h as well as in the GSH-treated cells compared to control in 21% O_2 (**Figure 7A**). To distinguish between the amount of protein and changes in the pluripotency markers' gene expression, we also performed quantitative real-time PCR (qRT-PCR) of NANOG, POU5F1, and SOX2 comparing cells cultivated in 21 and 5% O_2 and cells with ROS scavenged by GSH (10 mM) in 21% O_2 (**Figure 7B**). We observed an increase in NANOG, POU5F1,

and SOX2 expression following the GSH treatment comparable to levels of expression seen in cells grown in 5% O_2. qRT-PCR results correlate with the observed significant changes in protein amount, emphasizing the importance of ROS signaling in pluripotency maintenance.

DISCUSSION

hPSCs are routinely cultivated in media supplemented with FGF2 to support their undifferentiated growth (Dvorak et al., 2005; Xu et al., 2005a; Levenstein et al., 2006; Eiselleova et al., 2009) in atmospheric oxygen pressure (21% O_2). FGF2 promotes pluripotency and self-renewal through activation of PI3K/AKT and MAPK pathways (Armstrong et al., 2006; Li et al., 2007; Yu et al., 2011; Singh et al., 2012; Hossini et al., 2016; Wang et al., 2017; Haghighi et al., 2018). Previous studies have shown an enhancement of proliferation, transcription of pluripotency markers, generation of iPSCs, and inhibition of differentiation in low oxygen tension (Ezashi et al., 2005; Covello et al., 2006; Yoshida et al., 2009; Forristal et al., 2010; Mathieu et al., 2014), characteristic for the blastocyst's native niche (Fischer and Bavister, 1993; Okazaki and Maltepe, 2006). Hypoxia was described to induce or mediate the upregulation of PI3K/AKT (Alvarez-Tejado et al., 2001; Lee et al., 2013) and MAPK (Miyamoto et al., 2015) pathways in various cell lines. Surprisingly, a recent study conducted on mouse embryonic stem cells (mESCs) showed that PI3K/AKT and MAPK pathways are downregulated in hypoxia (Kučera et al., 2017) despite the fact that PI3K/AKT and MAPK pathways are considered to play an essential role in pluripotency maintenance. In light of this observation, it was of utmost importance to dissect mechanisms employed in hPSCs.

ROS Upregulate AKT Phosphorylation in hPSCs and Are Downregulated in Mild Hypoxia

We show that the 5% O_2 environment (referred to as mild hypoxia for the purpose of this study) stabilizes HIF-1α and downregulates AKT phosphorylation in hPSCs, while it does not have a significant effect on MEK1/2–ERK1/2 pathway (**Figures 1A,B** and **Supplementary Figures 1A,B**). Hypoxia was previously associated with decreased ROS levels (Kučera et al., 2017), and ROS were shown to regulate various cellular signaling pathways (Rhee, 2006; Genestra, 2007; Zhang et al., 2016). ROS were even found to be upregulating the MAPK and PI3K/AKT signaling in mESCs where hypoxia was associated with downregulation of these pathways (Kučera et al., 2017).

Decreased ROS levels are associated with mild hypoxia in hESCs as well (**Figure 1C**). Their selective downregulation by GSH (**Figure 2A**) led to PI3K/AKT downregulation independent of oxygen status (**Figure 2C** and **Supplementary Figures 2A,B**). Vice versa, selective upregulation of ROS by H_2O_2 (**Figure 2B**) independent of oxygen concentration led to PI3K/AKT and MAPK upregulation (**Figure 2C** and **Supplementary Figures 2A,B**). Considering that ROS levels directly respond to oxygen concentration (**Figure 1B**), ROS seem to act as second messengers responsible for PI3K/AKT upregulation in response to oxygen level. H_2O_2 also upregulated ERK1/2 phosphorylation in hPSCs, but ERK1/2 phosphorylation changed neither upon O_2 concentration changes (**Figure 1A** and **Supplementary Figures 1A,B**) nor in the presence of GSH in hPSCs (**Figure 2C** and **Supplementary Figures 2A,B**) contrary to mESCs (Kučera et al., 2017). A possible explanation is that MAPK serves different roles in mESCs and hESCs. Upregulation of MAPK in mESCs leads to lineage commitment (Kunath et al., 2007), but self-renewal of hPSCs relies on highly active MAPK (Dvorak et al., 2005; Eiselleova et al., 2009). Thus, high MAPK activity upon FGF2 induction possibly makes hPSCs less sensitive to subtle changes in ROS induced by O_2 concentration changes. Above that, our data also indicate that the MEK1/2–ERK1/2 pathway attenuates ROS (**Figure 5B**); the existence of a positive feedback loop from ROS toward mitogenic pathways is, therefore, possible, perhaps on the level of the FGF2 receptor.

O_2 Activates FGFR1 and PI3K via ROS in hPSCs

ROS have been described to activate receptor tyrosine kinases (RTKs) through dimerization induced by the oxidation-mediated formation of disulfide bonds between the cysteines of neighboring monomers (Chiarugi and Buricchi, 2007) or by inhibition of protein tyrosine phosphatases via cysteine oxidation (Chiarugi and Cirri, 2003; Chiarugi and Buricchi, 2007). Indeed, phosphorylation of FGFR1, the most abundantly expressed FGFR in hESCs (Dvorak et al., 2005), was upregulated by both ROS and O_2 in hPSCs (**Figures 3A,B** and **Supplementary Figures 3A,B**), suggesting this may contribute to the ROS-mediated upregulation of AKT phosphorylation. The upregulation of FGFR1 phosphorylation by H_2O_2 and O_2 was observed without the exogenous FGF2 stimulation as well (**Figure 3B**), implying that oxidation mediates the FGFR1 phosphorylation either via promoting its dimerization and autophosphorylation or via inhibition of FGFR1-associated phosphatases.

We also observed ROS-induced phosphorylation of the PI3K regulatory subunit p85, which is necessary for the release and activation of the catalytic p110 subunit. Possibly, this is a result of upstream ROS-mediated FGFR1 phosphorylation. Nevertheless, the lack of O_2-induced FGFR1–MEK1/2–ERK1/2 response denotes that ROS could directly modulate PI3K p85 in hPSCs (**Figure 3C** and **Supplementary Figures 3C,D**) as previously described in human mammary epithelial cells (Okoh et al., 2013). ROS-induced p85 phosphorylation would explain the ROS-induced increase in AKT phosphorylation (**Figure 2C**). Alternatively, ROS could inhibit phosphatases involved in PI3K/AKT regulation, for example PTEN, PP2A, or SHIP2. Such mechanism has been described in mouse skeletal muscle cells, embryonic fibroblasts, or HeLa cells (Lee et al., 2002; Zhang et al., 2007; Kim et al., 2018; Raman and Pervaiz, 2019).

AKT Phosphorylation Is Upregulated by ROS-Mediated Downregulation of PTEN Activity

To elucidate the mechanism behind the downregulation of AKT phosphorylation by ROS, we focused on PTEN—a

well-established PI3K antagonist (Leslie and Downes, 2002). Indeed, PTEN is probably involved in the attenuation of AKT phosphorylation in hPSCs because the downregulation of AKT phosphorylation can be reverted by PTEN silencing (**Figure 6C** and **Supplementary Figures 6E,G**). According to the literature, ROS-mediated cysteine oxidation renders PTEN inactive (Lee et al., 2002; Covey et al., 2007). Furthermore, we found the effect of PTEN silencing on AKT phosphorylation to be more profound in mild hypoxia than in 21% O_2 (**Figure 6C** and **Supplementary Figures 6E,G**) and confirmed that ROS are capable of oxidizing PTEN in hPSCs (**Figure 6E**). ROS scavenging by GSH in 21% O_2 also led to lower AKT phosphorylation, which was rescued by PTEN silencing (**Figure 6D** and **Supplementary Figures 6F,G**). These findings further support the hypothesis that ROS mediate downregulation of PTEN activity in hPSCs. AKT itself was also shown to be reversibly oxidized by ROS, which strengthens its PIP_3 binding pocket, recruitment to the plasma membrane, and its activation (Su et al., 2019). Our results show that the possible AKT oxidation does not induce phosphorylation without the activity of PI3K (**Figure 2D**). Seemingly, the ROS-mediated strengthening of the PIP_3 binding pocket on the AKT molecule (Su et al., 2019) cooperates with the reversible oxidation of PTEN to induce AKT phosphorylation.

PTEN was shown to be also regulated on the level of transcription, protein stability, and localization (Leslie and Downes, 2002). Since the total amount of PTEN remained stable when comparing 21 and 5% O_2 (**Figure 6A** and **Supplementary Figures 6A,B**) and cells treated with GSH and H_2O_2 (**Figure 6B** and **Supplementary Figures 6C,D**), downregulation of AKT phosphorylation in hPSCs does not appear to be driven by changes in PTEN total amount or stability. The extent of PTEN phosphorylation can impact its localization (Vazquez et al., 2000), but similarly to the total amount, we did not detect any changes in PTEN phosphorylation in different oxygen tensions (**Figure 6A** and **Supplementary Figures 6A,B**) or in the presence of a different amount of ROS (**Figure 6B** and **Supplementary Figures 6C,D**). These data together suggest the involvement of only cysteine oxidation in the ROS-mediated regulation of PTEN activity in hPSCs.

We also analyzed the role of SH2-domain-containing inositol-5′-phosphatase (SHIP2). This enzyme is known to antagonize PI3K in a manner similar to PTEN and is described to be regulated by ROS (Zhang et al., 2007). As expected, 2-h inhibition of SHIP2 by AS19 had no effect on AKT phosphorylation in hPSCs (**Figure 6F** and **Supplementary Figures 7A,B**) since the effect of SHIP2 on AKT phosphorylation starts to appear after 6 h (Fafilek et al., 2018). While SHIP2 probably does play a role in long-term hypoxia-induced regulation of AKT, our data suggest that it is not involved in the immediate dynamic response to O_2-induced ROS regulation of PI3K/AKT pathway in hPSCs.

ERK1/2 and AKT dephosphorylation have also been previously attributed to protein phosphatase 2A (PP2A). PP2A has been described to be negatively regulated by ROS, which might contribute to its activation in mild hypoxia (Rao and Clayton, 2002; Raman and Pervaiz, 2019). However, PP2A inhibition had no significant effect on AKT phosphorylation in hPSCs cultivated in 5 or 21% O_2 (**Figure 6G** and **Supplementary Figures 7C,D**). Similarly, no changes in ERK1/2 phosphorylation were detected in our cells (**Figure 1A** and **Supplementary Figures 1A,B**). Therefore, PP2A does not seem to play a significant role in O_2-induced ROS regulation of the PI3K/AKT pathway in hPSCs.

HIF-1α Silencing Upregulates ROS/PI3K/AKT and Inhibits MAPK in Mild Hypoxia

HIFs 1 and 2 are master regulators of cellular adaptation to hypoxic conditions (Semenza, 2001; Keith et al., 2012). $CoCl_2$ is a known hypoxia mimetic, stabilizing α subunits of HIFs, but it only transcriptionally activates HIF-1 (Befani et al., 2013). Mimicking hypoxia with $CoCl_2$ led to stabilization of HIF-1α and downregulation of AKT phosphorylation (**Figure 4A**). Previously, HIF-1-deficient fibroblasts were shown to accumulate ROS (Zhang et al., 2008). Indeed, we found hESCs with downregulated HIF-1α to have significantly elevated ROS levels (**Figure 4C**) and upregulated AKT phosphorylation even in the absence of ligand FGF2 (**Figure 4B** and **Supplementary Figure 4A**). Together with our observations describing ROS-induced regulation of FGFR1 (**Figure 3B**) and PTEN (**Figures 6C–E**), these data suggest that HIF-1 driven downregulation of ROS regulates activation of FGFR and PTEN inactivation in mild hypoxia. This is strikingly different from the mechanism in mESCs, where the ROS-mediated downregulation of PI3K/AKT and MAPK pathways is HIF-1 independent (Kučera et al., 2017). It is also important to mention that ROS probably influence other pathways converging on PI3K/AKT through different RTKs (Chiarugi and Buricchi, 2007; Kruk et al., 2013) and different phosphatases (Chiarugi and Cirri, 2003; Esposito et al., 2003; Chiarugi and Buricchi, 2007; Raman and Pervaiz, 2019), for example, the insulin or insulin-like signaling pathway (Papaconstantinou, 2009; Dalton, 2013).

MAPK Downregulate PI3K/AKT and FGFR1 Phosphorylation via ROS

The silencing of HIF-1α expression led to downregulation of ERK1/2 phosphorylation and simultaneous upregulation of AKT phosphorylation in hPSCs (**Figure 4B** and **Supplementary Figure 4A**). MAPK was previously shown to downregulate PI3K/AKT regulating the adaptor protein Gab1 (Yu et al., 2002) or by recruitment of PTEN to the plasma membrane (Zmajkovicova et al., 2013). In hPSCs, MEK1/2 inhibition also upregulated AKT phosphorylation (**Figure 5A** and **Supplementary Figures 5A,B**). MEK1/2 inhibition in mild hypoxia was also accompanied by an elevation of ROS (**Figure 5B**). Even though MEK1/2 inhibition-mediated elevation of ROS was not statistically significant in 21% O_2, AKT phosphorylation was rescued by downregulation of ROS (**Figure 5C** and **Supplementary Figures 5C,D**). These data implicate that MAPK attenuates PI3K/AKT via ROS as second messengers. Moreover, MEK1/2 inhibition led to upregulation of FGFR1 phosphorylation in 21% O_2, which can be prevented by ROS scavenging (**Figure 5D**, **Supplementary Figures 5C,E**).

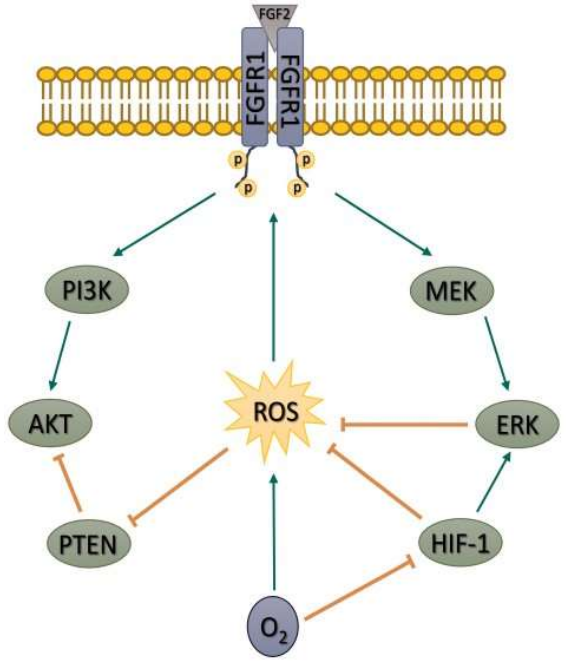

FIGURE 8 | Schematic depiction of our proposed model of the role of ROS in the regulation of FGF2-induced AKT phosphorylation in hPSCs. Based on our artificial manipulations of the MEK1/2–ERK1/2 pathway and ROS levels, we propose that MEK1/2–ERK1/2 pathway and mild hypoxia (5% O_2) downregulate AKT phosphorylation using ROS as second messengers. We further show that ROS contribute to AKT phosphorylation by FGFR1 transactivation and inhibition of PTEN activity in hPSCs. ROS, reactive oxygen species; FGF2, fibroblast growth factor 2; AKT, protein kinase B; hPSCs, human pluripotent stem cells; MAPK, mitogen-activated protein kinase; FGFR1, fibroblast growth factor receptor 1; PTEN, phosphatase and tensin homolog deleted on chromosome 10; MEK1/2, mitogen-activated protein kinase kinase 1 and 2; ERK1/2, extracellular signal-regulated kinase 1 and 2; HIF-1, hypoxia-inducible factor 1; PI3K, phosphatydylinositol-4,5-bisphosphate 3-kinase.

Even though our results stem from an artificial MEK1/2–ERK1/2 manipulation, MEK1/2–ERK1/2-induced inhibition of ROS suggest this mechanism may serve as a negative feedback loop from MAPK toward FGFR1. A similar negative feedback loop involving p38 has already been described in the literature (Zakrzewska et al., 2019). The detailed mechanism by which MEK1/2–ERK1/2 contributes to the ROS downregulation is so far unclear, but the MAPK pathway was shown to play an important role in metabolic reprogramming and upregulation of glycolysis (Papa et al., 2019). Glycolysis provides its intermediates to the pentose phosphate pathway (PPP), a significant NADPH source. NADPH is known to contribute to the ROS scavenging by providing its reductive potential to GSH and thioredoxins, consequently utilized to neutralize ROS (Hanschmann et al., 2013). It is, therefore, possible that MEK1/2–ERK1/2 may downregulate ROS in hPSCs via upregulation of NADPH production in PPP.

ROS Scavenging Upregulates Pluripotency Markers

Several studies have shown that a hypoxic environment improves hPSCs pluripotency (Ezashi et al., 2005; Mathieu et al., 2013), which was linked to HIFs-induced pluripotency gene expression (Forristal et al., 2010; Mathieu et al., 2014). Mild hypoxia-induced ROS downregulation might contribute to the pluripotency maintenance, at least according to our data showing that ROS scavenging with GSH in 21% O_2 upregulates pluripotency markers on levels similar to those observed in 5% O_2 (**Figures 7A,B**). This is in concert with a previous study showing that ROS are able to induce hPSCs differentiation (Ji et al., 2010). The role of PI3K/AKT attenuation due to ROS downregulation in pluripotency maintenance is unclear, but it could be an interesting topic of further studies, since PI3K/AKT signaling directs cell fate decision upon differentiation priming (Yu and Cui, 2016).

Another possible mechanism for ROS-mediated regulation of pluripotency is integrative nuclear FGFR1 signaling (INFS), which was shown to downregulate the expression of core pluripotency genes and to be instrumental in neural differentiation (Terranova et al., 2015). INFS-induced localization of FGFR1 in the nucleus is induced by activation of cell surface receptors (Stachowiak et al., 2007) and may include interaction with p85α (Dunham et al., 2004). Cell surface FGFR1 phosphorylation can be promoted by ROS as shown by us (**Figures 3A,B**) and others (Chiarugi and Cirri, 2003; Chiarugi and Buricchi, 2007). Similarly, the nuclear localization of FGFR2 negatively regulates HIFs in prostate cancer (Lee et al., 2019). We observed both the cytoplasmic and nuclear localization of FGFR1 in hPSCs using ICC (**Supplementary Figure 8**). We did not observe downregulation of FGFR1 nuclear localization after GSH or 5% O_2 treatment, but it is possible that this mechanism is employed in hPSCs but is under the ICC detection threshold. Such a mechanism would lead to FGFR1-activation-dependent downregulation of the pluripotency signaling network in response to ROS and consequent differentiation.

Taken together, our data show that the PI3K/AKT pathway in hPSCs is upregulated by ROS. The upregulation is secured by an increase in FGFR1-activating Tyr653/654 phosphorylation, PI3K p85 phosphorylation, and a decrease in PTEN activity. We further show that MAPK pathway and also mild hypoxia (in HIF-1-dependent manner) attenuate ROS and thus downregulate but do not completely shut off the PI3K/AKT signaling (**Figure 8**)—a pathway essential for hPSCs pluripotency maintenance, self-renewal, and cell fate decision. Such mechanism differs from observations made in mESCs (Kučera et al., 2017), possibly due to a different pluripotency status. Pluripotency maintenance and iPSCs reprogramming was shown to benefit from mild hypoxia, an environment native to the blastocyst; therefore, it is counterintuitive that it leads to PI3K/AKT downregulation. Higher PI3K/AKT activity in 21% O_2 could theoretically compensate for the missing hypoxia-induced pluripotency signaling. On the other hand, the PI3K/AKT pathway has also been implicated in the regulation of differentiation, as summarized by Yu and Cui (Yu and Cui, 2016). It seems

that a precise balance in signaling pathways activity helps to maintain pluripotency, and swings or disbalances in their activity induced by signaling molecules and external factors can affect the fragile balance between pluripotency and differentiation. We hypothesize that a mildly hypoxic environment via HIF-1 and also the MEK1/2–ERK1/2 pathway might help to maintain such balance in PI3K/AKT (and possibly other ROS-sensitive pathways) activity in hPSCs by controlling levels of second messengers—ROS. We propose that introducing ROS control into the hPSCs maintenance and differentiation protocols might thus lead to their significant improvement (**Figures 7A,B**). Because of the similarity between hPSCs and cancer stem cells and because the PI3K/AKT pathway often undergoes an oncogenic transformation, our results might also help deepen the current understanding of cancer biology.

DATA AVAILABILITY STATEMENT

The original contributions presented in the study are included in the article/**Supplementary Materials**, further inquiries can be directed to the corresponding author/s.

AUTHOR CONTRIBUTIONS

PF performed cell cultivation, WB with analysis, ROS analysis, and ICC analysis. DB performed qRT-PCR and analyzed the data. KH performed cell cultivation and Western blot analysis. MŠ performed WB and ICC. VR and PF wrote the manuscript and designed all experiments. All authors contributed to the article and approved the submitted version.

FUNDING

This work was supported by the Ministry of Education, Youth, and Sports of the Czech Republic (https://www.msmt.cz/?lang=2) and the European Regional Development Fund (https://ec.europa.eu/regional_policy/en/funding/erdf/) Project ENOCH No. CZ.02.1.01/0.0/0.0/16_019/0000868 (PF, VR, and DB) and by the project no. LQ1605 (PF, VR, and MŠ) from the National Program of Sustainability II (Ministry of Education, Youth, and Sports of the Czech Republic). This project was further supported by Grant Agency of the Ministry of Health of the Czech Republic (http://www.azvcr.cz/en), grant no. NU20-06-00156 (VR), and Brno Ph.D. Talent 2015 (PF) from South Moravian Centre for International Mobility, Czech Republic (https://www.jcmm.cz/projekt/brno_phd_talent_2020_en).

ACKNOWLEDGMENTS

We thank Pavel Krejčí, Ph.D. (Department of Biology, Faculty of Medicine, Masaryk University, Brno) for providing us with AS1938909 and Monika Štětková, MD for a grammar check.

SUPPLEMENTARY MATERIAL

The Supplementary Material for this article can be found online at: https://www.frontiersin.org/articles/10.3389/fcell.2020.607444/full#supplementary-material

REFERENCES

Adewumi, O., Aflatoonian, B., Ahrlund-Richter, L., Amit, M., Andrews, P. W., Beighton, G., et al. (2007). Characterization of human embryonic stem cell lines by the international stem cell initiative. *Nat. Biotechnol.* 25, 803–816. doi: 10.1038/nbt1318

Aksamitiene, E., Kiyatkin, A., and Kholodenko, B. N. (2012). Cross-talk between mitogenic Ras/MAPK and survival PI3K/Akt pathways: a fine balance. *Biochem. Soc. Trans.* 40, 139–146. doi: 10.1042/BST20110609

Alvarez-Tejado, M., Naranjo-Suárez, S., Jiménez, C., Carrera, A. C., Landázuri, M. O., and Del Peso, L. (2001). Hypoxia induces the activation of the phosphatidylinositol 3-kinase/Akt cell survival pathway in PC12 cells. Protective role in apoptosis. *J. Biol. Chem.* 276, 22368–22374. doi: 10.1074/jbc.M011688200

Armstrong, L., Hughes, O., Yung, S., Hyslop, L., Stewart, R., Wappler, I., et al. (2006). The role of PI3K/AKT, MAPK/ERK and NFκβ signalling in the maintenance of human embryonic stem cell pluripotency and viability highlighted by transcriptional profiling and functional analysis. *Hum. Mol. Genet.* 15, 1894–1913. doi: 10.1093/hmg/ddl112

Befani, C., Mylonis, I., Gkotinakou, I. M., Georgoulias, P., Hu, C. J., Simos, G., et al. (2013). Cobalt stimulates HIF-1-dependent but inhibits HIF-2-dependent gene expression in liver cancer cells. *Int. J. Biochem. Cell Biol.* 45, 2359–2368. doi: 10.1016/j.biocel.2013.07.025

Chiarugi, P., and Buricchi, F. (2007). Protein tyrosine phosphorylation and reversible oxidation: two cross-talking posttranslation modifications. *Antioxid. Redox Signal.* 9, 1–24. doi: 10.1089/ars.2007.9.1

Chiarugi, P., and Cirri, P. (2003). Redox regulation of protein tyrosine phosphatases during receptor tyrosine kinase signal transduction. *Trends Biochem. Sci.* 28, 509–514. doi: 10.1016/S0968-0004(03)00174-9

Covello, K. L., Kehler, J., Yu, H., Gordan, J. D., Arsham, A. M., Hu, C. J., et al. (2006). HIF-2α regulates Oct-4: effects of hypoxia on stem cell function, embryonic development, and tumor growth. *Genes Dev.* 20, 557–570. doi: 10.1101/gad.1399906

Covey, T. M., Edes, K., and Fitzpatrick, F. A. (2007). Akt activation by arachidonic acid metabolism occurs via oxidation and inactivation of PTEN tumor suppressor. *Oncogene* 26, 5784–5792. doi: 10.1038/sj.onc.1210391

Dalton, S. (2013). Signaling networks in human pluripotent stem cells. *Curr. Opin. Cell Biol.* 25, 241–246. doi: 10.1016/j.ceb.2012.09.005

Dunham, S. M., Pudavar, H. E., Prasad, P. N., and Stachowiak, M. K. (2004). Cellular signaling and protein-protein interactions studied using fluorescence recovery after photobleaching. *J. Phys. Chem. B* 108, 10540–10546. doi: 10.1021/jp0400972

Dvorak, P., Dvorakova, D., Koskova, S., Vodinska, M., Najvirtova, M., Krekac, D., et al. (2005). Expression and potential role of fibroblast growth factor 2 and its receptors in human embryonic stem cells. *Stem Cells* 23, 1200–1211. doi: 10.1634/stemcells.2004-0303

Eiselleova, L., Matulka, K., Kriz, V., Kunova, M., Schmidtova, Z., Neradil, J., et al. (2009). A complex role for FGF-2 in self-renewal, survival, and adhesion of human embryonic stem cells. *Stem Cells* 27, 1847–1857. doi: 10.1002/stem.128

Esposito, F., Chirico, G., Gesualdi, N. M., Posadas, I., Ammendola, R., Russo, T., et al. (2003). Protein kinase B activation by reactive oxygen species is independent of tyrosine kinase receptor phosphorylation and requires Src activity. *J. Biol. Chem.* 278, 20828–20834. doi: 10.1074/jbc.M211841200

Ezashi, T., Das, P., and Roberts, R. M. (2005). Low O_2 tensions and the prevention of differentiation of hES cells. *Proc. Natl. Acad. Sci. U.S.A.* 102, 4783–4788. doi: 10.1073/pnas.0501283102

Fafilek, B., Balek, L., Bosakova, M. K., Varecha, M., Nita, A., Gregor, T., et al. (2018). The inositol phosphatase SHIP2 enables sustained ERK

activation downstream of FGF receptors by recruiting Src kinases. *Sci. Signal.* 11:eaap8608. doi: 10.1126/scisignal.aap8608

Fischer, B., and Bavister, B. D. (1993). Oxygen tension in the oviduct and uterus of rhesus monkeys, hamsters and rabbits. *J. Reprod. Fertil.* 99, 673–679. doi: 10.1530/jrf.0.0990673

Forristal, C. E., Wright, K. L., Hanley, N. A., Oreffo, R. O. C., and Houghton, F. D. (2010). Hypoxia inducible factors regulate pluripotency and proliferation in human embryonic stem cells cultured at reduced oxygen tensions. *Reproduction* 139, 85–97. doi: 10.1530/REP-09-0300

Genestra, M. (2007). Oxyl radicals, redox-sensitive signalling cascades and antioxidants. *Cell. Signal.* 19, 1807–1819. doi: 10.1016/j.cellsig.2007.04.009

Haghighi, F., Dahlmann, J., Nakhaei-Rad, S., Lang, A., Kutschka, I., Zenker, M., et al. (2018). BFGF-mediated pluripotency maintenance in human induced pluripotent stem cells is associated with NRAS-MAPK signaling 06 biological sciences 0601 biochemistry and cell biology. *Cell Commun. Signal.* 16:96. doi: 10.1186/s12964-018-0307-1

Hanschmann, E. M., Godoy, J. R., Berndt, C., Hudemann, C., and Lillig, C. H. (2013). Thioredoxins, glutaredoxins, and peroxiredoxins-molecular mechanisms and health significance: from cofactors to antioxidants to redox signaling. *Antioxid. Redox Signal.* 19, 1539–1605. doi: 10.1089/ars.2012.4599

Hossini, A. M., Quast, A. S., Plötz, M., Grauel, K., Exner, T., Küchler, J., et al. (2016). PI3K/AKT signaling pathway is essential for survival of induced pluripotent stem cells. *PLoS ONE* 11:e0154770. doi: 10.1371/journal.pone.0154770

Hung, S.-C., Pochampally, R. R., Chen, S.-C., Hsu, S.-C., and Prockop, D. J. (2007). Angiogenic effects of human multipotent stromal cell conditioned medium activate the PI3K-akt pathway in hypoxic endothelial cells to inhibit apoptosis, increase survival, and stimulate angiogenesis. *Stem Cells* 25, 2363–2370. doi: 10.1634/stemcells.2006-0686

Jelinkova, S., Fojtik, P., Kohutova, A., Vilotic, A., Marková, L., Pesl, M., et al. (2019). Dystrophin deficiency leads to genomic instability in human pluripotent stem cells via NO synthase-induced oxidative stress. *Cells* 8:53. doi: 10.3390/cells8010053

Ji, A. R., Ku, S. Y., Cho, M. S., Kim, Y. Y., Kim, Y. J., Oh, S. K., et al. (2010). Reactive oxygen species enhance differentiation of human embryonic stem cells into mesendodermal lineage. *Exp. Mol. Med.* 42, 175–186. doi: 10.3858/emm.2010.42.3.018

Keith, B., Johnson, R. S., and Simon, M. C. (2012). HIF1 α and HIF2 α: sibling rivalry in hypoxic tumour growth and progression. *Nat. Rev. Cancer* 12, 9–22. doi: 10.1038/nrc3183

Khacho, M., Clark, A., Svoboda, D. S., Azzi, J., MacLaurin, J. G., Meghaizel, C., et al. (2016). Mitochondrial dynamics impacts stem cell identity and fate decisions by regulating a nuclear transcriptional program. *Cell Stem Cell* 19, 232–247. doi: 10.1016/j.stem.2016.04.015

Kim, J. H., Choi, T. G., Park, S., Yun, H. R., Nguyen, N. N. Y., Jo, Y. H., et al. (2018). Mitochondrial ROS-derived PTEN oxidation activates PI3K pathway for mTOR-induced myogenic autophagy. *Cell Death Differ.* 25, 1921–1937. doi: 10.1038/s41418-018-0165-9

Kruk, J. S., Vasefi, M. S., Heikkila, J. J., and Beazely, M. A. (2013). Reactive oxygen species are required for 5-HT-induced transactivation of neuronal platelet-derived growth factor and TrkB receptors, but not for ERK1/2 activation. *PLoS ONE* 8:e77027. doi: 10.1371/journal.pone.0077027

Krutá, M., Šeneklová, M., Raška, J., Salykin, A., Zerzánková, L., Pešl, M., et al. (2014). Mutation frequency dynamics in hprt locus in culture-adapted human embryonic stem cells and induced pluripotent stem cells correspond to their differentiated counterparts. *Stem Cells Dev.* 23, 2443–2454. doi: 10.1089/scd.2013.0611

Kučera, J., Netušilová, J., Sladeček, S., Lánová, M., Vašíček, O., Štefková, K., et al. (2017). Hypoxia downregulates MAPK/ERK but not STAT3 signaling in ROS-dependent and HIF-1-independent manners in mouse embryonic stem cells. *Oxid. Med. Cell. Longev.* 2017:438647. doi: 10.1155/2017/4386947

Kunath, T., Saba-El-Leil, M. K., Almousailleakh, M., Wray, J., Meloche, S., and Smith, A. (2007). FGF stimulation of the Erk1/2 signalling cascade triggers transition of pluripotent embryonic stem cells from self-renewal to lineage commitment. *Development* 134, 2895–2902. doi: 10.1242/dev.02880

Lee, H. H., Chang, C. C., Shieh, M. J., Wang, J. P., Chen, Y., Te, Y., et al. (2013). Hypoxia enhances chondrogenesis and prevents terminal differentiation through pi3k/akt/foxo dependent anti-apoptotic effect. *Sci. Rep.* 3:2683. doi: 10.1038/srep02683

Lee, J. E., Shin, S. H., Shin, H. W., Chun, Y. S., and Park, J. W. (2019). Nuclear FGFR2 negatively regulates hypoxia-induced cell invasion in prostate cancer by interacting with HIF-1 and HIF-2. *Sci. Rep.* 9:3480. doi: 10.1038/s41598-019-39843-6

Lee, S. R., Yang, K. S., Kwon, J., Lee, C., Jeong, W., and Rhee, S. G. (2002). Reversible inactivation of the tumor suppressor PTEN by H_2O_2. *J. Biol. Chem.* 277, 20336–20342. doi: 10.1074/jbc.M111899200

Leslie, N. R., and Downes, C. P. (2002). PTEN: the down side of PI 3-kinase signalling. *Cell. Signal.* 14, 285–295. doi: 10.1016/S0898-6568(01)00234-0

Levenstein, M. E., Ludwig, T. E., Xu, R.-H., Llanas, R. A., VanDenHeuvel-Kramer, K., Manning, D., et al. (2006). Basic fibroblast growth factor support of human embryonic stem cell self-renewal. *Stem Cells* 24, 568–574. doi: 10.1634/stemcells.2005-0247

Li, J., Wang, G., Wang, C., Zhao, Y., Zhang, H., Tan, Z., et al. (2007). MEK/ERK signaling contributes to the maintenance of human embryonic stem cell self-renewal. *Differentiation* 75, 299–307. doi: 10.1111/j.1432-0436.2006.00143.x

Maddalena, L. A., Selim, S. M., Fonseca, J., Messner, H., McGowan, S., and Stuart, J. A. (2017). Hydrogen peroxide production is affected by oxygen levels in mammalian cell culture. *Biochem. Biophys. Res. Commun.* 493, 246–251. doi: 10.1016/j.bbrc.2017.09.037

Mathieu, J., Zhang, Z., Nelson, A., Lamba, D. A., Reh, T. A., Ware, C., et al. (2013). Hypoxia induces re-entry of committed cells into pluripotency. *Stem Cells* 31, 1737–1748. doi: 10.1002/stem.1446

Mathieu, J., Zhou, W., Xing, Y., Sperber, H., Ferreccio, A., Agoston, Z., et al. (2014). Hypoxia-inducible factors have distinct and stage-specific roles during reprogramming of human cells to pluripotency. *Cell Stem Cell* 14, 592–605. doi: 10.1016/j.stem.2014.02.012

Mendoza, M. C., Er, E. E., and Blenis, J. (2011). The Ras-ERK and PI3K-mTOR pathways: cross-talk and compensation. *Trends Biochem. Sci.* 36, 320–328. doi: 10.1016/j.tibs.2011.03.006

Miyamoto, L., Yagi, Y., Hatano, A., Kawazoe, K., Ishizawa, K., Minakuchi, K., et al. (2015). Spontaneously hyperactive MEK-Erk pathway mediates paradoxical facilitation of cell proliferation in mild hypoxia. *Biochim. Biophys. Acta Gen. Subj.* 1850, 640–646. doi: 10.1016/j.bbagen.2014.12.006

Okazaki, K., and Maltepe, E. (2006). Oxygen, epigenetics and stem cell fate. *Regen. Med.* 1, 71–83. doi: 10.2217/17460751.1.1.71

Okoh, V. O., Felty, Q., Parkash, J., Poppiti, R., and Roy, D. (2013). Reactive oxygen species via redox signaling to PI3K/AKT pathway contribute to the malignant growth of 4-hydroxy estradiol-transformed mammary epithelial cells. *PLoS ONE* 8:e54206. doi: 10.1371/journal.pone.0054206

Östman, A., Frijhoff, J., Sandin, Å., and Böhmer, F. D. (2011). Regulation of protein tyrosine phosphatases by reversible oxidation. *J. Biochem.* 150, 345–356. doi: 10.1093/jb/mvr104

Papa, S., Choy, P. M., and Bubici, C. (2019). The ERK and JNK pathways in the regulation of metabolic reprogramming. *Oncogene* 38, 2223–2240. doi: 10.1038/s41388-018-0582-8

Papaconstantinou, J. (2009). Insulin/IGF-1 and ROS signaling pathway cross-talk in aging and longevity determination. *Mol. Cell. Endocrinol.* 299, 89–100. doi: 10.1016/j.mce.2008.11.025

Raman, D., and Pervaiz, S. (2019). Redox inhibition of protein phosphatase PP2A: potential implications in oncogenesis and its progression. *Redox Biol.* 27:101105. doi: 10.1016/j.redox.2019.101105

Rao, R. K., and Clayton, L. W. (2002). Regulation of protein phosphatase 2A by hydrogen peroxide and glutathionylation. *Biochem. Biophys. Res. Commun.* 293, 610–616. doi: 10.1016/S0006-291X(02)00268-1

Rhee, S. G. (2006). H_2O_2, a necessary evil for cell signaling. *Science* 312, 1882–1883. doi: 10.1126/science.1130481

Semenza, G. L. (2001). HIF-1 and mechanisms of hypoxia sensing. *Curr. Opin. Cell Biol.* 13, 167–71. doi: 10.1016/S0955-0674(00)00194-0

Shiojima, I., and Walsh, K. (2002). Role of Akt signaling in vascular homeostasis and angiogenesis. *Circ. Res.* 90, 1243–1250. doi: 10.1161/01.RES.0000022200.71892.9F

Singh, A. M., Reynolds, D., Cliff, T., Ohtsuka, S., Mattheyses, A. L., Sun, Y., et al. (2012). Signaling network crosstalk in human pluripotent cells: a Smad2/3-regulated switch that controls the balance between self-renewal and differentiation. *Cell Stem Cell* 10, 312–326. doi: 10.1016/j.stem.2012.01.014

Stachowiak, M. K., Maher, P. A., and Stachowiak, E. K. (2007). Integrative nuclear signaling in cell development - A role for FGF receptor-1. *DNA Cell Biol.* 26, 811–826. doi: 10.1089/dna.2007.0664

Su, Z., Burchfield, J. G., Yang, P., Humphrey, S. J., Yang, G., Francis, D., et al. (2019). Global redox proteome and phosphoproteome analysis reveals redox switch in Akt. *Nat. Commun.* 10:5486. doi: 10.1038/s41467-019-13114-4

Takahashi, K., Tanabe, K., Ohnuki, M., Narita, M., Ichisaka, T., Tomoda, K., et al. (2007). Induction of pluripotent stem cells from adult human fibroblasts by defined factors. *Cell* 131, 861–872. doi: 10.1016/j.cell.2007.11.019

Terranova, C., Narla, S. T., Lee, Y. W., Bard, J., Parikh, A., Stachowiak, E. K., et al. (2015). Global developmental gene programing involves a nuclear form of fibroblast growth factor receptor-1 (FGFR1). *PLoS ONE* 10:e0123380. doi: 10.1371/journal.pone.0123380

Vazquez, F., Grossman, S. R., Takahashi, Y., Rokas, M. V., Nakamura, N., and Sellers, W. R. (2001). Phosphorylation of the PTEN tail acts as an inhibitory switch by preventing its recruitment into a protein complex. *J. Biol. Chem.* 276, 48627–48630. doi: 10.1074/jbc.C100556200

Vazquez, F., Ramaswamy, S., Nakamura, N., and Sellers, W. R. (2000). Phosphorylation of the PTEN tail regulates protein stability and function. *Mol. Cell. Biol.* 20, 5010–5018. doi: 10.1128/MCB.20.14.5010-5018.2000

Wang, X. Q., Lo, C. M., Chen, L., Ngan, E. S. W., Xu, A., and Poon, R. Y. C. (2017). CDK1-PDK1-PI3K/Akt signaling pathway regulates embryonic and induced pluripotency. *Cell Death Differ.* 24, 38–48. doi: 10.1038/cdd.2016.84

Ward, P. S., and Thompson, C. B. (2012). Metabolic reprogramming: a cancer hallmark even warburg did not anticipate. *Cancer Cell* 21, 297–308. doi: 10.1016/j.ccr.2012.02.014

Xu, C., Rosler, E., Jiang, J., Lebkowski, J. S., Gold, J. D., O'Sullivan, C., et al. (2005a). Basic fibroblast growth factor supports undifferentiated human embryonic stem cell growth without conditioned medium. *Stem Cells* 23, 315–323. doi: 10.1634/stemcells.2004-0211

Xu, R. H., Peck, R. M., Li, D. S., Feng, X., Ludwig, T., and Thomson, J. A. (2005b). Basic FGF and suppression of BMP signaling sustain undifferentiated proliferation of human ES cells. *Nat. Methods* 2, 185–190. doi: 10.1038/nmeth744

Yoshida, Y., Takahashi, K., Okita, K., Ichisaka, T., and Yamanaka, S. (2009). Hypoxia enhances the generation of induced pluripotent stem cells. *Cell Stem Cell* 5, 237–241. doi: 10.1016/j.stem.2009.08.001

Yu, C. F., Liu, Z. X., and Cantley, L. G. (2002). ERK negatively regulates the epidermal growth factor-mediated interaction of Gab1 and the phosphatidylinositol 3-kinase. *J. Biol. Chem.* 277, 19382–19388. doi: 10.1074/jbc.M200732200

Yu, J. S. L., and Cui, W. (2016). Proliferation, survival and metabolism: the role of PI3K/AKT/ mTOR signalling in pluripotency and cell fate determination. *Development* 143, 3050–3060. doi: 10.1242/dev.137075

Yu, P., Pan, G., Yu, J., and Thomson, J. A. (2011). FGF2 sustains NANOG and switches the outcome of BMP4-induced human embryonic stem cell differentiation. *Cell Stem Cell* 8, 326–334. doi: 10.1016/j.stem.2011.01.001

Zakrzewska, M., Opalinski, L., Haugsten, E. M., Otlewski, J., and Wiedlocha, A. (2019). Crosstalk between p38 and Erk 1/2 in downregulation of FGF1-induced signaling. *Int. J. Mol. Sci.* 20:1826. doi: 10.3390/ijms20081826

Zeng, L., Zhou, H. Y., Tang, N. N., Zhang, W. F., He, G. J., Hao, B., et al. (2016). Wortmannin influences hypoxia-inducible factor-1 alpha expression and glycolysis in esophageal carcinoma cells. *World J. Gastroenterol.* 22, 4868–4880. doi: 10.3748/wjg.v22.i20.4868

Zhang, H., Bosch-Marce, M., Shimoda, L. A., Yee, S. T., Jin, H. B., Wesley, J. B., et al. (2008). Mitochondrial autophagy is an HIF-1-dependent adaptive metabolic response to hypoxia. *J. Biol. Chem.* 283, 10892–10903. doi: 10.1074/jbc.M800102200

Zhang, J., Liu, Z., Rasschaert, J., Blero, D., Deneubourg, L., Schurmans, S., et al. (2007). SHIP2 controls PtdIns(3,4,5)P3 levels and PKB activity in response to oxidative stress. *Cell. Signal.* 19, 2194–2200. doi: 10.1016/j.cellsig.2007.06.022

Zhang, J., Wang, X., Vikash, V., Ye, Q., Wu, D., Liu, Y., et al. (2016). ROS and ROS-mediated cellular signaling. *Oxid. Med. Cell. Longev.* 2016:4350965. doi: 10.1155/2016/4350965

Zhang, L., Liu, Q., Lu, L., Zhao, X., Gao, X., and Wang, Y. (2011). Astragaloside IV stimulates angiogenesis and increases hypoxia-inducible factor-1α accumulation via phosphatidylinositol 3-kinase/akt pathway. *J. Pharmacol. Exp. Ther.* 338, 485–491. doi: 10.1124/jpet.111.180992

Zhang, Y., and Yang, J. H. (2013). Activation of the PI3K/Akt pathway by oxidative stress mediates high glucose-induced increase of adipogenic differentiation in primary rat osteoblasts. *J. Cell. Biochem.* 114, 2595–2602. doi: 10.1002/jcb.24607

Zmajkovicova, K., Jesenberger, V., Catalanotti, F., Baumgartner, C., Reyes, G., and Baccarini, M. (2013). MEK1 is required for PTEN membrane recruitment, AKT regulation, and the maintenance of peripheral tolerance. *Mol. Cell* 50, 43–55. doi: 10.1016/j.molcel.2013.01.037

Conflict of Interest: The authors declare that the research was conducted in the absence of any commercial or financial relationships that could be construed as a potential conflict of interest.

Copyright © 2021 Fojtík, Beckerová, Holomková, Šenfluk and Rotrekl. This is an open-access article distributed under the terms of the Creative Commons Attribution License (CC BY). The use, distribution or reproduction in other forums is permitted, provided the original author(s) and the copyright owner(s) are credited and that the original publication in this journal is cited, in accordance with accepted academic practice. No use, distribution or reproduction is permitted which does not comply with these terms.

6.6. Annex 6

Cardiovascular progenitor cells and tissue plasticity are reduced in a myocardium affected by Becker muscular dystrophy

Pesl M, Jelinkova S, Caluori G, Holicka M, Krejci J, Nemec P, Kohutova A, Zampachova V, Dvorak P, ***Rotrekl V***

Pesl et al. Orphanet Journal of Rare Diseases (2020) 15:65
https://doi.org/10.1186/s13023-019-1257-4

Orphanet Journal of Rare Diseases

RESEARCH Open Access

Cardiovascular progenitor cells and tissue plasticity are reduced in a myocardium affected by Becker muscular dystrophy

Martin Pesl[1,2,3], Sarka Jelinkova[1,2], Guido Caluori[2,4], Maria Holicka[5], Jan Krejci[3], Petr Nemec[6], Aneta Kohutova[1,2], Vita Zampachova[7], Petr Dvorak[1] and Vladimir Rotrekl[1,2*]

Abstract: We describe the association of Becker muscular dystrophy (BMD) derived heart failure with the impairment of tissue homeostasis and remodeling capabilities of the affected heart tissue. We report that BMD heart failure is associated with a significantly decreased number of cardiovascular progenitor cells, reduced cardiac fibroblast migration, and ex vivo survival.

Background: Becker muscular dystrophy belongs to a class of genetically inherited dystrophin deficiencies. It affects male patients and results in progressive skeletal muscle degeneration and dilated cardiomyopathy leading to heart failure. It is a relatively mild form of dystrophin deficiency, which allows patients to be on a heart transplant list. In this unique situation, the explanted heart is a rare opportunity to study the degenerative process of dystrophin-deficient cardiac tissue. Heart tissue was excised, dissociated, and analyzed. The fractional content of c-kit$^+$/CD45$^-$ cardiovascular progenitor cells (CVPCs) and cardiac fibroblast migration were compared to control samples of atrial tissue. Control tissue was obtained from the hearts of healthy organ donor's during heart transplantation procedures.

Results: We report significantly decreased CVPCs (c-kit$^+$/CD45$^-$) throughout the heart tissue of a BMD patient, and reduced numbers of phase-bright cells presenting c-kit positivity in the dystrophin-deficient cultured explants. In addition, ex vivo CVPCs survival and cardiac fibroblasts migration were significantly reduced, suggesting reduced homeostatic support and irreversible tissue remodeling.

Conclusions: Our findings associate genetically derived heart failure in a dystrophin-deficient patient with decreased c-kit$^+$/CD45$^-$ CVPCs and their resilience, possibly hinting at a lack of cardioprotective capability and/or reduced homeostatic support. This also correlates with reduced plasticity of the explanted cardiac tissue, related to the process of irreversible remodeling in the BMD patient's heart.

Keywords: Becker muscular dystrophy, Dystrophin, Cardiovascular progenitor cells, C-kit, Cardiomyopathy, Heart failure

Background

Dystrophinopathies are a class of inherited X-linked genetic disorders that impair the proper synthesis of dystrophin, a scaffolding protein found in skeletal and cardiac muscle [1]. More than 70% of patients suffering from Becker muscular dystrophy (BMD), a mild form of dystrophin deficiency, are diagnosed with dilated cardiomyopathy (DCM) [2, 3], which is uncorrelated with skeletal muscle degeneration [4]. Heart failure is the most common cause of death in those with BMD [5], and patients are, in individual cases, referred for heart transplantation [6].

The cellular dynamics of DCM development in dystrophinopathies are still unclear. Although this condition involves mostly cardiomyocytes, increasing attention has been directed at understanding the features and progression of DCM in the non-muscular cell fractions. These mainly include cardiac fibroblasts [7–9] and endothelial

* Correspondence: vrotrekl@med.muni.cz
[1]Department of Biology, Faculty of Medicine, Masaryk University, Kamenice 5, Brno 62500, Czech Republic
[2]International Clinical Research Center, (ICRC), St. Anne's University Hospital, Pekarska 53, Brno 65691, Czech Republic
Full list of author information is available at the end of the article

© The Author(s). 2020 **Open Access** This article is distributed under the terms of the Creative Commons Attribution 4.0 International License (http://creativecommons.org/licenses/by/4.0/), which permits unrestricted use, distribution, and reproduction in any medium, provided you give appropriate credit to the original author(s) and the source, provide a link to the Creative Commons license, and indicate if changes were made. The Creative Commons Public Domain Dedication waiver (http://creativecommons.org/publicdomain/zero/1.0/) applies to the data made available in this article, unless otherwise stated.

cells [10–13], which are, in part, known to affect extracellular matrix and vascular remodeling. Other stromal cells possibly involved in cardiac homeostasis, survival, and disease dynamics are cardiovascular progenitor cells (CVPC) [14], which include the $CD117^{+}$ (or c-kit)/$CD45^{-}$ fraction, and has been the main focus of several recent studies [15, 16]. Currently, the evidence shows that c-kit^{+}/$CD45^{-}$ are activated by cardiac injury [17] supporting the hypothesis of paracrine regulation of cardiac function under pathophysiological conditions [16, 18, 19]; however, their role and fate in the human heart remains to be elucidated.

Here we describe the first comparative characterization of c-kit^{+}/$CD45^{-}$ CVPC occurrence and tissue plasticity in myocardium obtained during a rare case of a BMD heart transplant in our center, and only the third such transplantation in the Czech Republic during the past three decades of the transplantation program [20]. This unique sample from our BMD patient was compared to healthy control cardiac samples from healthy heart donors for cardiac transplantation.

Results

Patients' history

A patient with muscular dystrophy developed mild disease-related symptoms at the age 9 yrs. and Gowers' sign was pronounced by the age 15; additionally, there was calf pseudohypertrophy. To this day (age 48), the patient does not require a wheelchair and has no signs of intellectual impairment (for recent neurological report, see Additional file 1: Supplementary materials). Slowly progressing cardiomyopathy was detected in 2004 (age 33) and an internal cardiac defibrillator (ICD) was implanted in 2012 (the ICD was magnetic resonance incompatible, and no MRI scans could be performed). In 2014, the patient presented with heart failure. A cardiac evaluation found a reduced left ventricular ejection fraction (15%) with severe mitral regurgitation (3rd degree, hemodynamically graded as moderate for echo visualization; for a detailed description see Additional file 1: Supplementary materials and Additional file 2: Video 1; Additional file 3: Video 3; Additional file 4: Video 4), and borderline pulmonary hypertension, all of which responded to pharmacological intervention. Ischemic cardiomyopathy was excluded using coronary angiography (see Additional file 1: Supplementary materials). Due to progressive worsening of dyspnea up to the point of pulmonary edema, which required repeated hospital admissions, the patient was put on the non-urgent heart transplantation waiting list. The prescribed heart failure medication included beta-blockers, loop and mineralocorticoid diuretics, digoxin, angiotensin-converting enzyme (ACE) inhibitors, and proton pump inhibitors. A bicaval orthotropic cardiac transplantation took place shortly before the patient turned 44. He was discharged to out-patient care and follow-up 18 days post-transplantation. During the patient's procedure and the five subsequent heart transplant procedures, surgically available left atrial (LA) tissue, from LA reductions (i.e., surgically required LA shaping and reductions in order to fit the transplant to the left atria of the recipient), were collected for use as healthy controls for this study.

The patient had been screened for genetic mutations, in his twenties, i.e., exon sequencing of the *DMD* gene, but no known mutations were found. Due to the evident clinical presentation, other genes were not screened. A single point mutation c.3328 G > T, (p. Glu1110X) in exon 25, causing a stop codon, was later identified in a sample from the patient's first-degree cousin, which was done as part of a family pedigree (see Fig. 1). The patient was subsequently diagnosed with the same mutation. This mutation would normally result in a DMD phenotype. Nevertheless the BMD phenotype of our patient, with a similar stop codon mutation in exon 25, was explained by the presence of alternatively spliced mRNA, in which a deletion bridges the non-sense mutation and thus partially suppresses its effect [21]. The patient has

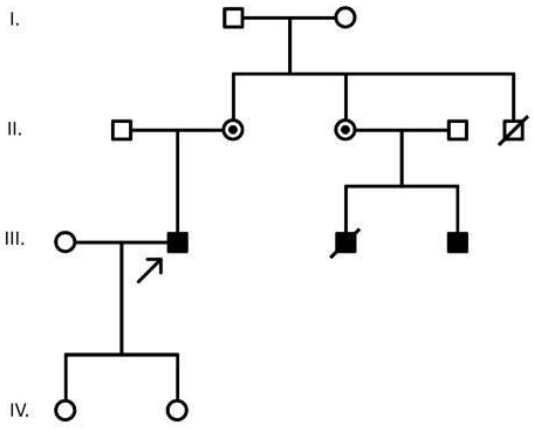

Fig. 1 Family history and pedigree. Proband has no siblings, his father has no signs of muscular dystrophy nor cardiovascular disease and is 70 years old. Mother of patient is alive, with no cardiac involvement, genetic analysis was not performed. Mother's sister, aunt of the proband, was diagnosed as a carrier of an identified mutation, has limited contact with the family, but no cardiac involvement could be traced. Her sons, proband's first cousins, were both confirmed to carry the mutation. The older one (born 1971) died from heart failure in his early thirties, suffering frequent epileptic seizures, aggravating an already unfavorable status, with dystrophy signs since the age of 10. More detailed data could not be retrieved since he was more than 10 years deceased during manuscript preparation. The younger cousin, born 1982 is alive, in his late thirties, with severe myopathy, loss of ambulation since age 14 and was diagnosed with dilated cardiomyopathy. Mother's brother died at 40 years, further details could not be retrieved from the family. The proband has two healthy daughters. Otherwise, the traceable family cardiac history was irrelevant

daughters, however, cascade mutation screening was not performed among female relatives, based on their preference. Creatine kinase (CK) levels before transplantation were only mildly increased, oscillating between 20 and 30 μkat/l (reference value under 3.17 μkat/l); the CK muscle brain (CK-MB) fraction was increased between 0.8–0.9 μkat/l, which normalized after transplantation (under 0.4 μkat/l). A skeletal muscle biopsy was not performed since the diagnosis was genetically verified.

Gross pathologic description of BMD heart

The heart explant (size 150 × 120 × 70 mm) presented bilateral atrial and ventricular dilatation. Both coronary arteries showed sporadic fibrous and atheromatic plaques, without stenosis, and without perivascular inflammation. The wall thickness of the right ventricle (RV) was 4 mm along the anterior basal side and 3 mm along the posterior apical side. RV outflow was partially obstructed by a left ventricle (LV) septal mass. The ventricle walls presented with irregular fibrosis, a thinned or absent myocardial layer, and thickened or prevalent adipose tissue. The LV posterior wall, in particular, was irregularly thick, with the subvalvular wall being 5 mm with a non-compaction appearance (the non-compacted/spongiotic layer: compacted layer ratio was approximately 1). The middle part of the LV posterior wall had a thickness of 8 mm, with fibrosis and thinning toward the apex. The anterior LV wall was irregularly thick (5–10 mm) with focal fibrosis. The IVS thickness was 12 mm. A myxoid transformation of the tricuspid and mitral valves was observed. Histologically, there were partial and non-specific myocardial changes, i.e., dilated cardiomyopathy with hypertrophic cardiomyocytes and interstitial fibrosis. The free LV wall had foci of non-compaction, prominent adipose tissue, and small residual groups of cardiomyocytes. Similar changes were seen in the LV papillary muscles and the RV outflow tract. Laminar fibrosis was present mostly in the subepicardial and middle layers of the compact myocardium regions. Cardiomyocytes showed no signs of acute regressive changes, nor the pathologic changes typical of storage disorders. A slight focal intimal thickening with sporadic incipient atheromatic plaques was found in the coronary arteries.

BMD samples were compared with myocardial samples from hearts explanted due to ischemic heart disease. The controls showed more or less diffuse membranous dystrophin staining. The BMD patient's samples showed a mosaic pattern with an absence of membranous staining and only sporadic isolated myocytes (< 0.1‰) with partial and weak membranous staining. These immunohistopathological findings are shown in Fig. 2.

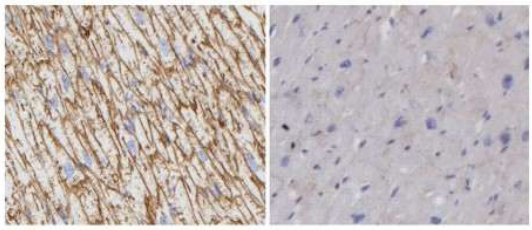

Fig. 2 Immunohistopathology of human myocardium stained for presence of dystrophin. Left image: healthy ventricular myocardium showing membranous aggregation of dystrophin. Right image: Becker muscular dystrophy-affected ventricular myocardium, showing weak membranous distribution of dystrophin. Magnification 400X

C-kit$^+$ /CD45$^-$ cells are depleted in BMD-affected myocardium

We quantified the number of c-kit$^+$/CD45$^-$ cells to detect significant alterations in the cardiac c-kit$^+$/CD45$^-$ population fraction in heart tissue affected by BMD-DCM. Tissue samples from myocardium were dissociated, and single-cell suspensions were quantified with anti-CD117 (c-kit) and anti-CD45 fluorophore-conjugated antibodies. Tissue samples were excised from the whole myocardium of the explanted BMD heart (i.e., LA, right atrium (RA), LV, RV, and intraventricular septum (IVS)) and compared to LA samples of healthy heart donors (HD). While the HD atrial samples contained an average of 1.54% (1.39; 1.62, and 1.62% for each HD sample) c-kit$^+$/CD45$^-$ cells, samples from the BMD myocardium contained 0.28 and 0.35% c-kit$^+$/CD45$^-$ cells (RA and LA, respectively; see Fig. 3a top row), which was less than a quarter of the HD average. The BMD ventricular samples contained 0.42, 0.58, and 0.13% c-kit$^+$ /CD45$^-$ cells (RV, LV, and IVS, respectively; see Fig. 3a bottom row). The BMD c-kit$^+$/CD45$^-$ mean fraction was significantly lower with respect to the mean value of the HD atrial samples ($p = 0.036$, calculated using the Mann-Whitney statistical test, Fig. 3b).

BMD heart tissue shows ex vivo reduced plasticity and phase-bright cells resilience

We evaluated the ability of mildly dissociated tissue explants (< 1 mm^3 pieces) to adhere to culture dishes, in order to prove their ability to retain tissue plasticity. While BMD explants samples required 7 days of ex-vivo cultivation before starting to attach, the HD samples started to attach within 4 days. We then observed and evaluated cardiac fibroblast cell migration from 19 HD and 13 BMD explants-derived samples to estimate the remodeling capacity of the original tissue. The maximal migration distance of fibroblasts from the explant border after 9 days in vitro was 1031.2 ± 351.2 μm in HD samples, but only 330.9 ± 224.4 μm in BMD ($p < 0.001$, Mann-Whitney, Fig. 3c and d top row). We later observed phase-bright

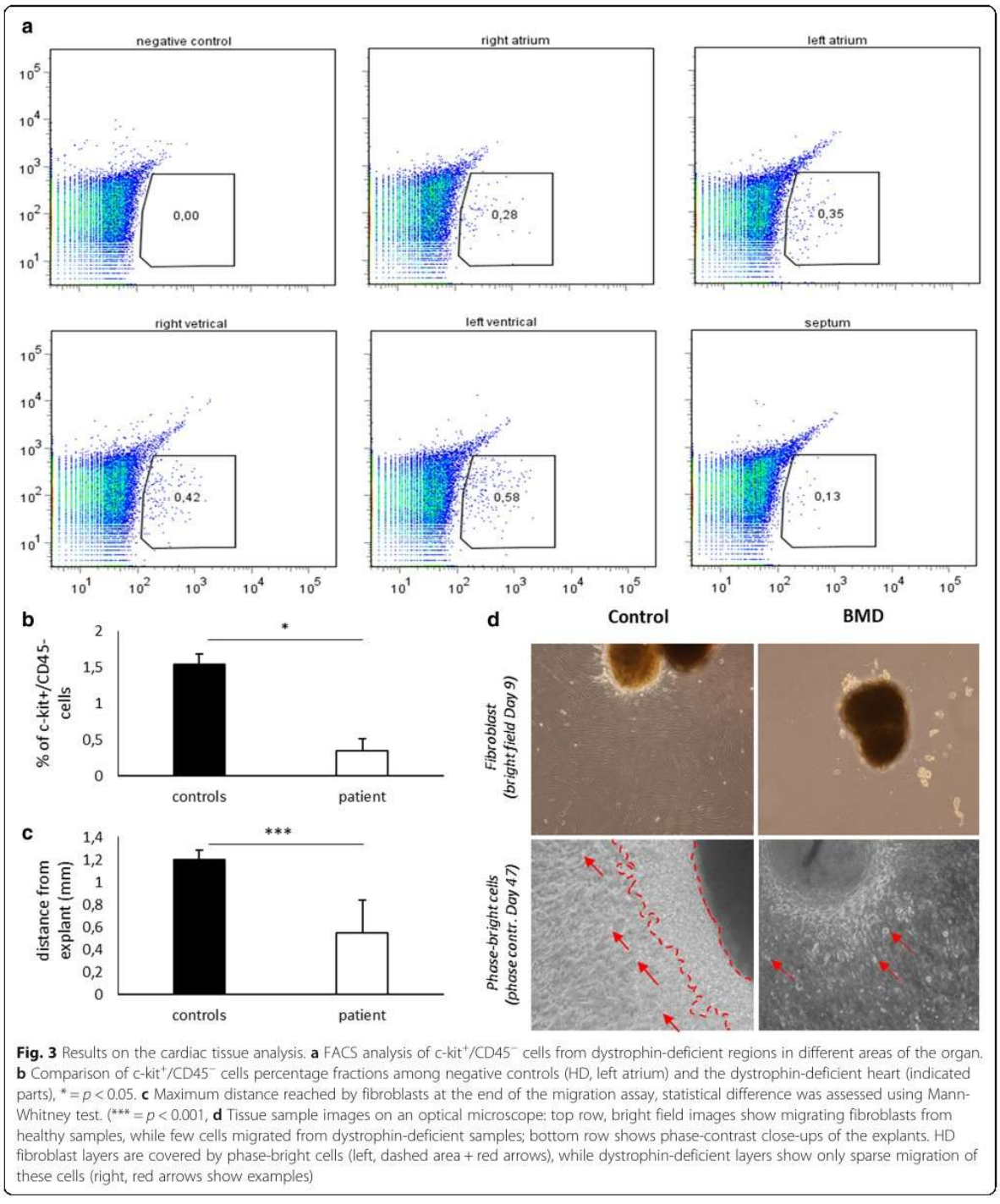

Fig. 3 Results on the cardiac tissue analysis. **a** FACS analysis of c-kit$^+$/CD45$^-$ cells from dystrophin-deficient regions in different areas of the organ. **b** Comparison of c-kit$^+$/CD45$^-$ cells percentage fractions among negative controls (HD, left atrium) and the dystrophin-deficient heart (indicated parts), * = $p < 0.05$. **c** Maximum distance reached by fibroblasts at the end of the migration assay, statistical difference was assessed using Mann-Whitney test. (*** = $p < 0.001$, **d** Tissue sample images on an optical microscope: top row, bright field images show migrating fibroblasts from healthy samples, while few cells migrated from dystrophin-deficient samples; bottom row shows phase-contrast close-ups of the explants. HD fibroblast layers are covered by phase-bright cells (left, dashed area + red arrows), while dystrophin-deficient layers show only sparse migration of these cells (right, red arrows show examples)

cells on fibroblasts. Phase-bright cells have been previously reported to contain a c-kit$^+$ fraction [22]. These loosely adherent cells were thus stained for the presence of the c-kit marker, which revealed a 61 ± 20% positive fraction (6 explant samples analyzed, see Additional file 1: Supplementary materials). Phase-bright cells in HD samples started to appear on the fibroblast layer after 9 days in vitro. In contrast, phase-bright cells in BMD samples

only appeared on fibroblasts after 28 days. BMD explants showed few isolated phase-bright cells on the surrounding fibroblast layer, while HD sample had a dense covering on the surrounding explant tissue (Fig. 3D bottom row). Overall, 32.45% (37/114) of the HD explants showed phase-bright cells, while only 15.64% (23/147) of BMD samples showed phase-bright cells. After 90 days, the HD phase-bright cells had grown enough to allow immunolabelling. The BMD phase-bright cells started to disappear before reaching the quantity necessary for immunolabeling and were no longer observable after 51 days of cultivation, which impaired the comparative analysis.

Discussion

Heart failure due to DCM is a common clinical manifestation in patients with BMD [5]. It has been shown that CVPCs, including c-kit$^+$/CD45$^-$ cells, are involved in cardiac injury and degeneration [17, 23], resulting, for example, in capillary rarefaction, fibrosis, and other pathogeneses of an affected heart [24, 25]. The pathogenesis of dystrophinopathy was previously linked to increased DNA damage and to increased mutagenesis in pluripotent stem cells reprogrammed from DMD patients and lacking dystrophin, as we showed previously [26]. This could affect different organ tissue stem cells or niche supporting cells similar to satellite cells [27]. In this study, we investigated the presence of CVPCs in one model BMD-affected myocardium, as well as tissue remodeling capabilities. We observed that the CVPC fraction found in the dystrophic LA was more than four times lower than the average found in HD samples. The detected values of BMD c-kit$^+$/CD45$^-$ fractions were also comparable to previously reported numbers in idiopathic DCM [28]. This CVPCs depletion resembles DCM associated with accelerated aging [29] and can be caused by an increased turnover concomitant with cell damage. These mechanisms of depletion have been shown, for instance, in hematopoietic stem cells with mutated Sirt1 [30], or dystrophin-deficient ckit$^+$/CD45$^-$ in the GRMD dog model [31]. The reduced tissue plasticity in our model, observed through decreased adherence and cell migration from diseased tissue, also might point to impaired remodeling properties of the BMD-DCM heart. In concert with this hypothesis, only one-tenth of the BMD tissue fragments adhered to gelatin-coated culture dishes, which was almost three-times less than for HD tissue. Dystrophic samples also required nearly twice as much time to attach. Decreased culture dish adherence of BMD heart explanted tissue was accompanied by reduced migration ability of the outgrowing cells. Such behavior could originate in the presence of an activated myofibroblast subpopulation, due to a chronic state of myocardial injury and inflammation [32] with progressive fibrosis [33, 34]. Myofibroblasts are a specialized cell type in between the phenotype of cardiac fibroblasts and smooth muscle myocytes that express α-smooth muscle actinin (SMA) and play an important role in cardiac remodeling [35, 36]. Their motility is reduced due to overexpression of focal adhesion proteins [37] and reduced production of collagen VIII, the lack of which has been associated with decreased migratory abilities [38]. Thus, the presence of terminally differentiated myofibroblasts might explain the reduced adhesion and migration of the cells in vitro.

Ultimately, impaired survival rate of phase-bright cells in BMD samples was observed, while these cells appeared and persisted in the HD fibroblast layer. Moreover, in the BMD samples they were only sparsely identifiable and prematurely disappeared from the BMD fibroblast layer. Their limited in vitro survival in dystrophin-deficient heart explants might hint at altered c-kit$^+$/CD45$^-$ cell resilience also in vitro and subsequently could promote BMD-DCM progression.

The main limitation of the study is the unique characteristic of the human BMD heart sample since only one specimen was available and opportunities to study a heart affected by dystrophinopathy are extremely rare. A comparable sampling of healthy human ventricular tissue was impossible and clearly unethical; thus, atrial tissue controls came from transplants, considered healthy from a cardiac point of view and thus suitable for heart transplantation. We chose donors of similar age to the BMD patient to remove the age bias; with one exception, all were males. Still, tissue availability was limited with only minimal information regarding the medical backgrounds of the donors and families.

In non-ischemic DCM, LA remodeling was observed in functional and morphological changes [39], making this heart area a valid control source. The wide age interval of the donor cohort (see Additional file 1: Supplementary materials) is common in other similar studies [28], and was not significantly different from the age of the BMD patient, as shown using the one-sample t-test ($p = 0.625$). To the best knowledge of the authors, this analysis is the first to directly quantify c-kit$^+$/CD45$^-$ cells from BMD-DCM heart tissue. It contributes to the present understanding of the occurrence and role of c-kit$^+$/CD45$^-$ cells by showing a comparative reduction in this cell fraction, which can be correlated with reduced plasticity and cellular resilience in the BMD heart.

Conclusions

Our findings give further insights into the correlation between c-kit$^+$/CD45$^-$ CVPCs levels, irreversible remodeling, and heart failure in BMD. Future studies aimed at describing c-kit$^+$/CD45$^-$ mechanisms of activation, paracrine modulation, and genetic impairment can provide new therapeutic perspectives into the management of cardiomyopathies. The analysis of c-kit$^+$/CD45$^-$ cells or possibly their secretome might serve as a helpful biomarker for early

stages of cardiomyopathy, possibly not limited only to BMD patients.

Methods

Flow cytometry assay

Tissue samples were excised (in BMD) or extracted during a left atrial biopsy (from heart donors HD). Reduced dystrophin expression was confirmed by immunohistochemistry of myocardial samples. BMD samples were taken from different sections of the heart (left and right atrium, left and right ventricle, and the interventricular septum). As for the healthy donors, only adult patients were included (age 24–62 years, variance statistically insignificant $p = 0.625$) to exclude the bias of pediatric patients that have increased CVPC levels [23]. Due to the unavailability of ventricular samples, only atrial samples, which were obtained from surgical reduction before placing the healthy heart into the chest cavity during transplantations, were used. No other differences in CVPC levels were reported. Samples were treated as previously described by Messina et al. [22]. Briefly, tissue samples were immersed in a 60 mm Petri dish (TPP, Trasadingen, CH) filled with 1xPBS + 2% Pen/Strep (BioSera, Nuaille, France) and cut into 1–2 mm^3 pieces with scissors. Tissue fragments were digested in a dissociating solution composed of 0.1% Collagenase IV in DMEM-F12 (both from Life Technologies, Carlsbad, CA, USA). Dissociation was carried out for 2 h at 37 °C with gentle manual agitation every 15 mins. The dissociation was stopped by adding an equal volume of explant IMDM medium (Life Technologies) supplemented with FBS 10% (Life Technologies), β mercaptoethanol 1% (Sigma-Aldrich, St. Louis, MO), Pen/Strep 1%, and L-glutamine 1% (both from BioSera). Samples were collected and pipetted vigorously with a 1 ml tip to release cells from tissue blocks. The dissociated cell suspension was filtered through a 40 μm strainer (Costar, Washington DC, USA) and spun in a conical tube at 200×g for 5 min. The supernatant was removed, and the cell pellet was resuspended in FACS-PBS, made from 1xPBS with 0.5% BSA (Sigma Aldrich) and 2 mM EDTA (Penta, Prague, CZ). Spinning and resuspension were repeated 3 times to ensure enzyme removal and cell separation. Antibodies were finally added to the suspension (CD45-FITC, cl. 30F11; CD117-APC, cl.3C11, all from Miltenyi Biotech, Bergisch Gladbach, DE) and the analysis was run on a BD FACS Canto II (BD Biosciences, New Jersey, NJ-USA). The negative control for FACS was an unlabeled cell suspension. Data were analyzed using FlowJo (FlowJo LLC, Ashland, OR-USA).

Cell migration assay and immunocytochemistry

Samples were cut into 1–2 mm^3 pieces, as described in the previous paragraph. For the migration assay and c-$kit^+/CD45^-$ cell cultivation, the tissue explants were collected in a dissociation solution and incubated for 5 mins at 37 °C. The enzymatic solution was then removed and replaced with a fresh solution. Incubation and enzyme replacement was repeated three times. Dissociation was stopped by adding an equal volume of explant medium. The samples were spun at 200×g for 2 min, then resuspended with explant medium. The tissue explants were distributed evenly on a 0.1% gelatin-treated 6-well plates (TPP), in 5 ml of explant medium. The dishes were not moved for 4 days to allow attachment of the tissue. The medium was changed every 4 days, and photos were taken on the same days using an inverted Olympus IX71 microscope (Tokyo, Japan), and QuickPhoto Camera software (Promicra, Prague, CZ). Pictures were analyzed using ImageJ open-source software to measure migration [40] distance and phase-bright cells. C-kit+ cells were detected using CD117-APC (Miltenyi Biotec, Bergisch Gladbach, DE) dissolved in 1:100 proportion in IMDM + 0.5% BSA. Photos were taken using a Zeiss LSM700 confocal laser scanning microscope (Zeiss, Oberkochen, DE).

Histopathological methods

The heart explants were dissected according to standard procedures, samples were taken from right atrium, tricuspid valve; the anterior and posterior wall, and outflow tract of the right ventricle; the right coronary artery; the right atrium and mitral valve; anterior papillary muscles; multiple samples from the anterior and posterior wall of the left ventricle; the septum and left coronary arteries. For immune-histological identification of dystrophin, formalin-fixed, paraffin-embedded tissue sections were treated with heat antigen retrieval (95 °C for 45 min, pH 9), and then treated with primary antibodies (Dystrophin Mouse Monoclonal Antibody, Leica, clone 34C5) using the avidin-biotin-immunoperoxidase method according to the manufacturer's protocol.

Statistical analysis

Descriptive statistics and comparisons between sample groups were performed using Prism 5.0 software (GraphPad, La Jolla, CA-US). Available normality tests were performed, and the non-parametric Mann-Whitney test was used to estimate statistical differences between samples. A p-value less than 0.05 was considered significant.

Supplementary information

Supplementary information accompanies this paper at https://doi.org/10.1186/s13023-019-1257-4.

Additional file 1. Supplementary materials.
Additional file 2: Video 1. Coronarography – right coronary artery.
Additional file 3: Video 2. Coronarography – left coronary artery.
Additional file 4: Video 3. Echocardiography.

Abbreviations
BMD: Becker muscular dystrophy; DCM: Dilated cardiomyopathy; HTx: Heart transplantation; IVS: Interventricular septum; LV: Left ventricle; PBC: Phase-bright cells; RV: Right ventricle

Acknowledgements
The authors would like to thank geneticist Dr. Gaillyova and attending neurologists Dr. Vohanka and Dr. Peslova for assistance in clarifying the available documentation.

Authors' contributions
MP was responsible for the design of the study and the coordination, conducted clinical follow-up of the patient, and obtained the informed consent as well as the collection of samples. SJ was responsible for the cellular laboratory sample preparation, the cellular experiments, and their evaluation. GC was responsible for results collection, drafting the manuscript, and figures preparation. MH and JK were attending the cardiologists of the patient. PN was responsible for the surgical preparation of the samples during heart transplantation and the surgeon on the case. AK performed part of the ex vivo analysis of the samples. VZ provided the histological examination of the dystrophic heart samples. PD and VR secured funding of the project and supervised the production of the results and the manuscript. All authors read and approved the final manuscript.

Funding
This work was supported by the Ministry of Education, Youth, and Sports of the Czech Republic (7AMB13FR011, No. CZ.02.1.01/0.0/0.0/16_019/0000868, projects no. LQ1605 and no. LQ1601 from the National Program of Sustainability II) and supported by funds from the Faculty of Medicine MU to junior researchers Martin Pesl and Sarka Jelinkova.

Availability of data and materials
The data that support the findings of this study are available from the corresponding author V.R. upon reasonable request.

Ethics approval and consent to participate
This study was carried out in accordance with the recommendations of the Masaryk University Ethics Committee and St. Ann's University Hospital Ethics Committee, issuing approval nr. 51 V/2015 - approved consent for heart tissue sampling and analysis, and genetic information analysis (DNA and circulating free DNA), protocol was approved on 12th August 2015. The "healthy donor" (HD) control samples were obtained from donors diagnosed with brain death. The hearts were brought to the transplantation center for transplantation and were provided for scientific analysis after the anonymization of donor data. Thus, individual information, such as names of donors, was not available to investigators. Samples from deceased donors were not further addressed by the ethics committee since the transplantation system is opt-out according to the law 285/2002 Sb. in the Czech Republic. At the same time, due to anonymization, family members were not reachable.

Consent for publication
The study subject gave written informed consent regarding explanted organ sampling and publication of results.

Competing interests
The authors declare that they have no competing interests.

Author details
[1]Department of Biology, Faculty of Medicine, Masaryk University, Kamenice 5, Brno 62500, Czech Republic. [2]International Clinical Research Center, (ICRC), St. Anne's University Hospital, Pekarska 53, Brno 65691, Czech Republic. [3]1st Department of Cardiovascular Diseases, St. Anne's University Hospital and Masaryk University, Pekarska 53, Brno 65691, Czech Republic. [4]Central European Institute of Technology (CEITEC MU), Nanobiotechnology, Kamenice 5, Brno 62500, Czech Republic. [5]Department of Cardiology, University Hospital Brno, Jihlavska 20, Brno 62500, Czech Republic. [6]Center for Cardiovascular Surgery and Transplantation, Pekarska 53, Brno 65691, Czech Republic. [7]1st Department of Pathology, Faculty of Medicine, Masaryk University and St. Anne's University Hospital in Brno, Pekarska 53, Brno 65691, Czech Republic.

Received: 23 July 2019 Accepted: 19 November 2019
Published online: 05 March 2020

References

1. Ho R, Nguyen M-L, Mather P. Cardiomyopathy in Becker muscular dystrophy: overview. World J Cardiol. 2016;8:356.
2. Yilmaz A, Gdynia H-J, Baccouche H, Mahrholdt H, Meinhardt G, Basso C, et al. Cardiac involvement in patients with Becker muscular dystrophy: new diagnostic and pathophysiological insights by a CMR approach. J Cardiovasc Magn Reson. 2008;10:50.
3. Panovský R, Pešl M, Holeček T, Máchal J, Feitová V, Mrázová L, et al. Cardiac profile of the Czech population of Duchenne muscular dystrophy patients: a cardiovascular magnetic resonance study with T1 mapping. Orphanet J Rare Dis. 2019;14:10.
4. Finsterer J, Stöllberger C. Cardiac involvement in Becker muscular dystrophy. Can J Cardiol. 2008;24:786–92.
5. Papa AA, D'Ambrosio P, Petillo R, Palladino A, Politano L. Heart transplantation in patients with dystrophinopathic cardiomyopathy: review of the literature and personal series. Intractable Rare Dis Res. 2017;6:95–101.
6. Darras BT, Miller DT, Urion DK. Dystrophinopathies. Seattle: University of Washington; 1993. http://www.ncbi.nlm.nih.gov/pubmed/20301298.
7. Furtado MB, Nim HT, Boyd SE, Rosenthal NA. View from the heart: cardiac fibroblasts in development, scarring and regeneration. Development. 2016; 143:387–97.
8. Furtado MB, Costa MW, Pranoto EA, Ekaterina S, Pinto Alexander R, Lam Nicholas T, et al. Cardiogenic genes expressed in cardiac fibroblasts contribute to heart development and repair. Circ Res. 2014;114:1422–34.
9. Lajiness JD, Conway SJ. The dynamic role of cardiac fibroblasts in development and disease. J Cardiovasc Transl Res. 2012;5:739–48.
10. Talman V, Kivelä R. Cardiomyocyte—endothelial cell interactions in cardiac remodeling and regeneration. Front Cardiovasc Med. 2018;5. https://doi.org/10.3389/fcvm.2018.00101.
11. Mathison M, Rosengart TK. Heart regeneration: the endothelial cell comes first. J Thorac Cardiovasc Surg. 2018;155:1128–9.
12. Hui Z, Lui Kathy O, Bin Z. Endocardial cell plasticity in cardiac development, diseases and regeneration. Circ Res. 2018;122:774–89.
13. Gray G, Toor I, Castellan R, Crisan M, Meloni M. Resident cells of the myocardium: more than spectators in cardiac injury, repair and regeneration. Curr Opin Physiol. 2018;1:46–51.
14. Leong YY, Ng WH, Ellison-Hughes GM, Tan JJ. Cardiac stem cells for myocardial regeneration: they are not alone. Front Cardiovasc Med. 2017;4. https://doi.org/10.3389/fcvm.2017.00047.
15. Zhou B, Wu SM. Reassessment of c-kit in cardiac cells: a complex interplay between expression, fate, and function. Circ Res. 2018;123:9–11.
16. Hodgkinson CP, Bareja A, Gomez JA, Dzau VJ. Emerging concepts in paracrine mechanisms in regenerative cardiovascular medicine and biology. Circ Res. 2016;118:95–107.
17. Finan A, Demion M, Sicard P, Guisiano M, Bideaux P, Monceaux K, et al. Prolonged elevated levels of c-kit+ progenitor cells after a myocardial infarction by beta 2 adrenergic receptor priming. J Cell Physiol. 2019;234: 18283–96.
18. Hong KU, Guo Y, Li Q-H, Cao P, Al-Maqtari T, Vajravelu BN, et al. c-kit+ Cardiac stem cells alleviate post-myocardial infarction left ventricular dysfunction despite poor engraftment and negligible retention in the recipient heart. PLoS ONE. 2014;9:e96725.
19. Davis DR. Cardiac stem cells in the post-Anversa era. Eur Heart J. 2019;40: 1039–41.
20. Viklicky O, Fronek J, Trunecka P, Pirk J, Lischke R. Organ transplantation in the Czech Republic. Transplantation. 2017;101:2259.
21. Fajkusová L, Lukáš Z, Tvrdíková M, Kuhrová V, Hájek J, Fajkus J. Novel dystrophin mutations revealed by analysis of dystrophin mRNA: alternative splicing suppresses the phenotypic effect of a nonsense mutation. Neuromuscul Disord. 2001;11:133–8.
22. Messina E, De Angelis L, Frati G, Morrone S, Chimenti S, Fiordaliso F, et al. Isolation and expansion of adult cardiac stem cells from human and murine heart. Circ Res. 2004;95:911–21.
23. Matuszczak S, Czapla J, Jarosz-Biej M, Wiśniewska E, Cichoń T, Smolarczyk R, et al. Characteristic of c-kit+ progenitor cells in explanted human hearts. Clin Res Cardiol Off J Ger Card Soc. 2014;103:711–8.
24. Lombardi R, Chen SN, Ruggiero A, Gurha P, Czernuszewicz GZ, Willerson JT, et al. Cardiac fibro-adipocyte progenitors express desmosome proteins and

preferentially differentiate to adipocytes upon deletion of the desmoplakin gene. Circ Res. 2016;119:41–54.
25. Kazakov A, Laufs U. Healthy and unhealthy cardiac progenitor cells modify the pathogenesis of myocardial diseases. Circ Res. 2016;119:10–2.
26. Jelinkova S, Fojtik P, Kohutova A, Vilotic A, Marková L, Pesl M, et al. Dystrophin deficiency leads to genomic instability in human pluripotent stem cells via NO synthase-induced oxidative stress. Cells. 2019;8(1):53.
27. Dumont NA, Wang YX, von Maltzahn J, Pasut A, Bentzinger CF, Brun CE, et al. Dystrophin expression in muscle stem cells regulates their polarity and asymmetric division. Nat Med. 2015;21:1455–63.
28. Matuszczak S, Czapla J, Jarosz-Biej M, Winiewska E, Cichoń T, et al. Characteristic of c-Kit + progenitor cells in explanted human hearts. Clin Res Cardiol. 2014;103(9):711–8. https://doi.org/10.1007/s00392-014-0705-3.
29. Saheera S, Nair RR. Accelerated decline in cardiac stem cell efficiency in spontaneously hypertensive rat compared to normotensive Wistar rat. PLoS One. 2017;12:e0189129.
30. Rimmelé P, Bigarella CL, Liang R, Izac B, Dieguez-Gonzalez R, Barbet G, et al. Aging-like phenotype and defective lineage specification in SIRT1-deleted hematopoietic stem and progenitor cells. Stem Cell Rep. 2014;3:44–59.
31. Cassano M, Berardi E, Crippa S, Toelen J, Barthelemy I, Micheletti R, et al. Alteration of cardiac progenitor cell potency in GRMD dogs. Cell Transplant. 2012;21:1945–67.
32. Kharraz Y, Guerra J, Pessina P, Serrano AL, Muñoz-Cánoves P. Understanding the process of fibrosis in Duchenne muscular dystrophy. Biomed Res Int. 2014;2014:965631.
33. Mann CJ, Perdiguero E, Kharraz Y, Aguilar S, Pessina P, Serrano AL, et al. Aberrant repair and fibrosis development in skeletal muscle. Skelet Muscle. 2011;1:21.
34. Fan D, Takawale A, Lee J, Kassiri Z. Cardiac fibroblasts, fibrosis and extracellular matrix remodeling in heart disease. Fibrogenesis Tissue Repair. 2012;5:15.
35. Dostal D, Glaser S, Baudino TA. Cardiac fibroblast physiology and pathology. In: Terjung R, editor. Comprehensive physiology. Hoboken: John Wiley & Sons, Inc.; 2015. p. 887–909. https://doi.org/10.1002/cphy.c140053.
36. Li L, Zhao Q, Kong W. Extracellular matrix remodeling and cardiac fibrosis. Matrix Biol. 2018;68–69:490–506.
37. Santiago J-J, Dangerfield AL, Rattan SG, Bathe KL, Cunnington RH, Raizman JE, et al. Cardiac fibroblast to myofibroblast differentiation in vivo and in vitro: expression of focal adhesion components in neonatal and adult rat ventricular myofibroblasts. Dev Dyn. 2010;239:1573–84.
38. Skrbic B, Engebretsen KVT, Strand ME, Lunde IG, Herum KM, Marstein HS, et al. Lack of collagen VIII reduces fibrosis and promotes early mortality and cardiac dilatation in pressure overload in mice. Cardiovasc Res. 2015;106:32–42.
39. Hoit BD, Ohio C. Left atrial size and function role in prognosis. J Am Coll Cardiol. 2014;63:493–505.
40. Treloar KK, Simpson MJ. Sensitivity of edge detection methods for quantifying cell migration assays. PLoS One. 2013;8:e67389.

Publisher's Note

Springer Nature remains neutral with regard to jurisdictional claims in published maps and institutional affiliations.

Ready to submit your research? Choose BMC and benefit from:

- fast, convenient online submission
- thorough peer review by experienced researchers in your field
- rapid publication on acceptance
- support for research data, including large and complex data types
- gold Open Access which fosters wider collaboration and increased citations
- maximum visibility for your research: over 100M website views per year

At BMC, research is always in progress.

Learn more biomedcentral.com/submissions

BMC

6.7. Annex 7

Dystrophin Deficiency Causes Progressive Depletion of Cardiovascular Progenitor Cells in the Heart

Jelinkova S, Sleiman Y, Fojtik P, Aimond F, Finan A, Hugon G, Scheuermann V, Beckerova D, Cazorla O, Vincenti M, Amedro P, Richard S, Jaros J, Dvorak P, Lacampagne A, Carnac G, ***Rotrekl V****, Meli AC*

International Journal of
Molecular Sciences

MDPI

Article

Dystrophin Deficiency Causes Progressive Depletion of Cardiovascular Progenitor Cells in the Heart

Sarka Jelinkova [1,2], Yvonne Sleiman [3], Petr Fojtík [1,2], Franck Aimond [3], Amanda Finan [3], Gerald Hugon [3], Valerie Scheuermann [3], Deborah Beckerová [1,2], Olivier Cazorla [3], Marie Vincenti [3,4], Pascal Amedro [3,4], Sylvain Richard [3], Josef Jaros [2,5], Petr Dvorak [1], Alain Lacampagne [3], Gilles Carnac [3], Vladimir Rotrekl [1,2,*,†] and Albano C. Meli [3,*,†]

1 Department of Biology, Faculty of Medicine, Masaryk University, Kamenice 5/A3, 62500 Brno, Czech Republic; sarka.jelinkova89@gmail.com (S.J.); petrfoj@hotmail.com (P.F.); deborah.beckerova@gmail.com (D.B.); pdvorak@med.muni.cz (P.D.)
2 ICRC, St Anne's University Hospital, Pekařská 53, 65691 Brno, Czech Republic; jaros@med.muni.cz
3 PhyMedExp, University of Montpellier, INSERM, CNRS, 34295 Montpellier, France; yvonne.sleiman@umontpellier.fr (Y.S.); franck.aimond@inserm.fr (F.A.); amandafinan@yahoo.com (A.F.); gerald.hugon@inserm.fr (G.H.); valerie.scheuermann@inserm.fr (V.S.); olivier.cazorla@inserm.fr (O.C.); m-vincenti@chu-montpellier.fr (M.V.); p-amedro@chu-montpellier.fr (P.A.); sylvain.richard@inserm.fr (S.R.); alain.lacampagne@inserm.fr (A.L.); gilles.carnac@inserm.fr (G.C.)
4 Pediatric and Adult Congenital Cardiology Department, M3C Regional Reference CHD Center, CHU Montpellier, 371 Avenue du Doyen Giraud, 34295 Montpellier, France
5 Department of Histology and Embryology, Faculty of Medicine, Masaryk University, Kamenice 5/A1, 62500 Brno, Czech Republic
* Correspondence: vrotrekl@med.muni.cz (V.R.); albano.meli@inserm.fr (A.C.M.); Tel.: +420-549-498-002 (V.R.); +33-4-67-41-52-44 (A.C.M.); Fax: +420-549-491-327 (V.R.); +33-4-67-41-52-42 (A.C.M.)
† Both authors contributed equally as supervising researchers.

check for updates

Citation: Jelinkova, S.; Sleiman, Y.; Fojtík, P.; Aimond, F.; Finan, A.; Hugon, G.; Scheuermann, V.; Beckerová, D.; Cazorla, O.; Vincenti, M.; et al. Dystrophin Deficiency Causes Progressive Depletion of Cardiovascular Progenitor Cells in the Heart. *Int. J. Mol. Sci.* **2021**, *22*, 5025. https://doi.org/10.3390/ijms22095025

Academic Editor: Hector Barajas-Martinez

Received: 1 April 2021
Accepted: 7 May 2021
Published: 10 May 2021

Publisher's Note: MDPI stays neutral with regard to jurisdictional claims in published maps and institutional affiliations.

Copyright: © 2021 by the authors. Licensee MDPI, Basel, Switzerland. This article is an open access article distributed under the terms and conditions of the Creative Commons Attribution (CC BY) license (https://creativecommons.org/licenses/by/4.0/).

Abstract: Duchenne muscular dystrophy (DMD) is a devastating condition shortening the lifespan of young men. DMD patients suffer from age-related dilated cardiomyopathy (DCM) that leads to heart failure. Several molecular mechanisms leading to cardiomyocyte death in DMD have been described. However, the pathological progression of DMD-associated DCM remains unclear. In skeletal muscle, a dramatic decrease in stem cells, so-called satellite cells, has been shown in DMD patients. Whether similar dysfunction occurs with cardiac muscle cardiovascular progenitor cells (CVPCs) in DMD remains to be explored. We hypothesized that the number of CVPCs decreases in the dystrophin-deficient heart with age and disease state, contributing to DCM progression. We used the dystrophin-deficient mouse model (*mdx*) to investigate age-dependent CVPC properties. Using quantitative PCR, flow cytometry, speckle tracking echocardiography, and immunofluorescence, we revealed that young *mdx* mice exhibit elevated CVPCs. We observed a rapid age-related CVPC depletion, coinciding with the progressive onset of cardiac dysfunction. Moreover, *mdx* CVPCs displayed increased DNA damage, suggesting impaired cardiac muscle homeostasis. Overall, our results identify the early recruitment of CVPCs in dystrophic hearts and their fast depletion with ageing. This latter depletion may participate in the fibrosis development and the acceleration onset of the cardiomyopathy.

Keywords: duchenne muscular dystrophy; *mdx* mouse; cardiovascular progenitors; c-kit; genomic instability; dilated cardiomyopathy

1. Introduction

Duchenne muscular dystrophy (DMD, prevalence 1/5000) is an X-linked genetic disorder causing the wasting of skeletal muscles, resulting in severe disability and premature death in young men [1]. In addition to skeletal muscle loss of function, cardiac muscle is nearly always affected in DMD [2] with the development of a dilated cardiomyopathy

(DCM) starting by the end of the second decade of the DMD patient's life [3,4]. As DMD patient care has improved over the years, heart failure has become the prevalent cause of mortality worldwide in DMD patients [5,6] and also in patients suffering from the less severe Becker muscular dystrophy (BMD). Both forms of the disease are related to dystrophin gene mutations.

The dystrophin deficiency in cardiomyocytes eventually leads to contractile failure followed by death [7]. The molecular and cellular mechanisms causing myocyte death are unclear and have been mostly investigated for skeletal muscle [8]. These reports have suggested impairment of calcium (Ca^{2+}) homeostasis and other ion fluxes [9–11] either due to a compromised plasma membrane integrity, deregulation of stretch-activated channels, or stretch-activated-channel-induced release of reactive oxygen species (ROS) that can trigger a sarcoplasmic reticulum (SR) Ca^{2+} leak [10]. Dystrophin deficiency also causes a leaky ryanodine receptor/Ca^{2+} release channel (RyR1) associated with early post-translational modifications including S-nitrosylation and calstabin1 depletion in *mdx* skeletal muscle [12]. Abnormal intracellular Ca^{2+} handling increases the influx of Ca^{2+} that triggers necrosis and cell death in DMD. We and others have described similar defects in the heart with abnormal Ca^{2+} homeostasis and ryanodine receptor (RyR2) dysfunction [12,13]. The deregulation of other ion complexes such as the voltage gated channel Nav1.5 in dystrophin-deficient cardiomyocytes has been reported [14].

In skeletal muscle, the population of satellite cell progenitors is affected, which has been implicated in the disease progression [15,16]. Dystrophinopathy results in myocyte death inducing muscle satellite cell activation [17] and increased differentiation [18,19] resulting in their eventual depletion [20]. Such a mechanism is unclear in the heart. Higher age-dependent fibrosis in *mdx* muscle and heart has been reported with early sarcolemmal damage induced by inflammation and macrophage infiltration [21,22]. Although DCM involves primarily cardiomyocyte damage, increasing attention has been given to non-muscular cell fractions, including cardiac fibroblasts [23–25] and endothelial cells [26–29], respectively involved in extracellular matrix and vascular remodeling. Other stromal cells possibly involved in cardiac homeostasis, survival, and disease dynamics are cardiovascular progenitor cells (CVPCs) [30], among which the $CD117^+$ (also named c-kit)/$CD45^-$ fraction is the main focus of recent studies [31–33]. We recently showed that CVPCs are activated and recruited to the site of cardiac injury [34], supporting the hypothesis of their paracrine regulation of cardiac function in pathophysiological conditions [31,35,36]. We found a CVPC depletion associated with late-stage pathological remodeling of cardiac muscle in BMD patients [37]. Nevertheless, the role and fate of CVPCs in the heart and cardiac pathology, particularly DMD-associated DCM, remains to be elucidated. Thus, in this study we investigated the chronological involvement of the CVPC population, in particular the c-kit^+/$CD45^-$ cells, in the progression of DMD-associated DCM in *mdx* dystrophic hearts.

2. Results

2.1. Mdx Cardiac Tissue Displays Decreasing Levels in C-Kit Receptor mRNA Expression with Ageing

We first analyzed the relative gene expression of *c-KIT* gene in different age-matched groups of 9, 24, 52, and 88 week-old (wo) WT and *mdx* mice. Based on previous work, these ages span the full range of the cardiac symptoms from young adult without symptoms through to adult with onset of cardiac symptoms to fully developed cardiac symptoms in old animals with late-stage heart failure [13]. The relative gene expression of *c-KIT* was evaluated by RT-PCR. At 9 and 24 wo, we observed similar expression between WT and *mdx* mice. A severe decrease with ageing was observed in older *mdx* animals ($p = 0.0151$ for mutation factor, $p = 0.0121$ for ageing factor). Interestingly, WT animals presented change in *c-KIT* expression only at 88 wo of age and not at the previously investigated age (Figure 1A).

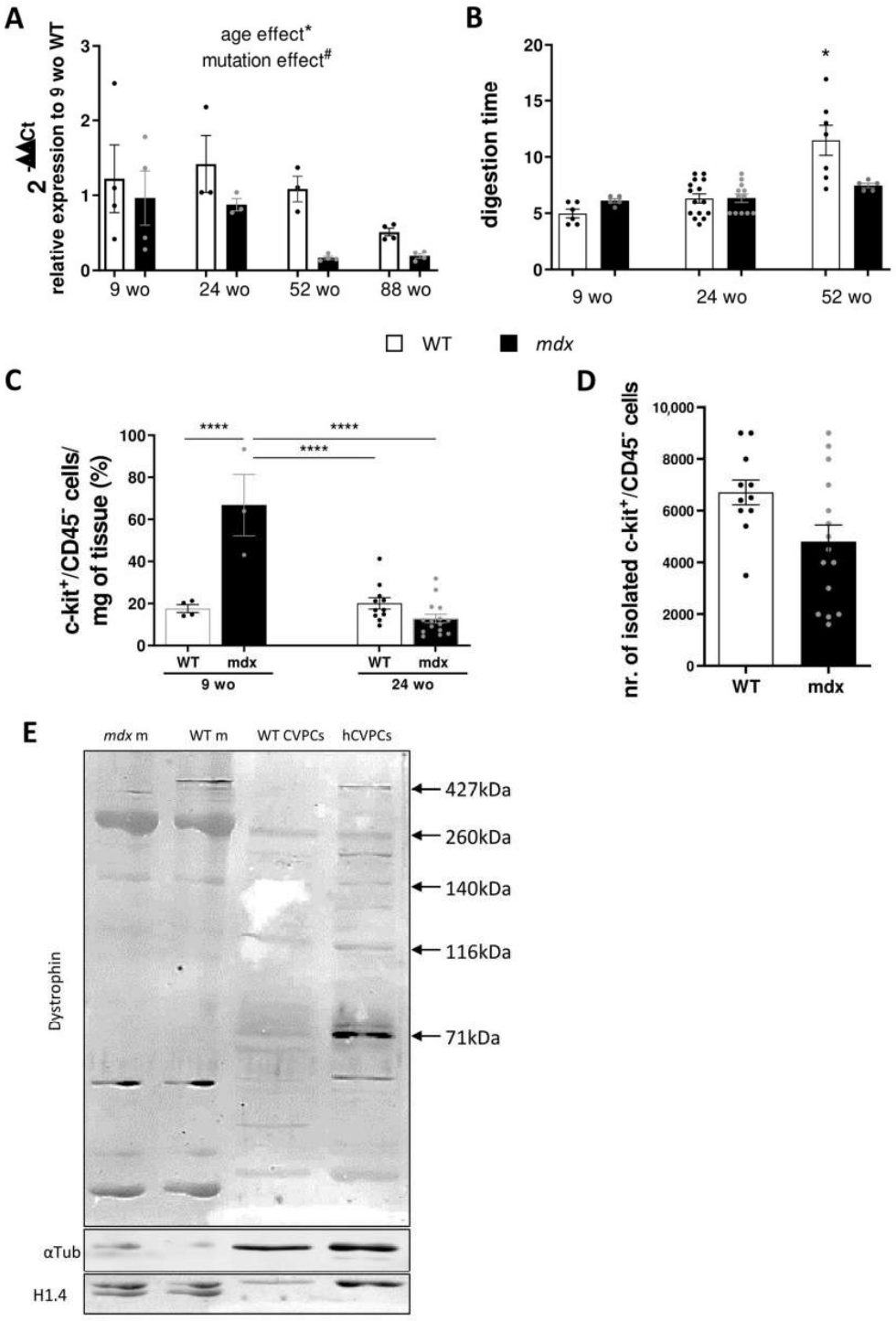

Figure 1. C-kit expression decreases in *mdx* animals in an age-dependent manner. (**A**) Bar graphs summarizing the relative *c-KIT* gene expression analyzed by RT-PCR in WT (open bars and black dots) and *mdx* (black bars and grey dots) cardiac left ventricles. Data are shown as mean ± SEM (n = 3–4 animals in each group). The presented value was calculated as $2^{-\Delta\Delta Ct}$ compared to housekeeping gene and 9 wo WT animals. Statistical difference was calculated by two-way ANOVA with Tukey's post-hoc test with mutation (# $p < 0.05$ for WT compared to *mdx*) and age (* $p < 0.05$ for *mdx* ageing mouse) as evaluation criteria. (**B**) Bar graphs summarizing the digestion time (in minutes) to dissociate the mouse heart. Data are shown

as mean ± SEM (n = 5–15 animals in each group). Kruskal–Wallis test with Dunn's multiple comparison was used for statistical evaluation (* $p < 0.05$). (**C**) Ratio of c-kit$^+$/CD45$^-$ cells isolated by MACS after cardiomyocyte filtration from 9 wo and 24 wo WT (open bars and black dots, n = 4–11) and *mdx* (black bars and grey dots, n = 3–16) mice, normalized by heart weight. Data are shown as mean ± SEM. Statistical significance was calculated using two-way ANOVA with Tukey's post-hoc test (**** $p < 0.0001$). (**D**) Number of c-kit$^+$/CD45$^-$ cells isolated by MACS after cardiomyocyte filtration in 24 wo WT mice (open bars and black dots, n = 11 animals) and 24 wo *mdx* mice (black bars and grey dots, n = 15 animals). (**E**) Illustrative images of Western blot (n = 3 repetitions) to evaluate the dystrophin expression in mouse (WT CVPCs) and human c-kit$^+$ (hCVPCs) isolated cells. The WT mouse skeletal muscle tissue (WT m) was used as positive control, while *mdx* skeletal muscle tissue (*mdx* m) was used to show no expression of the long isoform of dystrophin (Dp427) in *mdx* animal. The α-tubulin and basic histone H1.4 were used as loading controls.

2.2. Mdx CVPCs Show Early In Vivo Amplification Followed by Depletion and Low Resilience in In Vitro Culture

We next isolated the c-kit$^+$/CD45$^-$ cells in control and *mdx* hearts by enzymatic digestion through the Langendorff perfused heart method followed by magnetic sorting of the cell suspension. As cardiac fibrotic deposit is known to occur in *mdx* hearts [38], we evaluated whether the fibrosis could affect the digestion efficiency by evaluating the full digestion time. No significant difference was seen with an exception for the oldest WT animals with prolonged digestion time caused by blood clot formation (Figure 1B). The quality, viability, number, and shape of the cardiomyocytes were checked under a microscope. The ratio of isolated c-kit$^+$/CD45$^-$ cells over mg of cardiac tissue was higher in 9 wo *mdx* mice compared with age-matched WT (17.6 ± 1.8% in WT vs. 66.8 ± 14.5% in *mdx*, $p \leq 0.0001$, Figure 1C). There was no difference in 24 wo control and *mdx* mice (20.1 ± 2.7% in WT vs. 12.8 ± 2.0% in *mdx*, Figure 1C). Using MACS, we estimated lower isolated cell numbers in adult *mdx* samples (4800 ± 2500 cells vs. 6700 ± 1600 cells from *mdx* and WT respectively, $p = 0.0362$, Figure 1D). These cells were cultivated in vitro for further investigation. However, the plating efficacy was much lower compared to WT, with only sparse cells attaching to the cultivation surfaces, and thus in vitro cultivation could not be established. Further experiments on the CVPCs were thus conducted immediately after isolation without prolonged in vitro cultivation.

2.3. Different Expressed Dystrophin Isoforms in Mouse and Human CVPCs

Next, we evaluated whether the CVPC population expresses dystrophin isoforms that could impair the function of CVPCs in *mdx* mice. Dystrophin expression was analyzed by Western blot. Skeletal muscle of WT and *mdx* mice was loaded as reference. As expected, we found no expression for the high molecular weight (Dp427) dystrophin isoform in the *mdx* muscle compared to the WT muscle (Figure 1E). The mouse WT CVPCs only express shorter isoforms including bands at 260, 140, 116, and 71 kDa but no Dp427. In contrast, the human control CVPCs have a different expression pattern of the dystrophin isoforms, including the high molecular weight (Dp427) and ubiquitous isoform Dp71 (Figure 1E).

2.4. Increased Resident CVPCs at Early Stage Followed by Premature Depletion in Dystrophin-Deficient Heart

To further explore the quantity of c-kit$^+$/CD45$^-$ in *mdx* mice along with ageing, immunofluorescence analysis was performed on cryosections of flash frozen heart. We determined the proportion of c-kit$^+$/CD45$^-$ cells relative to all cells identified by DAPI staining in the myocardium. We found a higher number of CVPCs in 9 wo *mdx* hearts (0.09 ± 0.07%) compared with WT hearts (0.01 ± 0.02%) (Figure 2A,B). This difference remained in older animals between *mdx* (0.12 ± 0.08%) and WT mice (0.003 ± 0.008%) at the age of 24 wo, corresponding to the onset of the cardiac fibrosis (Figure 2A,B). In WT hearts, only individual cells were randomly found localized throughout the myocardium as illustrated in Figure 3A. The localization of the CVPCs in *mdx* hearts was mostly in the right atrium and sporadically in the epicardial area in the 9 wo age group with re-localization into ventricular myocardium in 24 wo suggesting injury activated recruitment of the

CVPCs as illustrated in Figure 3B. As CVPCs are thought to be involved in cardiac injury, we next evaluated whether inflammatory cell population is increased in the *mdx* heart. To that effect, we focused on the mast cells, known to be involved in the inflammatory process and specifically expressing the c-kit$^+$/CD45$^+$ markers [39]. We found that the *mdx* hearts exhibited a higher level of c-kit$^+$/CD45$^+$ mast cells at 9 wo. While the percentage of mast cells increased at 28 wo in the WT heart, no change was observed in the *mdx* heart at the same age (Figure 2C). However, *mdx* heart displayed deep depletion of the mast cells at 52 wo in contrast with those in WT heart. When ages were pooled, the *mdx* heart exhibited a higher percentage of mast cells compared to the WT heart (1.37 ± 1.30% in *mdx* to 0.08 ± 0.09% in WT; Figure 2C).

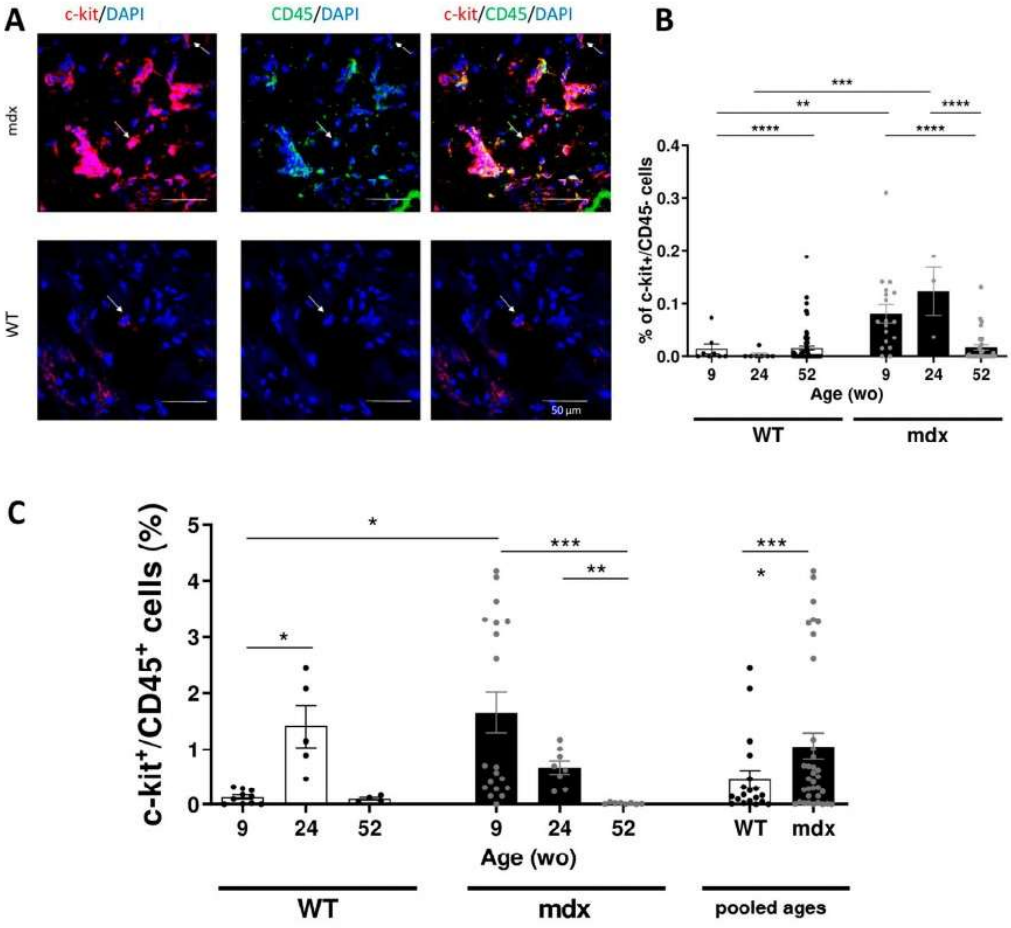

Figure 2. Recruitment of CVPCs in *mdx* hearts. (**A**) Representative histological analysis images of c-kit and CD45 immunolabeling. CVPCs were evaluated only as cells with positive signal for c-kit (red) and without signal for CD45 (green). Individual cells with these criteria are identified by arrows on the images. C-kit$^+$/CD45$^-$ cells were evaluated as mast cells. Scale bars: 50 µm. (**B**) Bar graphs showing the percentage of c-kit$^+$/CD45$^-$ cells relative to the total number of cells in WT (open bar and black dots) and *mdx* (black bar and grey dots). Data are shown as mean ± SEM (n = 3–20 sections per group; three animals were analyzed for the 9 wo and 52 wo groups, and two animals were analyzed for the 24 wo group). The statistical significance was calculated by two-way ANOVA and Tukey's multiple comparison test (* $p < 0.05$, ** $p < 0.01$, *** $p < 0.001$). (**C**) Bar graphs showing the percentage of inflammatory mast cells (c-kit$^+$/CD45$^-$) at different ages in WT (white bars and black dots) and *mdx* (black bars and grey dots) hearts. These mast cells were evaluated from the labeled sections shown in Figure 2A. Data are shown as mean ± SEM. Statistical significance was calculated by Kruskal–Wallis test and Dunn's multiple comparisons for each individual age group of WT and *mdx* hearts and by Student's t-test for pooled age groups (* $p < 0.05$, ** $p < 0.01$, *** $p < 0.001$, **** $p < 0.0001$).

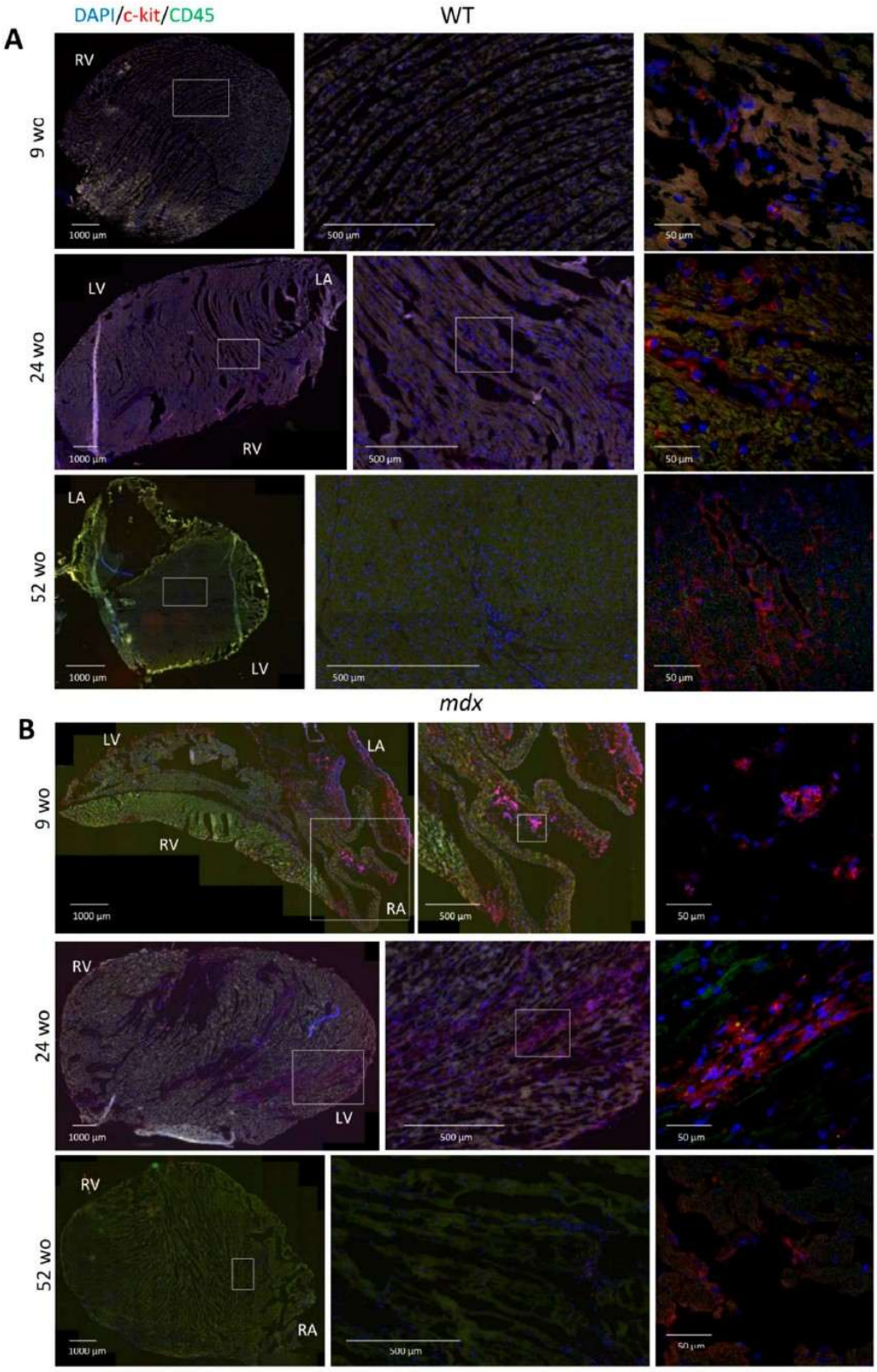

Figure 3. Abnormal age-dependent CVPC localization in the *mdx* heart. (**A**) Representative images of CVPC localization in WT hearts at the age of 9 (upper panels, n = 3 animals), 24 (middle panels, n = 2 animals), and 52 wo (lower panels,

n = 4 animals). (**B**) Representative images of CVPC localization in *mdx* hearts at the age of 9 wo (upper panel, three animals), 24 wo (middle panel, two animals) and 52 wo (lower panel, four animals). RV: right ventricle, LV: left ventricle, RA: right atrium, LA: left atrium. The c-kit protein was labeled in red, CD45 protein in green, and the nuclear DNA was counterstained with DAPI in blue. The detailed CVPC image taken by confocal microscopy was supplemented to the overview of the slice taken on fluorescent microscope and exactly positioned in the figure relative to the overall slice (left panels taken by confocal microscope, right and middle panel show detailed section marked in white rectangle). For each image the scale bar is indicated.

2.5. Early-Stage CVPC Recruitment Followed by Depletion Is Correlated with Fibrotic Development and Cardiac Dysfunction in Mdx Hearts

Next, we hypothesized that the progressive CVPC depletion in *mdx* is correlated with pathological cardiac remodeling known to be associated with fibrosis and left ventricular dysfunction. We first evaluated the progression of the cardiac remodeling with ageing by analyzing the collagen deposition as a main marker of fibrosis. We employed Masson's trichrome staining on WT and *mdx* left ventricle of 9, 24, and 52 wo animals (Figure 4A,B). We observed similar collagen deposition in the *mdx* and WT hearts of 9 wo animals (0.8 $\pm$ 0.4% and 1.8 $\pm$ 1.1% of aniline blue positive tissue for WT and *mdx*, respectively). This level of collagen remained constant in WT animals with ageing (3.1 $\pm$ 1.3% in 24 wo and 1.4 $\pm$ 0.9% in 52 wo). However, the collagen content increased progressively in the *mdx* hearts with ageing (3.8 $\pm$ 1.3% at 24 wo and 4.2 $\pm$ 2% at 52 wo, Figure 4A,B). We next analyzed the composition of collagen isoforms, including collagen 1A1 and 3, by Western blotting (Figure 4C). We observed no statistical difference in the collagen 1A1 protein expression in the WT and *mdx* hearts, although a tendency was visible for a higher expression in the *mdx* (Figure 4C). We found no difference in the collagen 3 protein expression between WT and *mdx* hearts. We evaluated the protein expression level of the matrix metalloprotease MMP-9 as this protein has been suggested to have important roles in the skeletal muscle dystrophy progression [40]. However, no change was observed between WT and mdx hearts at any age, although the 52 wo heart displayed a tendency for higher MMP-9 expression compared to WT (Figure 4C). To further evaluate the inflammation level in the mdx hearts, we also assayed the cyclooxygenase-2 (COX-2) protein as it has been involved in DMD [41]. No change was observed at any age in WT and *mdx* hearts (Figure 4C).

We next evaluated the age-dependent cardiac dysfunction in WT and *mdx* mice using conventional M-mode and high-frequency ultrasound-based two-dimensional speckle-tracking echocardiography of the left ventricle. With the conventional echocardiography, no change was observed in the percentage of LV fractional shortening (LVFS), although there was a tendency to slow decrease in LVFS in both groups (Figure 5A,B). However, with the highly sensitive ultrasound technique, we found an age-dependent decreasing slope of the global radial strain in *mdx* mice when compared to WT. At 52 wo, a decrease in LV global strain was found (42.8 $\pm$ 2.9% vs. 29.3 $\pm$ 3.7% in WT and *mdx*, respectively) (Figure 5C,D).

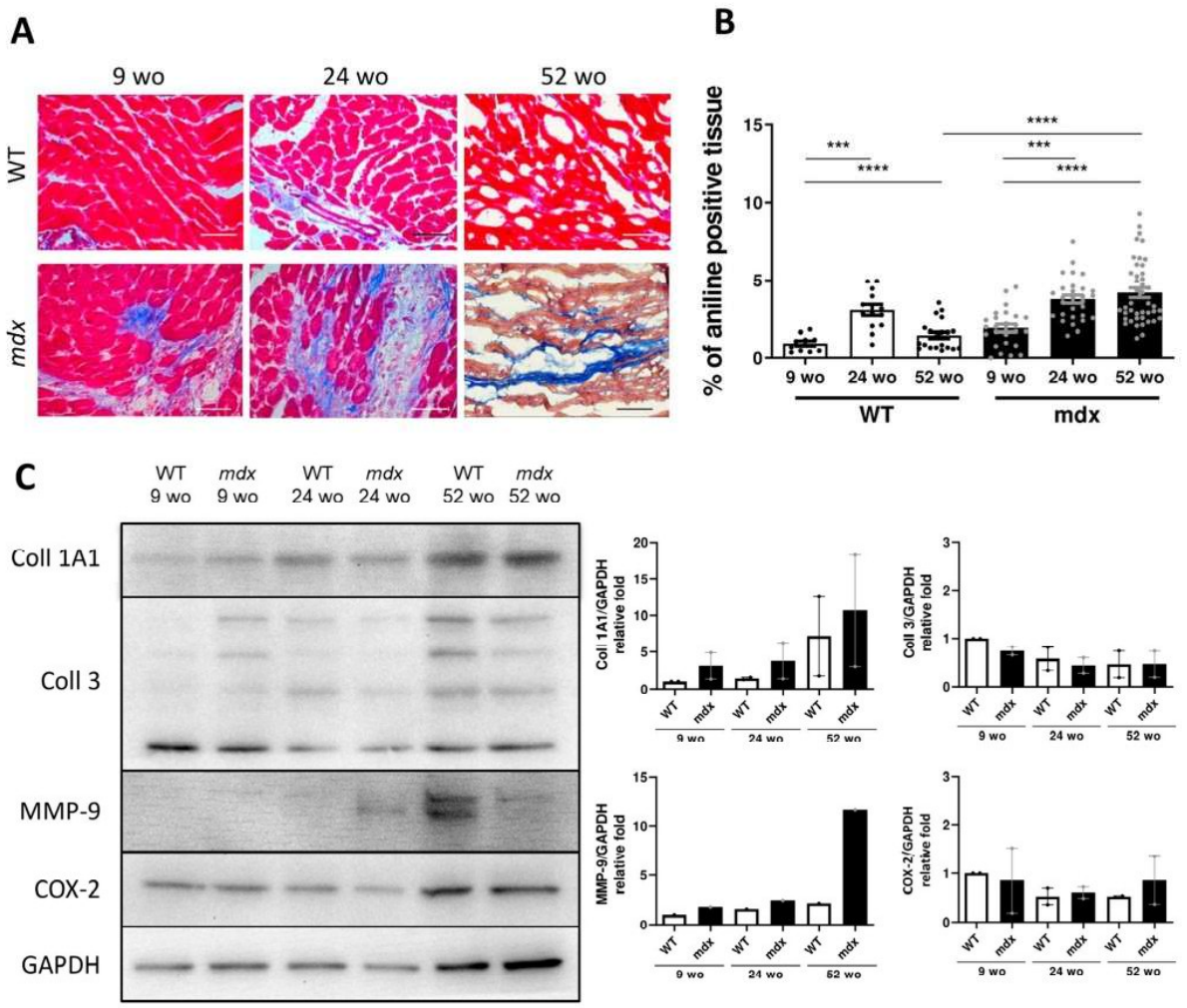

Figure 4. Fibrotic deposit and cardiac dysfunction correlate with decreasing CVPC presence in *mdx* heart. (**A**) Representative images of histological analysis stained using Masson trichrome technique showing myocytes (in red) and collagenous fibrotic tissue (in blue) in the left ventricle of WT and *mdx* hearts at 9, 24, and 52 wo. Line represents 100 µm. (**B**) The ratio of red and blue stained tissue was evaluated in WT hearts (open bars and black dots, n = 4–11 slices/3 animals per group) and *mdx* hearts (black bars and grey dots, n = 3–16 slices/3 animals per group) at the age of 24 wo and further at 52 wo. Statistical significance was calculated by Kruskal–Wallis test and Dunn's multiple comparison post-hoc test (*** $p < 0.001$, **** $p < 0.0001$). (**C**) Western blot analysis of collagen proteins and inflammatory proteins in the cardiac tissues. Left panel shows representative images of collagen 1A1 (Coll 1A1), collagen 3 (Coll 3), cyclooxygenase 2 (COX-2), and matrix metalloproteinase 9 (MMP-9) compared to the GAPDH control. The right panels show the normalized densitometry of each protein normalized by GAPDH content of WT (open bars, n = 2 animals) and *mdx* (black bars, n = 2 animals).

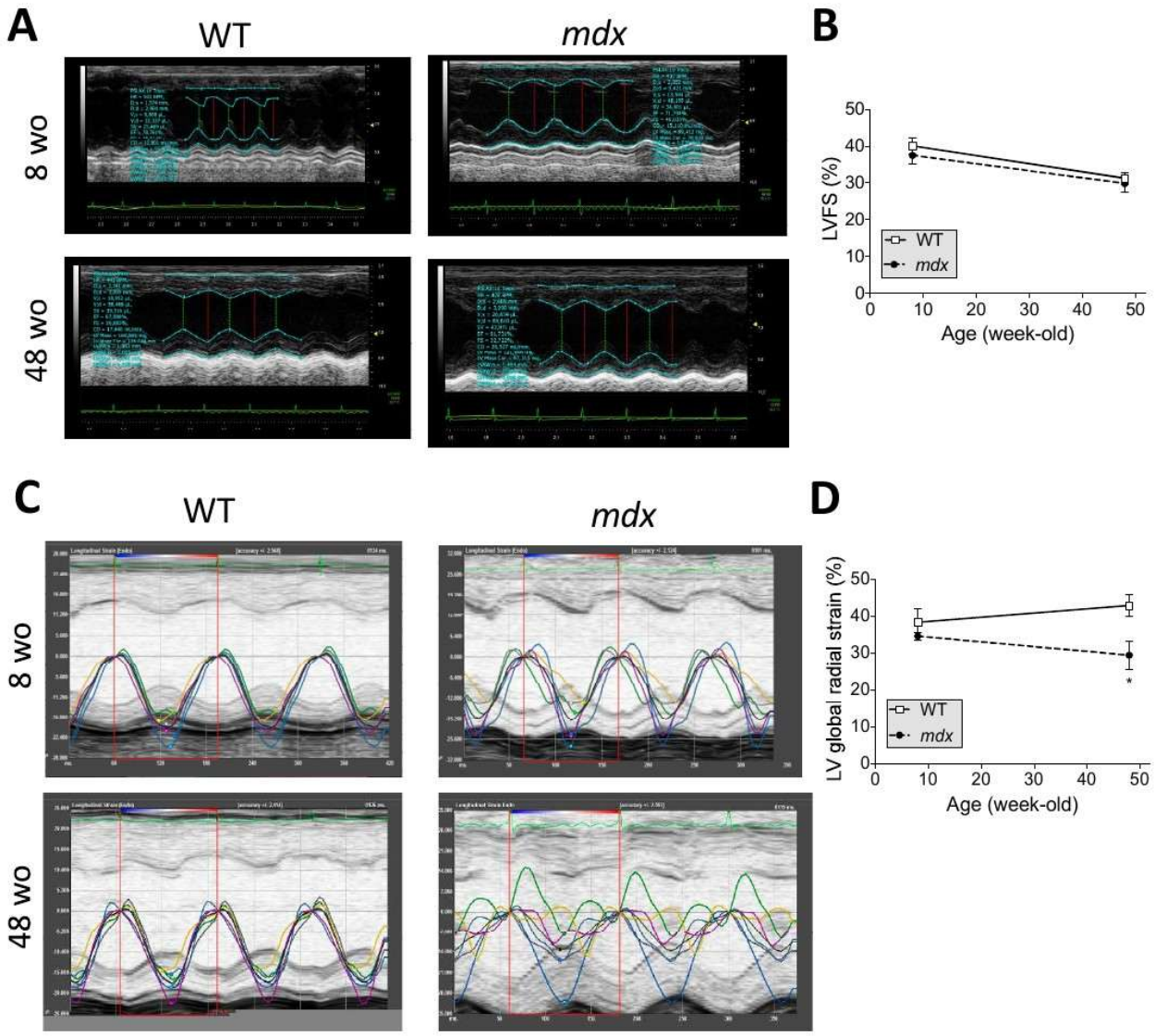

Figure 5. LV global strains are altered before LV ejection fraction in *mdx* mice. (**A**) M-mode images in WT and *mdx* at 8 and 48 wo. (**B**) Percentage (%) of the left ventricular fractional shortening (LVFS) in WT and *mdx* mice from 8 to 48 wo. (**C**) High-frequency ultrasound-based two-dimensional speckle-tracking (STE) images in WT and *mdx* at 8 and 48 wo. (**D**) Percentage (%) of the left ventricular (LV) global radial global strain in WT and *mdx* mice from 8 to 48 wo. Data are shown as mean ± SEM (n = 10 animals/group). A two-way ANOVA test was performed. * $p < 0.05$, *mdx* vs. WT mice at the same age.

2.6. DNA Damage and Oxidative Stress in CVPCs

Recently, we showed that dystrophin deficiency causes oxidative stress and DNA double strand breaks in DMD human pluripotent stem cells [42]. Thus, we aimed to verify whether dystrophin deficiency leads to similar defects in the isolated CVPC population in *mdx* mice. Since we have shown drastic depletion of CVPCs in 52 wo animals, we hypothesized that the damage occurs before 52 wo. Therefore, we explored the DNA damage in the isolated CVPCs using immunocytological analysis in the 24 wo mice. Evaluation of the accumulated histone H2A phosphorylated on Ser192 (γH2AX) was performed, detecting double stranded breaks as foci in the nucleus (Figure 6A). The CVPCs from *mdx* animals showed a significant increase (4 times more) in DNA damage compared to CVPCs from

age-matched WT animals. As DNA damage is associated with oxidative stress [42], we also evaluated the oxidative stress in the CVPCs. We observed no difference in oxidative stress, evaluated with the CellROX probe, between *mdx* and WT CVPCs (Figure 6B).

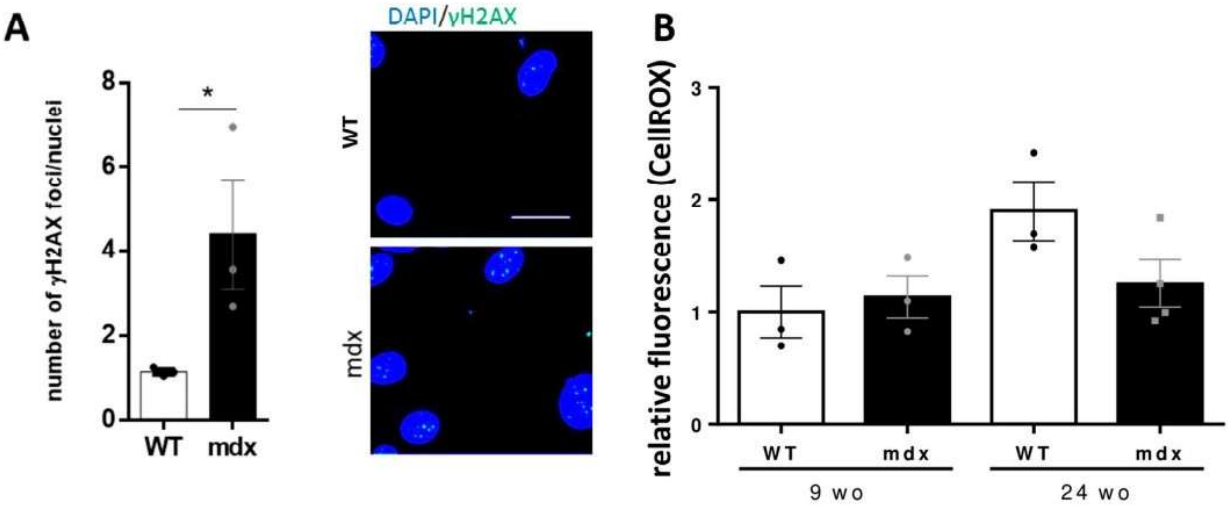

Figure 6. DNA damage is increased in *mdx* CVPCs. (**A**) Bar graphs showing the DNA double stranded breaks in isolated CVPCs from 24 wo WT and *mdx* mice as illustrated with the two images on the right. The DNA damage was evaluated as the ratio of γH2AX foci number (in green) per total number of nuclei (DAPI labeled, in blue) per image. At least 20 cells were evaluated from each animal; the average from each animal was used for statistics with three animals per group (* $p < 0.05$). The scale bar represents 20 μm. (**B**) Bar graphs showing the relative fluorescence of ROS production using CellROX dye on freshly isolated CVPCs of 9 and 24 wo mice. At least three animals per group were used. The values are represented in the bar graphs for WT (open bars and black circles/dots) and *mdx* (black bars and grey dots). The statistical difference was calculated using two-way ANOVA.

3. Discussion

In the present study, we showed, for the first time, that the dynamics of the CVPC population change with ageing in the *mdx* heart and correlate with the progression of the cardiac disease onset. Most of the studies related to DMD-associated DCM have focused on the pathological mechanisms related to dysfunction of the myocardium and morphological damage. Here, for the first time, we aimed at evaluating the impact of dystrophin deficiency on the capacity of the cardiac tissue to maintain its CVPC population and therefore its regenerative capacity. CVPCs were previously isolated from the heart of the golden retriever muscular dystrophy (GRMD) model of DMD [15]. They showed longer cell number doubling time in culture and lower telomere copy number, pointing to the limitations in expansion capabilities. A lower efficacy in cardiac differentiation was also found in GRMD-CVPCs compared to WT. Furthermore, it has been proven that CVPCs do not differentiate into cardiomyocytes in vivo [43,44]. Thus, studies mostly focused on the CVPC paracrine function enabling cardiac organ homeostasis [31,45–47], for which the injury triggered recruitment would be necessary. Interestingly, it was recently shown that the CVPC transplantation or even just the secreted exosomes are beneficial to the dystrophic heart [48,49]. While the beneficial effect of CVPCs was demonstrated, the dynamics and recruitment of the heart's own CVPC population remained unclear.

Our findings demonstrate that dystrophin deficiency induces a CVPC proliferation in young *mdx* mice, consistent with the CVPC proliferation in failing human hearts [50,51]. With ageing, we observed a depletion of CVPC population, consistent with the decrease of the progenitor cells in dystrophin-deficient skeletal muscle [20]. Therefore, although CVPCs and satellite cells have different functions, our findings likely reveal a common

phenomenon involving an early-stage recruitment triggered by cardiac injury as also previously shown [34,52], but followed by rapid depletion of the CVPC pool. We summarize our findings and a proposed mechanism of the CVPC in the dystrophin-deficient heart in the diagram of Figure 7.

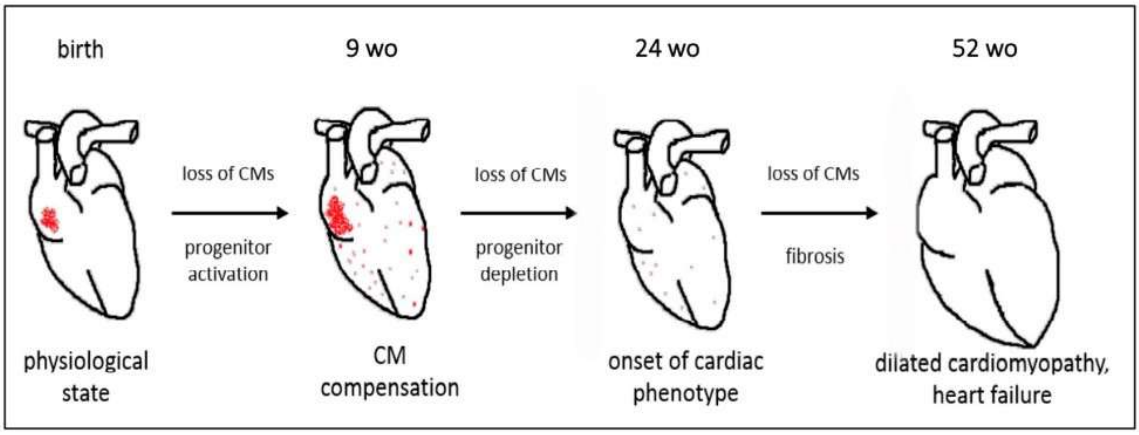

Figure 7. Diagram of the proposed mechanism for the fate of CVPCs in the dystrophin-deficient heart. Dystrophin deficiency induces CVPC proliferation and hyperplasia in 9 wo *mdx* mice associated with an age-dependent depletion and simultaneous progressive fibrosis of the heart during ageing leading to development of cardiac dysfunction by 52 wo.

Some studies showed that myocyte apoptosis precedes the fibrosis in both *mdx* skeletal muscle [53,54] and cardiac muscle as well as in DMD patients [55–58]. It has been also shown that the cardiomyocyte damage is caused by dystrophin deficiency, chronic inflammatory response, and collagen deposition [13,59,60]. Based on these claims, we hypothesized that increased fibrosis in old *mdx* hearts would impair the enzymatic heart digestion via the Langendorff perfusion. Although we observed increased fibrotic tissue in the old *mdx* hearts, the time for digestion was unchanged. The old WT hearts exhibited less fibrosis but increased digestion time due to some unexpected blood clots not seen in *mdx*. The production of fibrosis in the heart is mainly ensured by the cardiac fibroblasts that are activated in myofibroblasts at the site of injury [61]. It is very likely that the cardiac fibroblast activation causes the progressive increase in fibrosis we observed in *mdx* mice. In parallel, the expression of the matrix metalloproteinases, in particular the MMP-9 (also called gelatinase B), was shown to be upregulated in the dystrophin-deficient heart [62]. However, their activity has been revealed to be dysregulated in dystrophin/utrophin-deficient mice [61]. In the present study, we did not find any difference in the MMP-9 protein expression, although a tendency for higher expression was seen in the old (52 wo) *mdx* heart. Based on these previous studies, we cannot exclude that the MMP-9 dysregulation plays a role in the pathological fibrotic progression and CVPC depletion.

DMD is characterized by the absence of full-length dystrophin (Dp427) in myocytes, including cardiac myocytes. One group revealed retarded maturity and impaired contractile properties in DMD hiPSC-CMs lacking Dp427, suggesting functional consequences at the early stage of cardiac development [63]. Here, we evaluated the dystrophin isoforms expressed in the human and mouse CVPCs and found a key difference in Dp427 expression. The human control CVPCs express several dystrophin isoforms, including Dp427 and ubiquitous isoform Dp71. In contrast, the mouse WT CVPCs only express shorter isoforms including bands at 260, 140, 116, and 71 kDa. The reason of such difference between mouse and human CVPCs is unknown and would require further experiments. Based on several previous studies, including ours, *mdx* mice developed cardiac dysfunction by 20 wo, with myocardial fibrosis, increased collagen expression, ventricular hypertrophy, and arrhythmias as well as left ventricular dysfunction [13,64–68]. These studies clearly support the age-dependent cardiac dysfunction in the *mdx* mice. Here, for the first time,

we found that cardiomyocyte damage is associated with increased proliferation of the CVPCs and recruitment into the damaged sites. Although we did not observe any dramatic change in the extracellular matrix component production and inflammation, the evaluation of the age-dependent cardiac dysfunction in *mdx* mice using STE revealed a decrease of LV radial global strain in *mdx* mice at 52 wo, suggesting a cardiac dysfunction. Hence, *mdx* mice are known to have a mild global cardiac phenotype, despite cellular cardiac dysfunctions as early as few weeks of age as we have shown before [13]. Our results show that conventional echocardiography indicates normal cardiac function in *mdx* and WT mice. Using conventional ultrasound measures, cardiac dysfunction usually appears at a late stage after 48 wo in *mdx*. In both groups, a tendency to slow decrease in LVFS was observed from 40 to 30%. To compare, Spurney et al. previously described similar LVFS (32.2%) at 48 wo in WT mice [69], which is concordant with our results. Advanced imaging techniques, such as cardiac magnetic resonance imaging, Doppler tissue imaging or two-dimensional (2D) speckle-tracking echocardiography (STE), and cardiac distortion have shown cardiac dysfunction as early as the age of 32 wo in *mdx* [70–72]. Our data confirm these previous studies. STE imaging can be used to quantitatively measure the myocardial strain for potentially sensitive markers for early myocardial dysfunction in *mdx* mice. There is a major difference between conventional fractional shortening determination and the LV segmental STE analysis that takes into account the deformation of all segments. Moreover, the fractional shortening depends on loading conditions and heart rate. The STE analysis is not sensitive to loading conditions or heart rate.

As the functionality of the myocardium decreases, the CVPCs become sparse. These CVPCs possibly contribute to the cardiac muscle homeostasis maintenance via processes such as paracrine signalization by exosome secretion of cardiac cytokines improving damaged myocardium survival as previously proposed [45–47,73–77] or even endothelial differentiation and increased vascularization [78] employing progenitor populations as previously shown (e.g., Sca1 and/or c-kit+ cells) [79].

Furthermore, we recently showed that the delayed but progressive cardiac phenotype accelerated in the second decade of life may suggest involvement of CVPC depletion in the heart of patients with Becker muscular dystrophy [37], a milder form of muscular dystrophy than DMD. The first signs of the defective stem cell population in DMD were shown as defective asymmetric division due to dystrophin deficiency limiting the production of the satellite cells in *mdx* skeletal muscles via the Mark2 and EGFR/AurkA kinases [16,80]. In another study, we also showed that deregulated NOS causes damage in the DMD human pluripotent stem cell genome via ROS accumulation [42]. ROS production induces DNA mutations [81] via oxidative DNA damage [82]. This is in agreement with previous findings showing elevated ROS in dystrophic cardiomyocytes and skeletal myocytes [13,83]. We have shown that ROS level plays a role in the satellite cell survival in dystrophin-deficient skeletal muscle [84]. Here, we evaluated the level of oxidative stress in CVPCs but found no significant difference between WT and *mdx* mice. Of note, a similar result was obtained using *mdx* cardiosphere-derived cells that have similar properties to CVPCs. They found no difference either in expression of stem cell markers or myogenic differentiation potential, but both groups were impaired with ageing [85]. The lack of difference could also possibly be caused by the strong antioxidant properties of the supplements added into the culturing medium of the CVPCs, such as vitamins and selenium, which are essential components of several antioxidant enzymes [86–88]. As other groups have revealed the presence of oxidative stress in the *mdx* cardiomyocytes and its role in the related DCM development [64,89], we cannot exclude the possibility that the *mdx* CVPCs exhibit oxidative stress that contributes to increased DNA damage at 24 wo, right before the CVPC population depletion.

We thus suggest that impaired cardiac function in *mdx* mice, as we have shown here and previously [13], and shorter cardiomyocyte lifespan [54] combined with inflammation [59] and collagen deposition lead to upregulation of CVPC proliferation in young *mdx* mice. At the same time, normal CVPCs express dystrophin similarly to the muscle

satellite cells [16,90] and human pluripotent stem cells [42]. Dystrophin deficiency may thus weaken CVPCs as demonstrated by accumulation of DNA damage, and eventually cause their depletion in the heart. Thus, the dystrophin deficiency not only impairs the CVPC pool but also causes DNA damage in this pool. Altogether, there are fewer CVPCs in *mdx* mice, and these cells are damaged with age. Such a mechanism was described in depletion of other tissue-specific stem cells, including melanocyte and hematopoietic stem cells [91–93]. Although no information on CVPC mutagenesis is available, the DNA damage may lead to accelerated ageing [94,95], subsequent depletion, and diminished stem cell potential, including paracrine signaling and homeostatic function of the CVPC niche. Such a mechanism is in concert with lower CVPC expansion and differentiation capacity, shortened lifespan, and premature senescence in the DMD (GRMD) canine model [15]. While at early stage the CVPCs may have a paracrine function for cardiac regeneration, their disappearance may then lead to rapid deterioration, finally exacerbated by fast progressing cardiac fibrosis.

4. Materials and Methods

4.1. Ethical Statements

Animal procedures were conducted according to the guidelines of the Declaration of Helsinki, approved by the Institutional Ethics Committee for animal experiments, and received agreement from the national "Ministère de l' Enseignement Supérieur et de la Recherche" (No. #16473-2018082016141320). This research complied with the commonly accepted "3Rs". C57BL/10-Dmd^{mdx} male mice were chosen because of the appropriate lifespan to follow up the CVPC pool in the dystrophin-deficient heart. They were obtained from a colony maintained at a local animal facility network (RAM, Montpellier) [96]. C57BL/6 mice were purchased from Janvier Laboratories (Le Genest-Saint-Isle, France). Animals were housed conventionally in controlled humidity and temperature, operating on 12 h of light and dark cycles with food and water available ad libitum. Overall, 76 WT and 74 *mdx* mice were used for this study.

4.2. Immunohistology

The mice were sacrificed by cervical dislocation, and the heart was extracted from the chest. The organ was placed onto a Langendorff setup for aorta cannulation and perfused at 37 °C with a modified Tyrode solution (113 mM NaCl, 4.7 mM KCl, 0.6 mM KH_2PO_4, 0.6 mM Na_2HPO_4, 1.2 mM $MgSO_4 \cdot 7H_2O$, 12 mM $NaHCO_3$, 10 mM $KHCO_3$, 10 mM HEPES, 30 mM Taurine) with heparin (50 µL of 1000 U/mL solution) to remove blood residue. The heart was then removed and flash frozen in isopentane cooled by liquid nitrogen for cryoprotection of the tissues. The hearts were sectioned (5 µm) on a cryotome at a temperature of −20 to −25 °C. At least 20 (and up to 100) sections were analyzed for each animal. For histological staining of collagen deposits, a Masson's trichrome staining protocol was used. Briefly, sections were fixed with 4% paraformaldehyde and stained with Wiegert's hematoxylin. Then, the samples were fixed in Bouin's solution for 1 h and stained with fuchsin, differentiated in phosphomolybdic/phosphotungstic acid, and collagen was stained with aniline blue. Samples were then dried, clarified with xylene, and mounted with Pertex. The images were taken with an automatic TissueFAXS system (Tissuegnostics, Vienna, Austria) and Observer.Z1 microscope (Carl Zeiss, Oberkochen, Germany), and images were analyzed using QuPath software [97]. For the analysis of CVPC presence, the sections were fixed with 4% paraformaldehyde, incubated in blocking solution (0.1% BSA, 1% goat serum, 0.2% triton-X in 1× PBS), and then with primary antibodies against CD117 (AF1356, 1:100, R&D) and CD45 (cl. 30-F11, NB-100-77417SS, 1:50, Novus Biologicals, Cenntenial, CO, USA) overnight. Secondary antibodies (anti-rat Alexa488, anti-mouse Alexa594, Invitrogen, both 1:500) were applied after washing for one hour at room temperature. Nuclei were counterstained with DAPI. The microscopic images were taken with the automatic Tissue FAXS system (Tissuegnostics) and Observer.Z1

microscope (Carl Zeiss) for the whole overview and focused areas. Detailed images of areas of interest were acquired with an LSM700 confocal microscope system (Carl Zeiss).

4.3. Mouse Heart Dissociation

Heart dissociation was conducted according to the Langendorff method [98] with buffer containing 0.1 g/mL liberase/dispase (Roche, France) as previously described [13]. Isolated cells were transferred to an enzyme-free solution containing 1 mM $CaCl_2$ and 10% FBS, and the small cell population was separated from the myocytes with a cell strainer of 40 µm (Corning, New York, NY, USA).

4.4. CVPC Analysis

Following mouse heart dissociation, the suspension of small cells was labeled with CD45 (130-052-301) and CD117 (130-091-224) microbeads to obtain the desired population of $CD117^+/CD45^-$ cells with MACS columns (Miltenyi Biotec, Bergisch Gladbach, Germany). These cells were resuspended in CVPC medium (90% DMEM/F12 with glutamine (D8437, Sigma-Aldrich, Saint Louise, MO, USA), 10% ESC FBS (ES-009-B, Merck Millipore, Burlington, MA, USA), 1% penicillin/streptomycin, 1% insulin/transferrin/selenium, 10 ng/mL mouse bFGF, 10 ng/mL mouse EGF, 50 µg/mL gentamycin) and left to attach onto gelatin coated cover slips. The cells were analyzed within 10 days after isolation. For control of protein expression, a human sample of CVPCs was used. Following informed consent of the patient, discarded human right atrial appendages were collected during routine open heart procedures from Montpellier University Hospital, Arnaud de Villeneuve. Collection of the tissues followed the protocol approved by the French Ministry of National Education and Research (DC-2013-2023). CVPCs were isolated following the protocol in [99]. Fat was removed from atrial appendage specimens, and after washing with cold PBS, the tissues were cut into small pieces (roughly 1 mm). The minced tissue was enzymaticallly digested with collagenase II (30 U/mL; Thermo Fisher, Waltham, MA, USA) in PBS at 37 °C, shaking for one hour after which the remaining tissue was mechanically digested. The undigested tissue was left to settle by gravity, and the supernatant containing the CVPCs was collected. A second round of enzymatic and mechanical digestion was performed on the remaining tissue fragments. CVPCs were pelleted, resuspended, and plated in growth media: Ham's F12 (Sigma-Aldrich), 10% FBS (Hyclone, Logan, UT, USA), 10 ng/mL bFGF (Miltenyi Biotec), 0.2 mM glutathione (Sigma-Aldrich), 0.005 U/mL erythropoietin (Sigma), and penicillin/streptomycin. At passage 2, CVPCs were magnetically sorted using the Miltenyi Biotec MACS magnet for the $CD117^+$ population.

4.5. ROS and DNA Damage Analysis

For the detection of ROS, the adherent cells were incubated with CellROX Green reagent (Life technologies, detecting both ROS and RNS) for 1 h. Cells were then harvested using 0.5 mM EDTA solution and counted. Fluorescence in the green spectrum was measured using the monochromometer Tecan Infinite 200 PRO, and the signal of green was normalized by the total number of cells.

For immunofluorescent labeling of proteins, cells were cultivated on glass cover slips covered in gelatin, washed with PBS, and fixed using 4% paraformaldehyde at room temperature for 15 min. Cells were incubated with pre-extraction buffer (25 mM HEPES, 50 mM NaCl, 1 mM EDTA, 3 mM MgCl2, 200 mM sucrose, 0.5% Triton X-100) before continuing to blocking steps. The cells were permeabilized and blocked with blocking solution 1 (1% BSA, Triton X-100 0.2% in PBS, 15 min on ice) and blocking solution 2 (1% BSA, 1% NaN3, 0.05% Tween 20 in PBS, 60 min on ice). γH2AX Ser139 antibody (mouse monoclonal, 613402, BioLegend, San Diego, CA, USA) was incubated overnight at 4 °C. Samples were extensively washed with PBS/Tween (0.05%) and incubated with a fluorescently labeled secondary antibody against mouse for 1 h at room temperature. DAPI was used as a nuclear counterstain. Microscopy was performed using a confocal LSM700 microscope (Carl Zeiss), and images were processed using the ZEN system (Carl

Zeiss). For analysis of DNA double stranded breaks, the total number of γH2AX foci per image was divided by the total nuclei count per image.

4.6. Quantitative RT-PCR

For total c-kit expression in the heart, quantitative PCR was performed on frozen left ventricle samples of the chosen age WT and *mdx* groups. Total mRNA was extracted using the NucleoSpin RNA kit (Macherey-Nagel, Hoerdt, France) followed by reverse transcription with the RevertAid RT Reverse Transcription Kit (Thermo Fisher). qPCR was performed using LightCycler® 480 SybrGreen I Master (Roche) and a LightCycler® 480 Instrument II (Roche Life sciences). We used the following primers: c-kit forward 5′-ACTCGCACGGGGACATA-3′and reverse 5′-GGAGAGATTTCCCATCACACT-3′, the ribosomal protein large subunit P0 (*Rplp0*) as the housekeeping gene, forward 5′-ACATCAT CCCTGCCTCTAC-3′, and reverse 5′-CCTGCTTCACCACCTTCTT-3′. The presented value was calculated as ΔΔCt compared to housekeeping gene and 9 wo WT animals.

4.7. Western Blot Analysis

Protein extracts in radioimmunoprecipitation assay (RIPA) buffer were separated by SDS-PAGE 8–10% gradient gel electrophoresis and transferred overnight at 4 °C to nitrocellulose membranes, blocked at room temperature with Odyssey blocking buffer (Eurobio, France) and probed with a H4 (1/1000) rabbit polyclonal anti-dystrophin [100], rabbit polyclonal anti-histone H1.4 (Sigma-Aldrich; 1/5000, ref H7665), and mouse monoclonal anti α-tubulin (Sigma-Aldrich, 1/1000, ref: T9026) followed by IRDye® 680RD (α-tubulin) or IRDye® 800RD (H1.4) secondary antibodies (Eurobio, Les Ulis, France). Fluorescence was quantified with the Odyssey software (West Henrietta, NY, USA). Data were normalized to histone H1.4 expression and α-tubulin. For collagen and inflammation markers, cardiac tissue was homogenized in RIPA buffer and separated by SDS-PAGE 10% gel electrophoresis and transferred to nitrocellulose membranes. After blocking at room temperature with 5% milk, membranes were incubated with primary antibodies against collagen 1A1 (COL1A1, rabbit polyclonal, ref PA5-29569, Thermo Fisher), collagen 3 (rabbit polyclonal, ref PA5-34787, Thermo Fisher), mouse matrix metalloproteinase 9 (MMP-9, goat polyclonal, ref AF909-SP, R&D), and human/Mouse cyclooxygenase 2 (COX-2, goat polyclonal ref AF4198-SP, R&D). The GAPDH antibody (rabbit polyclonal, ref 2118, Cell Signal) was used as loading control for these markers.

4.8. Echocardiography

Cardiac function was evaluated in vivo in *mdx* and WT (C57BL/10ScSnJ) mice from 8 to 48 week-old (wo) (n = 10) by 2D transthoracic echocardiography using a high frequency ultrasound system (Vevo 2100, Visualsonics, Toronto, ON, Canada) equipped with a probe (30 MHz) operating at a frame rate of 200–250 per second. M-mode images were obtained using the LV short-axis view at the mid papillary muscle level. The M-mode gate was set in the middle between the two papillary muscles for fractional shortening analysis. For 2D STE studies, the short-axis B mode at the mid LV level and long-axis B mode cine loops were recorded with a scanhead placed at the mid-LV level, i.e., along the left sternal border with a clear view of both the apex and the outflow tract of LV. Three consecutive 2D videos of cardiac and stable cycles were recorded. Recordings were performed in anesthetized mice (1.5% isoflurane, 100% O_2). Animals were placed in a dorsal position on a heat-warming tray (37 °C) controlling heart rate (HR) > 400 beats/min for the duration of the study (with adjustment of level of anesthesia as necessary). All measurements and calculations were performed with the Vevo 2100 Software and were averaged from a minimum of three cycles and followed the standards of the American Society of Echocardiography and the Vevo 2100 guidelines.

4.9. Statistical Analysis

Normality was tested using the Shapiro–Wilk test. An unpaired *t*-test was used to compare 2 independent groups with parametric distribution. Two-way ANOVA was performed to analyze the age and mutation involvement in analyzed groups. Specific tests for each analysis are reported in individual figure legends. All data are expressed as mean ± SEM. A value of $p < 0.05$ was considered significant. Prism 6 (GraphPad, San Diego, CA, USA) was used for data analysis and statistics.

5. Conclusions

Dystrophin deficiency induces changes in *mdx* heart leading to cardiac dysfunction and excessive recruitment of CVPCs in injured sites, likely to maintain the tissue homeostasis. The dystrophinopathy impairs the CVPC pool by increasing DNA damage and need for extensive proliferation, causing early exhaustion of the cardiac tissue homeostasis maintenance capacity. Such a mechanism of progressive CVPC pool depletion, together with the cardiac pathophysiological condition associated with DMD, may be the major reason for progressive fibrosis in the heart of the DMD patients.

6. Contribution to the Field

Early cardiac dysfunction in DMD is clinically associated with left ventricular strain reduction due to fibrosis, hypocontractility, and arrhythmias. This leads to fully developed cardiomyopathy, which has become the leading cause of mortality in DMD patients. The cardiac dysfunction is primarily attributed to cardiomyocyte damage. This mechanism, however, is not sufficient to fully explain the delayed onset of DCM in the teenage years. Our present results reveal a link between CVPC activation in the heart and the progressive damage upon their depletion. The CVPCs are thought to primarily differentiate into an endothelial lineage but can provide important positive paracrine effects to the damaged myocardium. Our findings reveal a possible role of the CVPCs in the age-dependent cardiac dysfunction, which may eventually provide a target to improve the cardiac muscle homeostasis maintenance and lifespan in DMD patients. Our findings may help to reveal the molecular mechanisms involving the CVPCs that might be shared in other cardiac disorders.

Author Contributions: S.J. conducted the isolation and culture of the cells, histological analysis and evaluation of the data, wrote the initial manuscript draft; Y.S. performed the cell culture and RT-PCR; F.A. dissociated the animal hearts; P.F. and G.H. performed the Western blot analyses; V.S. performed the RT-PCR analysis and evaluation; O.C., M.V. and P.A. performed and analyzed the echocardiography evaluation; A.F. and S.R. provided the human samples and helped with data interpretation; J.J. and D.B. performed the evaluation of the histological data; G.C. and A.F. contributed to the project preparation, conception, and evaluation; P.D. and A.L. contributed to the project preparation, conception, and funding; V.R. and A.C.M. were supervising members of the team. All authors have read and agreed to the published version of the manuscript.

Funding: This work was supported by the Ministry of Education, Youth, and Sports of the Czech Republic (7AMB13FR011, No. CZ.02.1.01/0.0/0.0/16_019/0000868, project no. LQ1605 and no. LQ1601 from the National Program of Sustainability II) and funds from the Faculty of Medicine MU to junior researcher Sarka Jelinkova. This work was also supported by grants of the French Muscular Dystrophy Association (AFM; project 16073, MNM2 2012 and 20225), "Fondation pour la Recherche Médicale" (FRM; SPF20130526710), PHC Barrande (Duchenstem No. 28379TE), and "Institut National de la Santé et de la Recherche Médicale" (INSERM). Supported also by the European Regional Development Fund—Project ENOCH (No. CZ.02.1.01/0.0/0.0/16_019/0000868) and Project INBIO (No. CZ.02.1.01/0.0/0.0/16_026/0008451).

Institutional Review Board Statement: Not Applicable.

Informed Consent Statement: Not Applicable.

Conflicts of Interest: The authors declare that the research was conducted in the absence of any commercial or financial relationships that could be construed as a potential conflict of interest.

References

1. Mah, J.K.; Korngut, L.; Dykeman, J.; Day, L.; Pringsheim, T.; Jette, N. A Systematic Review and Meta-Analysis on the Epidemiology of Duchenne and Becker Muscular Dystrophy. *Neuromuscul. Disord.* **2014**, *24*, 482–491. [CrossRef]
2. Nigro, G.; Comi, L.I.; Politano, L.; Bain, R.J. The Incidence and Evolution of Cardiomyopathy in Duchenne Muscular Dystrophy. *Int. J. Cardiol.* **1990**, *26*, 271–277. [CrossRef]
3. Clarac, F.; Massion, J.; Smith, A.M. Duchenne, Charcot and Babinski, Three Neurologists of La Salpetrière Hospital, and Their Contribution to Concepts of the Central Organization of Motor Synergy. *J. Physiol.* **2009**, *103*, 361–376. [CrossRef]
4. Amedro, P.; Vincenti, M.; De La Villeon, G.; Lavastre, K.; Barrea, C.; Guillaumont, S.; Bredy, C.; Gamon, L.; Meli, A.C.; Cazorla, O.; et al. Speckle-Tracking Echocardiography in Children with Duchenne Muscular Dystrophy: A Prospective Multicenter Controlled Cross-Sectional Study. *J. Am. Soc. Echocardiogr.* **2019**, *32*, 412–422. [CrossRef] [PubMed]
5. Manzur, A.Y.; Kinali, M.; Muntoni, F. Update on the Management of Duchenne Muscular Dystrophy. *Arch. Dis. Child.* **2008**, *93*, 986–990. [CrossRef]
6. Fayssoil, A.; Nardi, O.; Orlikowski, D.; Annane, D. Cardiomyopathy in Duchenne Muscular Dystrophy: Pathogenesis and Therapeutics. *Heart Fail. Rev.* **2010**, *15*, 103–107. [CrossRef] [PubMed]
7. Straub, V.; Rafael, J.A.; Chamberlain, J.S.; Campbell, K.P. Animal Models for Muscular Dystrophy Show Different Patterns of Sarcolemmal Disruption. *J. Cell Biol.* **1997**, *139*, 375–385. [CrossRef]
8. Niggli, E.; Shirokova, N. A Guide to Sparkology: The Taxonomy of Elementary Cellular Ca^{2+} Signaling Events. *Cell Calcium* **2007**, *42*, 379–387. [CrossRef] [PubMed]
9. Williams, I.A.; Allen, D.G. Intracellular Calcium Handling in Ventricular Myocytes from Mdx Mice. *Am. J. Physiol. Heart Circ. Physiol.* **2007**, *292*, H846–H855. [CrossRef] [PubMed]
10. Jung, C.; Martins, A.S.; Niggli, E.; Shirokova, N. Dystrophic Cardiomyopathy: Amplification of Cellular Damage by Ca^{2+} Signalling and Reactive Oxygen Species-Generating Pathways. *Cardiovasc. Res.* **2008**, *77*, 766–773. [CrossRef]
11. Poláková, E.; Shirokova, N. Abnormal Sodium Handling and Mitochondrial Metabolism in Cardiac Dystrophy. *Biophys. J.* **2011**, *100*, 81a. [CrossRef]
12. Bellinger, A.M.; Reiken, S.; Carlson, C.; Mongillo, M.; Liu, X.; Rothman, L.; Matecki, S.; Lacampagne, A.; Marks, A.R. Hypernitrosylated Ryanodine Receptor Calcium Release Channels Are Leaky in Dystrophic Muscle. *Nat. Med.* **2009**, *15*, 325–330. [CrossRef] [PubMed]
13. Fauconnier, J.; Thireau, J.; Reiken, S.; Cassan, C.; Richard, S.; Matecki, S.; Marks, A.R.; Lacampagne, A. Leaky RyR2 Trigger Ventricular Arrhythmias in Duchenne Muscular Dystrophy. *Proc. Natl. Acad. Sci. USA* **2010**, *107*, 1559–1564. [CrossRef] [PubMed]
14. Koenig, X.; Dysek, S.; Kimbacher, S.; Mike, A.K.; Cervenka, R.; Lukacs, P.; Nagl, K.; Dang, X.B.; Todt, H.; Bittner, R.E.; et al. Voltage-Gated Ion Channel Dysfunction Precedes Cardiomyopathy Development in the Dystrophic Heart. *PLoS ONE* **2011**, *6*, e20300. [CrossRef] [PubMed]
15. Cassano, M.; Berardi, E.; Crippa, S.; Toelen, J.; Barthelemy, I.; Micheletti, R.; Chuah, M.; Vandendriessche, T.; Debyser, Z.; Blot, S.; et al. Alteration of Cardiac Progenitor Cell Potency in GRMD Dogs. *Cell Transplant.* **2012**, *21*, 1945–1967. [CrossRef]
16. Dumont, N.A.; Wang, Y.X.; von Maltzahn, J.; Pasut, A.; Bentzinger, C.F.; Brun, C.E.; Rudnicki, M.A. Dystrophin Expression in Muscle Stem Cells Regulates Their Polarity and Asymmetric Division. *Nat. Med.* **2015**, *21*, 1455–1463. [CrossRef]
17. Sohn, J.; Lu, A.; Tang, Y.; Wang, B.; Huard, J. Activation of Non-Myogenic Mesenchymal Stem Cells during the Disease Progression in Dystrophic Dystrophin/Utrophin Knockout Mice. *Hum. Mol. Genet.* **2015**, *24*, 3814–3829. [CrossRef] [PubMed]
18. Colussi, C.; Gurtner, A.; Rosati, J.; Illi, B.; Ragone, G.; Piaggio, G.; Moggio, M.; Lamperti, C.; D'Angelo, G.; Clementi, E.; et al. Nitric Oxide Deficiency Determines Global Chromatin Changes in Duchenne Muscular Dystrophy. *FASEB J.* **2009**, *23*, 2131–2141. [CrossRef]
19. Saccone, V.; Consalvi, S.; Giordani, L.; Mozzetta, C.; Barozzi, I.; Sandoná, M.; Ryan, T.; Rojas-Muñoz, A.; Madaro, L.; Fasanaro, P.; et al. HDAC-Regulated MyomiRs Control BAF60 Variant Exchange and Direct the Functional Phenotype of Fibro-Adipogenic Progenitors in Dystrophic Muscles. *Genes Dev.* **2014**, *28*, 841–857. [CrossRef]
20. Lu, A.; Poddar, M.; Tang, Y.; Proto, J.D.; Sohn, J.; Mu, X.; Oyster, N.; Wang, B.; Huard, J. Rapid Depletion of Muscle Progenitor Cells in Dystrophic Mdx/Utrophin-/- Mice. *Hum. Mol. Genet.* **2014**, *23*, 4786–4800. [CrossRef] [PubMed]
21. Van Erp, C.; Loch, D.; Laws, N.; Trebbin, A.; Hoey, A.J. Timeline of Cardiac Dystrophy in 3-18-Month-Old MDX Mice. *Muscle Nerve* **2010**, *42*, 504–513. [CrossRef]
22. Nitahara-Kasahara, Y.; Hayashita-Kinoh, H.; Chiyo, T.; Nishiyama, A.; Okada, H.; Takeda, S.; Okada, T. Dystrophic Mdx Mice Develop Severe Cardiac and Respiratory Dysfunction Following Genetic Ablation of the Anti-Inflammatory Cytokine IL-10. *Hum. Mol. Genet.* **2014**, *23*, 3990–4000. [CrossRef] [PubMed]
23. Furtado, M.B.; Nim, H.T.; Boyd, S.E.; Rosenthal, N.A. View from the Heart: Cardiac Fibroblasts in Development, Scarring and Regeneration. *Development* **2016**, *143*, 387–397. [CrossRef]
24. Furtado Milena, B.; Costa Mauro, W.; Pranoto Edward, A.; Salimova, E.; Pinto, A.R.; Lam, N.T.; Park, A.; Snider, P.; Chandran, A.; Harvey, R.P.; et al. Cardiogenic Genes Expressed in Cardiac Fibroblasts Contribute to Heart Development and Repair. *Circ. Res.* **2014**, *114*, 1422–1434. [CrossRef] [PubMed]
25. Lajiness, J.D.; Conway, S.J. The Dynamic Role of Cardiac Fibroblasts in Development and Disease. *J. Cardiovasc. Transl. Res.* **2012**, *5*, 739–748. [CrossRef] [PubMed]

26. Talman, V.; Kivelä, R. Cardiomyocyte—Endothelial Cell Interactions in Cardiac Remodeling and Regeneration. *Front. Cardiovasc. Med.* **2018**, *5*, 101. [CrossRef]
27. Mathison, M.; Rosengart, T.K. Heart Regeneration: The Endothelial Cell Comes First. *J. Thorac. Cardiovasc. Surg.* **2018**, *155*, 1128–1129. [CrossRef] [PubMed]
28. Zhang, H.; Lui, K.O.; Zhou, B. Endocardial Cell Plasticity in Cardiac Development, Diseases and Regeneration. *Circ. Res.* **2018**, *122*, 774–789. [CrossRef]
29. Gray, G.; Toor, I.; Castellan, R.; Crisan, M.; Meloni, M. Resident Cells of the Myocardium: More than Spectators in Cardiac Injury, Repair and Regeneration. *Curr. Opin. Physiol.* **2018**, *1*, 46–51. [CrossRef]
30. Leong, Y.Y.; Ng, W.H.; Ellison-Hughes, G.M.; Tan, J.J. Cardiac Stem Cells for Myocardial Regeneration: They Are Not Alone. *Front. Cardiovasc. Med.* **2017**, *4*, 47. [CrossRef] [PubMed]
31. Hodgkinson, C.P.; Bareja, A.; Gomez, J.A.; Dzau, V.J. Emerging Concepts in Paracrine Mechanisms in Regenerative Cardiovascular Medicine and Biology. *Circ. Res.* **2016**, *118*, 95–107. [CrossRef]
32. Maxwell, J.T.; Trac, D.; Shen, M.; Brown, M.E.; Davis, M.E.; Chao, M.S.; Supapannachart, K.J.; Zaladonis, C.A.; Baker, E.; Li, M.L.; et al. Electrical Stimulation of Pediatric Cardiac-Derived c-Kit+ Progenitor Cells Improves Retention and Cardiac Function in Right Ventricular Heart Failure. *Stem Cells* **2019**, *37*, 1528–1541. [CrossRef]
33. Zhou, B.; Wu, S.M. Reassessment of C-Kit in Cardiac Cells: A Complex Interplay Between Expression, Fate, and Function. *Circ. Res.* **2018**, *123*, 9–11. [CrossRef] [PubMed]
34. Finan, A.; Demion, M.; Sicard, P.; Guisiano, M.; Bideaux, P.; Monceaux, K.; Thireau, J.; Richard, S. Prolonged Elevated Levels of C-Kit+ Progenitor Cells after a Myocardial Infarction by Beta 2 Adrenergic Receptor Priming. *J. Cell. Physiol.* **2019**, *234*, 18283–18296. [CrossRef]
35. Hong, K.U.; Guo, Y.; Li, Q.-H.; Cao, P.; Al-Maqtari, T.; Vajravelu, B.N.; Du, J.; Book, M.J.; Zhu, X.; Nong, Y.; et al. C-Kit+ Cardiac Stem Cells Alleviate Post-Myocardial Infarction Left Ventricular Dysfunction Despite Poor Engraftment and Negligible Retention in the Recipient Heart. *PLoS ONE* **2014**, *9*, e96725. [CrossRef] [PubMed]
36. Davis, D.R. Cardiac Stem Cells in the Post-Anversa Era. *Eur. Heart J.* **2019**, *40*, 1039–1041. [CrossRef]
37. Pesl, M.; Jelinkova, S.; Caluori, G.; Holicka, M.; Krejci, J.; Nemec, P.; Kohutova, A.; Zampachova, V.; Dvorak, P.; Rotrekl, V. Cardiovascular Progenitor Cells and Tissue Plasticity Are Reduced in a Myocardium Affected by Becker Muscular Dystrophy. *Orphanet J. Rare Dis.* **2020**, *15*, 65. [CrossRef]
38. Meyers, T.A.; Townsend, D. Early Right Ventricular Fibrosis and Reduction in Biventricular Cardiac Reserve in the Dystrophin-Deficient Mdx Heart. *Am. J. Physiol. Heart Circ. Physiol.* **2015**, *308*, H303–H315. [CrossRef]
39. Chisholm, K.M.; Merker, J.D.; Gotlib, J.R.; Gitana, G.; Lefterova, M.; Zehnder, J.L.; George, T.I.; Arber, D.A.; Ohgami, R.S. Mast Cells in Systemic Mastocytosis Have Distinctly Brighter CD45 Expression by Flow Cytometry. *Am. J. Clin. Pathol.* **2015**, *143*, 527–534. [CrossRef] [PubMed]
40. Shiba, N.; Miyazaki, D.; Yoshizawa, T.; Fukushima, K.; Shiba, Y.; Inaba, Y.; Imamura, M.; Takeda, S.; Koike, K.; Nakamura, A. Differential Roles of MMP-9 in Early and Late Stages of Dystrophic Muscles in a Mouse Model of Duchenne Muscular Dystrophy. *Biochim. Biophys. Acta* **2015**, *1852*, 2170–2182. [CrossRef]
41. De Oliveira, F.; Flavia, D.O.; Quintana, H.T.; Bortolin, J.A.; Gomes, O.A.; Liberti, E.A.; Ribeiro, D.A. Cyclooxygenase-2 Expression in Skeletal Muscle of Knockout Mice Suffering Duchenne Muscular Dystrophy. *Histochem. Cell Biol.* **2013**, *139*, 685–689. [CrossRef]
42. Jelinkova, S.; Fojtik, P.; Kohutova, A.; Vilotic, A.; Marková, L.; Pesl, M.; Jurakova, T.; Kruta, M.; Vrbsky, J.; Gaillyova, R.; et al. Dystrophin Deficiency Leads to Genomic Instability in Human Pluripotent Stem Cells via NO Synthase-Induced Oxidative Stress. *Cells* **2019**, *8*, 53. [CrossRef]
43. Van Berlo, J.H.; Kanisicak, O.; Maillet, M.; Vagnozzi, R.J.; Karch, J.; Lin, S.-C.J.; Middleton, R.C.; Marbán, E.; Molkentin, J.D. C-Kit+ Cells Minimally Contribute Cardiomyocytes to the Heart. *Nature* **2014**, *509*, 337–341. [CrossRef]
44. Sultana, N.; Zhang, L.; Yan, J.; Chen, J.; Cai, W.; Razzaque, S.; Jeong, D.; Sheng, W.; Bu, L.; Xu, M.; et al. Resident C-Kit(+) Cells in the Heart Are Not Cardiac Stem Cells. *Nat. Commun.* **2015**, *6*, 8701. [CrossRef]
45. Chimenti, I.; Smith, R.R.; Li, T.-S.; Gerstenblith, G.; Messina, E.; Giacomello, A.; Marbán, E. Relative Roles of Direct Regeneration versus Paracrine Effects of Human Cardiosphere-Derived Cells Transplanted into Infarcted Mice. *Circ. Res.* **2010**, *106*, 971–980. [CrossRef] [PubMed]
46. Li, T.-S.; Cheng, K.; Lee, S.-T.; Matsushita, S.; Davis, D.; Malliaras, K.; Zhang, Y.; Matsushita, N.; Smith, R.R.; Marbán, E. Cardiospheres Recapitulate a Niche-Like Microenvironment Rich in Stemness and Cell-Matrix Interactions, Rationalizing Their Enhanced Functional Potency for Myocardial Repair. *Stem Cells* **2010**, *28*, 2088–2098. [CrossRef] [PubMed]
47. Tseliou, E.; Pollan, S.; Malliaras, K.; Terrovitis, J.; Sun, B.; Galang, G.; Marbán, L.; Luthringer, D.; Marbán, E. Allogeneic Cardiospheres Safely Boost Cardiac Function and Attenuate Adverse Remodeling After Myocardial Infarction in Immunologically Mismatched Rat Strains. *J. Am. Coll. Cardiol.* **2013**, *61*, 1108–1119. [CrossRef]
48. Rogers, R.G.; Fournier, M.; Sanchez, L.; Ibrahim, A.G.; Aminzadeh, M.A.; Lewis, M.I.; Marbán, E. Disease-Modifying Bioactivity of Intravenous Cardiosphere-Derived Cells and Exosomes in *Mdx* Mice. *JCI Insight* **2019**, *4*. [CrossRef] [PubMed]
49. Aminzadeh, M.A.; Rogers, R.G.; Fournier, M.; Tobin, R.E.; Guan, X.; Childers, M.K.; Andres, A.M.; Taylor, D.J.; Ibrahim, A.; Ding, X.; et al. Exosome-Mediated Benefits of Cell Therapy in Mouse and Human Models of Duchenne Muscular Dystrophy. *Stem Cell Rep.* **2018**, *10*, 942–955. [CrossRef] [PubMed]

50. Kubo, H.; Jaleel, N.; Kumarapeli, A.; Berretta, R.M.; Bratinov, G.; Shan, X.; Wang, H.; Houser, S.R.; Margulies, K.B. Increased Cardiac Myocyte Progenitors in Failing Human Hearts. *Circulation* **2008**, *118*, 649–657. [CrossRef]
51. Matuszczak, S.; Czapla, J.; Jarosz-Biej, M.; Wiśniewska, E.; Cichoń, T.; Smolarczyk, R.; Kobusińska, M.; Gajda, K.; Wilczek, P.; Sliwka, J.; et al. Characteristic of C-Kit+ Progenitor Cells in Explanted Human Hearts. *Clin. Res. Cardiol.* **2014**, *103*, 711–718. [CrossRef] [PubMed]
52. Leite, C.F.; Lopes, C.S.; Alves, A.C.; Fuzaro, C.S.C.; Silva, M.V.; de Oliveira, L.F.; Garcia, L.P.; Farnesi, T.S.; de Cuba, M.B.; Rocha, L.B.; et al. Endogenous Resident C-Kit Cardiac Stem Cells Increase in Mice with an Exercise-Induced, Physiologically Hypertrophied Heart. *Stem Cell Res.* **2015**, *15*, 151–164. [CrossRef]
53. Tidball, J.G.; Albrecht, D.E.; Lokensgard, B.E.; Spencer, M.J. Apoptosis Precedes Necrosis of Dystrophin-Deficient Muscle. *J. Cell. Sci.* **1995**, *108*, 2197–2204. [CrossRef] [PubMed]
54. Mikhaĭlov, V.M.; Komarov, S.A.; Nilova, V.K.; Shteĭn, G.I.; Baranov, V.S. Ultrastructural and morphometrical analysis of apoptosis stages in cardiomyocytes of MDX mice. *Tsitologiia* **2001**, *43*, 729–737. [PubMed]
55. Bridges, L.R. The Association of Cardiac Muscle Necrosis and Inflammation with the Degenerative and Persistent Myopathy of MDX Mice. *J. Neurol. Sci.* **1986**, *72*, 147–157. [CrossRef]
56. Megeney, L.A.; Kablar, B.; Perry, R.L.S.; Ying, C.; May, L.; Rudnicki, M.A. Severe Cardiomyopathy in Mice Lacking Dystrophin and MyoD. *Proc. Natl. Acad. Sci. USA* **1999**, *96*, 220–225. [CrossRef]
57. Rubi, L.; Todt, H.; Kubista, H.; Koenig, X.; Hilber, K. Calcium Current Properties in Dystrophin-deficient Ventricular Cardiomyocytes from Aged Mdx Mice. *Physiol. Rep.* **2018**, *6*, e13567. [CrossRef]
58. Jelinkova, S.; Vilotic, A.; Pribyl, J.; Aimond, F.; Salykin, A.; Acimovic, I.; Pesl, M.; Caluori, G.; Klimovic, S.; Urban, T.; et al. DMD Pluripotent Stem Cell Derived Cardiac Cells Recapitulate in Vitro Human Cardiac Pathophysiology. *Front. Bioeng. Biotechnol.* **2020**, *8*, 535. [CrossRef]
59. Messina, S.; Altavilla, D.; Aguennouz, M.; Seminara, P.; Minutoli, L.; Monici, M.C.; Bitto, A.; Mazzeo, A.; Marini, H.; Squadrito, F.; et al. Lipid Peroxidation Inhibition Blunts Nuclear Factor-KappaB Activation, Reduces Skeletal Muscle Degeneration, and Enhances Muscle Function in Mdx Mice. *Am. J. Pathol.* **2006**, *168*, 918–926. [CrossRef]
60. Radley, H.G.; Davies, M.J.; Grounds, M.D. Reduced Muscle Necrosis and Long-Term Benefits in Dystrophic Mdx Mice after CV1q (Blockade of TNF) Treatment. *Neuromuscul. Disord.* **2008**, *18*, 227–238. [CrossRef]
61. Delfín, D.A.; Zang, K.E.; Schill, K.E.; Patel, N.T.; Janssen, P.M.L.; Raman, S.V.; Rafael-Fortney, J.A. Cardiomyopathy in the Dystrophin/Utrophin-Deficient Mouse Model of Severe Muscular Dystrophy Is Characterized by Dysregulation of Matrix Metalloproteinases. *Neuromuscul. Disord.* **2012**, *22*, 1006–1014. [CrossRef] [PubMed]
62. Dahiya, S.; Givvimani, S.; Bhatnagar, S.; Qipshidze, N.; Tyagi, S.C.; Kumar, A. Osteopontin-Stimulated Expression of Matrix Metalloproteinase-9 Causes Cardiomyopathy in the Mdx Model of Duchenne Muscular Dystrophy. *J. Immunol.* **2011**, *187*, 2723–2731. [CrossRef] [PubMed]
63. Pioner, J.M.; Guan, X.; Klaiman, J.M.; Racca, A.W.; Pabon, L.; Muskheli, V.; Macadangdang, J.; Ferrantini, C.; Hoopmann, M.R.; Moritz, R.L.; et al. Absence of Full-Length Dystrophin Impairs Normal Maturation and Contraction of Cardiomyocytes Derived from Human-Induced Pluripotent Stem Cells. *Cardiovasc. Res.* **2020**, *116*, 368–382. [CrossRef]
64. Khouzami, L.; Bourin, M.-C.; Christov, C.; Damy, T.; Escoubet, B.; Caramelle, P.; Perier, M.; Wahbi, K.; Meune, C.; Pavoine, C.; et al. Delayed Cardiomyopathy in Dystrophin Deficient Mdx Mice Relies on Intrinsic Glutathione Resource. *Am. J. Pathol.* **2010**, *177*, 1356–1364. [CrossRef] [PubMed]
65. Siemionow, M.; Malik, M.; Langa, P.; Cwykiel, J.; Brodowska, S.; Heydemann, A. Cardiac Protection after Systemic Transplant of Dystrophin Expressing Chimeric (DEC) Cells to the Mdx Mouse Model of Duchenne Muscular Dystrophy. *Stem Cell Rev. Rep.* **2019**, *15*, 827–841. [CrossRef] [PubMed]
66. Au, C.G.; Butler, T.L.; Sherwood, M.C.; Egan, J.R.; North, K.N.; Winlaw, D.S. Increased Connective Tissue Growth Factor Associated with Cardiac Fibrosis in the Mdx Mouse Model of Dystrophic Cardiomyopathy. *Int. J. Exp. Pathol.* **2011**, *92*, 57–65. [CrossRef] [PubMed]
67. Fayssoil, A.; Renault, G.; Guerchet, N.; Marchiol-Fournigault, C.; Fougerousse, F.; Richard, I. Cardiac Characterization of Mdx Mice Using High-Resolution Doppler Echocardiography. *J. Ultrasound Med.* **2013**, *32*, 757–761. [CrossRef]
68. Stuckey, D.J.; Carr, C.A.; Camelliti, P.; Tyler, D.J.; Davies, K.E.; Clarke, K. In Vivo MRI Characterization of Progressive Cardiac Dysfunction in the Mdx Mouse Model of Muscular Dystrophy. *PLoS ONE* **2012**, *7*, e28569. [CrossRef]
69. Spurney, C.; Yu, Q.; Nagaraju, K. Speckle Tracking Analysis of the Left Ventricular Anterior Wall Shows Significantly Decreased Relative Radial Strain Patterns in Dystrophin Deficient Mice after 9 Months of Age. *PLoS Curr.* **2011**, *3*, RRN1273. [CrossRef]
70. Taqatqa, A.; Bokowski, J.; Al-Kubaisi, M.; Khalil, A.; Miranda, C.; Alaksham, H.; Fughhi, I.; Kenny, D.; Diab, K.A. The Use of Speckle Tracking Echocardiography for Early Detection of Myocardial Dysfunction in Patients with Duchenne Muscular Dystrophy. *Pediatr. Cardiol.* **2016**, *37*, 1422–1428. [CrossRef]
71. Soslow, J.H.; Xu, M.; Slaughter, J.C.; Stanley, M.; Crum, K.; Markham, L.W.; Parra, D.A. Evaluation of Echocardiographic Measures of Left Ventricular Function in Patients with Duchenne Muscular Dystrophy: Assessment of Reproducibility and Comparison to Cardiac Magnetic Resonance Imaging. *J. Am. Soc. Echocardiogr.* **2016**, *29*, 983–991. [CrossRef]
72. Mertens, L.; Ganame, J.; Claus, P.; Goemans, N.; Thijs, D.; Eyskens, B.; Van Laere, D.; Bijnens, B.; D'hooge, J.; Sutherland, G.R.; et al. Early Regional Myocardial Dysfunction in Young Patients with Duchenne Muscular Dystrophy. *J. Am. Soc. Echocardiogr.* **2008**, *21*, 1049–1054. [CrossRef] [PubMed]

73. Sahoo, S.; Losordo, D.W. Exosomes and Cardiac Repair after Myocardial Infarction. *Circ. Res.* **2014**, *114*, 333–344. [CrossRef] [PubMed]
74. Kishore, R.; Khan, M. More Than Tiny Sacks: Stem Cell Exosomes as Cell-Free Modality for Cardiac Repair. *Circ. Res.* **2016**, *118*, 330–343. [CrossRef] [PubMed]
75. Singla, D.K. Stem Cells and Exosomes in Cardiac Repair. *Curr. Opin. Pharmacol.* **2016**, *27*, 19–23. [CrossRef] [PubMed]
76. Suzuki, E.; Fujita, D.; Takahashi, M.; Oba, S.; Nishimatsu, H. Stem Cell-Derived Exosomes as a Therapeutic Tool for Cardiovascular Disease. *World J. Stem Cells* **2016**, *8*, 297–305. [CrossRef]
77. Saha, P.; Sharma, S.; Korutla, L.; Datla, S.R.; Shoja-Taheri, F.; Mishra, R.; Bigham, G.E.; Sarkar, M.; Morales, D.; Bittle, G.; et al. Circulating Exosomes Derived from Transplanted Progenitor Cells Aid the Functional Recovery of Ischemic Myocardium. *Sci. Transl. Med.* **2019**, *11*. [CrossRef]
78. Fang, S.; Wei, J.; Pentinmikko, N.; Leinonen, H.; Salven, P. Generation of Functional Blood Vessels from a Single C-Kit+ Adult Vascular Endothelial Stem Cell. *PLoS Biol.* **2012**, *10*, e1001407. [CrossRef]
79. Hosoda, T. C-Kit-Positive Cardiac Stem Cells and Myocardial Regeneration. *Am. J. Cardiovasc. Dis.* **2012**, *2*, 58–67.
80. Wang, Y.X.; Feige, P.; Brun, C.E.; Hekmatnejad, B.; Dumont, N.A.; Renaud, J.-M.; Faulkes, S.; Guindon, D.E.; Rudnicki, M.A. EGFR-Aurka Signaling Rescues Polarity and Regeneration Defects in Dystrophin-Deficient Muscle Stem Cells by Increasing Asymmetric Divisions. *Cell Stem Cell* **2019**, *24*, 419–432. [CrossRef] [PubMed]
81. Hsie, A.W.; Recio, L.; Katz, D.S.; Lee, C.Q.; Wagner, M.; Schenley, R.L. Evidence for Reactive Oxygen Species Inducing Mutations in Mammalian Cells. *Proc. Natl. Acad. Sci. USA* **1986**, *83*, 9616–9620. [CrossRef]
82. Douki, T.; Rivière, J.; Cadet, J. DNA Tandem Lesions Containing 8-Oxo-7,8-Dihydroguanine and Formamido Residues Arise from Intramolecular Addition of Thymine Peroxyl Radical to Guanine. *Chem. Res. Toxicol.* **2002**, *15*, 445–454. [CrossRef] [PubMed]
83. Khairallah, M.; Khairallah, R.; Young, M.E.; Dyck, J.R.B.; Petrof, B.J.; Des Rosiers, C. Metabolic and Signaling Alterations in Dystrophin-Deficient Hearts Precede Overt Cardiomyopathy. *J. Mol. Cell. Cardiol.* **2007**, *43*, 119–129. [CrossRef]
84. El Haddad, M.; Jean, E.; Turki, A.; Hugon, G.; Vernus, B.; Bonnieu, A.; Passerieux, E.; Hamade, A.; Mercier, J.; Laoudj-Chenivesse, D.; et al. Glutathione Peroxidase 3, a New Retinoid Target Gene, Is Crucial for Human Skeletal Muscle Precursor Cell Survival. *J. Cell. Sci.* **2012**, *125*, 6147–6156. [CrossRef] [PubMed]
85. Hsiao, L.-C.; Perbellini, F.; Gomes, R.S.M.; Tan, J.J.; Vieira, S.; Faggian, G.; Clarke, K.; Carr, C.A. Murine Cardiosphere-Derived Cells Are Impaired by Age but Not by Cardiac Dystrophic Dysfunction. *Stem Cells Dev.* **2014**, *23*, 1027–1036. [CrossRef] [PubMed]
86. Saito, Y.; Takahashi, K. Selenoprotein P: Its Structure and Functions. *J. Health Sci.* **2000**, *46*, 409–413. [CrossRef]
87. Takahashi, K.; Avissar, N.; Whitin, J.; Cohen, H. Purification and Characterization of Human Plasma Glutathione Peroxidase: A Selenoglycoprotein Distinct from the Known Cellular Enzyme. *Arch. Biochem. Biophys.* **1987**, *256*, 677–686. [CrossRef]
88. Yarimizu, J.; Nakamura, H.; Yodoi, J.; Takahashi, K. Efficiency of Selenocysteine Incorporation in Human Thioredoxin Reductase. *Antioxid. Redox Signal.* **2000**, *2*, 643–651. [CrossRef]
89. Williams, I.A.; Allen, D.G. The Role of Reactive Oxygen Species in the Hearts of Dystrophin-Deficient Mdx Mice. *Am. J. Physiol. Heart Circ. Physiol.* **2007**, *293*, H1969–H1977. [CrossRef]
90. Dick, E.; Kalra, S.; Anderson, D.; George, V.; Ritso, M.; Laval, S.H.; Barresi, R.; Aartsma-Rus, A.; Lochmüller, H.; Denning, C. Exon Skipping and Gene Transfer Restore Dystrophin Expression in Human Induced Pluripotent Stem Cells-Cardiomyocytes Harboring DMD Mutations. *Stem Cells Dev.* **2013**, *22*, 2714–2724. [CrossRef]
91. Inomata, K.; Aoto, T.; Binh, N.T.; Okamoto, N.; Tanimura, S.; Wakayama, T.; Iseki, S.; Hara, E.; Masunaga, T.; Shimizu, H.; et al. Genotoxic Stress Abrogates Renewal of Melanocyte Stem Cells by Triggering Their Differentiation. *Cell* **2009**, *137*, 1088–1099. [CrossRef] [PubMed]
92. Rossi, D.J.; Bryder, D.; Seita, J.; Nussenzweig, A.; Hoeijmakers, J.; Weissman, I.L. Deficiencies in DNA Damage Repair Limit the Function of Haematopoietic Stem Cells with Age. *Nature* **2007**, *447*, 725–729. [CrossRef]
93. Pilzecker, B.; Buoninfante, O.A.; van den Berk, P.; Lancini, C.; Song, J.-Y.; Citterio, E.; Jacobs, H. DNA Damage Tolerance in Hematopoietic Stem and Progenitor Cells in Mice. *Proc. Natl. Acad. Sci. USA* **2017**, *114*, E6875–E6883. [CrossRef]
94. Mandal, P.K.; Rossi, D.J. DNA-Damage-Induced Differentiation in Hematopoietic Stem Cells. *Cell* **2012**, *148*, 847–848. [CrossRef] [PubMed]
95. Burkhalter, M.D.; Rudolph, K.L.; Sperka, T. Genome Instability of Ageing Stem Cells–Induction and Defence Mechanisms. *Ageing Res. Rev.* **2015**, *23*, 29–36. [CrossRef]
96. Amancio, G.D.C.S.; Grabe-Guimarães, A.; Haikel, D.; Moreau, J.; Barcellos, N.M.S.; Lacampagne, A.; Matecki, S.; Cazorla, O. Effect of Pyridostigmine on in Vivo and in Vitro Respiratory Muscle of Mdx Mice. *Respir. Physiol. Neurobiol.* **2017**, *243*, 107–114. [CrossRef]
97. Bankhead, P.; Loughrey, M.B.; Fernández, J.A.; Dombrowski, Y.; McArt, D.G.; Dunne, P.D.; McQuaid, S.; Gray, R.T.; Murray, L.J.; Coleman, H.G.; et al. QuPath: Open Source Software for Digital Pathology Image Analysis. *Sci. Rep.* **2017**, *7*, 1–7. [CrossRef]
98. Broadley, K.J. The Langendorff Heart Preparation—Reappraisal of Its Role as a Research and Teaching Model for Coronary Vasoactive Drugs. *J. Pharmacol. Methods* **1979**, *2*, 143–156. [CrossRef]
99. He, J.-Q.; Vu, D.M.; Hunt, G.; Chugh, A.; Bhatnagar, A.; Bolli, R. Human Cardiac Stem Cells Isolated from Atrial Appendages Stably Express C-Kit. *PLoS ONE* **2011**, *6*, e27719. [CrossRef] [PubMed]
100. Chazalette, D.; Hnia, K.; Rivier, F.; Hugon, G.; Mornet, D. Alpha7B Integrin Changes in Mdx Mouse Muscles after L-Arginine Administration. *FEBS Lett.* **2005**, *579*, 1079–1084. [CrossRef] [PubMed]